Studies on the mechanism of Rho dependent transcription termination in *Escherichia coli*

Thesis submitted to
Manipal University

For the Degree of

Doctor of Philosophy

By

Jisha Chalissery
Registration Number : 050100022

CENTRE FOR DNA FINGERPRINTING AND DIAGNOSTICS
Hyderabad

2010

DECLARATION

The research work embodied in this thesis entitled **"Studies on the mechanism of Rho dependent transcription termination in *Escherichia coli*"**, has been carried out by me at the Centre for DNA Fingerprinting and Diagnostics, Hyderabad, under the guidance of Dr. Ranjan Sen. I hereby declare that this work is original and has not been submitted in part or full for any degree or diploma of any other university or institution.

Jisha Chalissery
Centre for DNA Fingerprinting
and Diagnostics, Hyderabad.

CERTIFICATE

This is to certify that this thesis entitled **"Studies on the mechanism of Rho dependent transcription termination in *Escherichia coli*"**, submitted by Ms. Jisha Chalissery, for the Degree of Doctor of Philosophy to Manipal University is based on the work carried out by her at the Centre for DNA Fingerprinting and Diagnostics, Hyderabad. This work is original and has not been submitted in part or full for any degree or diploma of any other university or institution.

Dr. Ranjan Sen
Thesis Supervisor
Centre for DNA Fingerprinting
and Diagnostics, Hyderabad.

Dr. Shekhar C Mande
Dean, Academic Affairs
Centre for DNA Fingerprinting
and Diagnostics, Hyderabad

Table of Contents

Acknowledgements

I take this opportunity with much pleasure to thank all the people who have helped me through the course of my journey towards producing this thesis. The work in this thesis was carried out at Center for DNA Fingerprinting and Diagnostics (CDFD), Hyderabad. My utmost gratitude goes to my thesis advisor, Dr. Ranjan Sen for his constant guidance, help and support. His hard working nature and persistent attempts to solve the problems really motivated me to face the challenges. He was always accessible and willing to help his students with their research. I also thank other members of doctoral committee Drs. Abhijit Sardesai and Rupinder Kaur for their helpful suggestions.

I gratefully acknowledge Dr. J. Gowrishankar, director CDFD for his advice and intellectually stimulating discussions. I am grateful to the Vice Chancellor, Registrar and the Head, Dept of Biotechnology of the Manipal University for allowing me to register as a graduate student. I am also very grateful to Dr. Shekhar C. Mande, head Structural Biology lab and Dean, Academics section, CDFD for his constant encouragement throughout this work. I would like to acknowledge the CDFD staff of instrumentation, academic, accounts and administrative section for providing the necessary support for this research.

I am grateful to the University Grants Commission (UGC), India for providing me with Junior and Senior research fellowships, during the period of my work. The research at our laboratory has been supported financially by research grants to Dr. Ranjan Sen from Wellcome Trust, UK and CDFD. I would like to express my gratitude to all these institutions.

Thanks are due to my labmates with whom I share tons of fond memories. My seniors, Anoop and Bibhusita taught me new techniques and helped me to work without any trouble especially during my initial days in the lab. Bibhs, Megha and Jineta also provided for some much needed humor and entertainment in what could have otherwise been a somewhat stressful laboratory environment. I would also like to thank my juniors Ghazala, Amitabh, Rajesh and Sourabh for contributing to a very pleasant working environment. Amitabh’s and Jisha V’s enthusiasm and readiness to help made my work so much

smoother. Other past and present lab members that I have had the pleasure to work with or along side are Sharmistha, Dipak, Nisha, Irfan, Kalyani and Shalini. I would like to thank my good friend Nisha not only for her excellent comments, but also for listening to me whenever I was excited about a new idea. I am especially grateful to Nancy and Gowresh for their sincere efforts in organizing the lab and for all the help provided by them in carrying out the experiments.

I acknowledge Drs. Anupama and Hari Narayanan for their advice and their willingness to share their ideas with me, which was of great value for me in designing various *in vivo* experiments during this research. I was fortunate to have seniors like Gokul, Aravind, Akif, Santhosh and Prabhat with whom I had extensive discussions about my work and their guidance have been of great value in this study. I wish to extend my warmest thanks to my collegues Vaibhav, Sudhish, KV, Senthil, Kshama, Uma, Pankaj, Shafiqque, Pavani, Dhananjay, Fiona, Neeraja and Ashwanth. I would also like to thank JRF 2004: Devi, Tej, Debashree, Ratheesh, Sandeep, Shiny, Kaiser, Yusuf, Aisha, Gita and Tabrez for being a great company. I would specially like to thank my roommates and friends Sheeba, Abira, Shivalika and Yashaswini for the time spent with them.

I am grateful to my daddy and mammy for their love, support and allowing me to be as ambitious as I wanted. They taught me to set high goals for myself and work hard to achieve them. I am deeply indebted to Achan and Amma for their care and support especially during the preparation of this thesis. My special gratitude is due to my brother Josan, Dimpy Chechi, Saju ettan, Ramya etathi, Aneena and Adidev for their loving support. I am, thankful to my daughter Apoorva for giving me happiness and joy. I can’t express my gratitude for my husband Suneesh in words, whose unconditional love has been my greatest strength. I cannot be what I am without him who stands beside me in all my times. Without his encouragement and understanding it would have been impossible for me to finish this work.

Finally, my greatest regards to the Almighty for bestowing upon me the courage to face the complexities of life and complete this project successfully.

Jisha

Abbreviations

$A_{600\ nm}$	:	Absorbance at 600 nm
Å	:	Angstrom
aa	:	Amino acid
ADP	:	Adenosine di phosphate
APS	:	Ammonium-per-Sulphate
ApU	:	Adenylyl- (3', 5') Uridine
ATP	:	Adenosine tri phosphate
bp	:	Base pair
BSA	:	Bovine Serum Albumin
CC	:	Coiled coil
CnBr	:	Cyanogen Bromide
C-terminal	:	Carboxy terminal
CTD	:	C-Terminal Domain
CTP	:	Cytosine Tri Phosphate
DMF	:	DiMethyl Formamide
DNA	:	Deoxyribonucleic acid
dNTP	:	Deoxynucleotide
ds	:	double stranded
DTT	:	Di thiothreitol
EC	:	Elongation Complex
E. coli	:	*Escherichia coli*
EDTA	:	Ethylene diamine tetra acetic acid
FP	:	Forward primer
hr	:	hour
g	:	gram
GTP	:	Guanosine Tri Phosphate
IPTG	:	Isopropyl β-D thiogalactopyranoside
kb	:	Kilo base
KD	:	Kilo Dalton

L	:	Litre
LB	:	Luria Broth
M	:	Molar
mg	:	Milligram
μg/ml	:	Microgram per millilitre
μl	:	Microlitre
min	:	Minute
mg/ml	:	Milligram per millilitre
mM	:	MilliMolar
μM	:	Micromolar
MOI	:	Multiplicity of infection
nt	:	Nucleotide
N-terminal	:	Amino terminal
NTD	:	N-terminal domain
NTP	:	Nucleoside triphosphate
OD	:	Optical density
O/N	:	Overnight
ONPG	:	O-Nitro phenyl-β-D-Galactoside
PAGE	:	Polyacrylamide Gel Electrophoresis
PCR	:	Polymerase Chain Reaction
pfu	:	Plaque forming units
P_i	:	Inorganic phosphate
PKA	:	Protein Kinase A
PMSF	:	Phenyl methyl sulphonyl fluoride
Ppi	:	Pyrophosphate
RB	:	Road Block
RBS	:	Ribosome binding site
RNA	:	Ribonucleic Acid
RNAP	:	RNA polymerase
RP	:	Reverse primer
rpm	:	Revolutions per minute

SDS	:	Sodium Dodecyl Sulphate
sec	:	Seconds
TAE	:	Tris-acetate EDTA
TBE	:	Tris-borate EDTA
TE	:	Tris-EDTA
TEMED	:	N,N,N',N'-Tetramethylethylenediamine
TEC	:	Ternary Elongation Complex
Tris	:	2-amino-2-hydroxymethyl propane-1,3-diol
Tris-Cl	:	Tris Chloride buffer
ts	:	Temperature sensitive
UTP	:	Uracil tri phosphate
UV	:	Ultra violet
WT	:	Wild type
X-Gal	:	5-Bromo 4-chloro 3-indolyl β-D-galactopyranoside

Synopsis

Transcription is the process of synthesizing an RNA that is complimentary to the template strand of DNA. The final step in transcript formation is termination, which occurs when the elongating complex moves into one or more terminator sites along DNA template that may serve as transcription regulators within genes or mark the end of a gene or an operon, where the RNA polymerase releases the RNA transcript and dissociates from the DNA template. Specific termination sites on the DNA fall into two classes – factor independent (intrinsic) terminators having a stem loop structure (GC-rich palindromic element) followed by the U rich sequence; and factor dependent termination, where factors like Rho and Nun acts. The transcription termination factor Rho of *Escherichia coli* is a homohexameric protein that is essential for the viability of the cell (Banerjee et al., 2006). Rho is a RNA binding protein which can translocate along the RNA and unwind the RNA: DNA hybrid using the RNA-dependent ATPase activity. Unlike the conserved and highly localized intrinsic termination signals, Rho dependent terminators are bipartite sequences that are present over 200 bp of DNA. The proximal Rho binding site called *rut* (for Rho utilization), spanning a region of around 70-80 nucleotides rich in Cytosine and a distal sequence comprising the termination zone (Banerjee et al., 2006). Interaction of Rho with the elongation factor NusG facilitates the RNA release process from the elongation complex (EC) which is an essential step *in vivo*. NusG causes early termination at several terminators including *trp t'* and can overcome the defects of certain *rho* mutants (Sen et al., 2008).

In order to investigate the involvement of each of the different functions of Rho in releasing RNA from the EC, random mutagenesis of *rho* gene and the subsequent screening for viable Rho mutants defective for Rho dependent transcription termination, was carried out which are described in Chapter III. It also gives a detailed account of the purification and *in vitro* characterization of Rho mutants and the localization of these substitutions in the crystal structure of Rho. Further this chapter describes the design of stalled EC to uncouple the different functions of Rho from RNA release step for studying the effect of ATP and NusG on RNA-release efficiency of the Rho mutants. The major

results from these studies are as follows. Different termination defective mutants of Rho are isolated and they are located within the two different domains of Rho; the N-terminal RNA binding domain (G51V, G53V, and Y80C) and in the C-terminal ATP binding domain (Y274D, P279S, P279L, G324D, N340S, I382N) including the two important structural elements, the Q-loop (P279S, P279L) and R-loop (G324D). Termination defects of the mutants in primary RNA binding domain and Q-loop could not be restored under any conditions that we tested and these were also defective for most of the other functions of Rho. The termination defects of the mutants (Y274D, G324D and N340S), which were mainly defective for secondary RNA binding and likely defective for translocase activity, could be restored under relaxed *in vitro* conditions. We also show that a mutation in a primary RNA binding domain (Y80C) can cause a defect in ATP binding and induce distinct conformational changes in the distal C-terminal domain and this domain may act as a "master switch" that governs all the other functions of Rho. The primary RNA binding domain and the Q-loop are the most crucial structural elements for the RNA release function. The rate of ATP hydrolysis is directly correlated with the efficiency of RNA release and involvement of NusG is restricted only to the final step of RNA release from the EC (Chalissery et al., 2007).

The exact binding surface involved in the Rho-NusG complex is not yet known and the knowledge of which is essential for understanding the mechanism of termination process. To learn more about how the structure of NusG affects its functions in Rho-mediated termination, two domains of NusG were purified serparately and were tested for their effects on the modulation of Rho dependent termination and the ability to compete with WT NusG, which are described in Chapter IV. *In vivo* pulldown of Rho was attempted by individual NusG-NTD and NusG-CTD to identify the domain of NusG involved in interaction with Rho. Chapter IV also describes the mutational, cross-linking and direct binding analyses for the determination of binding surface of NusG on Rho. Here we demonstrate that isolated NusG-CTD can specifically bind to Rho. The amino acid residues G146, V148, L158, V160 and I164 of NusG are important for interactions with Rho. Experiments involving site-specific Cys-Cys di-sulphide bond formation between Rho and NusG revealed that whole face of NusG comprising of NusG-CTD and a part of

NusG-NTD interacts with a dimer of Rho in the absence of EC and the surface exposed amino acids 202, 221 and 224 of Rho located in the well conserved P-loop domain interacts with NusG. In the presence of EC, the β' subunit of RNA polymerase interacts with the hydrophobic pocket at the opposite face and may remove the NusG-NTD interaction with Rho (Chalissery et al., Manuscript Communicated).

References

1. **Chalissery, J.,** Muteeb, G., Jisha, V., Mohan, S. and Sen, R. Interaction surface required for the complex formation between a transcription terminator and an antiterminator. Manuscript Communicated.
2. Sen, R., **Chalissery, J.** and Muteeb, G. (2008). Nus factors of *Escherichia coli*. Invited chapter of the book *Escherichia coli* and *Salmonella*: Cellular and Molecular Biology, ASM press. http://www.ecosal.org.
3. **Chalissery, J.**, Banerjee, S., Bandey, I. and Sen, R. (2007). Transcription termination defective mutants of Rho: role of different functions of Rho in releasing RNA from the elongation complex. Journal of Molecular Biology. 371, 855-872.
4. Banerjee, S., **Chalissery, J.**, Bandey, I and Sen, R. (2006). Rho-dependent transcription termination. More questions than answers. Journal of Microbiology, 44(1), 11-22.

CHAPTER I

Review of Literature

1.1 Prokaryotic transcription

Transcription is the process in which the portions of the template strand of the DNA genome that corresponds to genes are 'copied' into RNA transcripts (mRNA, tRNA or rRNA). It is the first step in gene expression and a major point of gene regulation. Numerous factors regulate transcription by influencing the ability of the RNA polymerase (RNAP) to access, bind and transcribe specific genes in response to appropriate signals. The three main phases of the transcription cycle are known as initiation, elongation and termination, and each stage is subject to regulation. During transcription initiation, a transcription-competent RNAP complex forms at the promoter and the DNA template is aligned in the active site of the polymerase. The active site is where nucleotides are paired with the template and are joined processively during elongation to produce the RNA transcript. Termination of transcription involves release of the RNA transcript and the dissociation of the transcription complex from the DNA template.

1.2 RNA polymerase

The transcription process is carried out by RNAP (Greive and von Hippel, 2005; Landick, 2001; von Hippel, 1998), a multisubunit molecular motor, the basic structure of which is conserved from bacteria to eukaryotes (Ebright, 2000). Each cell contains approximately 2000–5000 RNAP molecules (Grigorova et al., 2006; Ishihama, 2000). *E. coli* core RNAP is a ~400 kDa complex of 5 subunits, α_2, β, β' and ω. Assembly of *E. coli* RNAP proceeds via the pathway $\alpha + \alpha \rightarrow \alpha_2 + \beta \rightarrow \alpha_2\beta + \beta' \rightarrow \alpha_2\beta\beta' + \omega \rightarrow \alpha_2\beta\beta'\omega$ (Ghosh et al., 2001; Ishihama, 1981). RNAP can be crudely described as a crab claw whose active site is positioned at the base of its two pincers. The largest subunit β' makes up one pincer and part of the floor of the active-center cleft; the second-largest subunit β makes up the other pincer and the other part of the floor of the active-center cleft. The active center is located on the floor of the active-center cleft, immediately adjacent to the junction of the active center cleft and the secondary channel. The active center contains a tightly bound catalytic Mg^{2+} ion, coordinated by three Asp residues, and contains binding sites for NTP substrates (Sosunov et al., 2005; Zaychikov et al., 1996; Zhang et al., 1999).

RNAP possess five interior tunnels – the downstream binding site (DBS) tunnel for the double stranded (ds) DNA, the RNA exit tunnel, the template strand (T) tunnel, the non-

template strand (NT) tunnel, and the secondary tunnel through which NTP and small RNA diffuse to and from the active site (Figure 1.1). Downstream DNA, located in an internal channel formed between the jaws, separates into its two strands near the active site. The highly conserved structural feature called the β' rudder separates the two tunnels that enclose each strands of the DNA in the transcription bubble. The strands take different paths through the polymerase and reanneal to form the upstream duplex, which is at a right angle to the downstream DNA. Nascent RNA follows the template strand for about 9 bases and then exits the polymerase underneath a flap that juts out from the bottom of the jaws. RNA exit channel accommodates 5–6 bases of the nascent transcript. The β′ lid, a loop-like structure that protrudes into the main channel, contacts the nascent RNA at the upstream edge of the RNA-DNA hybrid, where the RNA gets separated from the DNA template-strand and upstream ds DNA is formed. RNAP has two moving parts that constitute a part of its active center: the F-bridge (bridge helix) and the G-loop (trigger loop), which have crucial roles during catalysis and RNA chain elongation (Figure 1.1). The highly flexible G (trigger)-loop together with the F (bridge)-helix is involved in selecting and binding correct NTP in the catalytic site, specifically, at the i + 1 site. After phosphodiester bond formation between i -1 and i + 1 NTPs and the release of pyrophosphate, the G (trigger)-loop interactions with the incorporated nucleotide are lost, so it moves away from the catalytic site and assumes an alternative (unfolded) conformation (Vassylyev et al., 2007; Wang et al., 2006).

The α subunit of RNAP comprises two independently folded domains connected by a highly flexible interdomain linker (Blatter et al., 1994; Fujita et al., 2000; Jeon et al., 1995; Jeon et al., 1997; Negishi et al., 1995; Zhang and Darst, 1998). The N-terminal domain (NTD;1 residues 8-235) is required and sufficient for the assembly of core enzyme (Igarashi et al., 1991a; Kimura and Ishihama, 1995a; Kimura and Ishihama, 1995b), while the C-terminal domain (CTD; residues 249-329) plays key roles in transcription activation by interacting with either a large group of transcription factors (class I factors) such as cAMP receptor protein (CRP) and OmpR (Igarashi et al., 1991b; Igarashi and Ishihama, 1991), or the upstream element (UP element), which is present in a certain class of strong promoters including ribosomal RNA promoters (Ross et al., 1993).

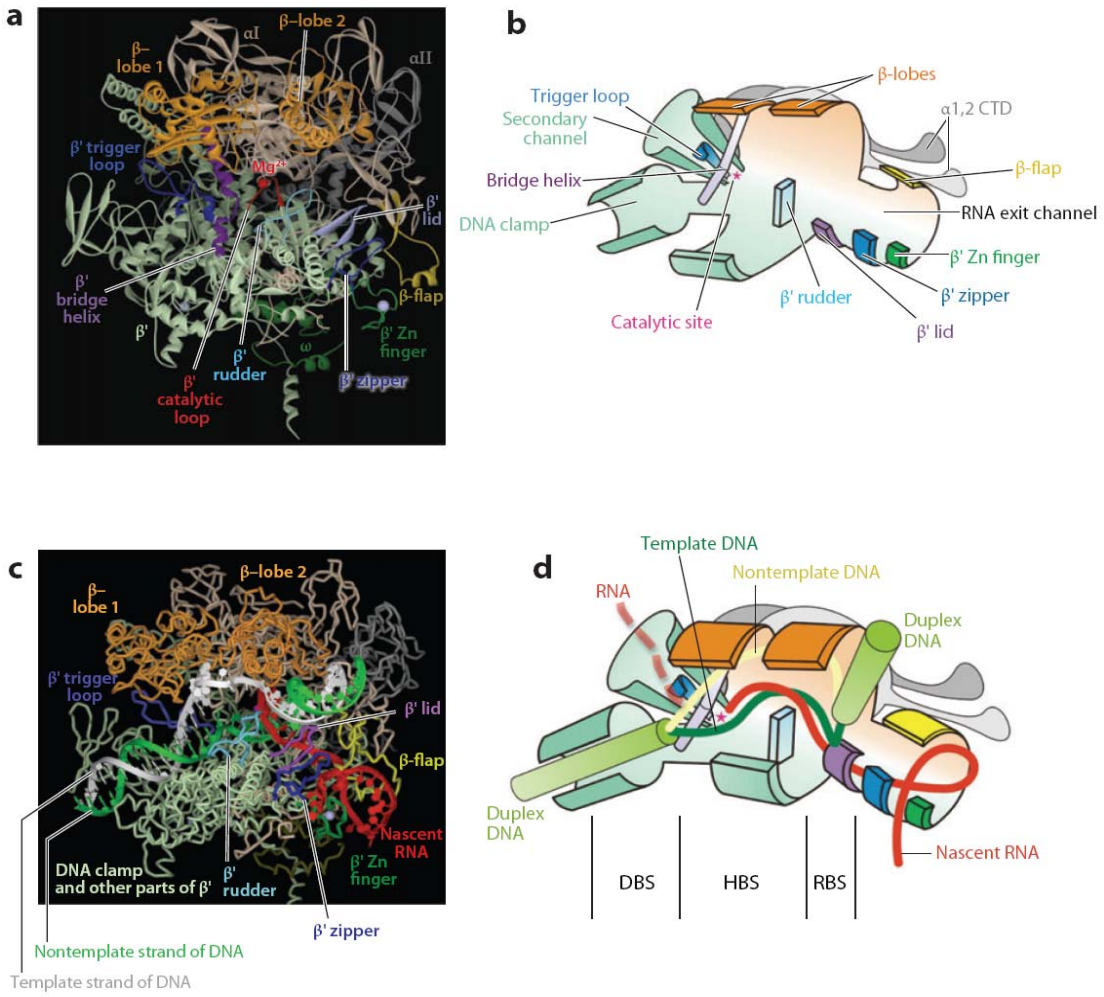

(Nudler, 2009)

Figure 1.1: Structural overview of the elongating complex (EC).

a) High-resolution crystal structure of the *Thermus aquaticus* RNAP core (Zhang et al., 1999) is shown as colored ribbons (αI, αII, β, β, and ω). This structure represents the main-channel view of RNAP. Mobile elements include β bridge helix (BH) [residues I705-V835 of *Thermus thermophilus* (T.t.) β]; β trigger loop (T1234-L1256); β zipper (V26-E47); β Zn finger (G51-S83); β lid (R525-S538); β rudder (N584-S602); β-lobe 1 (A29-D133, G337-S392); β-lobe 2 (R142-N330); and β-flap (G757-S789). b) A schematic representation of the RNAP structure in (a) shown as a simplified diagram with all the key structural elements labeled. c) Structural model of the EC using the T.t. EC structure (Vassylyev et al., 2007). d) The schematic representation of the structure with the same color code as in (b). The main channel secures the RNA-DNA hybrid in the hybrid-binding site (HBS). β domains clamp the downstream DNA in the DNA duplex-binding site (DBS). The β zipper, Zn finger, and lid along with β-flap form the RNA exit channel. The RNA-binding site (RBS) is located at the junction of HBS and the RNA exit channel and also functions as rear zip lock that separates the nascent transcript from the hybrid. The front zip lock formed by the BH and other elements of the catalytic center separates RNA (shown as a dashed red line) from the hybrid during backtracking, directing it into the secondary channel (shown as a funnel). Transcription goes from right to left.

The αCTD has a compact globular structure consisting of four helices, two helical turns, and a long C-terminal loop with defined structure. The dimer of αNTD has an elongated flat structure. All amino acid (aa) residues that are anticipated in the interaction with two large subunits, β and β' (Kimura and Ishihama, 1995a; Kimura and Ishihama, 1995b), are exclusively located on one face of the flat structure. On the other face of αNTD dimer exist the interdomain linkers to αCTDs. Thus two αCTDs are supposed to extrude out from the core part of RNAP, probably towards the upstream direction, through the long flexible linkers. The ω subunit, encoded by the *rpoZ* gene and consisting of 90 aa is necessary to restore denatured RNAP *in vitro* to its fully functional form. ω simultaneously binds the N-terminal and C-terminal regions of β' (Ghosh et al., 2001).

The principal enzymatic action of RNAP is the synthesis of RNA chain complementary to the DNA template strand from nucleoside triphosphate (NTP) substrates. The transfer of a nucleotidyl moiety from the incoming NTP substrate to the 3'-OH of the nascent RNA is followed by the release of pyrophosphate (PP_i) and translocation of RNAP by one nucleotide. The polymerization reaction is reversible. In the process known as pyrophosphorolysis, RNAP progressively degrades the nascent RNA in the presence of PP_i, releasing NTPs from the 3' end of the transcript (Rozovskaia et al., 1981). In backtracked EC, RNAP also mediates endonucleolytic cleavage of the nascent transcript near the 3'-end leading to the release of 5' NMPs (Surratt et al., 1991) (Figure 1.2). This reaction greatly facilitated by cleavage factors, such as GreA and GreB occurs at the active site of RNAP where two catalytic Mg^{2+} ions are coordinated by invariant aspartate residues (Orlova et al., 1995; Vassylyev et al., 2002). The resulting 5'-fragment remains stably bound to the RNAP and in the presence of nucleotides, the discarded RNA segment is correctly resynthesized. The energy of NTP hydrolysis is not directly used for translocation. According to the Brownian ratchet model, the energy gained from the coordinated binding of correct NTP coupled with reciprocating motion of the F (bridge)-helix–G (trigger)- loop unit results in the stepwise forward motion of RNAP with efficient incorporation of correct substrate (Abbondanzieri et al., 2005; Bar-Nahum and Nudler, 2001; Guajardo and Sousa, 1997).

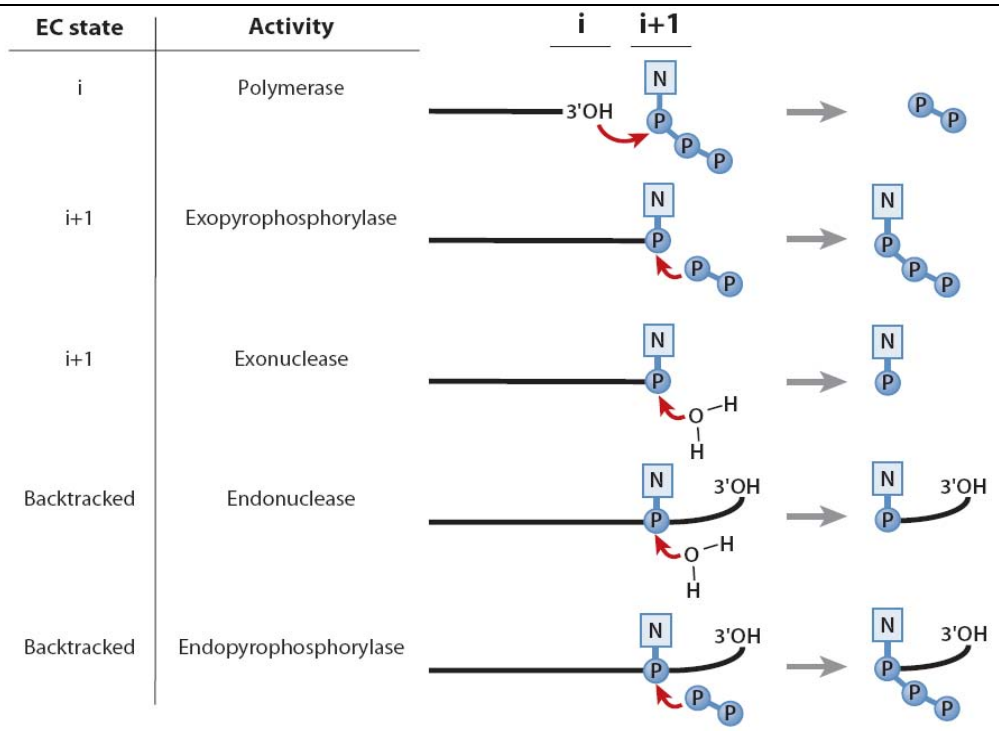

(Nudler, 2009)

Figure 1.2: Catalytic activities of RNAP.

Schematic representation of enzymatic reactions performed by the elongating complex in different states. i and i+1 represent the product- and substrate-binding sites of the catalytic center, respectively. Red arrows indicate the direction of the nucleophilic attack. Solid lines represent the nascent RNA. Abbreviations: P, phosphate group; N, nucleotide residue.

The rifamycins (rifampicin, rifapentine and rifabutin) bind to a site on bacterial RNAP adjacent to the RNAP active center and prevent extension of RNA beyond a length of 2–3 nt. However, rifampicin has no effect on RNAP once it has elongated past the promoter. Streptolydigin (Stl), on the other hand, blocks transcription immediately upon addition to elongating, as well as initiating, RNA polymerase. Stl binds to a site adjacent to but not overlapping the RNAP active center and encompasses the bridge helix and the trigger loop. Stl stabilizes catalytically inactive substrate bound transcription intermediate, thereby blocking structural isomerization of RNAP to an active configuration (Temiakov et al., 2005; Tuske et al., 2005). The α-pyrone antibiotic myxopyronin (Myx) inhibits bacterial RNAP by interacting with the RNAP ‘‘switch region’’ - the hinge that mediates opening and closing of the RNAP active center cleft - to prevent interaction of RNAP with promoter DNA (Belogurov et al., 2009; Mukhopadhyay et al., 2008).

1.3 Transcription initiation

Transcription initiation involves recognition of the promoter, opening the promoter to insert the RNAP in its proper orientation onto the template strand within the transcription bubble, initiating RNA synthesis by positioning 5' nucleotide of the transcript on the DNA template and polymerizing the first few complementary nucleotides along the template to extend the nascent RNA to 8-9 bp. Finally, σ factor is released and core RNAP leaves the promoter and becomes committed to productive chain elongation.

1.3.1 Promoter elements

The DNA sequences contacted by RNA polymerase in the initiating complex can be divided into two parts, the promoter recognition region (PRR), which spans from -60 to the start site (+1), and the initial transcribed sequence (ITS), which spans from +1 to +20. Specific promoter elements that may be used for promoter recognition include: UP elements (positioned between −60 and −40) that are bound by the C-terminal domains of the α subunits of core (α-CTDs), a −35 element a hexamer (TTGACA) that is recognized by residues in σ^{70} region 4, an 'extended -10 motif' (TG) located immediately upstream of the -10 region that is recognized by residues in σ^{70} region 3, and sequences within a −10 element, a hexamer (TATAAT), that is recognized by residues in σ^{70} region 2. The UP element, an AT rich region found predominantly in strong promoters, enhances the promoter activity by promoting RNA polymerase binding (Ellinger et al., 1994; Ross et al., 1993). The promoter spacer spanning 16-19 bp separates the -10 and -35 consensus hexamers and contributes to promoter function. The length of the spacer, but not its sequence, is an important determinant of promoter strength (Harley and Reynolds, 1987; Hawley and McClure, 1983; Mulligan et al., 1985; Stefano and Gralla, 1982; Warne and deHaseth, 1993). One exception is the "extended -10" promoters where TG at positions -15 and -16 is required in the spacer (Chan and Busby, 1989; Keilty and Rosenberg, 1987).

1.3.2 Role of sigma factors in transcription initiation

Although core RNAP can transcribe RNA, it must bind to an σ subunit to form holoenzyme in order to associate with specific DNA sequence located at the promoters. A rapid shift in global gene expression patterns is achieved by utilizing different σ factors in response to variation in conditions by redirecting RNAP to the appropriate classes of

genes. Regulatory proteins called antisigmas specifically bind to a sigma factor and prevent its interaction with RNAP core. Cascades of sigmas and corresponding antisigmas often orchestrate transcription switches from one set of genes to another (Hughes and Mathee, 1998). Of the 7 different σ factors (σ^{70}, $\sigma^{38/S}$, $\sigma^{32/H}$, $\sigma^{54/N}$, $\sigma^{28/F}$, $\sigma^{24/E}$ and σ^{19}) encoded by *E. coli*, σ^{70} the *rpoD* gene product is the major σ factor that governs the transcription of genes required for exponential growth (Gruber and Gross, 2003). During the stationary phase, σ^{S} binds the RNAP and up regulates the expression of genes required for cellular maintenance while the genes required for exponential growth are rapidly switched off (Hengge-Aronis, 1996). σ^{32} and σ^{24} transcribe the genes for heat shock proteins; σ^{54} transcribes the genes which are regulated by the availability of nitrogen and σ^{28} is needed for expression of the flagellar and chemotaxis genes. σ^{19}, the *fecI* gene product, originally identified as a regulatory gene for the ferric citrate transport system is involved in transcriptional regulation of the genes for extra cytoplasmic functions (Gruber and Gross, 2003).

The binding of σ factor results in the formation of a holoenzyme that can not only recognize promoter DNA but also trigger a series of structural transitions in RNAP required for initiation. According to the process described as “sigma cycle”, the σ subunit dissociates from the core enzyme once a stable elongation complex is formed after the synthesis of 9–12 nucleotides long RNA transcript (Figure 1.3). When RNAP dissociates at the terminator, it is free for reassembly with a new σ and begin another cycle of transcription (Travers and Burgess R. R., 1969).

Based on sequence conservations the housekeeping σ^{70} subunit is divided into four evolutionarily conserved regions, termed regions 1 through 4 (Lonetto et al., 1992). Two DNA binding determinants located in the regions 2.4 and 4.2 of σ^{70} recognise respectively the -10 and -35 sequence of prokaryotic promoter. Region 1.1, conserved only among primary σ^{s}, is an autoinhibitory domain that masks DNA binding determinants in free σ^{70} but also promotes open complex formation (Dombroski et al., 1993a; Dombroski et al., 1993b; Dombroski et al., 1992).

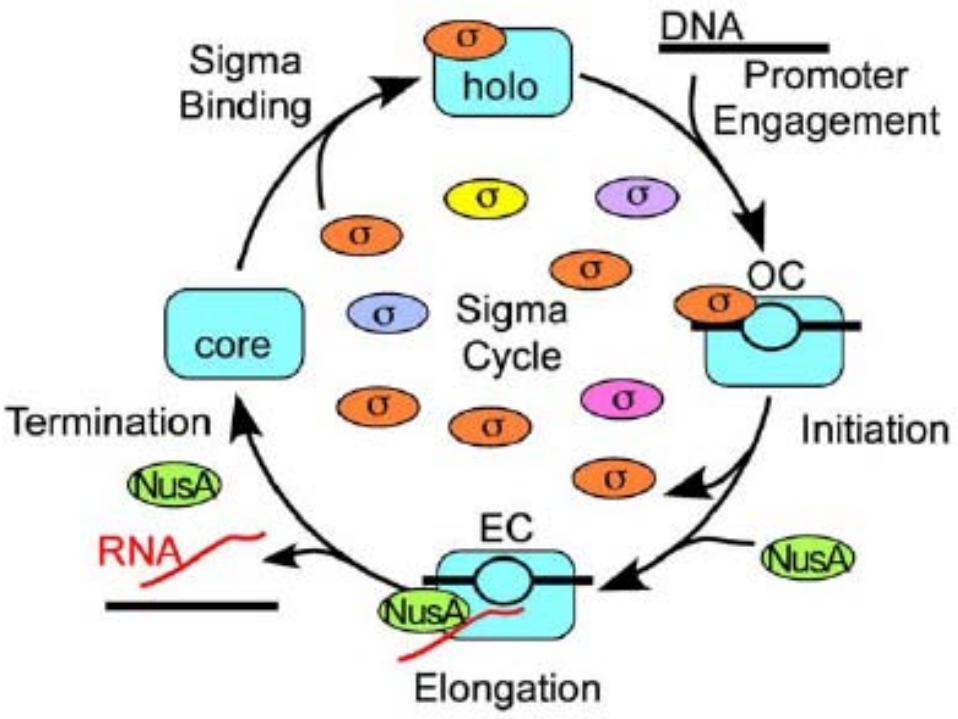

(Mooney et al., 2005)

Figure 1.3: The σ Cycle.

A pool of σ factors competes for binding to core RNAP to form a holoenzyme, which binds promoter DNA to form an open complex (OC). σ release from the elongating form of the enzyme (the EC) explains how σ can be reused to direct transcription initiation by multiple molecules of core RNAP. Competitive binding to the EC by NusA may help displace σ from the EC.

An interaction with core reorients regions 1.1 and 3.1–4.2 of σ^{70} relative to the central 1.2–2.4 domain (Callaci et al., 1998; Callaci et al., 1999) which removes autoinhibition by region 1.1 (Dombroski et al., 1993a; Dombroski et al., 1993b) and reorganizes region 2.3–2.4 to allow selective recognition of the nontemplate strand of the -10 region of the promoter (Callaci et al., 1999; Marr and Roberts, 1997; Young et al., 2001). Interaction of σ2 with the β' clamp in the upper pincer and σ3 with β1 in the lower pincer modulates the opening and closing of the downstream DNA channel. Likewise, interaction of σ4 with the β flap can alter the RNA exit channel (Murakami et al., 2002) (Figure 1.4).

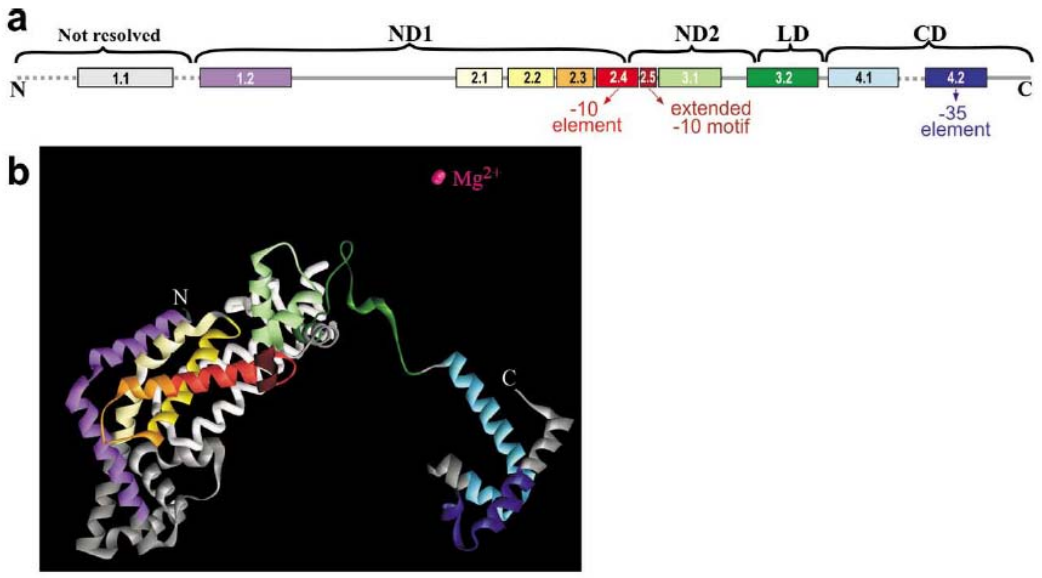

(Borukhov and Severinov, 2002)

Figure 1.4: Structure and amino acid sequence conservation of σ factors.

a) Schematic representation of σ structural domains and evolutionarily conserved regions. The linear structure represents a σ^{70}-like subunit. Evolutionarily conserved regions are represented by numbered boxes and are color-coded. Structural domains are indicated above. Below, the interactions made by DNA binding domains of σ are indicated. b) Ribbon diagram of σ^{A} factor from *T. thermophilus* RNAP holoenzyme structure (Vassylyev et al., 2002). The color coding is as in (a). The β subunit coiled-coil domain is shown in white. The positions of RNAP active site coincides with the positions of catalytic Mg^{2+} ions (magenta spheres).

1.3.3 Initiation of transcription

Holoenzyme first recognizes the two conserved hexamers in the promoter, located at -10 and -35 relative to the transcription start point of +1, then melts the DNA from -11 to +4 to form the open complex, and then begins synthesizing the nascent RNA. The complex lacking catalytic activity formed upon initial recognition and binding to the promoter DNA by RNAP, is referred to as closed complex, (RPc), because the DNA is fully double-stranded or closed. For transcription initiation to occur, RPc must transition into a species, RPo, in which the DNA is both bent and unwound (open), and polymerase has undergone major conformational changes, called isomerization. The stable RPo species is achieved when the DNA around the transcriptional start site is fully separated, creating a transcription bubble from around −11 to +3, the template strand is located in the active site with the +1 nucleotide ready for base paring with incoming NTPs, and the polymerase

‘clamp’ fully closes onto the DNA that is lying in the DNA channel (Brodolin et al., 2005; Davis et al., 2007; Kainz and Roberts, 1992; Lim et al., 2001; Nguyen and Burgess, 1997; Sasse-Dwight and Gralla, 1989; Sasse-Dwight and Gralla, 1991). In RPo, the nontemplate strand nucleotides of the −10 element interact with σ region 2.3, stabilizing the polymerase-promoter complex. Additionally, the nucleotide at −5 may be recognized by σ^{70} region 1.2 (Feklistov et al., 2006; Haugen et al., 2006; Zenkin et al., 2007).

At *de novo* initiation, NTP is brought in from the secondary channel and phosphodiester bond is formed between the nucleotide substrates positioned in the i and i+1 sites. In steps after the first phosphodiester bond, the i site is occupied by the 3’ OH nucleotide of the nascent transcript, while the i+1 site accommodates the successive NTP. Polymerase prefers to start transcripts with ATP followed by GTP, UTP, and then CTP. A translocation event follows rapidly to reposition the next template base at the new i+1 site before the catalysis of the next phosphodiester bond occurs. The RNA strand is bound to the template strand as an 8-bp RNA-DNA heteroduplex. RNA longer than 8 nt would be peeled away from the template strand and directed in to the RNA exit channel.

Promoter escape is the last step of transcription initiation and is intimately linked to the phenomenon of abortive initiation. The nascent RNA chain can dissociate rather rapidly from the polymerase, at least for the first two or three nucleotides (McClure et al., 1978), and studies of abortive initiation products suggest that a length of up to nine to ten nucleotides may be required for formation of a stable ternary complex at some promoters (Carpousis and Gralla, 1985; Goldman et al., 2009; Grachev and Zaychikov, 1980; Gralla et al., 1980; Munson and Reznikoff, 1981; Straney and Crothers, 1985). During abortive initiation, RNAP cycles repeatedly at the promoter without dissociating from the template but rather remains bound as open and initial transcribing complexes (Carpousis and Gralla, 1980). The RNAP active center translocates relative to DNA in initial transcription through a “scrunching" mechanism. According to this model, in each cycle of abortive initiation, RNAP pulls downstream DNA into itself, pulling in 1 bp per phosphodiester bond formed and accommodating the accumulated DNA as single-stranded bulges within the unwound region; on release of the abortive RNA, RNAP extrudes the accumulated DNA, which regenerates the initial state (Kapanidis et al., 2006). The accumulated DNA-scrunching

stress (DNA-unwinding stress and DNA-compaction stress) in the stressed intermediate provides the driving force for abortive initiation and also used to drive breakage of interactions between RNAP and promoter DNA and between RNAP and initiation factors during promoter escape (Kapanidis et al., 2006; Revyakin et al., 2006).

1.4 Transcription elongation

During elongation, RNAP functions as a part of the ternary elongation complex (TEC) in association with template DNA and RNA product. The EC is both highly stable and processive, rapidly extending RNA chains for thousands of nucleotides. The catalytic cycle of RNA chain elongation minimally involves (i) nucleoside triphosphate (NTP) binding, (ii) nucleophillic displacement of pyrophosphate from the NTP by the RNA 3' hydroxyl, (iii) pyrophosphate release, and (iv) translocation of the new RNA 3' nucleotide to vacate the NTP binding site.

1.4.1 Structure of elongation complex

The core enzyme conformations in the EC and the holoenzyme are not identical, demonstrating the most significant changes in those structural domains that switch their contacts from the σ-subunit in the holoenzyme to the nucleic acids in the EC. These alterations demarcate the transition from the initiation to the elongation phase and probably contribute to the high stability of the EC, a feature that distinguishes it markedly from the initiation complex. The most notable rearrangements involve the β and β' domains forming the pincers of the crab-claw-like structure of the core enzyme (Zhang et al., 1999) to constitute the main channel accommodating the downstream DNA and the RNA/DNA hybrid. First, the β'-pincer (the major part of the 'clamp' in the eukaryotic system) domain consisting of the amino-terminal α-helical coiled coil (β'CC1; residues 540–581), the major binding site for the σ subunit, and two loops ('rudder', β'582–602, and 'lid', β'525–539) moves away from its position in the holoenzyme by, 5.5 Å , bringing the lid into a stack with the upstream edge of the RNA/DNA hybrid and positioning the rudder right between the downstream DNA and the hybrid. Second, the movement of the coiled coil is accompanied by the corresponding shift of the adjacent β' N-terminal domain (β'951–499), which places it near the downstream edge of the DNA on one side (β'102–132; β'470–499) and contributes to the formation of the RNA exit channel on the other (β'51–

87). Third, in the β-pincer portion of the claws, the β-domain (β1–130; β335–396) that has lost its interactions with the σ-regions 2.4–3.1 (ND2 domain) moves by, 3.0 Å towards the RNA/DNA hybrid, whereas the adjacent β-domain (β140–332) approaches downstream DNA after the, 4.0 Å reorientation, thereby closing the downstream DNA-binding cleft in the EC. The latter movement is probably attributable to the presence of the downstream DNA rather than to the absence of the σ-subunit. Last, the entire β-flap (β703–830) domain that forms one wall of the RNA exit channel moves slightly (2.2 Å) towards the displaced transcript in the EC. However, this rearrangement is compensated for by the corresponding repositioning of the β' N-terminal domain forming another wall of the channel; thus, the size and shape of the RNA exit channel remain nearly unchanged. Overall, in comparison with the holoenzyme, the EC structure undergoes closure of the RNAP claws to reduce the size of the main channel substantially and probably to achieve surface complementarity between the protein and the nucleic acid chains, thereby favouring the high stability and processivity of the EC (Vassylyev et al., 2007).

1.4.2 Transcriptional pausing

Transcription elongation does not proceed at a uniform rate. In *E. coli*, the average rate of elongation is 50 nt/s (Uptain et al., 1997). RNAP tends to dwell transiently at certain template positions known as pause sites. Pauses, which are characterized by highly variable durations and efficiencies (Greive and von Hippel, 2005), are an ubiquitous aspect of transcription elongation and are known to play regulatory roles particularly in synchronizing transcription with other biological processes, such as translation in bacteria (Landick et al., 1985), factor-dependent and factor-independent termination (Nudler and Gottesman, 2002; Wilson and von Hippel, 1994), interactions with regulatory proteins (Nickels and Hochschild, 2004) and/or RNA folding. Antiterminators like N, Q, RfaH and PUT reduce the half life and /or efficiency of pausing at some sites thereby helping RNAP transcribe long operons (Artsimovitch and Landick, 2002; King et al., 1996; Rees et al., 1997; Yang and Roberts, 1989). Mutations in RNAP core subunits can either enhance or reduce pausing (Fisher and Yanofsky, 1983). Even though pauses are not associated with a consensus sequence, pause positions along the template are strongly sequence-dependent. This sequence dependence is encoded indirectly, through the effect of base-pairing nucleic

acid interactions on the motion of RNAP along DNA. The uridine-rich segment of intrinsic terminators induces pausing at the release site even in the absence of the hairpin, and certain Rho terminators are strong pausing sites in the absence of Rho (Dutta et al., 2008; Lau et al., 1983; Morgan et al., 1983).

Class I pauses (like *his*) are mediated by a stem–loop structure that interacts with RNAP and displace the 3' OH away from the catalytic center (Landick et al., 1996; Toulokhonov et al., 2001). Class II pauses (like *ops*) involve backtracking due to a weak DNA-RNA hybrid (Artsimovitch and Landick, 2000; Artsimovitch and Landick, 2002). The effects of NusA and NusG are pause class-specific: NusA enhances pausing at class I sites, whereas NusG inhibits pausing at class II sites. Pausing at both classes of sites is affected similarly by substitutions in RNAP that increase or decrease the rate of RNA synthesis (Artsimovitch and Landick, 2000).

1.4.3 Regulation of transcription elongation

Regulation of RNA chain elongation depend both on interruptions to transcription caused by pause, arrest, and termination signals encoded in the DNA and RNA and on auxiliary proteins that modify the response of RNAP to these signals. Auxiliary proteins such as NusA, NusG, GreA and GreB modulates the rate of transcription via direct protein:protein interactions with the RNAP. Recent genome-wide ChIP-chip study on *E. coli* revealed that σ^{70}, NusA, NusG, and Rho are distributed relatively uniformly among most transcribing RNAP molecules with apparent relative affinities for elongating RNAP of NusA ≈ NusG > Rho > σ^{70}. Rho and NusA appear to associate with RNAP as σ^{70} association decreases, with Rho slightly preceding NusA, whereas NusG associates with elongating RNAP more slowly (Mooney et al., 2009a).

1.4.3.1 Elongation factors NusA and NusG

NusA and NusG are the integral part of the transcription EC and modulate the transcription elongation rate, intrinsic and Rho dependent termination. NusA and NusG, are universally conserved among bacteria and archaebacteria (Ingham et al., 1999), are typically essential to cell viability (Bubunenko et al., 2007). Both of these Nus factors directly interact with

RNAP and Rho (Greenblatt and Li, 1981; Mason et al., 1992; Schmidt and Chamberlin, 1984).

NusA reduces the rate of elongation by enhancing the pausing of the EC at specific sequences (Burns et al., 1998; Burova et al., 1995). NusA was observed to enhance the class I pauses as in *his*- or *trp*- pause hairpins and suppresses forward translocation (Bar-Nahum et al., 2005). NusA is an important component of both λ N and Q antitermination complexes (Mason et al., 1992; Yarnell and Roberts, 1992). The multiple functionality of NusA could be reflected by its multidomain structural organization. NusA is a rod-shaped, elongated molecule consisting of distinct structural domains viz. an N-terminal RNAP binding domain, three RNA binding motifs, S1, K homology 1 (KH1), and KH2; two C-terminal acidic regions, AR1 and AR2 (Figure 1.5). Upon binding to RNAP through its N-terminal domain, the RNA binding domains of NusA become accessible to interact with 5'-end of the nascent RNA. Interaction of the C-terminal AR1 and AR2 domains with the α-subunit of RNAP may also help the RNA binding domain of NusA to interact with the RNA (Liu et al., 1996). Interaction of NusA with the single stranded region in the upstream end of the nascent RNA allows stable hairpin to form near the RNA exit channel by preventing unwanted pairing with the 5'- end of the RNA. The RNAP TL mutant, I1134V, which slows elongation, was resistant to NusA-mediated pausing and translocation. NusA is unable to exert any further effect on the TL/BH oscillation in this mutant suggesting that NusA decelerate elongation by decelerating F bridge oscillation (Bar-Nahum et al., 2005). Cross-linking experiments and RNA protection studies with functional ECs suggest that NusA could also make contacts near the RNA exit channel, around the β-flap domain. It has also been proposed that NusA stabilizes pause hairpin-flap interaction, which by widening the RNA exit channel may allosterically affect RNAP's active site. NusA no longer enhances pausing when the flap-tip helix of the β subunit is deleted, again suggesting an interaction with the β-flap domain in the NusA-pause hairpin-EC complex (Toulokhonov et al., 2001).

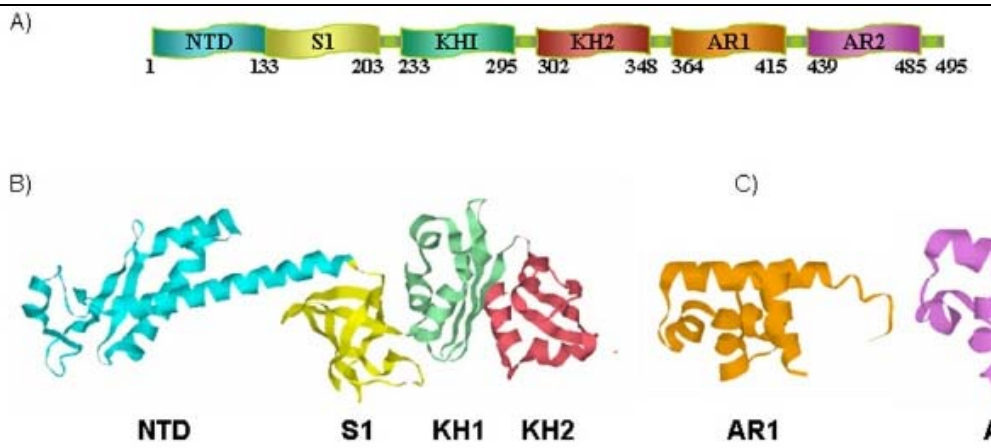

Figure 1.5: Crystal structures of NusA domains and complexes with RNA and N protein.

A) Cartoon showing different functional domains of *E. coli* NusA. The NTD and the Src homology (S1), KH1, and KH2 domains are highly conserved among different NusA molecules. Domains AR1 and AR2 are found in a few species, including *E. coli*. Numbers indicate amino acid positions. B) The crystal structure of conserved domains of NusA from *T. maritima* (Protein Data Bank [PDB] no. 1L2F) (Shin et al., 2003) shows that each functional domain has distinct tertiary folds and corresponds to a separate structural domain, as indicated. C) Two separate nuclear magnetic resonance structures of AR1 and AR2 domains (PDB nos. 1WCL and 1WCN, respectively) (Eisenmann et al., 2005) of *E. coli.*

NusG is a 21 kD monomeric protein involved in transcription elongation and termination (Richardson, 2002). The homology model of *E. coli* NusG (EcoNusG) derived from the crystal structure of *Aquifex aeolicus* NusG (AaeNusG) reveals that it is comprised of two distinct globular domains connected by a flexible linker (Knowlton et al., 2003; Steiner et al., 2002) (Figure 1.6). The N-terminal ribonucleo-protein (RNP) like domain (NTD) is proposed to be involved in protein and nucleic acid binding. AaeNusG has a unique ~70 residues long positively charged immunoglobulin like central domain which is replaced by a loop known as appended mini domain in *E. coli* NusG (EcoNusG) (Knowlton et al., 2003; Steiner et al., 2002). It is believed to serve as a structural element rather than involved in residue specific contact with other proteins (Richardson and Richardson, 2005). The KOW motif, which was first discovered in the C-terminal domain of NusG (CTD) is predicted to interact with both RNA and proteins concomitantly since different areas of this domain are implicated for these interactions (Knowlton et al., 2003; Steiner et al., 2002). The flexible linker between these two domains may allow independent degrees of freedom for each of the N- and C-terminal domains which enable inter-domain cross-

talks in response to the interactions with external factors. The 27 residues long KOW motif of NusG shares homology with different ribosomal proteins RL24 (from bacteria and chloroplast), RL26/RL27 (from eukaryotes) and with eukaryotic proteins Spt5 and DSIF (Kyrpides et al., 1996; Steiner et al., 2002; Wada et al., 1998).

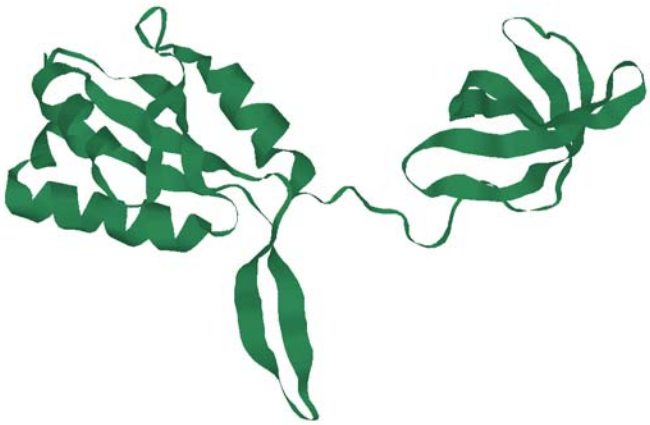

Figure 1.6: Homology model of *E. coli* NusG.

E. coli NusG consists of two largely independent N and C-terminal structural domains, NTD and CTD, respectively connected by a flexible linker.

NusG interacts directly with RNAP (Li et al., 1992) increases the rate of elongation by reducing the pausing and was found to be more effective in anti-pausing the EC at the class II pauses (Artsimovitch and Landick, 2000). Studies of the operon specific transcription factor RfaH, whose NTD is a close paralog of NusG, suggest strongly that NusG binds the same coiled-coil structure of the RNAP β' subunit as does σ^{70} region 2 (Belogurov et al., 2007; Sevostyanova et al., 2008). The likely interaction of NusG with RNAP near the active center helps the RNAP to hold the 3'-end of the nascent RNA at weak RNA:DNA hybrid sequences and thereby preventing the backtracking of EC at the class II pause sites. *In vitro* analysis of *E. coli* RNAP TL mutants suggests that NusG modifies RNAP the same way as does the TL G1136S mutation (which accelerates elongation), by stabilizing the EC in the posttranslocated (active) state. This "fast" mutant loses its responsiveness to NusG during elongation or translocation, suggesting that NusG is unable to promote TL/BH oscillation in this mutant enzyme (Bar-Nahum et al., 2005). The antitermination factor RfaH also accelerates elongation and stabilizes the posttranslocated state of the EC (Svetlov et al., 2007) and the eukaryotic homolog of NusG, DSIF, increase the rate of

RNAP II elongation (Wada et al., 1998). NTD of NusG alone is sufficient to suppress pausing and enhance transcript elongation *in vitro* suggesting that the NTD interacts with RNAP (Mooney et al., 2009b).

1.4.3.2 Transcript cleavage factors GreA and GreB

RNAP that has backtracked at pause sites can be rescued by internal hydrolysis of a 3' end segment of the transcript, which in turn provides a properly placed 3' primer end for resynthesis. In *E. coli*, transcription cleavage factors GreA and GreB induce cleavage of backtracked complexes *in vitro* (Borukhov et al., 1992; Borukhov et al., 1993). The gene encoding the GreA protein was first identified as a suppressor of a temperature-sensitive mutation in the largest subunit of *E. coli* RNAP (Sparkowski and Das, 1992). Disruption of either *greA* or *greB* has little phenotype in *E. coli*, but a double disruption renders the cells temperature sensitive (Orlova et al., 1995). A major function of cleavage factors *in vivo* may be error correction and proofreading of misincorporated nucleotides (Erie et al., 1993). Though GreA and GreB each with a molecular weight of about 19 kDa, have similar two-domain architectures (Koulich et al., 1997; Stebbins et al., 1995), they exhibit several differences (Figure 1.7). First, GreB binds to RNAP approximately 100-fold tighter than GreA (Koulich et al., 1997). Second, GreA-induced cleavage yields di- and trinucleotide products, whereas GreB stimulates the accumulation of excised products in a much wider size range (2–18 nucleotide long RNAs; (Borukhov et al., 1993; Kulish et al., 2000). Third, unlike GreA, which is only able to prevent arrest, GreB can also rescue the already arrested TECs (Borukhov et al., 1993). Gre-factor reaches into the secondary channel of the RNAP with its coiled-coil (CC) domain and donates the acidic side chains to the RNAP active site where, together with the RNAP catalytic residues, they coordinate the catalytic Mg^{2+} ions. The reaction yields a 3'-OH primer end in the active center and a 3'-terminal oligonucleotide that diffuses away through the secondary channel. Substitution of the two crucial acidic residues at the tip of the amino-terminal CC domain of the Gre factor resulted in a marked decrease in Gre-assisted cleavage (Laptenko et al., 2003; Opalka et al., 2003; Sosunova et al., 2003). The carboxy-terminal CC of the RNAP β'-subunit is the main binding site for Gre factors (Figure 1.7c) and substitutions of these residues and those in the GreB C-terminal domain hydrophobic cavity confer defects in

GreB activity and binding to RNAP (Vassylyeva et al., 2007). Gre proteins also promote the initial step of elongation by inhibiting abortive initiation, presumably by rescuing some state analogous to backtracked ECs and thereby stimulate promoter clearance (Feng et al., 1994; Hsu et al., 1995).

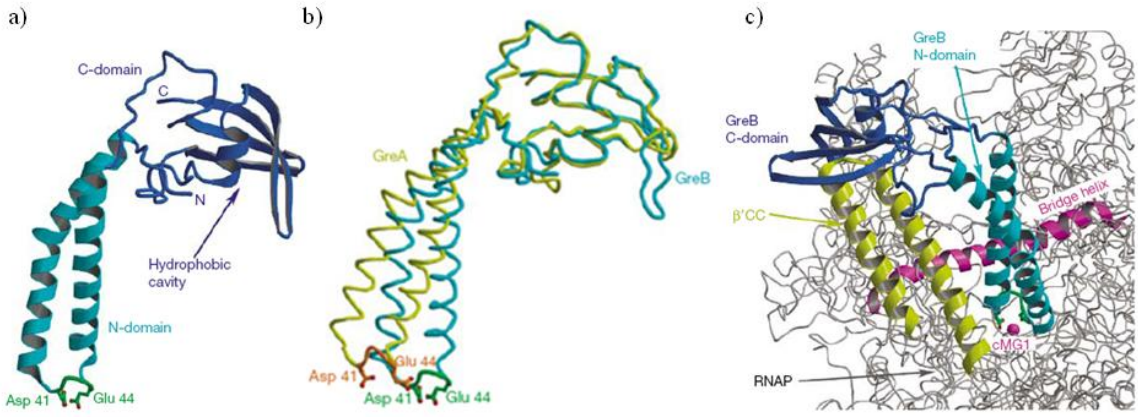

(Vassylyeva et al., 2007)

Figure 1.7

a) Structure of the GreB protein. The α-helical turn at the tip of the N-domain and the two principal acidic side chains are shown in green. b) Structures of GreB and GreA superimposed by the C-domains. c) Structural model of the RNAP–GreB complex. The structure of the *Thermus thermophilus* RNAP (Vassylyev et al, 2002), in which the β'CC tip residues were substituted for the *E. coli* counterparts, was used for the modelling. β'CC, β'-subunit coiled coil; cMG1, a high-affinity catalytic Mg^{2+} ion in the RNAP active site.

1.5 Transcription termination

Termination is defined as the (irreversible) dissociation of the protein and RNA components of the EC from the DNA of the genome. Several conformational changes that occur in the process of transcription termination include RNA–DNA hybrid unwinding, release of the nucleic-acid components of the EC by the RNAP, and, finally, transcription-bubble collapse as the DNA template and non-template strands re-anneal to form the stable dsDNA genome. Termination in *E. coli* proceeds by two distinct classes of mechanisms called intrinsic and factor dependent termination, respectively. Intrinsic terminators can stop transcription through the formation of an RNA stem-loop immediately upstream of a U-rich stretch in nascent RNA which disrupts the RNA-DNA base pairs within the transcription EC and destabilizes the complex (Gusarov and Nudler, 1999; Komissarova et

al., 2002; Yarnell and Roberts, 1999). In contrast, factor-dependent terminators recruit a termination factor to the nascent transcript for transcription termination. Rho is a homohexameric protein that binds to naked, non-translating RNA at a C-rich site called Rho utilization site (*rut* site). Once bound to RNA, it utilizes its own RNA-dependent ATPase activity and subsequently ATPase-dependent helicase activity to unwind RNA-DNA hybrids and release RNA from the transcribing EC (Richardson, 2002).

1.5.1 Factor independent (intrinsic) transcription termination

The intrinsic termination sites encoded in nucleic acid are so-called because they do not require the involvement of additional protein factors for their function. Intrinsic termination occurs at defined template sequences that code for a stable stem-loop (terminator) hairpin in the RNA, followed directly by a run of uridine residues. In general transcript release occurs after the termination hairpin has formed and 7–8 rU residues have been synthesized. Although the RNAP core can terminate at intrinsic termination sites, the reaction is stimulated by additional factors, e.g. NusA.

1.5.1.1 Terminator sequence

Intrinsic terminators include most defined termination sites in bacterial transcription units, although this may be in part because they are fairly well recognized by sequence analysis. These terminators are defined by a palindromic template sequence that codes for an RNA stem–loop (hairpin) structure immediately followed by an ~7-nucleotide sequence of ribo-uridine residues that forms a particularly weak RNA–DNA hybrid with the complementary deoxyribo-adenosine residues of the template DNA (Martin and Tinoco, 1980; Wilson and von Hippel, 1994). Intrinsic terminators might function by inducing the transcription complex to pause at this weak RNA–DNA hybrid position, with the EC being prevented from backsliding by interactions (with polymerase and RNA) that involve the terminator hairpin that forms within the nascent RNA. This pause increases the dwell time of the EC at the intrinsic termination positions, perhaps to allow time for the complete folding of the hairpin and/or to allow the occurrence of the conformational changes in the RNAP that might be required for this type of termination.

1.5.1.2 Mechanism of intrinsic transcription termination

Three different models have been proposed to describe the mechanism of transcription termination at intrinsic terminators. According to the "allosteric model" the hairpin might interact with either (or both) the flap and Zn^{2+} binding domains at the upstream end of RNAP to cause a conformational change that leads to hybrid melting, bubble collapse and complex dissociation, as deletion of each of these domains can reduce the termination efficiency (King et al., 2004; Toulokhonov et al., 2001; Toulokhonov and Landick, 2003) (Figure 1.8). The "hybrid-melting model" proposes that the termination hairpin destabilizes the EC by destabilizing the upstream end of the RNA–DNA hybrid, possibly by rearranging the domains of the RNA-binding region of the RNAP (the lid and rudder loops) and clashing with the TL. This may force the TL to move toward the active site and irreversibly trap the EC. The TL movement induces DNA-binding-clamp opening, triggering bubble collapse and the ultimate destabilization of the entire EC sufficiently to bring about transcript and RNAP release (Bar-Nahum et al., 2005; Epshtein et al., 2007; Gusarov and Nudler, 1999; Komissarova et al., 2002). In "forward translocation model", the transcription complex moves forwards, without RNA synthesis, along the DNA scaffold during hairpin formation (Figure 1.8).

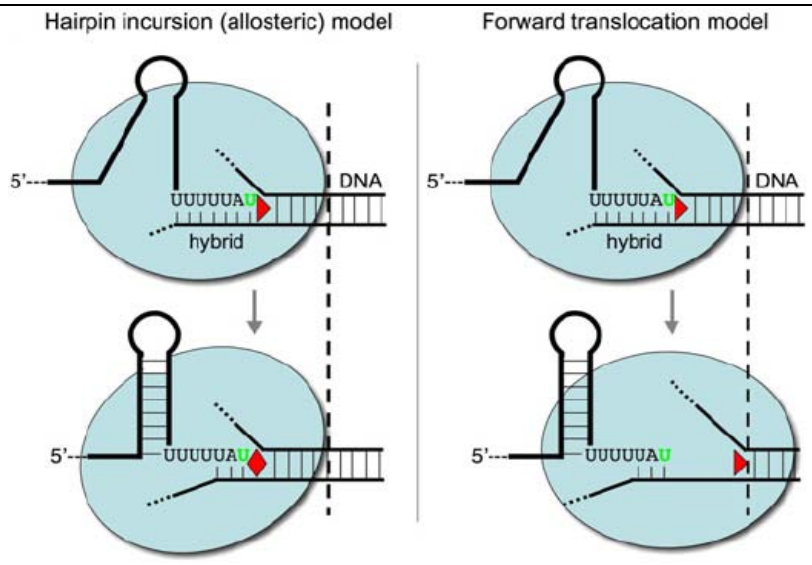

(Epshtein et al., 2007)

Figure 1.8: Alternative models of termination.

The forward translocation model (right) postulates that the hairpin forces the EC to move forward without RNA synthesis. Such movement should lead to downstream DNA duplex unwinding and RNA extraction (Santangelo and Roberts, 2004). The allosteric model (left) postulates that the hairpin does not induce forward translocation but instead enters the

RNA exit channel and main channel to melt the RNA:DNA hybrid and destabilize the EC (Gusarov and Nudler, 1999). Conformational change in the catalytic center (diamond) caused by the invading hairpin leads to irreversible EC inactivation.

The resulting decrease in the length of the RNA–DNA hybrid (at weak hybrid positions along the template) might then trigger dissociation of the transcription complex and release of the RNA transcript (Ryder and Roberts, 2003; Santangelo et al., 2003; Santangelo and Roberts, 2004; Yarnell and Roberts, 1999).

1.5.2 Factor dependent transcription termination

Factor-dependent termination is not very well defined by sequences at the site of termination, but reflects events that are not directly related to transcription, such as the release of ribosomes from nascent transcript or DNA damage. Two host termination factors have been identified, Rho, which acts at many sites on the bacterial chromosome (Roberts 1969; Richardson 1996), and MFD, which is responsible for releasing RNAP stalled at sites of UV induced DNA lesions (Selby & Sancar 1995a,b). Two non-host termination factors identified are Nun and Alc. Nun is a λ related bacteriophage HK022 encoded protein, which binds to *nut* site of transcribed RNA and causes transcription arrest by anchoring RNAP to DNA (Hung and Gottesman, 1995; Watnick and Gottesman, 1999). Alc encoded by bacteriophage T4 terminates transcription at multiple sites yet responds to specific DNA signals in the vicinity of each site (Drivdahl & Kutter 1990, Kashlev *et al*. 1993).

1.5.2.1 Rho dependent transcription termination

Rho is a hexameric RNA–DNA helicase of *E. coli* that binds to the nascent transcript at a 'loading site' called *rut* (Rho utilization site) that is rich in cytosine residues and also relatively unstructured (Brennan et al., 1987). *rut* is at least 40 nt long, whereas the minimal RNA segment required for termination is ≈ 80 nt (Hart and Roberts, 1994). There are few sequence similarities among *rut* sites from different genes. The sites where termination actually occurs are even less well defined, and can be distributed over a large region of DNA, up to 120 bp promoter distal to *rut*. Once loaded onto the transcript Rho translocates in a 5′→3′ direction along the nascent RNA by an ATP-driven process, moving towards the transcribing RNAP. Most Rho-dependent termination positions on the template are also pause sites allowing Rho to 'catch up' with the paused RNAP which

leads to termination. However, not all pause sites are termination points, and these include some of the strongest pause along a terminator (Dutta et al., 2008; Kassavetis and Chamberlin, 1981).

1.5.2.1.1 Physiology of Rho dependent termination

Rho is essential for viability of *E. coli* and many other species of bacteria (Richardson, 2002). Transcription termination of approximately half of the transcription units, or operons, in *E. coli* relies on Rho factor. Autogenous regulation of *rho* gene precisely regulates the level of expression of Rho protein and is constant (0.3% of total protein) over a wide range of growth rates in *E. coli* (Blumenthal et al., 1976). Partially defective *rho* mutants have markedly increased level of protein, while hyperactive mutants have lower than normal levels (Imai and Shigesada, 1978; Tsurushita et al., 1984). A recent study showed that, the reduced genome *E. coli* strain carrying deletion of horizontally acquired DNA, including cryptic prophages and transposons is less sensitive to the Rho inhibitor bicyclomycin, suggesting that high activity of Rho is required for cell survival. This is because bacteria uses Rho dependent termination to strongly represses transcription of the prophages and other horizontally acquired portions of the genome, some of which are detrimental to the host (Cardinale et al., 2008).

Premature arrest of translation and release of ribosomes from mRNA often cause inhibition of downstream transcription, a phenomenon known as polarity. Since transcription and translation are coupled in bacteria and the rates of both processes are similar, it is likely that ribosomes bound to mRNA block access of Rho to *rut* and/or to the TEC. Release of ribosomes at the nonsense mutation allows Rho to bind RNA and signals the elongating RNAP to terminate transcription (Adhya and Gottesman, 1978). This also explains why Rho-dependant termination normally occurs at the end of a gene, although potential *rut* sites are dispersed throughout the transcribed sequences. The transcript region, even from a WT gene, may fail to be translated in any of the following instances: (i) generation of a nonsense codon in the mRNA by transcriptional error (Bregeon et al., 2003; Bridges, 1999; Libby et al., 1989; Taddei et al., 1997), (ii) stochastic failure of ribosome binding to mRNA, (iii) ribosomal frameshifting on mRNA (Bregeon et al., 2001) leading to the premature termination of translation or (iv) endonucleolytic mRNA cleavage, resulting in

the absence of translation on the 3’ side of the cleavage site. Polarity can be suppressed by either a mutation in *rho* or by its inhibitor Psu protein from P4 bacteriophage (Das et al., 1976; Linderoth and Calendar, 1991).

Transcriptional polarity results in decreased expression not only of downstream genes in the same operon (intercistronic polarity) but also of the cistron in which termination occurs (intracistronic polarity) (de Smit et al., 2008; de Smit et al., 2009). Using chromatin immunoprecipitation and microarrays (ChIP-chip) ≈ 200 Rho-terminated loci were identified. Half of the Rho-dependent terminators were located at the 3’ ends of genes, including small RNAs (sRNAs) and transfer RNAs (tRNAs). The other half were found within the coding sequence of annotated genes (intragenic). For one set of intragenic terminators, the readthrough event was in the opposite direction of the gene, indicating antisense transcription (Peters et al., 2009). While the inability of Rho to terminate the transcription of tRNA and rRNA genes, which are not translated, is due, in part, to the extensive structure of these transcripts that prevents Rho loading. In addition a specific antitermination system modifies the TEC so that it is resistant to Rho, even in the presence of *rut* (Condon et al., 1995; Squires et al., 1993).

Uncoupling of translation with transcription leads to the accumulation of untranscribed naked RNAs. These untranslated RNAs may form duplex with single strand of DNA, displacing the other DNA strand as a loop. This condition, called ‘R’ loop formation, is unfavourable for the cell viability. Mutants deficient in either Rho or NusG had increased R-loops on the chromosome (Harinarayanan and Gowrishankar, 2003). Both R-loop formation and Rho mediated premature transcription termination are kinetic phenomena associated with the nascent untranslated and unstructured transcript as it emerges from the RNAP in the TEC, raising the possibility that the Rho-mediated termination has been selected in evolution to prevent the occurrence of the R-loop formation (Gowrishankar and Harinarayanan, 2004) (Figure 1.9).

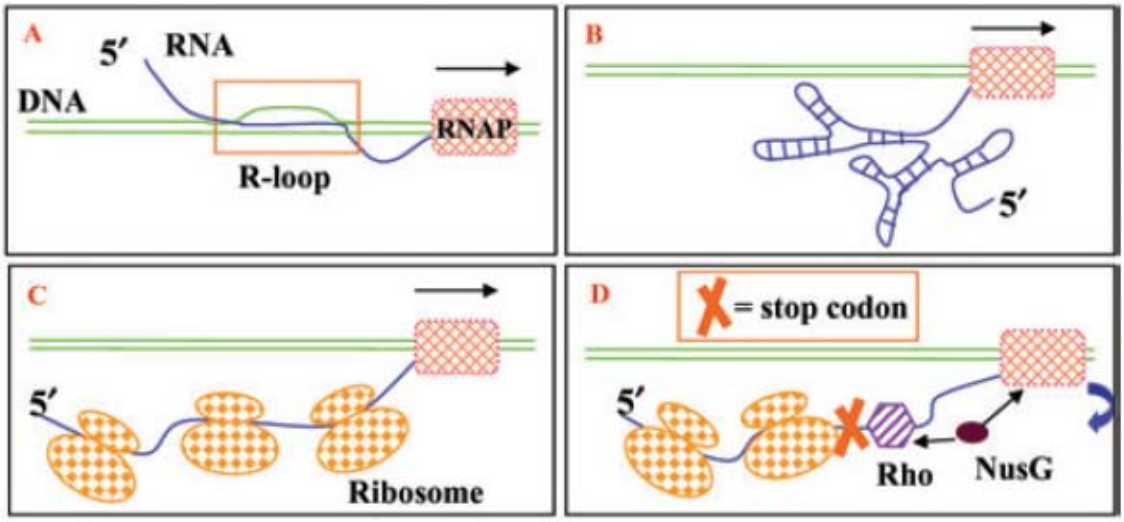

(Gowrishankar and Harinarayanan, 2004)

Figure 1.9: Schematic depiction of R-loop formation and its avoidance

A) R-loop formation by re-annealing of the nascent unstructured transcript to the template DNA strand upstream of the transcription elongation complex. B-D) Different ways of R-loop avoidance, B) RNA secondary structure formation C) coupling of translation with transcription D) Rho- and NusG-mediated termination of transcripts with premature stop codons.

Rho being a multifunctional protein with RNA binding, ATPase and helicase activities was speculated to have roles other than being a transcription terminator. In *Rhodobacter capsulatus* Rho was found as a major and firmly associated component of the RNA degradosome (Jager et al., 2001). Though Rho is essential in *E. coli*, some of the severe termination defective mutants of Rho, do not affect the overall growth of the cell. This raises the question whether the other role(s) of Rho is more important for viability and how important is rho-dependent transcription termination for *E. coli?*

1.5.2.1.2 Structure of Rho

Rho functions as a homohexamer of 47 kDa subunits each having 419 aa residues arranged in a closed ring structure (Skordalakes and Berger, 2006). Rho can self assemble in a solution with a variety of assembly states, the hexamer being the most predominant. Rho protomers assemble into dimeric or tetrameric forms under a high concentration of salt, low protein concentration and in the absence of cofactors. Almost a homogenous hexameric population of Rho can be obtained in a weak ionic environment of 50-100 mM

salt and a 2-10 μM of Rho, either in presence or absence of cofactors like RNA or ATP (Geiselmann et al., 1992). Rho can also exist as a lock washer variant in which the ring is separated at one monomer-monomer interface, allowing RNA to enter the cavity without a free end (Burgess and Richardson, 2001b; Skordalakes and Berger, 2003). The diameter of the Rho ring is 120 Å, with a large interior hole that varies in width from 20–35Å. The widest point of the hole is defined by the perimeter of the N-terminal domains, while the narrowest constriction is formed by the Q-loop signature sequence motifs.

Each subunit comprises an N-terminal RNA binding domain (residues 1-130) and a C-terminal domain (residues 131-419) with both RNA binding and ATPase activities (Bear et al., 1985; Dolan et al., 1990; Dombroski and Platt, 1988). Rho has two distinct nucleic acid binding sites. The primary RNA binding sites formed by the NTDs, which have ability to bind either ssDNA or RNA occupies the 5'-terminal segment of the RNA. The secondary RNA binding sites in the CTDs bind the 3' portion of the RNA and direct it through the cavity in the center of the hexamer (Figure 1.10). NTDs consist of three α-helices appended to five stranded β-barrel comprising the oligonucleotide or oligosaccharide-binding OB fold. The first nucleotide base packs into the hydrophobic pocket of Tyr80, Glu108 and Tyr110 enough to accommodate pyrimidines, while too small for larger molecules like purines (Skordalakes and Berger, 2003). This has been argued to be one of the reasons for the preference for 'pyrimidine'-rich sequence for Rho loading. No contacts are seen to the 2' hydroxyl of the bound nucleic acid, explaining why Rho is able to bind both ssDNA and ssRNA. The orientation of the N-terminal modulate primary RNA binding cleft face inwards, thus making mRNA to follow a somewhat zig-zag path that extends from the periphery to the center of each protomer for binding to the Rho molecule.

The CTD also carries three functionally important loops: a) phosphate-binding P-loop, associated with ATP binding and ATPase activity of Rho, spanning from 179-183 is highly conserved among RecA family of ATPase (Opperman and Richardson, 1994; Wei and Richardson, 2001a). b) Q-loop and c) R-loop comprises the secondary RNA binding site of Rho (Figure 1.10). Q-loop is formed by an 8-residue segment within 278-290 aa residues (Skordalakes and Berger, 2003; Wei and Richardson, 2001a; Wei and Richardson, 2001b; Xu et al., 2002) while R-loop span between 322-326 aa residues (Burgess and Richardson,

2001a; Miwa et al., 1995; Skordalakes and Berger, 2003). In the open-ring Rho structure, the Q-loops are only partly ordered in all six subunits (Skordalakes and Berger, 2003). In the closed ring structure each Q-loop forms a hairpin-like structure with a well-defined configuration. The principle translocation element of Rho, the Q-loop, adopts two markedly distinct configurations that alternate between adjacent protomers around the ring. RNA binds in a shallow channel formed by the interface of two adjacent ATPase domains, where it contacts Rho's second translocation element, the R-loop (Skordalakes and Berger, 2006).

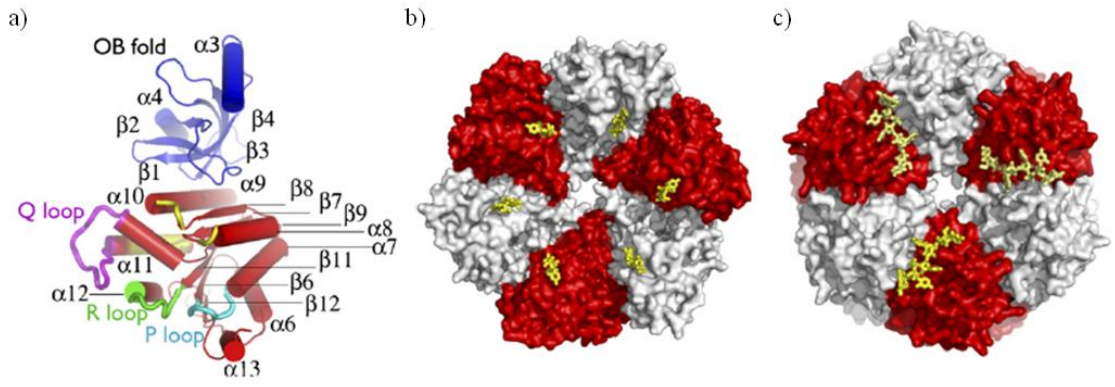

(Skordalakes and Berger, 2006)

Figure 1.10

a) Structure and topology of the closed-ring Rho protomer. The RecA domain is shown in red, and the OB fold is shown in blue. Translocation (Q and R) and catalytic (P) loops are highlighted in magenta, green, and cyan, respectively. Regions colored yellow indicate subunit-subunit contact points. Secondary structural elements are labeled. b) Surface representation of the closed-ring Rho hexamer (top-down view). RNA bound to primary RNA-binding sites is shown as yellow sticks. The Rho A and B subunits are alternately colored gray and red. c) Surface representation of the closed-ring Rho hexamer (bottom-up view) showing globally where RNA (yellow sticks) binds to the protein's RecA folds.

The active Rho assembly has six ATP binding pockets located at each of the interfaces between two adjacent CTDs and contains the Walker A and B signature sequence motifs common to all RecA-type ATPases. The side chains of two conserved aa, Met186 and Phe355, are responsible for sandwiching the adenine moiety of bound nucleotide. RNA interacts with a conserved lysine (Lys181) located within the Walker A motif, which lies just upstream of the catalytic lysine (Lys184) of the GKT triad in the P-loop motif of the

ATP binding pocket, thus linking the ATPase active site to the RNA substrate (Skordalakes and Berger, 2006).

According to the recent crystal structure of Rho, the hexamer appears to function as an asymmetric particle in which five subunits simultaneously contact nucleic acid, each in a unique manner. The structure also indicates that there is no handoff of the RNA from one subunit to the next; rather, a single subunit stays associated with one RNA nucleotide throughout the catalytic cycle and only engages every seventh (n+6) nucleotide in a chain (Thomsen and Berger, 2009). Six ATP molecules are hydrolyzed to move six nucleotides of RNA. Among hexameric helicases, RecA-family enzymes move 5'→3', while AAA+ proteins track 3'→5'. Comparison of Rho (Thomsen and Berger, 2009) and DNA bound structure of the AAA+ helicase E1 hexamers (Enemark and Joshua-Tor, 2006) reveals that the two motors bind nucleic acid substrates in a similar conformation and with the same relative polarity, but the two motors sequentially hydrolyze ATP in opposite directions. Both helicases contain an exchange/empty (E) ATP-binding site sequestered between a tightly bound ATP (T) state and a weakly bound product (D) state. However, the relative order of flanking active site states for Rho is flipped in comparison with E1. This configuration is responsible for biasing the direction of subunit movement; with the protomer linked to the T state effectively being locked down, and the subunit between the E and D states free to move upon ATP binding. This inverted orientation would lead to a counterclockwise shift of the ‘‘free’’ subunit upon binding ATP in Rho and a clockwise shift in E1. Thus, by reorienting a common motor domain within two different hexameric assemblies and by reversing the relative direction of movement between an ATP binding site and its adjoining arginine finger, nature has evolved two families of hexameric helicases with opposing translocation polarities (Thomsen and Berger, 2009).

1.5.2.1.3 Mechanism of Rho dependent termination

Rho-dependent termination has three basic steps, a) Rho loading b) Rho translocation and c) Rho unwinding of DNA-RNA duplex to release RNA (Figure 1.11). Rho binds to naked, non translating RNA at a C-rich site called Rho utilization site (*rut* site). The *rut* site binding of Rho is achieved by the N-terminal or primary binding domain. RNA binding to

the primary site triggers ring opening (Jeong et al., 2004; Skordalakes and Berger, 2003; Yu et al., 2000), which allows the RNA to enter the interior of the particle and associate with a secondary RNA-binding site that resides on C-terminal (Burgess and Richardson, 2001a; Miwa et al., 1995; Wei and Richardson, 2001a). RNA binding to the secondary site is thought to stimulate ring closure, an event that facilitates the formation of a catalytically competent ATPase and turns Rho into an active translocase (Gogol et al., 1991; Yu et al., 2000). Thus, there exists a time lag between the initial contact of Rho with RNA and the beginning of ATP hydrolysis and translocation (Kim and Patel, 2001).

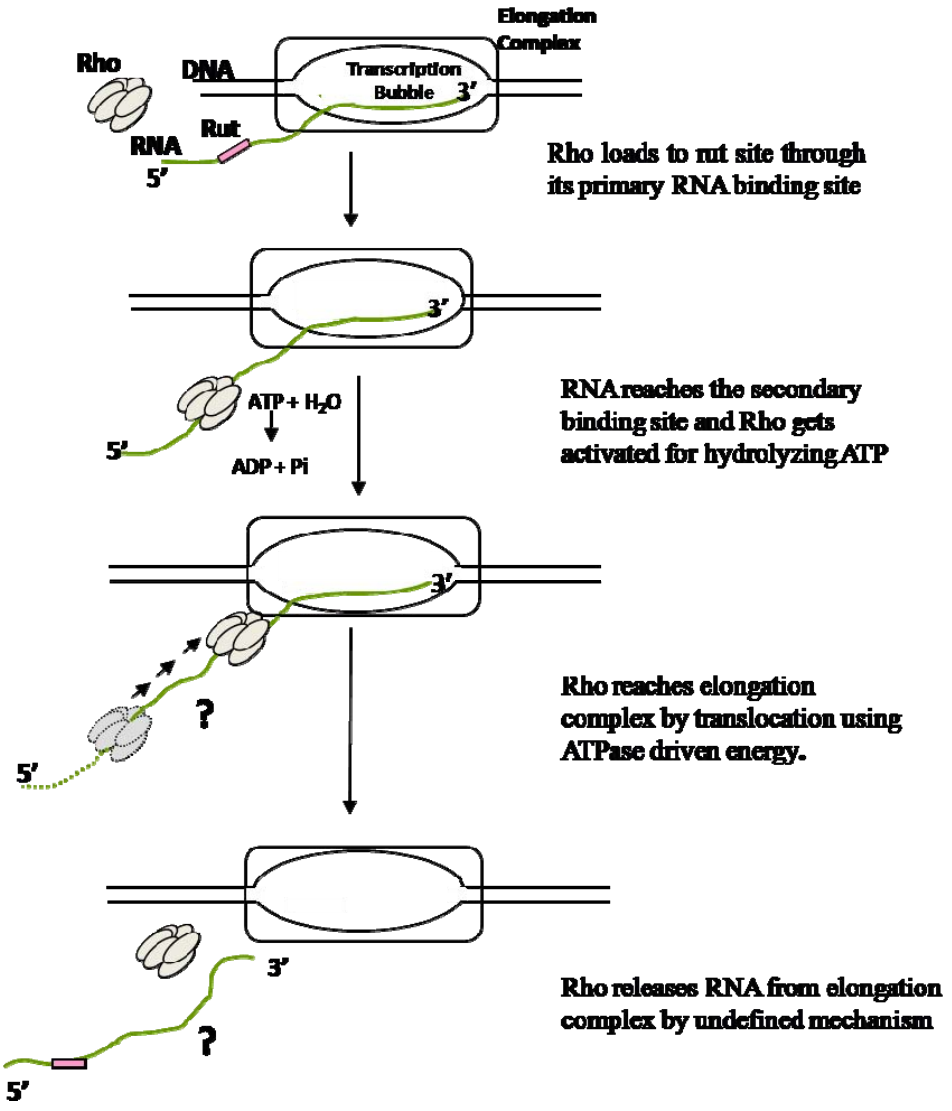

Figure 1.11: Steps leading to RNA release from an elongation complex at a Rho dependent terminator

During translocation, Rho is thought to successively fire its ATPase sites in a sequential manner as it moves along a nucleic-acid track (Kim and Patel, 1999; Stitt and Xu, 1998). The energy derived from ATP hydrolysis powers the translocase / helicase activity of Rho to unwind RNA/ DNA duplex (Banerjee et al., 2006). There have been following proposals explaining Rho movement: a) Tracking model: Rho leaves the *rut* site and translocates to reach EC. b) Looping model: Rho remains attached to the *rut* site and loops over to the EC at the site of termination, a proposal that has been overruled by the observation that a block of RNA-RNA could act as a conditional block to unwinding of a RNA-DNA duplex downstream to it (Steinmetz et al., 1990). c) Tethered tracking model: Rho remains attached to the *rut* site and moves along with the RNA in a zipper like manner (Steinmetz and Platt, 1994). Thus the widespread view was that Rho tracks along the RNA in a 5'-3' direction, presumably faster than RNAP emits RNA, and then effects termination when it catches up to RNAP. However recently increasing evidences shows that Rho molecule associates with RNAP throughout the transcription cycle and it does not require the nascent transcript for initial binding (Epshtein et al., 2010; Mooney et al., 2009a).

The force generated by ATP hydrolysis of Rho is the key factor in dislodging the EC through its molecular motor action, and the process is facilitated when the EC is in a catalytically competent state (Dutta et al., 2008). Different mechanisms are proposed for the release of RNA from EC by Rho: a) Spooling of RNA by Rho: Rho may act like a spool with the centre of axis passing through its hole to wind RNA from the binding pocket of RNAP. Compared to *E. coli* Rho, Rho analogue (Rv1297) from *Mycobacterium tuberculosis* with poor RNA-dependent ATP hydrolysis and inefficient DNA–RNA unwinding activities exhibited very robust and earlier transcription termination from the EC of *E. coli* RNAP. It has been proposed that spooling of large stretch of RNA by *M. tb* Rho brings it near the EC and is instrumental in pulling out RNA from the active center of the RNAP (Kalarickal et al., 2010). b) Forward translocation model for Rho function proposes that RNA release is facilitated by rewinding of DNA in the upstream transcription bubble region (Park and Roberts, 2006). c) Allosteric mechanism of termination: Recently it was shown that Rho dependent termination is a two-step process that involves rapid EC inactivation (trap) and a relatively slow dissociation. Inactivation is

the critical rate-limiting step that establishes the position of the termination site. The trap mechanism depends on the allosterically induced rearrangement of the RNAP catalytic centre by means of the evolutionarily conserved mobile trigger-loop domain, which is also required for EC dissociation (Epshtein et al., 2010).

1.5.2.1.4 Regulation of Rho dependent termination by NusA and NusG

Although NusA is essential in WT *E. coli*, in combination with other mutations or in a strain carrying deletion of horizontally acquired DNA *nusA* deletion can survive (Cardinale et al., 2008; Zheng and Friedman, 1994). Microarray expression analysis of the reduced genome cell reveals strikingly similar patterns of gene expression in three conditions: inhibition of Rho and deletion of either *nusA* or *nusG* (Cardinale et al., 2008). Because NusG stimulates Rho-dependent termination *in vitro* (Burns et al., 1999), the result is consistent with NusG acting as a cofactor of Rho *in vivo*. This result also clarifies the effect of NusA in Rho-dependent termination: Although NusA somewhat inhibits Rho function *in vitro*, this activity is probably irrelevant. Instead, NusA acts with Rho to stimulate termination *in vivo*, and an attractive model is that stimulation of pausing by NusA synchronizes Rho function with the emerging transcript by slowing RNAP and allowing Rho time to act.

The interactions between NusA and Rho have been studied in purified *in vitro* systems (Schmidt and Chamberlin, 1984). *In vitro* transcription assays in the presence of NusA revealed that NusA either inhibits or delays the Rho dependent termination process (Burns et al., 1998). While some experiments suggest that NusA stimulates Rho-dependent termination (Kainz and Gourse, 1998). It is possible that NusA-mediated sequence-specific modulation of the properties of the EC affects the Rho-dependent termination at different termination points.

The involvement of NusG in Rho-dependent termination was first identified genetically in the strains which either overexpress NusG or are depleted of NusG. Physiological levels of NusG are needed for Rho-dependent termination *in vivo.* In cells depleted of NusG, termination at most Rho-dependent terminators is greatly reduced (Sullivan and Gottesman, 1992; Sullivan et al., 1992). However, excess NusG can decrease Rho's

termination efficiency in WT cells (Burova and Gottesman, 1995). The overproduction of NusG suppresses termination defects of certain Rho mutants (Burns et al., 1999; Martinez et al., 1996). Rho-dependent termination *in vitro* is also enhanced by NusG (Burns and Richardson, 1995; Li et al., 1993; Nehrke and Platt, 1994; Nehrke et al., 1993). The retardation of Rho by a NusG column suggested physical contact between Rho and NusG (Li et al., 1993). NusG does not improve either the rate of unwinding of the RNA-DNA hybrid or ATP hydrolysis or the RNA binding properties of Rho (Nehrke et al., 1993). Kinetic studies revealed that NusG is required for Rho dependent termination when RNAP is elongating rapidly but not when elongation is slowed by low NTP concentrations (Burns et al., 1999), suggesting that NusG stimulates interaction of Rho with the EC. In fact, NusG enhances the rate of Rho-mediated RNA release from stalled ECs (Burns et al., 1998; Nehrke and Platt, 1994). NusG also causes a promoter-proximal shift in the end points of Rho-terminated RNA and allows Rho to use shorter segments of upstream RNA than NusG can use alone, both effects indicating that NusG enhances Rho interaction with RNA (Nehrke et al., 1993). Neither NTD nor CTD of NusG alone can enhance Rho-dependent termination indicating that interactions of both domains with ECs are required for this process (Mooney et al., 2009b). G146D and L158P mutations in CTD of NusG are defective for Rho-dependent termination indicating that most likely the CTD interacts with Rho (Harinarayanan and Gowrishankar, 2003; Mooney et al., 2009b). The ability of NusG to stimulate Rho activity but inhibit pausing appears paradoxical, because pausing is believed to be an essential prelude to Rho activity. Most likely, NusG stimulates Rho function in some way independent of its effect on pausing.

1.5.2.1.5 Inhibitors of Rho

As Rho is essential for the viability of many bacterial species, it is an attractive drug target for drug development. So far two Rho-specific protein inhibitors and two chemical inhibitors of transcription termination have been reported. The protein inhibitors of Rho include Psu of the satellite bacteriophage P4 and an *E. coli* protein YaeO. Chemical inhibitors that specifically target Rho are a naturally occurring antibiotic bicyclomycin and a chemical compound BI-K0058.

Psu, a unique 21 kDa protein encoded by *psu* (polarity suppression), a late gene of bacteriophage P4, is a non-essential capsid decoration protein (Dokland et al., 1993; Isaksen et al., 1992) that has been shown to suppress polarity in phage P2. The Psu protein inhibits Rho-dependent termination specifically and efficiently both *in vivo* (Linderoth and Calendar, 1991; Linderoth et al., 1997; Pani et al., 2006; Sauer et al., 1981; Sunshine and Six, 1976) and *in vitro* (Pani et al., 2006) and has no effect on intrinsic termination. Since Psu does not require any known antitermination sequence, the mode of action of Psu is different from the lambdoid phage-derived antiterminators (Linderoth and Calendar, 1991; Weisberg and Gottesman, 1999). C-terminal tail of this predominantly α-helical protein is involved in interaction with Rho (Pani et al., 2006; Pani et al., 2009). Psu affects the ATP binding and RNA-dependent ATPase activity of Rho, which in turn reduces the rate of RNA release from the EC (Pani et al., 2006).

YaeO a 9 kDa acidic protein from *E. coli* that binds tightly to Rho has been shown to reduce the Rho dependent termination (Pichoff et al., 1998). The solution structure revealed that YaeO is composed of an N-terminal helix and a seven-stranded beta sandwich. YaeO binds proximal to the primary nucleic acid binding site of Rho and acts as a competitive inhibitor of RNA binding (Gutierrez et al., 2007).

Bicyclomycin (BCM), a naturally occurring antibiotic, first isolated in 1972 from *Streptomyces sapporonensis* (Kamiya et al., 1972) and *S. aizumenses* (Miyamura et al., 1972; Miyamura et al., 1973), has been shown to specifically target Rho (Zwiefka et al., 1993). BCM is a heterocyclic compound that is biosynthetically derived from L-leucine and L-isoleucine (Iseki et al., 1980; Miyoshi et al., 1980) (Figure 1.12) and has antibacterial activity against gram-negative bacteria (Kamiya et al., 1972; Miyamura et al., 1972; Miyamura et al., 1973) and the gram-positive bacterium *Micrococcus luteus* (Nowatzke et al., 1997). BCM is a reversible, non-competitive inhibitor of Rho and prevents ATP turnover (Park et al., 1995). The antibiotic binds at a pocket located at the inter face between adjacent C-terminal domains that is formed in part by the P and R loops. Binding of BCM to Glu112 physically occlude the water molecule that attacks ATP (Skordalakes et al., 2005), thus hindering ATP hydrolysis. BCM also slows Rho's

movement along RNA and acts as a mixed-type inhibitor for RNA binding at the secondary site (Magyar et al., 1996).

BI-K0058 is a reversible, non-competitive inhibitor of Rho and is structurally unrelated to BCM (Figure 1.12). It inhibits the poly(C)-dependent ATPase activity of Rho as well as *in vitr*o transcription termination. BI-K0058 does not affect the ATP-binding activity of Rho, while it inhibits the formation of the ATP-independent high affinity Rho-RNA complex. Its antibiotic spectrum against Gram negative bacteria is limited to a smaller number of species than BCM. In addition, its antimicrobial activity against *Staphylococcus aureus*, a species in which Rho is not essential, implies that it is either the Rho–BI-K0058 complex that inhibits growth or that BI-K0058 acts on a different cellular target (Carrano et al., 2003).

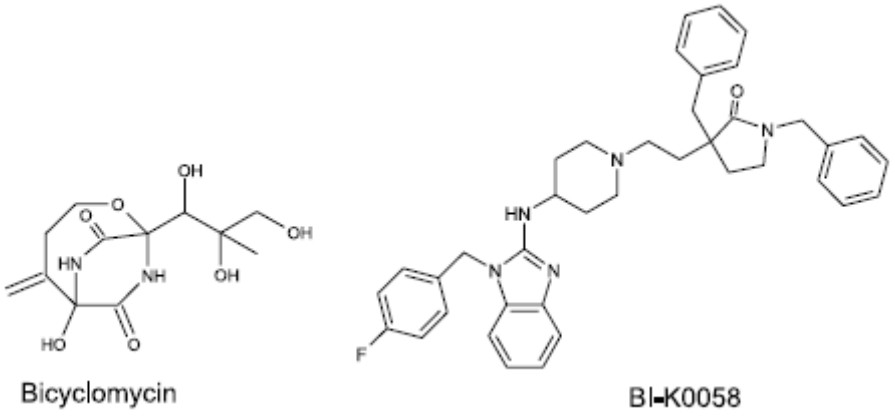

(Carrano et al., 2003)

Figure 1.12: Structures of bicyclomycin and BI-K0058.

1.5.2.2 Mfd dependent transcription termination

Mfd (*m*utation *f*requency *d*ecline–named for its activity to reduce mutagenesis through enhanced repair) is a 130-kDa monomeric protein that interacts with RNAP and the nucleotide excision repair (NER) component UvrA. Mfd consists of eight domains: a three-domain UvrB homology module, a single RNAP interaction domain (RID), a two-domain DNA-translocation module, a C-terminal regulatory domain, and a domain of unknown function (Deaconescu et al., 2006) (Figure 1.13). It has ATPase activity and binds DNA with little or no sequence specificity in an ATP-dependent manner. Mfd

simultaneously binds about 20 bp of DNA emerging upstream from the enzyme and a site on the β subunit of RNAP. When RNAP is stalled by DNA damage, Mfd is recruited which removes RNAP from the DNA so that it no longer acts as an obstacle to DNA repair (Selby and Sancar, 1993). Using the translocase activity and the energy of ATP, Mfd induces forward translocation of arrested back tracked ECs to force the enzyme downstream (Park et al., 2002). The interaction of Mfd with UvrA could enhance the rate of repair either by recruiting the repair proteins directly to the site of damage or by enhancing the rate of another step in the damage recognition and excision process.

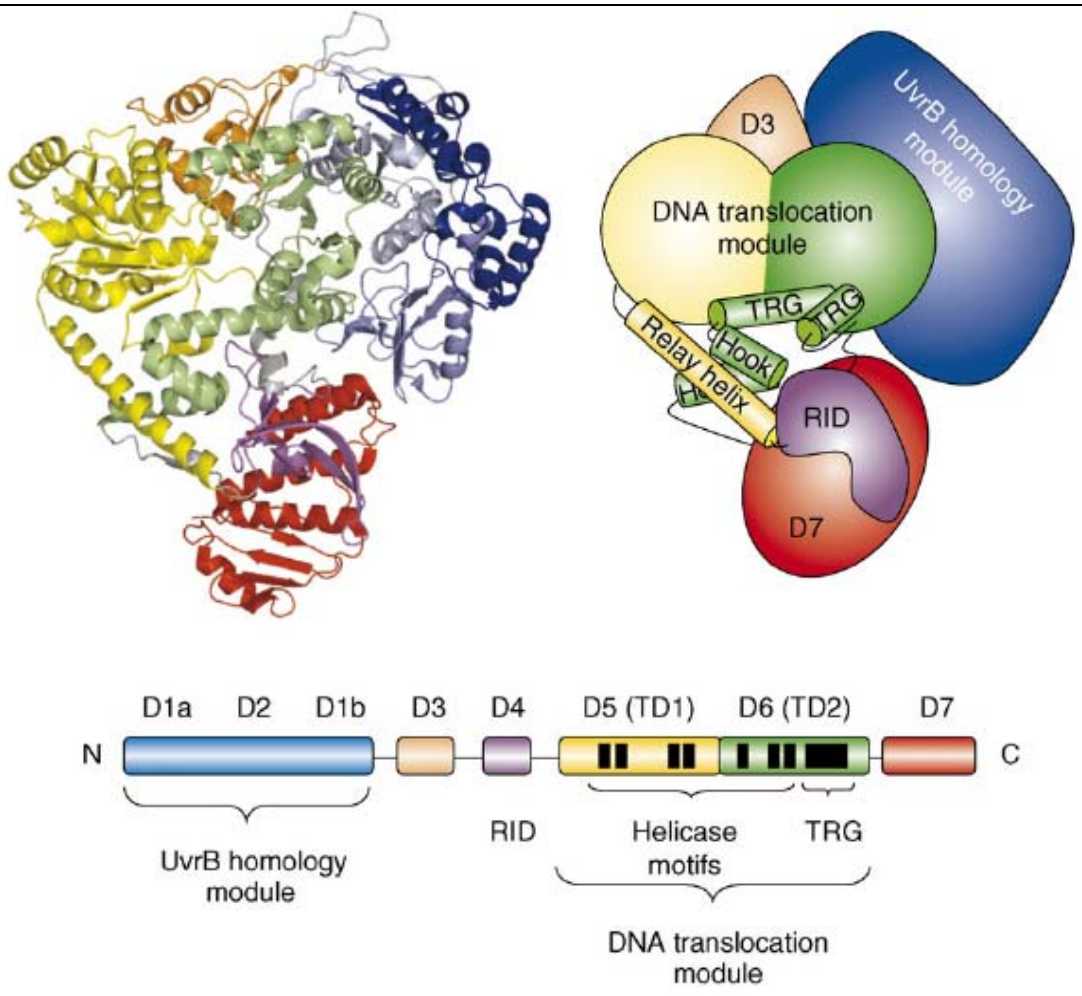

(Savery, 2007)

Figure 1.13: Structure and domain organization of *E. coli* Mfd.

The 3.2-A° crystal structure of Mfd reveals eight structural domains, denoted D1a, D2, D2b, D3, D4, D5, D6 and D7 (PDB no. 2EYQ (Deaconescu et al., 2006)).

1.5.2.3 Nun dependent transcription termination

Nun protein expressed by λ-related phage HK022 binds RNA as does λN, but has the opposite activity. Nun binding to Nut sites causes termination, not antitermination. Furthermore, Nun binding blocks translation of N protein mRNA (Kim et al., 2003). Constitutive expression of Nun by the HK022 lysogen arrests transcribing RNAP and destroys the transcription program of a sensitive phage (King et al., 2000; Robert et al., 1987), thereby preventing the superinfection by competing phages (Chattopadhyay et al., 1995; Oberto et al., 1993; Robert et al., 1987; Robledo et al., 1991). In a purified system with RNAP and λ DNA, Nun alone can cause transcription arrest (Hung and Gottesman, 1995), but NusA, NusB, NusE, and NusG enhance this arrest activity in vitro (Robledo et al., 1991). Several of the *nus* mutations that interfere with N-mediated antitermination also disrupt Nun function *in vivo*. NusA and NusG are not required for Nun-mediated arrest at *nutL* (Burova et al., 1999; Kim et al., 2006; Watnick and Gottesman, 1998). Despite this difference, the set of Nus factors required by N also is recruited by Nun to construct a particle around the *nut* site. The N-terminal segments (ARMs) of N and Nun are similar and contact *nut* identically (Chattopadhyay et al., 1995; Faber et al., 2001). The N-terminal portions of N and Nun can be interchanged without loss of function in either case, implying that the termination function of Nun resides in the C-terminus (Henthorn and Friedman, 1996). The C-terminus of Nun contains residues responsible for interaction with both RNAP and the DNA template, contacting RNAP in a Zn^{2+}-dependent manner through a cluster of histidine residues (Watnick and Gottesman, 1999; Watnick et al., 2000). The C-terminus of Nun also contains residues responsible for its interaction with the DNA template just downstream of the transcription bubble: A pair of charged residues (K106 and K107) binds the phosphate backbone of the DNA, and the penultimate residue (W108) is proposed to intercalate into the DNA strands (Kim and Gottesman, 2004; Watnick et al., 2000), causing the EC to arrest just downstream of the *nut* site (Watnick et al., 2000) (Figure 1.14). *In vivo*, arrested transcripts are terminated and released, whereas in a minimal in vitro system the transcripts remain associated with the EC (Hung and Gottesman, 1995; Robert et al., 1987; Sloan and Weisberg, 1993). Both *in vivo* and *in vitro*

the *E. coli* Mfd protein releases stalled transcription EC (Park et al., 2002; Selby and Sancar, 1993) and facilitates the release of Nun-arrested complexes (Washburn et al., 2003).

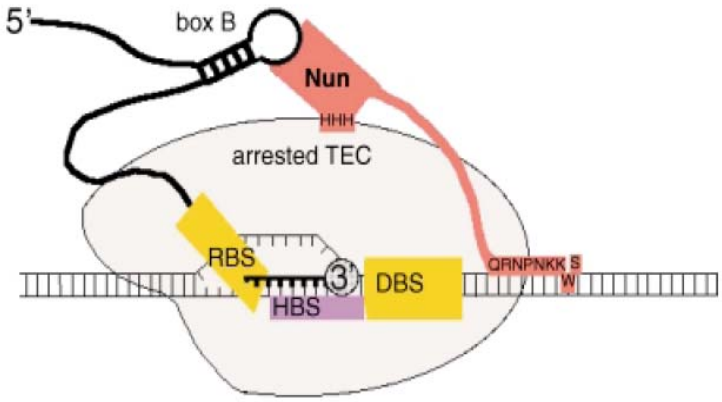

(Nudler and Gottesman, 2002)

Figure 1.14: Model for transcription arrest by Nun.

The N-terminal ARM motif of Nun interacts with BOXB, tethering Nun in proximity to the TEC. Histidine residues in the C-terminal region permit Nun to contact RNAP in a Zn^{2+}- dependent manner. The C-terminus contacts DNA, possibly by intercalation of the penultimate tryptophan residue into the DNA template. The arrested complex is released by MFD in the presence of ATP.

1.5.2.4 Alc dependent transcription termination

Alc, encoded by bacteriophage T4 terminates transcription at multiple sites (Drivdahl and Kutter, 1990) yet responds to specific DNA signals in the vicinity of each site (Kashlev et al., 1993). Soon after phage T4 infects *E. coli*, host transcription shuts down while the transcription of phage genes becomes highly active. This discrimination is due, at least in part, to the hydroxymethylated cytosines (hmCyt) in phage DNA. T4 mutants lacking hmCyt failed to express phage late genes and cannot propagate. Suppressor mutations, located at 134 kb of the phage genomic map, allow transcription of late phage genes on cytosine-containing DNA (*alc*) (Snyder et al., 1976). The 167 aa Alc protein is a site-specific termination factor that terminates transcription at multiple sites on non-modified DNA. hmCyt or mCyt within a few nucleotides of the termination site abolish Alc termination. The Alc protein has been shown to act only on fast moving RNAP, and the slowing of elongation due to low substrate concentration or mutation in the RNAP β subunit abolishes Alc dependent termination (Kashlev et al., 1993). Mutational analysis

shows that Alc interacts with the nonessential N-terminal domain of the RNAP β subunit (Severinov et al., 1994).

CHAPTER II

Objectives

2.1 Introduction

Transcription termination of approximately half of the transcription units, or operons, in *Escherichia coli* relies on Rho factor. Rho is a homo-hexameric RNA/DNA helicase or translocase capable of dissociating the elongating RNA polymerase from the template DNA by utilizing its RNA-dependent ATPase activity (Richardson, 2002; Richardson, 2003). It recognizes the Rho utilization (*rut*) site on the exiting mRNA through its N-terminal primary RNA binding domain (Modrak and Richardson, 1994). Binding of RNA to the primary binding site of Rho guides the 3'- end of the RNA into the central hole of the hexamer, which constitutes the secondary RNA binding domain. Interaction of the RNA with these two sites activates the ATP hydrolysis. By virtue of all these functions, Rho releases the nascent transcript and disengages the transcribing RNA polymerase.

In vivo, interaction of the transcription terminator Rho with the transcription elongation factor NusG is essential for efficient transcription termination. However, *in vitro*, Rho can induce RNA release in the absence of NusG, but the presence of the latter increases the efficiency and the speed of the process (Burns et al., 1999; Burova et al., 1995). NusG which increases the speed of transcription elongation at specific pause sites is an essential component of the N-mediated antitermination machinery and also promotes read-through of terminators within ribosomal *rrn* operons (Sen et al., 2008). Direct interaction of NusG with Rho in the *in vitro* experiments has also been demonstrated (Li et al., 1993; Pasman and von Hippel, 2000). However, the binding surface involved in the Rho-NusG complex is not known.

2.2 Questions framed for the study

2.2.1 Which of the functions of Rho are important for transcription termination?

Studies over the past four decades since its discovery and purification by J.W. Roberts in 1969 (Roberts, 1969), have highlighted Rho as a molecule and have revealed the structure and the physiological functions. Despite all these efforts, many of the fundamental questions pertaining to mechanistic properties of Rho remain obscure. How the individual properties of Rho, such as, ATPase activity, RNA:DNA unwinding etc. are linked to the RNA release step of transcription termination is not yet clear. In this work, an attempt is

made to address this question. It is important to obtain different Rho mutants defective for termination in order to understand the mechanism of Rho mediated transcription termination. Earlier mutagenesis approaches were restricted to identify the different functional domains of Rho (Martinez et al., 1996; Miwa et al., 1995; Xu et al., 2002). The approach used in present study is to randomly mutagenize the *rho* gene, isolate the termination defective mutants, characterize each of them for their defects in other functions and establish a structure– function relationship of the effects of these mutations based on the structure of Rho. Understanding various biochemical properties of these mutants can be useful in exploring the mechanism of Rho action. It is also aimed to establish an *in vitro* experimental set-up to measure the Rho mediated RNA release from a stalled EC, uncoupled from the transcription elongation process. This setup will enable us to understand the specific roles of ATP and NusG in the process of Rho-dependent termination.

2.2.2 Which is the binding site of NusG protein on the transcription termination factor Rho?

E. coli NusG has two distinct globular domains; the N-terminal domain, NusG-NTD and the C-terminal domain, NusG-CTD. These two domains are connected by a flexible linker (Knowlton et al., 2003; Steiner et al., 2002). A hydrophobic patch in the NusG-NTD has been implicated for the interaction of this domain with the transcription elongation complex (Mooney et al., 2009) and two point mutations, G146D and L158P, in the NusG-CTD have been shown to be defective for the Rho-dependent termination (Harinarayanan and Gowrishankar, 2003; Mooney et al., 2009). It is unknown how and where Rho contacts NusG and the mechanism of modulation of the Rho-dependent termination by NusG. We will be focusing on finding the binding surface of NusG on Rho, knowledge of which is essential for understanding the mechanism of the termination process. *In vitro* studies using individual domains of NusG can be done extensively to gain the knowledge of molecular basis of Rho-NusG interaction. Various deletion and point mutants will be generated in the domain involved in the interaction to further localize the binding region. These mutants will be an important tool in identifying the areas on the solvent-accessible surface of NusG that interact with Rho protein and this will in turn help us to understand the role of NusG in Rho-dependent termination.

CHAPTER III

Transcription termination defective mutants of Rho: Role of different functions of Rho in releasing RNA from the elongation complex

3.1 Introduction

Rho is a homo-hexameric RNA/DNA helicase or translocase that dissociates RNA polymerase from DNA template and releases RNA. RNA-dependent ATPase activity of Rho provides free energy for these activities (Banerjee et al., 2006; Richardson, 2002; Richardson, 2003). The primary RNA binding site (residues 22–116) can bind to a single-stranded DNA molecule as well as a single-stranded RNA molecule and is responsible for recognizing the Rho utilization (*rut*) site (Modrak and Richardson, 1994). Amino acid residues 179–183 form the P-loop, a highly conserved region among the RecA family of ATPases and is involved in ATP binding and ATPase activity (Wei and Richardson, 2001a). The Q-loop and R-loop have been defined as the secondary RNA binding sites. The Q-loop is formed by an eight residue segment within 278–290 amino acid residues (Burgess and Richardson, 2001; Wei and Richardson, 2001a; Wei and Richardson, 2001b; Xu et al., 2002), while the R-loop spans between 322–326 amino acid residues (Burgess and Richardson, 2001; Miwa et al., 1995; Skordalakes and Berger, 2003).

Rho-dependent termination involves a series of sequential events. At first Rho binds to the C-rich regions of the nascent RNA, called the *rut* site (Alifano et al., 1991; Bear et al., 1988; Morgan et al., 1985) through its primary RNA binding domain. This binding leads to the positioning of the RNA into the secondary RNA binding domain, which in turn activates the ATPase activity. It utilizes the free energy derived from the ATP hydrolysis for its translocase/ RNA–DNA helicase functions (Richardson, 2002; Richardson, 2003), which eventually leads to the release of the RNA from the elongation complex. It is commonly believed that the translocase / helicase activity of Rho is instrumental in pulling out RNA from the elongating RNA polymerase (Richardson, 2002). However, it is not well understood how each of these events is related to the RNA release process.

To investigate the involvement of different functions of Rho in releasing the RNA from the elongation complex the *rho* gene was randomly mutagenized and isolated the termination

defective mutants. Each of the mutants were characterized for their defects in other functions and established a structure–function relationship of the effects of these mutations based on the closed ring structure of Rho (Skordalakes and Berger, 2006). An *in vitro* experimental set-up was established to measure the Rho mediated RNA release from a stalled EC, uncoupled from the transcription elongation process. This setup enabled us to find the conditions under which some of these mutants regained the efficiency of RNA release and to understand the specific roles of ATP and NusG in the process of Rho-dependent termination.

3.2 Materials and Methods

3.2.1 Construction of the background strain for Rho mutant screening

For isolation of termination defective mutations in Rho the background strain should carry chromosomal deletion in the *rho* gene. Since *rho* is an essential gene, in this strain, Rho should be supplied from a shelter plasmid. The *E. coli* strain GJ3192 (MC4100 galEp3 Δrho::Kan^R with pHYD1201, Amp^R) was selected for strain constuction. pHYD1201 plasmid present in this strain carries WT *rho* gene and an IPTG dependent conditional replicon. This strain also bears a *galEp3* reporter system. The *galEp3* mutation is an IS2 (contains several Rho-dependent terminators) insertion situated between the promoter and structural genes of the gal operon, which confers a Gal^- phenotype because of Rho-dependent transcriptional polarity exerted by IS2 on the structural genes (Das et al., 1978). Rho mutants can release polarity in such a strain and can render the *galEp3* strain Gal^+, as determined by red color on D-galactose (Gal)-supplemented MacConkey medium.

Another reporter *trpE9851*(Oc) was moved by P1 transduction from GJ3183 into GJ3192 and designated as RS336. The *trpE9851*(Oc) mutation confers Rho-dependent transcriptional polarity on the downstream *trpCDBA* genes (Morse and Guertin, 1972), so that the strain is unable to utilize anthranilate to satisfy its Tryptophan auxotrophy in the

presence of functional Rho. The strain with WT Rho is incapable of growing on a minimal anthranilate plate while Rho mutant strains can overcome the polarity of the trpE9851(Oc) mutation.

Bacterial strains, phages, and plasmids used in this study are listed in Appendix I.

3.2.2 Random mutagenesis of Rho by mutator strain

The Rho cloned in a low copy number plasmid PCL1920 (pHYD567) was transformed in to competent cells of XL1-Red mutator strain (from Stratagene). This strain deficient in three of the primary DNA repair pathways: the *mutS* (error-prone mismatch repair), *mutD* (deficient in 3´- to 5´-exonuclease of DNA polymerase III) and *mutT* (unable to hydrolyze 8-oxodGTP) has random mutation rate ~5000-fold higher than that of WT strain. The transformants that appeared after 24 hr were inoculated in 100 ml of LB supplemented with spectinomycin and were grown overnight at 37 ºC. Plasmid was isolated using midiprep kits from Qiagen.

3.2.3 Genetic screen for isolation of termination defective mutations in Rho

The mutagenized *rho* plasmid library was transformed into the background strain RS336. The transformants were plated on MacConkey agar plates supplemented with Spectinomycin, Tetracycline, Kanamycin and 1% (w/v) galactose and grown at 37 °C. The strain was propagated in the absence of IPTG to remove the shelter plasmid so that the sole supply of Rho will be from the mutagenized plasmid library. gal^+ transformants were picked, purified three times by streaking in the same medium. Mutant strains were then streaked on a minimal anthranilate plate to confirm the mutations. Approximately 100,000 colonies were screened. The putative Rho mutant plasmids were isolated and re-transformed into the background strain for ensuring the mutant phenotypes. The full-length *rho* gene was sequenced from each of these plasmids to identify the mutation and to ensure that no other mutations were present in the gene (Figure 3.1).

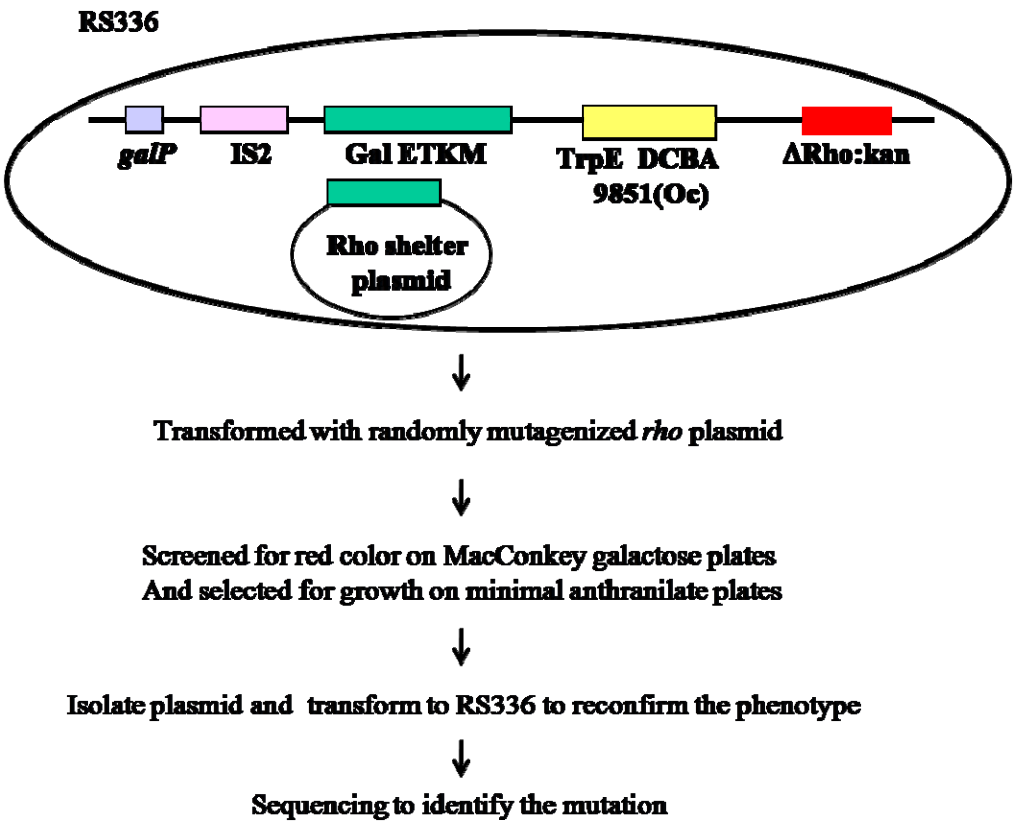

Figure 3.1: Schematic representation of genetic screen for isolation of termination defective mutations in Rho

3.2.4 Cloning of P_{lac}-*ΔnutR – lacZ* construct

Plasmid pK8628 (Neely and Friedman, 1998) carrying the P_{lac}-H-19B-*nutR*(T_{R1})-*lacZ* construct was used to make lambda monolysogens for estimating the *in vivo* termination efficiency at the H-19B T_{R1} rho-dependent terminator. The Rho dependent terminator T_{R1} present within the *nutR* region of this plasmid has to be removed to make the control plasmid carrying P_{lac}-*lacZ* construct. H-19B *nutR* sequence between BamHI and HindIII sites of plasmid pK8628 was deleted by restriction digestion. A 22-nucleotide adapter made by annealing two complementary oligos RS205 and RS206 was inserted between the BamHI and HindIII sites by ligation. Ligation mix was transformed into ultracompetant *E. coli* DH5α cells. The recombinants were screened using colony PCR with RS58/RK1 primers specific for the upstream and downstream regions of the sequence to be inserted. The clones were confirmed by sequencing and the plasmid was named as pRS431 (Figure 3.2).

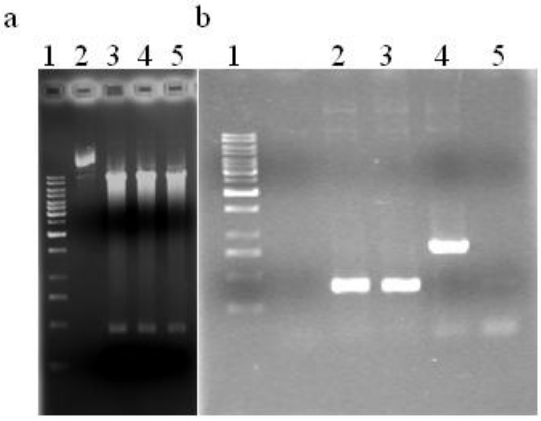

Figure 3.2: Cloning of P_{lac}-*ΔnutR–lacZ* construct a) Double digested vector. Lanes: 1. 1 kb DNA marker; 2. pK8628 plasmid purified; 3-5. BamHI and HindIII digested pK8628 plasmid. b) PCR to confirm *nutR* deletion using RS58/RK-1 primers. Lanes: 1. 1 kb DNA marker; 2-3. positive clones amplified to the expected size of 330 bp; 4. Control plasmid pK8601 amplified to the expected size of 750bp; 5. Negative control

3.2.5 Strain constructions by lambda transduction for measurement of *in vivo* termination

λRS45 and λRS88 are *lac* based lambda phage vector used for transferring fusions to single copy by homologous recombination *in vivo.* The DNA that is integrated between the recombination region of *bla*'- *lacZ* of the phage vector gets transferred into the recipient cell's chromosome at the phage λ attachment site (Simons et al., 1987). Recombinant lambda phage carrying P_{lac}-H-19B- *nutR*(T_{R1})-*lacZYA* construct was made by propagating λRS45 in *E. coli* strain MC4100, harboring the pK8628 plasmid. The recombinant λRS45 vector, harboring the P_{lac}-*nutR*(T_{R1})-*lacZYA* cassette was screened by the logic that the cassette contains T_{R1} Rho dependent terminator before *lacZ* gene and hence the recombinant λRS45 harboring this cassette will appear pale blue compared to the white plaques of the parent vector, on a bacterial lawn of MC4100 in an LB soft agar plate supplemented with X-Gal IPTG. By lambda transduction using this recombinant λRS45, P_{lac}-H-19B *nutR*(T_{R1})-*lacZYA* cassette was inserted as single copy at the phage λ attachment site of strain RS336, resulting in strain RS364. Colony PCR of the lysogens were carried out using the RS58/RK1 primers to confirm the presence of the cassette in the chromosome of MC4100. *E. coli att*B and λ *att*P specific primers SBM15, 16 and 17 were used for PCR to confirm that they were single copy insertions at the λ phage insertion site in the bacterial chromosome (Powell et al., 1994) (Figure 3.3). Refer Appendix III for protocol on λ lysate preparation and λ transduction.

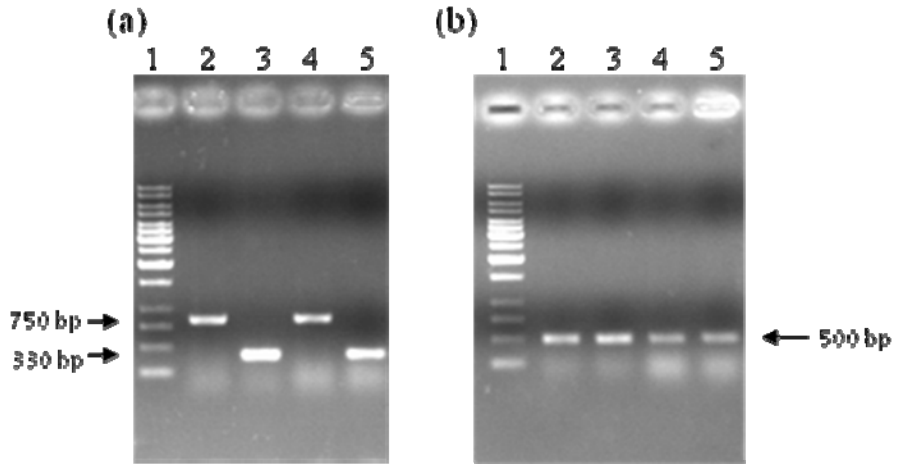

Figure 3.3: Colony PCR to confirm the T_{R1} and del T_{R1} lysogens

(a) T_{R1} and del T_{R1} lysogens PCR amplified with RS58/RK1 primers. Lanes: 1. 1 kb DNA ladder (MBI); 2. RS364 strain carrying P_{lac}-H-19B *nutR(T_{R1})-lacZYA* cassette amplified to the expected size of 750 bp; 3. RS391 strain carrying P_{lac}-*lacZYA* cassette amplified to the expected size of 330 bp; 4. RS449 strain carrying P_{lac}-H-19B *nutR(T_{R1})- lacZYA* cassette amplified to the expected size of 750 bp; 5. RS450 strain carrying P_{lac}-*lacZYA* cassette amplified to the expected size of 330 bp. (b) PCR to confirm monolysogens. Lane 1. 1 kb DNA ladder (MBI). Lanes 2-5. Monolysogen recombinants same as in panel 'a' amplified to the expected size of 500 bp using primers SBM 15, 16, and 17.

Similarly, recombinant λRS88 carrying P_{lac}-*lacZYA* construct was made by growing it on MG1655 transformed with pRS431. Multicopy plasmid pRS431 was incompatible with MC4100 (*lacI*^{q}) strain may be due to the full induction of the *lac* promoter leading to toxic effects of *lac* permease over-production. Recombinant phage which formed dark blue plaques on bacterial lawn of MC4100 in an LB soft agar plate supplemented with X-Gal IPTG was purified to homogeneity. Single copy fusion without H-19B T_{R1} *rho*-dependent terminator was constructed by lambda transduction using this recombinant λRS88 and designated as RS391. *rpoB8* and *rpoB2* genes (Jin and Gross, 1988) were moved into GJ3192 by P1 transduction and named as RS446 and RS451, respectively. P_{lac}-H-19B *nutR(T_{R1})- lacZYA* and P_{lac}-*lacZYA* were inserted into RS446 in single copy resulting in the strains RS449 and RS450, respectively. Strain RS445 was constructed by single copy insertion of P_{lac}-*lacZYA* in GJ3161.

3.2.6 *In vivo* characterization of Rho mutants

3.2.6.1 Measurement of *in vivo* termination defects of the Rho mutants through beta-Galactosidase assay

Beta-Galactosidase assay is commonly used to determine promoter strength, transcriptional activity, termination etc in a construct that have area of interest fused upstream to the Galactosidase gene. Beta-Galactosidase enzyme cleaves the lactose analog ONPG (O-Nitro phenyl-ß-D Galactosidase), a colorless compound into yellow colored ONP (O- Nitro phenol) and Galactose. The strains RS364 and RS391 were transformed with the mutants and WT Rho plasmids to estimate the *in vivo* termination efficiency at the H-19B T_{R1} rho-dependent terminator. Similarly RS449 and RS450 were transformed with the mutants and WT Rho plasmids to get the activities with B8 RNAP. The strains GJ3073 and RS445 were used to get the beta-Galactosidase activities in the presence of WT Rho. The measurements of beta-Galactosidase activities were done in a microtiter plate using a Spectramax plus plate reader following the procedure described in the Appendix III. Beta-Galactosidase values were average of five to six independent measurements. The ratio of beta–Galactosidase values in the presence and absence of T_{R1} terminator gives the efficiency of terminator read-through (%RT) (Figure 3.4).

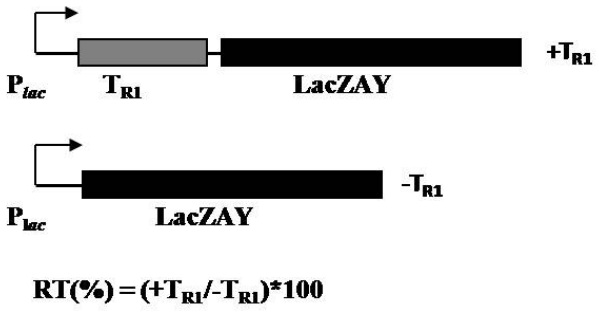

Figure 3.4: Cartoon representing the P_{lac}-H-19B- *nutR*(T_{R1})-*lacZYA* and P_{lac}-*lacZYA* cassettes used for measurement of *in vivo* termination are shown.

3.2.6.2 Temperature sensitivity of Rho mutant strains through culture spotting

RS336 strain transformed with Rho mutant plasmids were used to test the ability to Rho mutant strains to grow at high temperature. A single colony was picked and inoculated in 1 ml LB and incubated at 37 ˚C overnight in shaking waterbath. The culture density was then

normalized by measuring their OD at 600 nm. The normalized cultures were serially diluted and 5 µl were spotted on appropriate LB plates. The plates were incubated at 42 ºC over night and scanned next morning.

3.2.7 Cloning, expression and purification of proteins

3.2.7.1 Cloning and purification of Rho mutants

The WT and mutant *rho* genes were PCR amplified from pHYD567 and its derivatives using proof-reading DNA polymerase and primers RS84new and RS85a. The PCR product was double digested with NdeI and XhoI. They were cloned into the NdeI/XhoI site of pET21b to introduce a His-tag at the C-terminal end. The colony PCR positive transformants were confirmed by restriction digestion and sequencing (Figure 3.5).

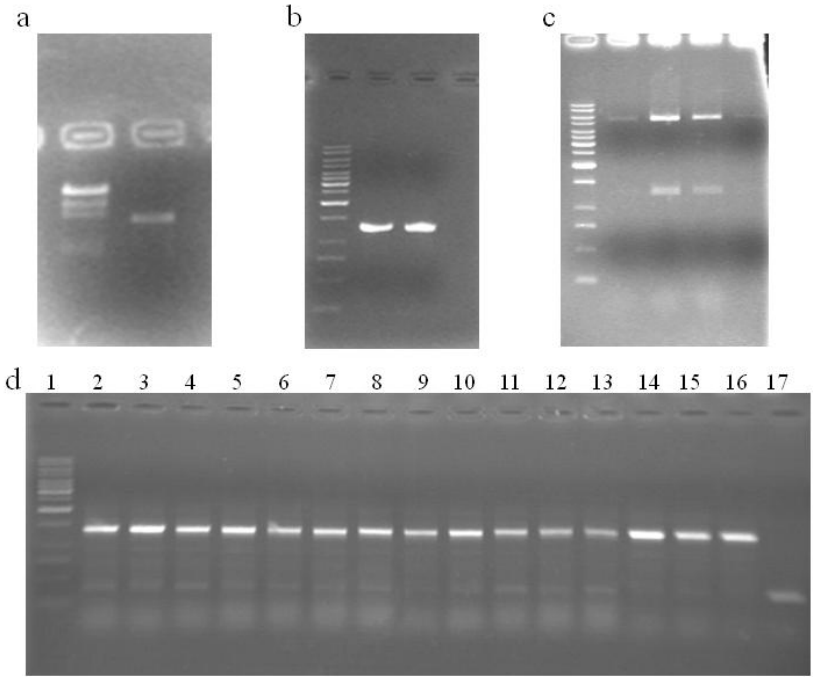

Figure 3.5: A representative figure showing cloning of Rho mutants into pET21b.

a) NdeI/XhoI double digested pET21b plasmid (vector) b) NdeI/XhoI double digested *rho* mutant genes (insert) used for cloning. c) NdeI/XhoI digestion of recombinant pET21b with *rho* cloned in. d) PCR screen to confirm *rho* gene. Lanes: 1. 1 kb DNA marker; 2-16 shows the His tagged *rho* gene amplified using RS78 and RS79 primers from the recombinant plasmids 17. Negative control

All the mutant (except Rho I382N) plasmids were then transformed into the BL21(DE3) over expressing strain. I382N was over expressed in salt-inducible strain BL21SI (Invitrogen). Protein expression in BL21(DE3) was done by inducing at OD_{600} of 0.5 with 1 mM IPTG for 3 hr at 32 °C. His tagged Rho was purified using Ni-NTA column. The cells were collected by centrifuging the cell culture at 10000 rpm for 5 min. The cells were then resuspended in lysis buffer (pH 8.0) containing 100 mM NaH_2PO_4, 10 mM Tris-HCl (pH 8.0), 300 mM NaCl, 10 mM imidazole, 1 mg/ml Lysozyme and 50 µg/ml PMSF. After resuspending the cells thoroughly, Lysozyme was added and incubated on ice with constant stirring for 30 min. The cells were sonicated till solution turns yellowish and complete lysis takes place. The cells were centrifuged after lysis at 4 °C, 12000 rpm for 30 min. Supernatant was transferred to prechilled fresh tube. The Ni-NTA beads were packed in column that works under gravity. And the columns were equilibrated with 5 bed volumes of lysis buffer. The supernatant was applied to the column (typically 5 ml bed volume). The unbound fraction was allowed to flow through. The fraction was collected for analysis. The column was washed with 10 bed volumes of wash buffer (pH 8.0) containing 100 mM NaH_2PO_4, 10 mM Tris-HCl (pH 8.0), 300 mM NaCl, 20 mM imidazole. The protein was eluted with 30 ml elution buffer composed of 100 mM NaH_2PO_4, 10 mM Tris-HCl (pH 8.0), 300 mM NaCl, 500 mM imidazole. Various fractions were then checked on 10% SDS-PAGE (Figure 3.6a). After dialyzing with TGED (10 mM Tris-HCl (pH 7.8), 0.1 mM EDTA, 0.1 mM DTT, 5% (v/v) glycerol) with 0.1 M NaCl the proteins were further loaded on heparin- sepharose column (Amersham) and the bound protein was eluted with increasing ionic strength (Figure 3.6b). Pure protein was dialysed for 10 hr against storage buffer (20 mM Tris-HCl (pH 7.9), 0.1 mM EDTA, 0.1 mM DTT, 100 mM KCl and 5% (v/v) glycerol) with three buffer changes and concentrated using Amicon YM100 (Millipore). Glycerol to the final concentration of 50% (v/v) was added to the concentrated pure protein and was aliquoted in to 100 µl fraction and stored at $^{-}$70 ºC (Figure 3.6).

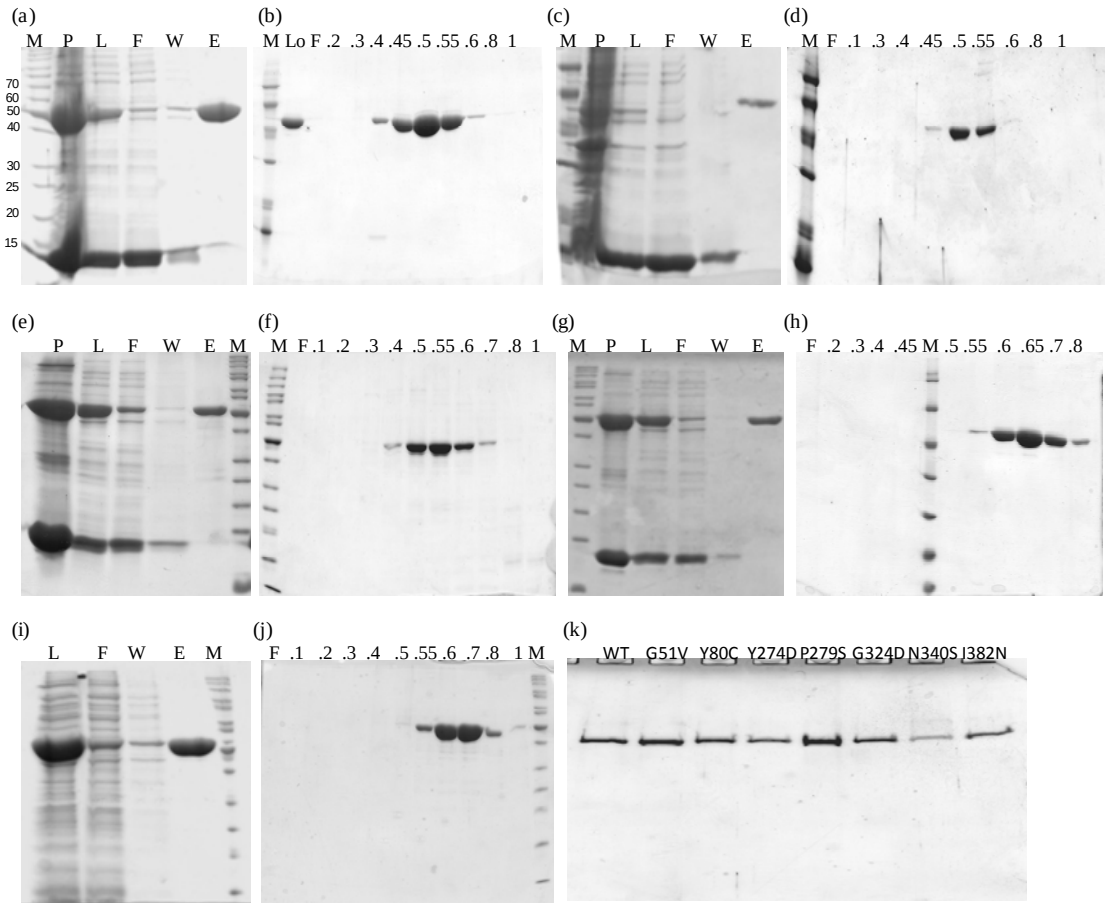

Figure 3.6: Purification of WT and Rho mutant proteins

(a) Purification of WT Rho through Ni-NTA column. (b) Purification of WT Rho through heparin column. The NaCl gradient (0.1 M to 1.0 M NaCl) batch elution fractions through the Heparin column are shown.(c) Purification of Rho Y80C through Ni-NTA column. (d) Purification of Rho Y80C through Heparin column by batch elution with NaCl gradient. (e) Purification of Rho G324D through Ni-NTA column. (f) Purification of Rho G324D through Heparin column by batch elution with NaCl gradient. (g) Purification of Rho N340S through Ni-NTA column. (h) Purification of Rho N340S through Heparin column by batch elution with NaCl gradient. (i) Purification of Rho I382N through Ni-NTA column. (j) Purification of Rho I382N through Heparin column by batch elution with NaCl gradient. (k) Purified WT and Rho mutant proteins. M, Marker; P, Pellet; L, Lysate; F, Flowthrough; W, Wash; E, Elute; Lo, Load.

The expression levels for all the mutants, except Y80C, were high and the majority of the proteins were present in the soluble fraction. As the expression level of Y80C was low, to avoid the contamination from the WT Rho expressed from chromosome, the purification was done in the presence of 1 M NaCl. For all the mutants the contamination from WT Rho protomers was also checked by passing the mutant Rho proteins through Ni-NTA columns in the presence of 1 M NaCl. Due to the dissociation of the subunits at high salt, non- His tagged WT protomers, if present, would be eluted in the wash-fractions only. The contamination from the WT protomer was estimated to be less than 5% for all the mutants.

3.2.7.2 Cloning and purification of HMK tagged WT Rho and Rho Y80C

An HMK (Heart Muscle Kinase) tag sequence cloned to the C terminus Rho can be radiolabelled and subsequently the labeled protein or the cleavage products from this protein can be visualized and analyzed in a phosphor imager screen, after electrophoresis. The labeling method utilizes the catalytic subunit of Protein Kinase A (PKA) to catalyze the transfer of the gamma phosphate of [γ-^{32}P] ATP to the Serine residue of the PKA recognition site (Arg Arg Ala **Ser** Val) present on fusion proteins.

WT Rho and Rho Y80C genes were PCR amplified using primers RS84new (upstream of *rho* gene with NdeI site) and RS153 (downstream of *rho* gene with HMK tag and XhoI site) and a proof reading DNA polymerase enzyme, Deepvent (NEB). The PCR product was double digested with NdeI/XhoI and was cloned into pET21b at its NdeI/XhoI site (Figure 3.7).

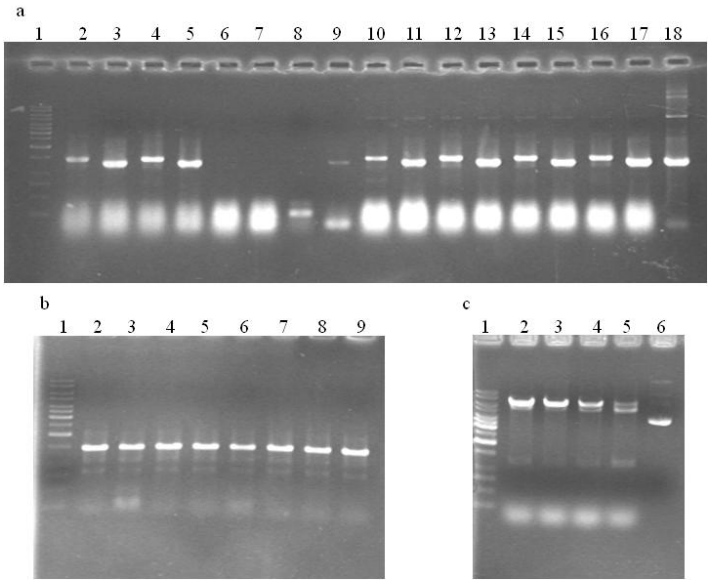

Figure 3.7: Cloning of HMK tagged WT Rho and Rho Y80C into pET21b.

a) PCR screen to confirm HMK tagged WT *rho* gene. Lanes: 1. 1 kb DNA marker (NEB); 2, 4, 10, 12, 14, 16 shows the HMK tagged WT *rho* gene amplified from the recombinant plasmids using vector specific primers RS78 and RS79; 3, 5, 11, 13, 15, 17 shows the HMK tagged WT *rho* gene amplified from the recombinant plasmids using gene specific primers RS84new and RS85a. b) PCR screen to confirm HMK tagged *rho* Y80C gene using RS78 and RS79 primers. Lanes: 1. 1 kb DNA marker; 2-9 shows *rho* gene amplified from the recombinant plasmids using vector specific primers RS78 and RS79. c) NdeI/XhoI digestion of recombinant pET21b with *rho* cloned in. Lanes: 1. 1 kb DNA marker; 2-5 are NdeI-XhoI double digested plasmids; 6. uncut plasmid DNA sample.

The plasmids were sequenced and was transformed into BL21(DE3). The resultant Rho proteins having both His and HMK-tags at the C terminal end was purified the same way as given above using Ni–NTA beads (Qiagen) and Heparin-agarose affinity column (Amersham) (Figure 3.8). The termination assays showed that these two tags did not interfere with the function of the WT Rho.

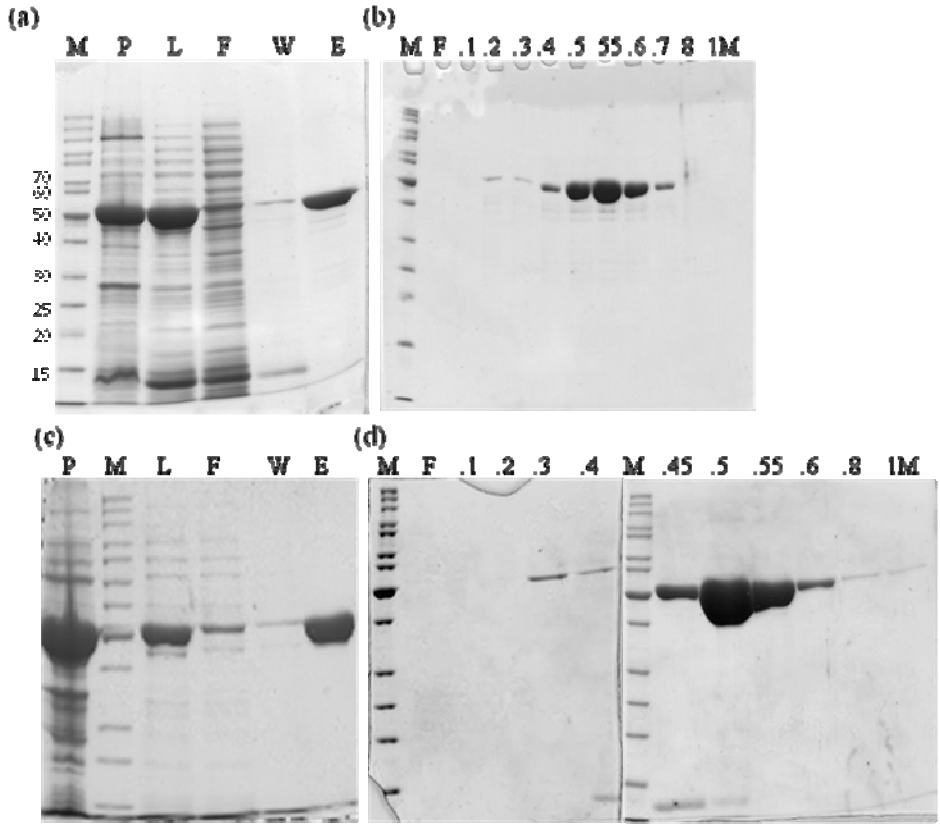

Figure 3.8: Purification of HMK tagged WT Rho and Rho Y80C:

(a) Purification of WT HMK Rho protein through Ni-NTA column: M, Marker; P, Pellet, L, Lysate; F, Flowthrough, W, Wash, E, Elute (b) Purification through Heparin column by batch elution with NaCl gradient. Rho eluted at 0.4 M- 0.7 M NaCl. (c) Purification of HMK Rho Y80C protein through Ni-NTA column: M, Marker; P, Pellet, L, Lysate; F, Flowthrough, W, Wash, E, Elute (d) Purification of HMK Rho Y80C through Heparin column by batch elution with NaCl gradient. Rho eluted at 0.45 M- 0.6 M NaCl.

3.2.7.3 Purification of mutant RNA polymerase

RNA polymerase mutant RpoB Q513P (B8) was purified from strain Rpob8, a MG1655 derivative. Strain was grown in 4 L of TB medium for 12 hr. The cells were harvested by centrifugation at 12000 rpm and the cell pellet was frozen. B8 RNAP was purified from 35 g of cells. To the pellet, 150 ml of buffer A (50 mM Tris-HCl (pH 8.0), 10 mM EDTA, 5%

(v/v) Glycerol, 1 mM DTT, 300 mM NaCl). It was mixed well by stirring, on ice. 0.5 mg/ml Lysozyme was added to this, and was mixed well by pipetting and by using a blender. This was then incubated on ice for 10 min. It was mixed well as above and incubated for 10 min, on ice. Sodium deoxycholate (4%) was added drop by drop with stirring, to a final concentration of 0.2% and was incubated at 4 °C in a cold room, with stirring. The cells were aliquoted to 25 ml each in fresh pre-cooled Falcon tubes and sonicated for 10 min for complete lysis.

The lysate was then centrifuged at 12000 rpm for 45 min at 4 °C. The supernatant was transferred to a clean beaker (pre-cleaned with chilled DEPC treated water) and 10% Polyethylamine (Polymin P, pH 7.9) was slowly added with constant stirring, to a final concentration of 0.8%. The stirring was continued for another 20 min (the solution turns turbid) at 4 °C. This was then centrifuged at 12000 rpm for 45 min at 4 °C. The pellet obtained was thoroughly resuspended in 100 ml TGED (10 mM Tris-HCl (pH 8.0), 0.5 mM EDTA, 5 % (v/v) Glycerol, 0.1 mM DTT) plus 0.5 M NaCl by mixing thoroughly in a blender in the cold room. The suspension is centrifuged at 12000 rpm for 15 min at 4 °C, the supernatant is stored for analysis, and the pellet is resuspended completely in TGED plus 0.5 M NaCl as before and the washing is repeated twice more. To elute RNAP from Polymin P, the pellet was resuspended in 100 ml of TGED plus 1 M NaCl. The mixture was centrifuged at 12000 rpm for 30 min at 4 °C. The clear supernatant was measured, transferred into a clean and pre-cooled glass beaker and finely ground Ammonium sulphate was added slowly to the supernatant with constant stirring, to an amount of 35 g to 100 ml solution. pH was adjusted to the range of 7-7.5 with 2 N NaOH. This was left with stirring for 30 min. The suspension was then centrifuged at 12000 rpm for 45 min at 4 °C. The pellet obtained was resuspended in TGED with 0.1 M NaCl (Figure 3.9a). The protein was then dialyzed against 1L of TGED plus 0.1 M NaCl, with two buffer changes O/N.

Next day, the protein was centrifuged at 12000 rpm for 15 min at 4 °C to remove any protein aggregates. The supernatant was loaded on to a Heparin column (Amersham), which was preequilibrated with TGED plus 0.1M NaCl. RNAP was eluted with a gradient of NaCl (0.2-1.0 M) in TGED buffer. The RNAP fraction elutes out in the range of 0.5-0.65 M NaCl. The fractions were checked for the presence of protein by running in an 8%

SDS-PAGE (Figure 3.9b). Those fractions were pooled and dialysed against 1L of TGED plus 0.1 M NaCl, with two buffer changes O/N.

The protein was passed through Mono-Q column (strong cation exchanger) using Biorad FPLC. Protein was eluted with a linear concentration gradient of NaCl in TGED buffer (Figure 3.9c). The purest fractions were pooled and were concentrated in a 100 KDa concentrator (Amicon) against 2x storage buffer (80 mM Tris-HCl; 0.4 M KCl; 2 mM EDTA, 2 mM DTT). Glycerol to the final concentration of 50% (v/v) was added to the concentrated pure protein, aliquoted into fresh sterile eppendorf tubes and stored in ⁻70 °C deep freezer.

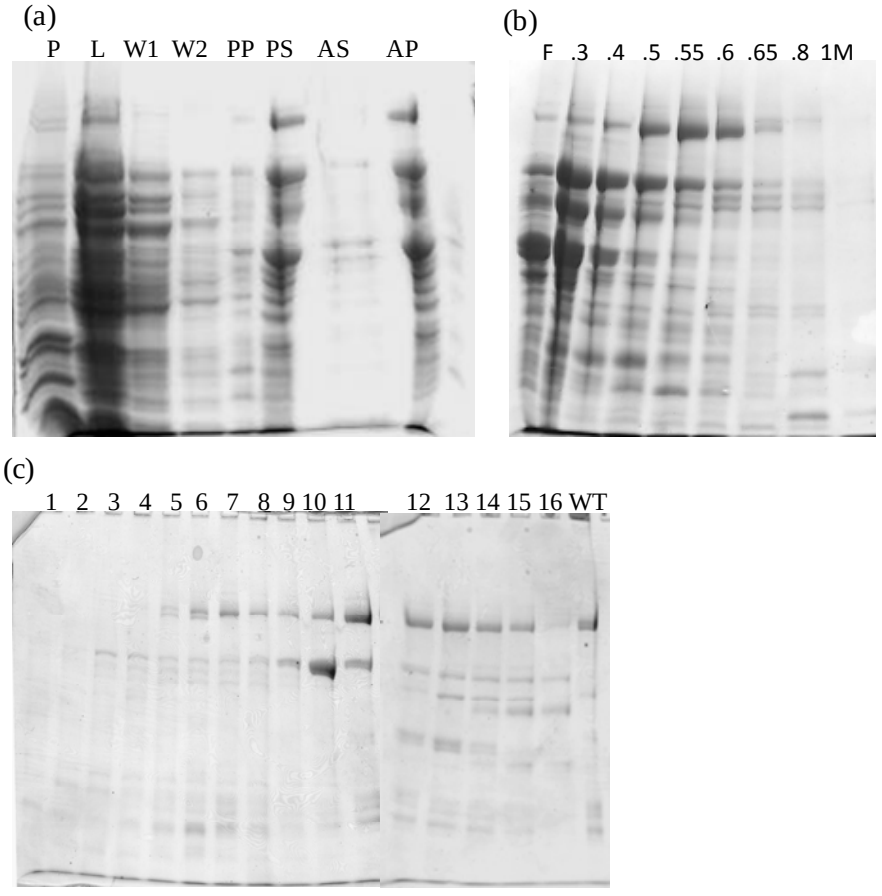

Figure 3.9: Purification of mutant RNA polymerase RpoB Q513P (B8):

a) P, Pellet; L, lysate; W1, first wash of Polymin P pellet; W2, second wash of Polymin P pellet; PP, Polymin P pellet; PS, Polymin P supernatant; AS, Ammonium sulphate supernatant, AP Ammonium sulphate pellet. b) Purification through Heparin column by batch elution with NaCl gradient. F, Flowthrough. RNAP eluted at 0.5 - 0.65 M NaCl. c) Purification through Mono Q column. 1-16 gradient elution fractions; WT, purified WT RNAP.

3.2.8. *In vitro* characterization of Rho mutants

3.2.8.1 Construction of templates for *in vitro* transcription

Plasmid pRS106 contain *trp t'* Rho dependent terminator following a strong T7A1 promoter. Linear DNA templates for *in vitro* transcription were made by PCR amplification using the plasmid pRS106. In order to immobilize the template on streptavidin- coated magnetic beads, a biotinylated upstream primer (RS83) was used. The lac-operator sequence was incorporated in a downstream primer (RS177) to make the templates with lac-operator at the downstream edge (Figure 3.10). RS140 was used as the reverse primer for making continuous transcription template without the lac operator sequence.

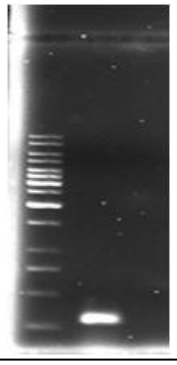

Figure 3.10: T7A1 *trp t'* template PCR amplified using RS83/ RS177 primers

3.2.8.2 Establishment of a functional Rho dependent transcription termination system

In vitro Rho-dependent termination reactions were performed in transcription buffer (T buffer: 25 mM Tris-HCl (pH 8.0), 5 mM $MgCl_2$, 50 mM KCl, 1 mM DTT and 0.1 mg/ml of BSA) at 37 °C. The template DNA was immobilized on the streptavidin-coated magnetic beads (Promega), wherever required, before starting the reaction. The reactions were initiated with 10 nM DNA, 40 nM WT RNA polymerase, 175 μM ApU, 5 μM each of GTP and ATP and 2.5 μM CTP to make a 23-mer elongation complex (EC23). [α-^{32}P]CTP (3000 Ci/mmol) was added to the reaction to label the EC23. The complex was chased with 20 μM NTPs in the presence of 10 μg/ml of rifampicin for 5 min at 37 °C. 50 nM WT Rho or Rho mutants and 200 nM NusG were added to the chase solution as indicated. The reaction was stopped by adding 20 μl of phenol after 5 min of incubation at 37 °C and the released RNA was phenol extracted. RNA was fractionated in a 10% sequencing gel. For the reactions with B8 RNAP, the enzyme concentration was 100 nM and the EC was chased with 100 μM NTPs.

3.2.8.3 CD spectroscopy

The Circular Dichorism (CD) spectroscopy was performed using JASCO 810 spectropolarimeter at 25 °C. Far-UV CD spectra were recorded in the 250 to 200 nm range, in a cuvette with 0.1 cm path length. The data pitch was set at 1 nm; bandwidth of 2 nm; response time of 2 s and scan speed of 100 nm/min was used for measurement. Each spectrum was an average of four accumulations. CD spectroscopy was carried out in the buffer containing 20 mM Tris-HCl (pH 8.0) and 100 mM NaCl. The estimation of secondary structure was done using the manufacturer's software for the instrument (Yang et al., 1986).

3.2.8.4 Gel retardation and filter retention assays

RNA binding to the primary RNA-binding site of the WT and mutant Rho proteins was measured by gel retardation and filter retention assays using an endlabeled 34-mer oligo(dC). 10 nM of labeled oligo was used for the binding assays in the transcription buffer (25 mM Tris-HCl (pH 8.0), 5 mM $MgCl_2$, 50 mM KCl, 1 mM DTT and 0.1 mg/ml of BSA) with the increasing concentrations of the WT or the mutant Rho (0.1 nM to 300 nM). The reactions were performed at 37 °C for 5 min before loading onto a 5% (w/v) native acrylamide gel. Fraction of bound species was quantified by Image Quant software of the phosphor-imager Typhoon 9200. Gel-shift assays with labeled rC_{10} were also done in the same way. The dissociation constant values were calculated by hyperbolic fitting of the binding isotherms. For the competition assays, 10 nM oligo$(dC)_{34}$ was allowed to bind to 50 nM of WT or mutant Rho proteins for 5 min at 37 °C followed by adding 10 nM (1:1), 50 nM (1:5) and 100 nM (1:10) of either cold oligo$(dC)_{34}$ or H-19B *cro* RNA and incubating the reaction for further 5 min at 37 °C. The amount of bound fraction that survived the competitor was estimated from the band intensities. For the filter retention assays, 10 nM of enlabelled oligo$(dC)_{34}$ was allowed to bind with the increasing concentrations of the WT or the mutant Rho (0.1 nM to 300 nM) at 37 °C for 5 min. 5 µl of this reaction mixtures were spotted onto a nitrocellulose membrane in duplicate and kept in a dot-blot apparatus (Bio-Rad). Each spot was washed with 500 µl of transcription buffer under vacuum. The fraction of bound oligo$(dC)_{34}$ was estimated from the ratio of the intensity of the washed (retained) and unwashed (total) spots using Image-Quant software.

3.2.8.5 ATPase assay

ATPase activity of the WT and mutant Rho proteins was measured from the release of inorganic phosphate (Pi) from ATP after separating on the polyethyleneimine TLC sheets (Macherey-Nagel) using 0.75 M KH_2PO_4 (pH 3.5) as the mobile phase. In all the ATPase assays the composition of the reaction mixtures was 25 mM Tris-HCl (pH 8.0), 50 mM KCl and 5 mM $MgCl_2$, 1 mM DTT and 0.1 mg/ml of BSA. The reactions were stopped with 1.5 M formic acid at the indicated time points. To determine the concentration of poly(C) required for half-maximal ATPase activity, 25 nM Rho was incubated with different concentrations of poly(C) at 37 °C. Reaction was initiated with 500 μM ATP together with [γ-^{32}P]ATP (6000 Ci/mmol) and was stopped after 15 min by formic acid. Release of Pi was analyzed by exposing the TLC sheets to a Phosphorimager screen for 5 min and subsequently by scanning using Typhoon 9200 (Amersham) and quantified by Image QuantTL software. The concentration of poly(C) corresponding to half-maximal ATPase activity was determined by fitting the plot of amount of Pi release against concentration of poly(C) to a sigmoidal curve. To determine the concentration of rC_{10} and rC_{25} corresponding to half-maximal ATPase activity, the titrations were done in the presence of 1 μM oligo$(dC)_{34}$. The concentration of ATP was 1 mM. Other conditions were similar to those described above.

To calculate the Km values of ATP for WT and Y80C mutant of Rho, in the same reaction mixture as described above, 5 nM of Rho was incubated with 10 μM of poly(C) at 30 °C for 10 min and ATP hydrolysis was initiated by the addition of different concentration of ATP (10 μM – 100 μM). Aliquots were removed and mixed with 1.5 M formic acid at various time points. The product formation was linear in the time range (up to 5 min) that we used for calculating the initial rate of reaction. The initial rates of the reaction were determined by plotting the amount of ATP hydrolyzed versus time using linear regression method. Then the Km values were determined from the double-reciprocal Lineweaver–Burk plots.

The rate of ATP hydrolysis in the presence of poly(C) was measured in the same reaction mixture as described above. The concentrations of Rho, ATP and poly(C) were 10 nM, 1 mM and 20 μM, respectively. Reactions were performed at 30 °C and aliquots were

removed at different time points (at 30 s intervals up to 5 min) and mixed with 1.5 M formic acid.

3.2.8.6 Photo-affinity labeling of ATP and rC_{10} to Rho

To determine the apparent dissociation constant ($K_{d,app}$) of ATP, UV cross-linking of labeled ATP was performed with 50 nM Rho and varying concentrations of [γ-^{32}P]ATP (30 Ci/mmol) in a 10 µl reaction mixture containing 25 mM Tris-HCl (pH 8.0), 50 mM KCl, 5 mM $MgCl_2$ and 1 mM DTT. The samples were irradiated for 5 min at room temperature in CL-1000 Ultraviolet cross-linker from UVP. This method of determining the apparent dissociation constant was used earlier. In a similar way the crosslinking of labeled rC_{10} to WT and Y80C mutant of Rho were performed. The samples were separated by SDS-PAGE, followed by scanning the gels in the phosphorimager Typhoon 9200 and quantified by Image-Quant software.

3.2.8.7 Fluorescence quenching and anisotropy measurements

All the fluorescence experiments were performed in the buffer containing 10 mM Tris-HCl (pH 7.0) and 100 mM KCl at 25 °C in a Perkin Elmer LS 55 Luminescence spectrometer. The scanning was done using FLWINLAB software. Changes in the tryptophan (W381) fluorescence at 350 nm of WT and Y80C Rho were monitored upon exciting at 295 nm. Fluorescence quenching was measured in the presence of different concentrations of a neutral quencher, acrylamide. Normalized emission was plotted against increasing concentrations of acrylamide and the quenching constant (K_{SV}) was obtained using Stern-Volmer equation: $(F_0/F)_{350}=1+ K_{SV}[Q]$, where, F_0 is the initial fluorescence intensity and Q is the concentration of acrylamide. TbGTP (3:1; 150 µM of terbium chloride and 50 µM of GTP) complex upon excitation at 295 nm gives rise to an emission signal characterized by two emission peaks at 488 nm and 545 nm. We measured the fluorescence anisotropies of this complex at 545 nm both in the absence and presence of either WT or Y80C Rho proteins. The anisotropy (r) of a fluorophore gives the measure of the rotational freedom of the species and reports the conformational flexibility of the surroundings (Kumar and Chatterji, 1990).

3.2.8.8 End-labeling of Rho

For the purpose of end-labeling the proteins, heart muscle protein kinase (HMK) tagged WT and Y80C Rho was used. HMK-tagged Rho proteins were radiolabeled with [γ-^{32}P]ATP (3000 Ci/mmol) using protein kinase A (Sigma). The labeling method utilizes the catalytic subunit of PKA to catalyze the transfer of the gamma phosphate of **γ-**^{32}P ATP to the serine residue of the PKA recognition site (Arg Arg Ala **Ser** Val) present on fusion proteins. The labeling reaction was done in buffer containing 20 mM Tris-HCl (pH 8.0), 150 mM NaCl, 10 mM $MgCl_2$ and 10 μM ATP. 30 μg of Rho were incubated with 60 units of the kinase for 2 hr at 21 °C.

3.2.8.9 Limited proteolysis of Rho by V8 protease

The conformational changes induced by the Y80C mutation were probed from the limited proteolysis pattern generated by V8 protease. 0.8 μM of labeled Rho were incubated with 0.05 μg of V8 protease in transcription buffer supplemented with 1 mM ATP for the indicated time at 37 °C. The reactions were stopped by adding 6X SDS-loading dye and were stored on ice. Samples were heated to 95 °C for 3 min, prior to loading onto a 12.5% SDS-PAGE. Gels were exposed overnight to a phosphorimager screen and were scanned using Phosphor-imager Typhoon 9200 and analyzed by Image-Quant software.

Molecular weight markers of end-labeled Rho were generated by cyanogen bromide (CNBr) and Sub-maxillary protease (Arg-C) mediated cleavages. Methionine-specific cleavage reactions using CNBr contained (pH adjusted to pH2 with 1 M HCl) 0.8 μM of labeled Rho, 1 M CNBr and 0.4% (w/v) SDS in a 10 μl reaction. Reaction mixtures for arginine specific cleavage contained 0.8 μM of labeled Rho, 2 μg of Sub-maxillary protease and 0.1% (w/v) SDS in a 10 μl reaction. Reactions were terminated after 10 min at 37 °C by addition of 6X SDS-loading dye followed by boiling.

3.2.8.10 RNA release from stalled elongation complex by WT and Rho mutants

trp t' template with the lac operator sequence at position 161 was used to study RNA release from stalled elongation complex (RB) by WT and Rho mutants. In order to make the stalled roadblocked complex on streptavidin beads, lac repressor was added before addition of the chasing solution. EC_{23} was made first and then was chased with 20 μM

NTPs and 10 μg/ml of rifampicin for 2 min to make the RB. This was followed by addition of 50 nM of either WT or mutant Rho proteins in the presence or absence of 200 nM NusG. The reaction was incubated at 37 °C for 5 min and the supernatant was separated from streptavidin beads on a magnetic stand to measure the released RNA from the EC. For the kinetics of RNA release from the RB, under different concentrations of ATP both in the presence or absence of NusG, RB was at first formed at position 161 of the *trp t'* template as described above, except that EC_{23} was chased with 50 μM NTPs. The RB was then washed extensively to remove the unincorporated NTPs and was re-suspended in T buffer supplemented with different concentrations of ATP. Following which 50 nM WT Rho or Rho mutants with or without 200 nM NusG were added to it. Half of the supernatant (S) was removed at various time points and added to the equal volume of RNA loading dye (Ambion). The rest of the reaction (half of the supernatant+pellet; P) was phenol extracted and mixed with the dye.

3.3 Results

3.3.1 Isolation of termination defective mutations in Rho

The whole *rho* gene was randomly mutagenized and screened for mutants defective for termination at two Rho-dependent terminators. After screening about 100,000 colonies, nine unique mutations in Rho which were severely defective for termination were isolated. These mutations are G51V, G53V, Y80C, Y274D, P279S, P279L, G324D, N340S and I382N. G51V and I382N mutations were independently isolated at least six times. Due to termination at the Rho-dependent terminators, WT Rho strain with *galEP3* reporter was unable to utilize galactose resulting in white coloured colonies on MacConkey galactose indicator plates. Red colonies formed due to the utilization of galactose by Rho mutant strains indicate the terminator read-through activity (Figure 3.11).

Strain with WT Rho carrying *trpE9851*(Oc) mutation was unable to grow on minimal anthranilate medium while Rho mutant strains were able to grow on minimal anthranilate medium. Utilization of anthranilate as indicated by growth on minimal plates is due to the release of Rho-dependent transcriptional polarity on the downstream genes at the *trp* locus (Figure 3.12). Termination defects exhibited by these mutations on three Rho-dependent terminators (defect for *nutR*/T_{R1} terminator is described below) suggest that the defect is not specific for a particular terminator.

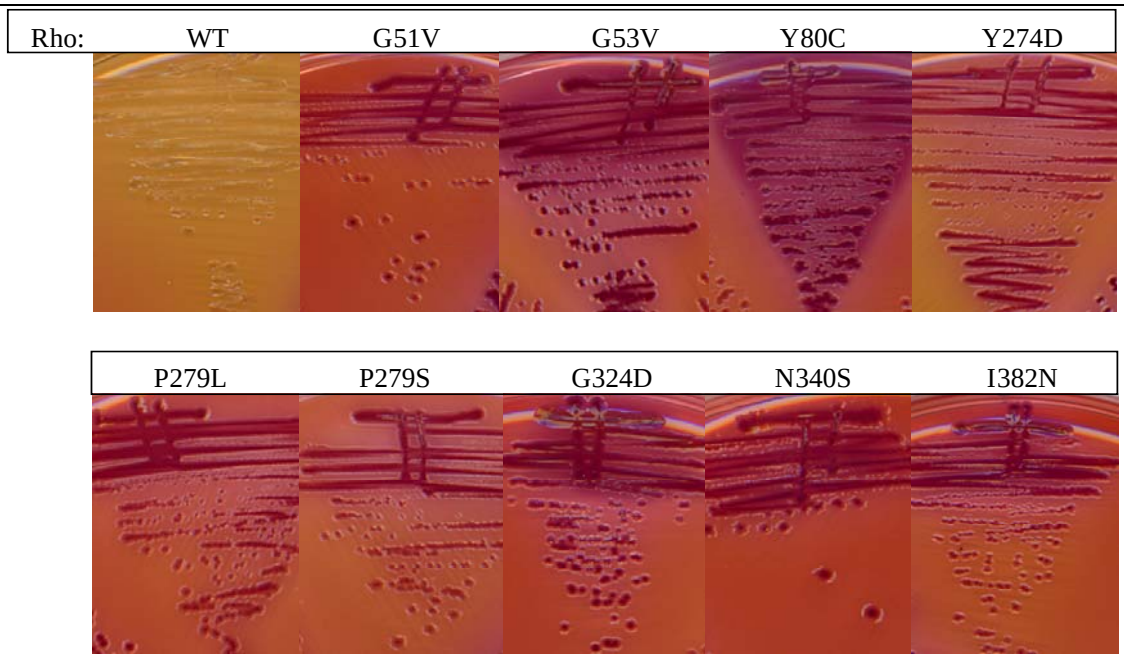

Figure 3.11

Plasmids with WT and mutant copies of *rho* were transformed to strain RS336 carrying *galEP3* reporter. The *rho* mutations were able to render the galEp3 strain Gal$^+$, as determined by color on D-galactose-supplemented MacConkey medium.

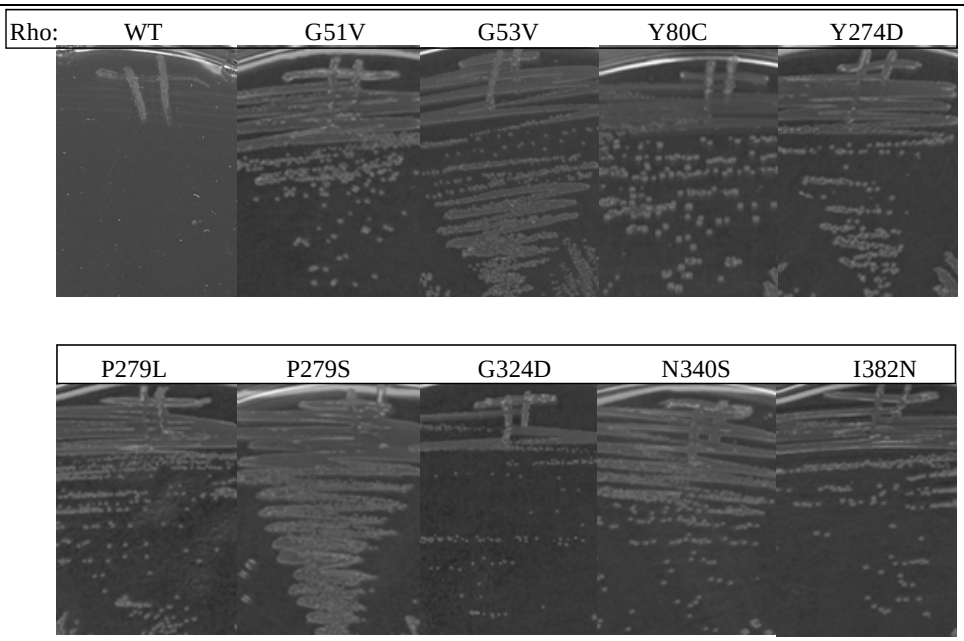

Figure 3.12

Plasmids with WT and mutant copies of *rho* transformed to strain RS336 carrying *trpE9851*(Oc) mutation were assessed for transcriptional polarity at the *trp* locus. The *rho* mutations were able to render the *trpE9851*(Oc) strain Anth$^+$, as determined by growth on minimal anthranilate plates.

3.3.2 *In vivo* termination defects of the Rho mutants

To get a quantitative measure of the termination defects of the Rho mutants, the ratio of β-galactosidase made from a *lacZ* reporter fused to a Rho dependent terminator (P_{lac}-H-19B *nutR/*T_{R1}*-lacZYA*) to that without the terminator (P_{lac}-*lacZYA*) was measured (read-through efficiency=%RT). This Rho-dependent terminator is derived from the *nutR-cro* region of a lambdoid phage H-19B (Neely and Friedman, 1998) and found to behave similar to the *nutR/*T_{R1} of λ phage. These reporter fusions were present as a single copy prophage. Different strains with these reporter fusions were transformed with the plasmids carrying the Rho mutants. The measurements were done in the presence of either WT or B8 (rpoB, Q513P) RNAP in the chromosome and either in the presence of a WT or chromosomal deletion of Rho (Table 1).

Table 1: *In vivo* termination defects of the Rho mutants in the presence of WT RNAP

Rho alleles	***β-galactosidase (arbitrary units)***					
	***Δrho: kan*[a]**			**WT *rho*[b]**		
	+tR1	-tR1	%RT	+tR1	-tR1	%RT
WT	42 ± 2	973 ± 28	4.3	37 ± 2	839 ± 68	4.4
G51V	334 ± 20	690 ± 24	49.0	360 ± 17	860.5 ± 62	41.8
G53V	548.5 ±54	678 ± 22	80.9	433 ± 11	1055 ± 45	41.0
Y80C	435 ± 12	687 ± 11	63.3	422 ± 23	1072 ± 46	39.3
Y274D	605.5 ± 45	729 ± 34	83.1	324 ±14	1183± 44	27.4
P279S	362 ± 8	677 ± 25	53.4	308 ± 6	870 ± 10	35.4
P279L	686 ± 39	1116 ± 39	61.5	317 ± 22	852 ± 42	37.2
G324D	636.5 ± 24	1074 ± 52	59.3	298± 13	839 ± 33	35.5
N340S	732± 45.5	1102 ± 35	66.4	284 ± 15.5	973 ± 33	29.2
I382N	750 ± 54	1158 ± 24	64.8	290± 11	1057 ±24	27.5

[a]Strains RS364 and RS391 with WT RNA polymerase and deletion of *rho* in the chromosome.
[b]Strains GJ3073 and RS445 with WT RNA polymerase and WT *rho* in the chromosome.
These above strains were transformed with the plasmids bearing different WT and *rho* mutants. The ratio of β galactosidase values in the presence and absence of T_{R1} terminator gives the efficiency of terminator read-through (%RT). This Rho-dependent terminator is derived from the *nutR-cro* region of a lambdoid phage H-19B and found to behave similar to the *nutR/*T_{R1} *of* λ phage. The averages of 5 to 6 independent measurements are shown.

Compared to WT Rho, all the mutants showed a significant defect in termination as evident from the 10 to 20-fold increase in terminator read-through efficiency (Table 1, column 4). Even in the presence of a WT copy of Rho, the read-through efficiency of the mutants was significantly high (Table 1, column 7). This could be attributed to the multi-copy (copy number of pCL1920 is ~5) dominance of the mutant Rho over WT Rho. The

partial suppression of the defects could also arise from the mixing of WT and mutant protomers of Rho.

The kinetic coupling model of Rho-dependent termination predicts that a slow moving RNAP can suppress the effect of defective Rho (Jin et al., 1992). So the ability of B8 (rpoB, Q513P), a slow elongating RNAP to suppress the defects of these mutants was tested. Similar measurements of termination read-through in the presence of B8 RNAP showed that defects of none of the Rho mutants were suppressed by the "slow" RNAP (Table 2, column 4), which is in contrast to earlier observations of different Rho mutants being suppressed by this RNAP (Guarente and Beckwith, 1978; Jin et al., 1992). According to the kinetic coupling model, slow RNAP will suppress only the Rho mutants which are defective in translocation along the RNA. Thus, either these mutants translocate too slow to catch up B8 RNAP or these mutants are defective in other steps of Rho-dependent termination. It is also noted that none of these mutants were compatible with a fast moving RNAP, B2 (rpoB, H526Y). It was difficult to obtain transformants in the strain having B2 RNAP in the chromosome with all the plasmids bearing Rho mutants. The defects of these Rho mutants might have amplified in the presence of a fast moving RNAP that caused this lethality. The increased read-through activity with the slow RNAP (B8), was unexpected (Table 2, column 4) and the reason for this is not clear.

Table 2: *In vivo* termination defects of the Rho mutants in the presence of B8 RNAP

Rho alleles	***β-galactosidase (arbitrary units)***		
	***Δrho: kan*[a]**		
WT	78.5 ± 10	564 ± 83	13.9
G51V	445 ± 32	782 ± 128	56.9
G53V	458 ± 48	636 ± 96	72.1
Y80C	645 ± 60	850 ± 180	75.8
Y274D	435 ± 45.5	623 ± 115	69.8
P279S	345 ± 42	633 ± 122	54.5
P279L	772 ± 36	1304 ± 84	59.2
G324D	847 ± 116	1127 ± 18.5	75.1
N340S	1272 ± 93	1553 ± 275	81.9
I382N	1050 ± 33	1247 ± 182	84.1

[a]Strains RS449 and RS450 with B8 RNA polymerase and deletion of *rho* in the chromosome.
These above strains were transformed with the plasmids bearing different WT and *rho* mutants. The ratio of galactosidase values in the presence and absence of T_{R1} terminator gives the efficiency of terminator read-through (%RT). This Rho-dependent terminator is derived from the *nutR-cro* region of a lambdoid phage H-19B and found to behave similar to the *nutR*/T_{R1} of λ phage. The averages of 5 to 6 independent measurements are shown.

3.3.4 Temperature sensitivity of Rho mutant strains

The normalized overnight cultures of RS336 strain transformed with WT and Rho mutant plasmids cultures were serially diluted and 5 µl were spotted on appropriate LB plates. The plates were incubated at 42 ºC over night. It was observed that mutants other than G51V, Y80C and Y274D caused a growth defect at 42 °C (Figure 3.13).

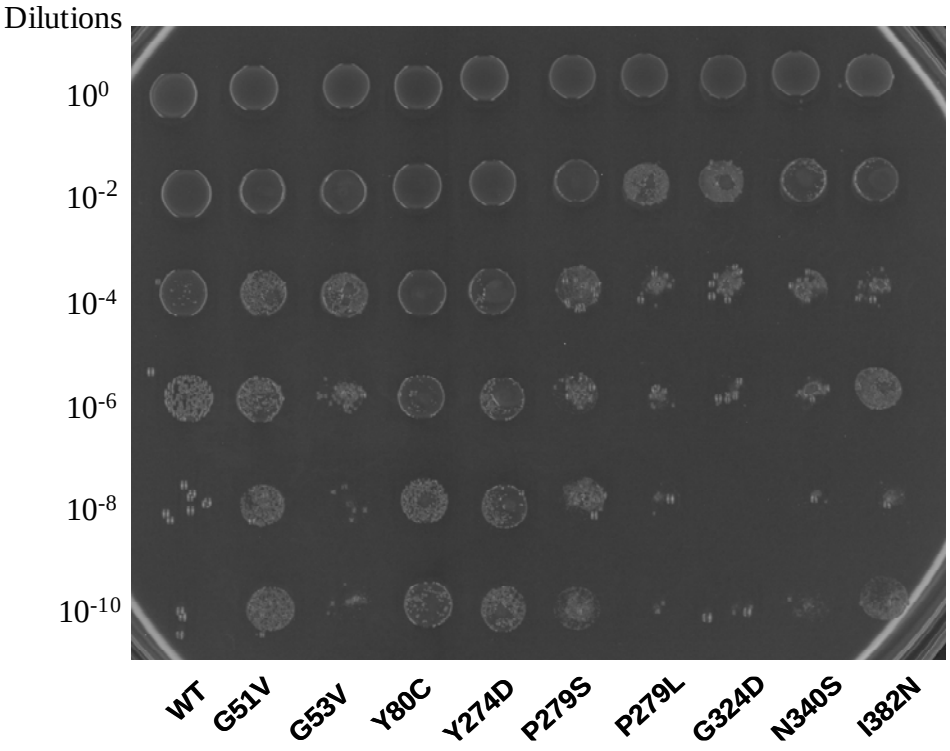

Figure 3.13
Growth of WT and Rho mutants on LB plate at 42 °C

3.3.5 Location of the mutations on the crystal structure of Rho

The positions of the mutations were mapped on the hexameric closed ring structure of Rho, which has both the primary and secondary RNA binding sites occupied with nucleic acids (Skordalakes and Berger, 2006) (Figure 3.14(a) and (b)). In general, the mutations are located within or close to the previously identified important functional domains of Rho. Among them, G51V, G53V and Y80C are in the primary RNA binding domain (Figure 3.14(c)). Y274D, P279S and P279L are in or close to the Q-loop (Figure 3.14(d)). G324D and N340S are close to the secondary RNA binding domain and G324D is in the R-loop (Figure 3.14(d)). The mutation I382N could not be located on the structure as the C-

terminal end of the closed ring structure of Rho is not resolved. Interestingly, mutations in these important structural elements of Rho did not have a lethal phenotype.

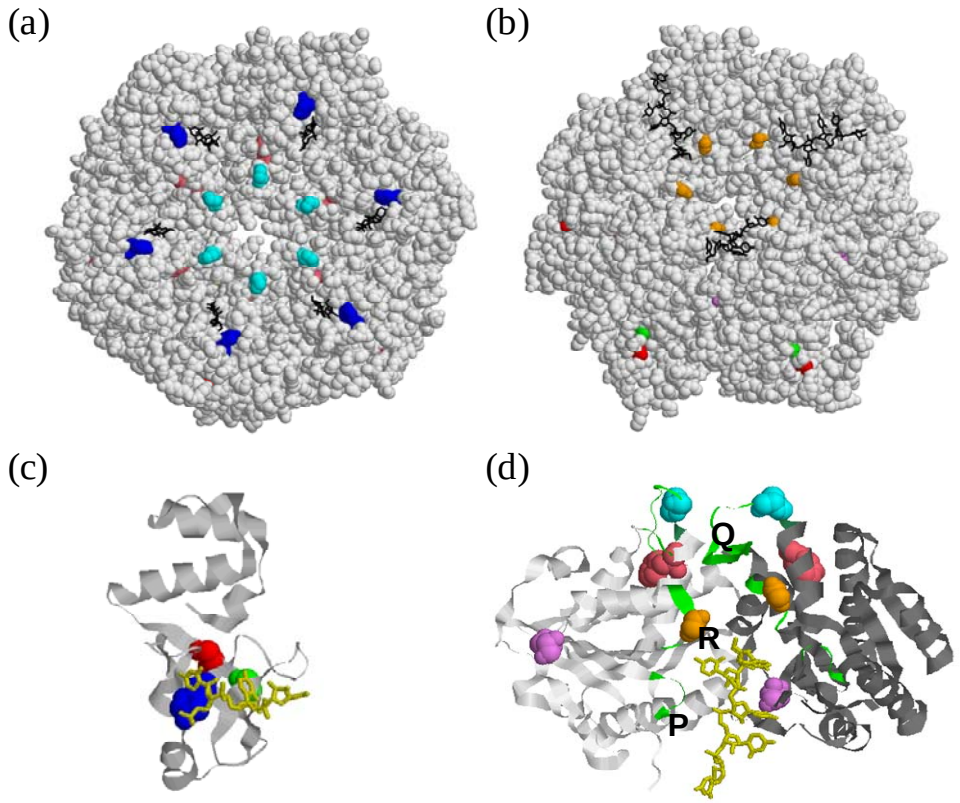

Figure 3.14: Location of the mutations on the crystal structure of Rho.

In (a) and (b) the space-filled model of hexameric closed ring structure of Rho was generated from the available co-ordinates of the dimeric unit of Rho (2HT1) and the figures were prepared using RASMOL. Positions of the mutations are indicated. The color codes are as follows. G51V, red; G53V, green; Y80C, blue; Y274D, pink; P279S/P279L, cyan; G324D, orange; N340S, violet. The position of I382N is not resolved in this structure. In a) the view is from primary RNA binding domain and that in b) is from secondary RNA binding domain. c) The primary RNA binding domain of Rho generated from the co-ordinates of the structure of N-terminal domain (2A8V) structure. RNA oligonucleotide is shown in yellow and locations of G51V, G53V and Y80C are also shown as spheres with the same color code as in a) and b). d) The secondary RNA binding domain is shown in the dimeric unit of the closed ring structure with the RNA (in yellow) bound at the interface of the two monomers (chains are shown in grey and black). P, Q and R loops are shown in green and the locations of Y274D, P279S/P279L, G324D and N340S are also indicated as spheres. Color codes for the mutations are same as in a) and b).

It is revealed from the structure that amino acid Y80 makes direct contact with the nucleic acid in the primary RNA binding domain (Bogden et al., 1999) (Figure 3.14(c)). So there is a high probability that Y80C change will affect the primary RNA binding drastically. Amino acids G51 and G53 also come within 12–14 Å of the nucleic acid in the crystal

structure and changes in these amino acids can also affect the primary RNA binding (refer the distance calculations in Table 3). The crystal structure revealed the binding of only two nucleotides, whereas about ten nucleotides can be occupied in the primary RNA binding site of a monomer (Geiselmann et al., 1992). Therefore it is likely that other amino acids of this domain (including G51 and G53) will take part in the primary RNA binding (Hitchens et al., 2006). Defect in the primary RNA binding due to the change in these three amino acids will subsequently affect the secondary RNA binding and the RNA release processes.

Table 3: Distances of the positions of different mutations from important functional domains

Mutant Rho	Distance to the 1° RNA binding site (A°)	Distance to the 2° RNA binding site (A°)	Distance to ATP binding site (A°)
G51V	14.3	48.6	38.5
G53V	12.3	41.5	32.0
Y80C	5.3	46.3	39.2
Y274D	17.6	22.2	22.7
P279S	16.2	29.4	32.2
G324D	34.1	4.9	17.1
N340S	36.0	14.2	19.6

The distances were calculated using RASMOL program. For calculating the distances from primary (1^{o}) and secondary (2^{o}) RNA binding domains, the nearest RNA residues were considered and that from the P-loop, C^{α} atom of residue 184 was considered.

The amino acids G324 and N340 are situated close to the RNA in the secondary RNA binding site (Figure 3.14(d) and Table 3). It is likely that G324, located in the R-loop, will take part directly in the interaction with RNA. Therefore, it can be predicted that changes in these two amino acids will cause a defect in the secondary RNA binding and in the ATP hydrolysis activities. This may in turn affect the processive translocation of Rho along the RNA, which will lead to a termination defect.

P279S and P279L changes in the Q-loop can alter the loop conformation by extending the length of the preceding helix. The closed ring structure of Rho revealed that the Q-loop is about 30 Å (Table 3) away from the nearest RNA residue in the secondary RNA binding site. In the closed ring structure of Rho, the Q-loop forms a hairpin-like structure from the disordered conformations observed in the open ring structure (Skordalakes and Berger, 2006). This alteration may be important for attaining the active conformation of Rho and the change in the loop conformation due to the mutations will affect its function. On the other hand Y274, which is located just outside this loop, may come on the pathway of the RNA passing through the dimeric interface of two Rho protomers (Figure 3.14(d)). So Y274D may have similar defects as G324D and N340S changes. In order to test these predictions of the additional defects of these mutants in different properties of Rho, their efficiencies for primary and secondary RNA binding as well as for their ATP binding and hydrolysis activities were assayed.

3.3.6 *In vitro* transcription termination defects of the Rho mutants

In vitro transcription termination activity of the Rho mutants was studied at the *trp t'* terminator using purified WT and all the mutant Rho proteins, except G53Vand P279L. G53V and P279L mutants were not purified as they formed inclusion bodies under overexpression conditions. A linear DNA template with the *trp t'* terminator cloned downstream to the strong T7A1 promoter was used for transcription assays. In order to observe the released RNA at the Rho-dependent termination points, the templates were immobilized on streptavidin-coated magnetic beads. In the assays, the supernatant fractions contain the released RNA. The WT Rho protein showed about 85% efficiency in termination. Consistent with their *in vivo* phenotype, all the Rho mutants except I382N showed significantly reduced termination efficiency (Figure 3.15(a) and (b)). The presence of NusG during the chase improved the termination efficiency of Y274D, G324D and N340S by about two fold (Figure 3.15(a) and (b)). NusG, however, did not bring about early termination in these mutants as observed for the WT Rho (Figure 3.15(a)).

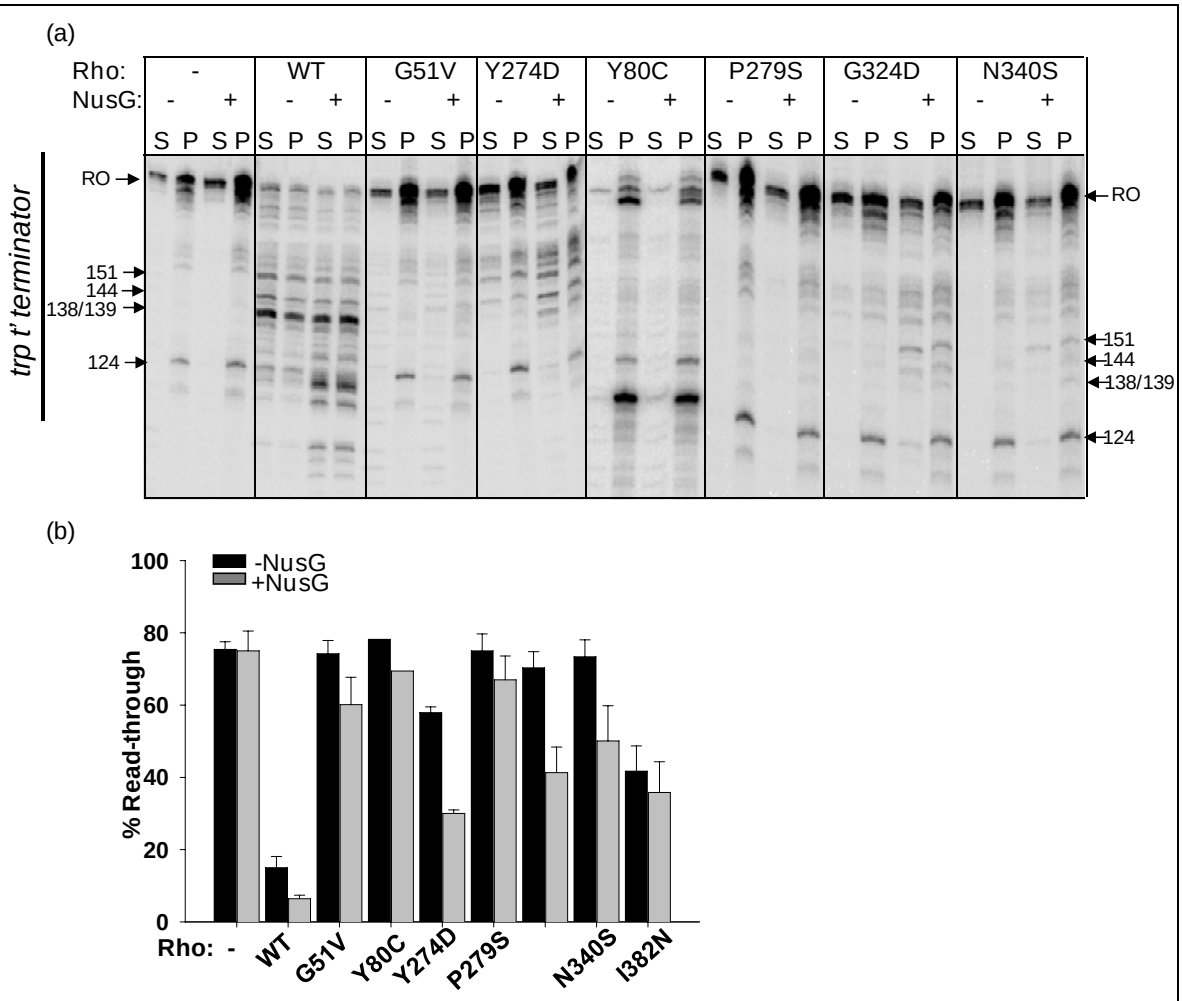

Figure 3.15: *In vitro* termination defects of the mutant Rho proteins in the presence of WT RNA polymerase

(a) Autoradiogram of the *in vitro* transcription termination by different Rho mutants both in the absence and presence of NusG. Transcription was initiated from T7A1 promoter. The DNA template was immobilized on magnetic beads. Rho-dependent RNA release starts from 100 nt downstream of the transcription start site in the *trp t'* terminator region (as indicated). Major termination positions are marked. Half of the supernatant (released RNA) is denoted as S and the rest of the reaction mixture containing half of the supernatant and pellet is denoted as P. RO denotes the run-off product. The read-through efficiency (RT) for each case was calculated from the S lanes as: RT=[RO product]/[RO product + all the products ≥100 nt]. (b) Measured RT for each of the mutants is shown as bar diagrams using WT RNA polymerase. Higher read through efficiencies of the Rho mutants reflect their termination defect.

In order to validate the *in vivo* observation that the termination defects of the Rho mutants could not be suppressed by B8 RNAP, *in vitro* transcriptions were also carried out with the B8 enzyme.

Consistent with the *in vivo* data (Table 2), the *in vitro* assays (Figure 3.16(a) and (b)) also showed that B8 RNAP does not improve the termination efficiency of the mutants significantly, except for Y274D. For Y274D and G324D mutants, termination efficiency was improved ~1.5-to two fold in the presence of NusG. These mutants (and N340S; see Figure 3.15(a) and (b)) might have defects in the RNA release step(s) from the EC, and NusG is likely to be involved in this step during the Rho-dependent termination process.

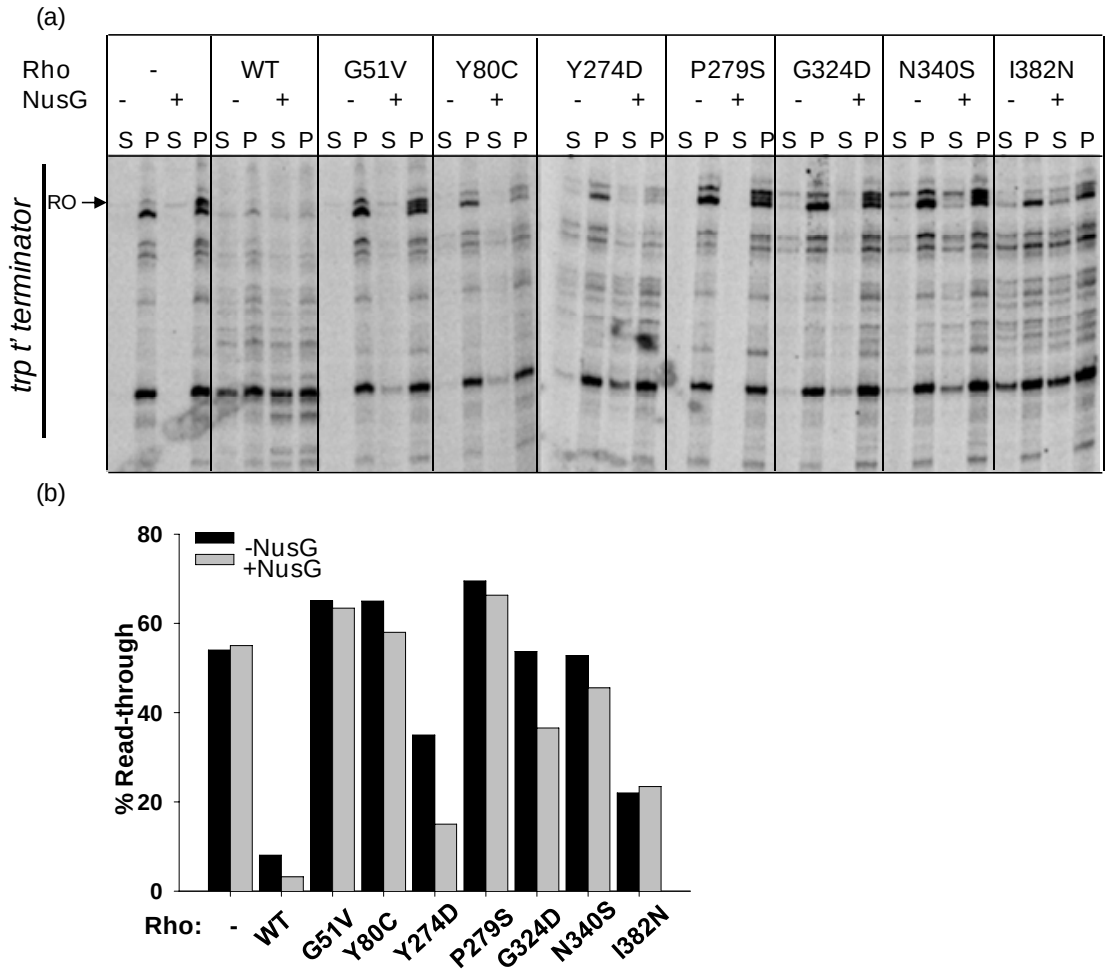

Figure 3.16: *In vitro* termination defects of the mutant Rho proteins in the presence of B8 RNA polymerase

(a) Autoradiogram of the *in vitro* transcription termination by different Rho mutants both in the absence and presence of NusG. The meaning of S and P is same as described for Figure 3.15. RO denotes the run-off product. (b) Bar diagrams showing read through efficiencies of the Rho mutants in the presence of B8 RNA polymerase. The read-through efficiency (RT) efficiencies are calculated in the same way as described in Figure 3.15.

3.3.7 Structural integrity of the Rho mutants

The Circular Dichorism spectra of different Rho mutants were similar to that of the WT Rho (Figure 3.17), indicating that the overall structural integrity of the mutants was maintained during the course of the experiments. The estimation of the secondary structure was done by using the reference file Yang US.jwr. The composition of the different secondary structural elements for WT and mutant Rho proteins are as follows. α–Helix, 25–29%; β–sheet, 24–32%; turn, 13–17%; random coil, 28–32%. So the differential activities and loss of specific functions of the mutants in various assays were not due to instability of the mutants or presence of inactive fractions in the preparations.

(a)

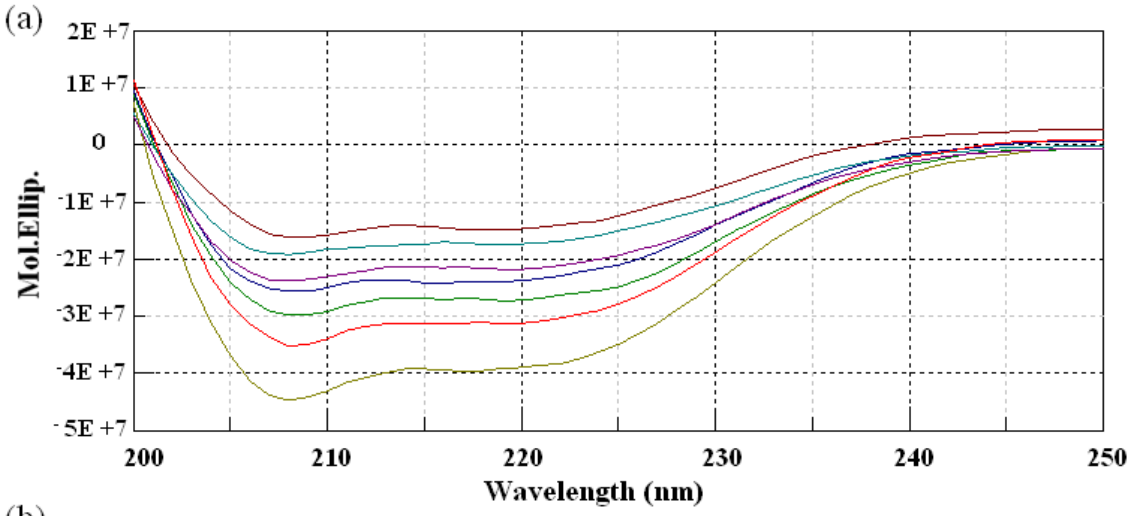

(b)

Secondary structure composition (%)	WT Rho	Rho G51V	Rho Y80C	Rho Y274D	Rho G324D	Rho N340S	Rho I382N
α-Helix	27.5	27.1	29.3	27.1	26.8	24.7	26.5
β-sheet	32.1	29.4	22.7	23.8	41.1	26.1	27.9
Turn	12.8	14.8	17.3	16.9	13.9	17.1	15.7
Random coil	27.7	28.6	30.6	32.1	18.2	32.1	29.9

Figure 3.17

(a) CD spectra of WT Rho and mutants. WT: Blue, G51V: Red, Y80C: Green, Y274D: Violet, G324D: Brown, N340S: olive green, I382N: cyan. CD spectroscopy was performed using a JASCO 810 system at 25 °C. The scanning was done from 250 to 200 nm in a cuvette with 0.1 cm path length. (b) The secondary structure composition of WT Rho and mutants. The estimation was done using the manufacturer's software for the instrument.

3.3.8 Primary RNA-binding properties of the Rho mutants

There are two distinct types of polynucleotide interaction sites in Rho (Richardson, 1982; Wei and Richardson, 2001a). The primary RNA binding site, located in the N-terminal region, recognizes both single-stranded DNA and RNA, whereas the secondary binding site located at the central hole of the oligomer, binds specifically to the RNA. To investigate whether interactions in these two sites were affected by these mutations, the interactions specifically at the primary binding site was monitored by estimating the dissociation constant (K_d) of each of the mutants for a 34-mer DNA oligonucleotide, $(dC)_{34}$. Occupancy of a DNA oligomer only in the primary RNA binding site of the Rho crystal (Skordalakes and Berger, 2003) and protection of primary RNA binding domain by DNA oligomer in the protein footprinting studies (Wei and Richardson, 2001a), strongly suggest that DNA can specifically bind to this site and not to the secondary RNA binding site.

The dissociation constants (K_d) for oligo$(dC)_{34}$ of different Rho mutants were measured by both gel retardation and filter binding assays (Table 4, column 2). The K_d value for WT Rho was ~10 nM. None of the mutants were defective for binding to oligo$(dC)_{34}$ except Y80C, which did not show significant binding in both the gel retardation and filter binding assays. In order to test whether this defect is specific for DNA oligo, the efficiency of binding of a radiolabeled RNA oligo, rC_{10} to Y80C was checked by UV cross-linking. This mutant showed significantly reduced cross-linking efficiency even at 20 μM of rC_{10} (Figure 3.18). The binding defect of this mutation is consistent with the fact that this amino acid directly stacks against the base of the oligonucleotide (Bogden et al., 1999) (Figure 3.14(c)). Previously reported mutants in this region also exhibited similar defects in primary RNA binding (Martinez et al., 1996).

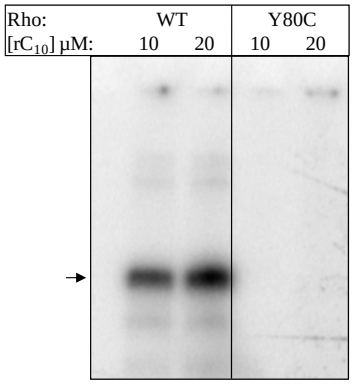

Figure 3.18

Autoradiogram of SDS-PAGE showing the amount of labeled rC_{10} crosslinked with WT (indicated by arrow) and Rho Y80C after UV cross-linking. 50 nM of WT or Rho Y80C was crosslinked with different concentrations of labeled rC_{10} as indicated.

3.3.9 Secondary RNA binding

Interaction of RNA in the secondary site is mandatory to activate ATP hydrolysis (Richardson, 1982; Wei and Richardson, 2001a) (Figure 3.19). It has been reported that due to the weak interactions at the secondary RNA binding site, it is difficult to observe the RNA binding at this site by using direct binding assays (Dolan et al., 1990; McSwiggen et al., 1988). So the concentrations of poly(C), oligos rC_{10} (10-mer) and rC_{25} (25-mer) required to elicit half-maximal ATPase activities in the presence of excess ATP was measured for estimating the binding efficiency to this site. For the oligos, rC_{10} and rC_{25}, measurements were done in the presence of oligo $(dC)_{34}$ at the primary site, because short RNA oligos ($rC_{5–8}$) can elicit ATPase activity by binding to the secondary site only in the presence of oligo(dC) (Miwa et al., 1995; Richardson and Carey III, 1982).

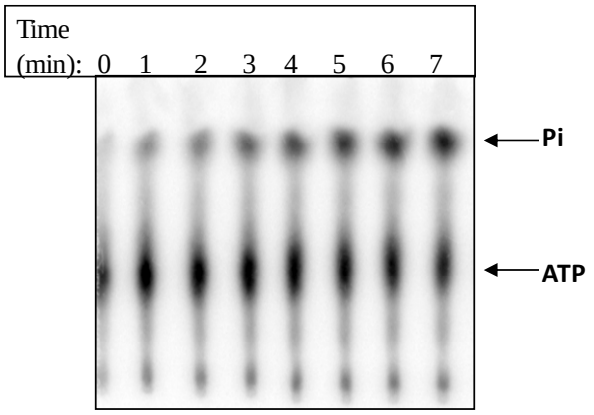

Figure 3.19

A representative autoradiogram showing the separation of Pi and ATP by thin layer chromatography (TLC) after ATP hydrolysis by Rho using poly(C) as cofactor.

None of the mutants showed a significant defect in utilizing poly(C) as substrate (Table 4, column 3). Only P279S and G324D showed slightly less affinity compared to others. This was further supported by the fact that the rates of ATP hydrolysis with poly(C) were also not significantly different for the mutants (Table 4, column 4). Since a strong substrate like poly(C) can mask the defects in secondary site binding (Chen and Stitt, 2004; Wei and Richardson, 2001b), two shorter RNA oligos, rC_{10} and rC_{25} were used to assess the binding defects in the secondary site. All the mutants, except I382N, failed to show significant amounts of ATP hydrolysis even at a very high concentration of the oligo, rC_{10} (Table 4, column 6). Even with the longer oligo rC_{25}, the affinity for G51V was only increased, but

still it showed ~100-fold weaker affinity compared to WT (Table 4, column 5). In general, we concluded that except I382N, all the mutants were defective in secondary RNA binding or they had an extremely slow rate of ATP hydrolysis. This defect should have contributed significantly in their inability to terminate.

Table 4: *In vitro* primary and secondary RNA binding properties of the Rho mutants

Rho mutants	K_d[a] $(dC)_{34}$ (nM)	[poly(C)] at half-maximal ATPase activity[b] (μM)	ATPase activity on poly(C) RNA[c] (nmoles of ATP/min/μg of Rho)	[rC_{25}] at half-maximal ATPase activity[d] (μM)	[rC_{10}] at half-maximal ATPase activity[e] (μM)
WT	10 ± 0.9	0.59 ± 0.02	29.1 ± 3.5	0.13 ± 0.01	13.2 ± 2.6
G51V	3 ± 0.3	0.46 ± 0.04	15.5 ± 0.2	15.45 ± 1.75	> 200
Y80C	>3000	0.14 ± 0.06	20.4 ± 0.2	> 500	> 200
Y274D	12 ± 1.4	0.43 ± 0.02	14.1 ± 1.0	> 500	> 200
P279S	3 ± 0.1	0.78 ± 0.03	33.1 ± 2.3	> 500	> 200
G324D	10 ± 2	0.72 ± 0.05	19.6 ± 4.0	> 500	> 200
N340S	11 ± 2	0.51 ± 0.09	23.6 ± 1.4	> 500	> 200
I382N	12 ± 3	0.30 ± 0.02	20.4 ± 0.05	0.39 ± 0.01	32.3 ± 1.0

[a] K_d values were average of those obtained from gel shift and filter binding assays using end-labeled $(dC)_{34}$. Fractions of bound complexes were plotted against the concentration of Rho and the plot was fitted to a hyperbolic binding isotherm to determine the dissociation constant. Concentration of oligo$(dC)_{34}$ is expressed in terms of DNA ends. For Y80C there was no binding up to 3 μM. I acknowledge Irfan Bandey for providing the data in column 2.

[b] Amount of radiolabeled inorganic phosphate release from [γ-^{32}P]ATP was plotted against the increasing concentration of poly(C). Concentration of poly(C) corresponding to the half-maximal ATPase activity was determined by fitting the plot to a sigmoidal curve. The concentration range of poly(C) was 0 to 5 μM, in terms of the nucleotides. The concentration of ATP was 500 μM. Poly(C) will bind both to the primary and secondary RNA binding sites. So the values obtained by this method will reflect binding defects, if any, in the secondary site.

[c] The initial rate of ATP hydrolysis in the presence of poly(C) as co-factor was determined by fitting the plot of the amount of un-hydrolyzed ATP against time to the equation $y = y_o \exp(-\lambda t)$, where λ is the rate constant. The time-points in the linear region (upto 5 min) were considered for the calculations. Concentrations of ATP and poly(C) were 1 mM and 20 μM, respectively.

[d] Except for WT, G51V and I382N, significant amount of ATPase activity was not observed up to 500 μM of rC_{25}. Concentration of rC_{25} is expressed in terms of RNA ends. Concentration of ATP was 1 mM.

[e] Except for WT and I382N, significant amount of ATPase activity was not observed up to 200 μM of rC_{10}. Concentration of rC_{10} is expressed in terms of RNA ends. Concentration of ATP was 1 mM.

Most likely, the defect in binding of oligo $(dC)_{34}$ to the primary site of the Y80C mutant did not stimulate the ATPase activity with the shorter oligos at the secondary site. In case of G51V, the unusual mode of binding of $(dC)_{34}$ in the primary site, might have failed to elicit the allosteric effect in the secondary site. Earlier, the reported tight binding mutant, G99V, also had a similar defect in binding to oligo rC_{10} (Pereira and Platt, 1995). Defects of G324D and N340S for secondary RNA binding were predictable from their locations close to this site. Although according to the crystal structure (Skordalakes and Berger, 2006) (Table 3), amino acids Y274 and P279 are more than 20 Å away from the closest RNA residue in the secondary site, these data and the previously obtained protein footprinting results with Q-loop mutants (Wei and Richardson, 2001b) strongly suggest that this region of Rho also takes part in interactions with the RNA in the secondary site.

3.3.10 ATP binding

The apparent dissociation constant ($K_{d,app}$) of ATP for WT and mutant Rho proteins in the absence of the RNA cofactor was measured by using the UV-cross-linking technique (Figure 3.20). The apparent affinity of ATP for mutants Y274D, P279S and G324D was observed to be reduced by five-to eight fold, whereas it was comparable to WT for mutants N340S, G51V and I382N (Table 5). Mutations in R and Q-loops might have allosteric effects on the proximal P-loop, the ATP binding site. Cross-talk between the R-loop and P-loop has also been proposed from the closed ring crystal structure of Rho (Skordalakes and Berger, 2006).

There was no significant cross-linking of ATP for the Y80C mutant. Cross-linking efficiency of the radiolabeled ATP varied among different mutants to the extent that it was negligible for Y80C. Absence of cross-linking means that either the binding affinity for ATP is very poor or some unusual conformational changes due to the mutation has impaired the chemistry of crosslinking. As Y80C can hydrolyze ATP in the presence of poly(C) (Table 4) the mutant must have the ability to bind ATP. Therefore, the Km value of ATP for this mutant using poly(C) as cofactor was measured and compared with the WT Rho (Table 5, data in parentheses). Y80C, indeed showed about four fold increase in Km value, which indicated that the binding of ATP has been affected due to this mutation. It is of interest to note that a mutation in the primary RNA binding domain can affect the conformations in the ATP binding domain which is located ~40 Å away (Table 3).

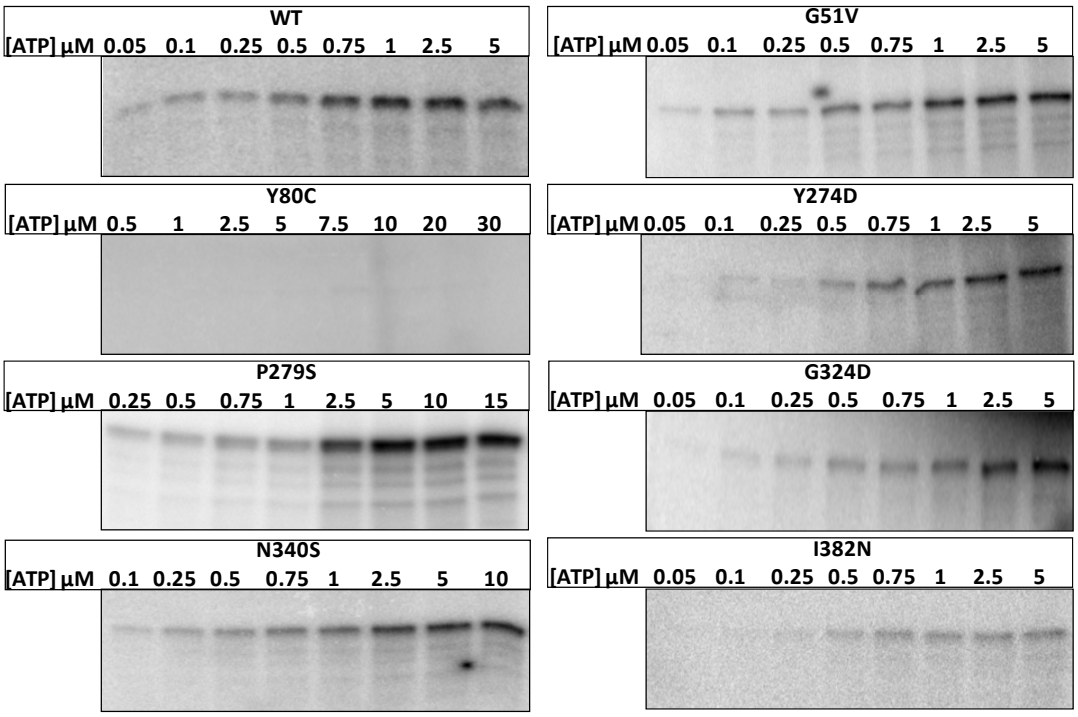

Figure 3.20

Autoradiograms of SDS-PAGE showing the amount of labeled ATP crosslinked with WT and different mutant Rho proteins after UV cross-linking. Varying concentrations of [γ-^{32}P]ATP was crosslinked with 50 nM of WT and mutant Rho proteins.

Table 5: ATP binding of the Rho mutants

Rho Mutants	$K_{d,\ app}$ µM
WT	0.54 ± 0.06 (11.7 ± 2.2)
G51V	1.35 ± 0.26
Y80C	No cross-linking (43.2 ± 0.8)
Y274D	3.15 ± 0.26
P279S	4.28 ± 0.54
G324D	2.45 ± 0.15
N340S	1.09 ± 0.12
I382N	0.60 ± 0.1

Apparent dissociation constant ($K_{d,app}$) of ATP was determined by UV-cross-linking. The intensities of the cross-linked species were plotted against increasing concentrations of [γ-P^{32}]ATP and K_d values were obtained from the hyperbolic fitting of the plots. For Y80C, no cross-linking was observed up to 30 µM of [γ-P^{32}]ATP. K_m values of ATP for WT and Y80C are shown in parenthesis. Concentration of WT and mutant Rho was 50 nM in hexamer.

3.3.11 Probing the conformational changes in the C-terminal domain of Rho Y80C compared to WT Rho

Besides impairing the primary RNA binding, the Y80C mutation also caused significant defect in ATP binding. This led us to hypothesize that this change may cause conformational changes in the distal (~40 Å) C-terminal domain allosterically. To test this hypothesis, the conformations of WT and mutant Rho was probed by limited proteolytic cleavages, fluorescence anisotropy and fluorescence quenching.

The surface accessibility of the single tryptophan residue (W381), located ~15 Å away from the ATP-binding site was monitored by the fluorescence quenching technique using acrylamide as a neutral quencher. This tryptophan residue emits a fluorescence signal at 350 nm upon excitation at 295 nm. Quenching of this signal was plotted against the increasing concentration of acrylamide to obtain the quenching constant (Ksv) (Figure 3.21). The value of Ksv increases as the tryptophan becomes more surface accessible. It was observed that this tryptophan in the Y80C mutant is more surface accessible compared to the WT.

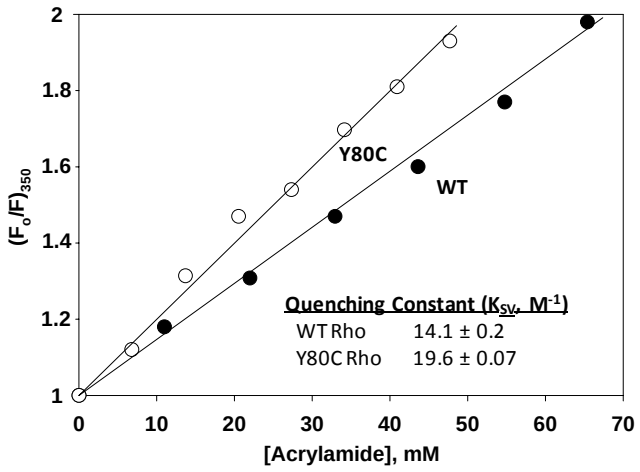

Figure 3.21

Stern-Volmer plots for acrylamide quenching of tryptophan fluorescence of WT and Y80C Rho proteins. The quenching constant (K_{SV}) was calculated from these plots using the equation: $(F_0/F)_{350} = 1 + K_{SV}[Q]$, Q is the concentration of the quencher, acrylamide.

A fluorescent analogue of GTP, Tb-GTP, which is a complex of terbium chloride and GTP (Kumar and Chatterji, 1990; Sen and Dasgupta, 2003), was used to see the local conformational flexibilities at the ATP binding pocket. It was assumed Tb-GTP will bind to the same ATP binding site as GTP is also a good substrate of Rho (Lowery and Richardson, 1977; Nowatzke and Richardson, 1996). The anisotropy (r) of the Tb-GTP moiety upon binding to the ATP binding pocket was measured. A higher value of r means less rotational freedom of the fluorescent probe. A lower value of r for Tb-GTP bound to Y80C compared to that obtained for WT Rho (Table 6) suggested more conformational disorders in the ATP-binding pocket.

Table 6: Fluorescence anisotropy (r) values of Tb-GTP

Species	***Anisotropy (r)***
Free Tb-GTP [150μM: 50μM]	0.096 ± .005
Tb-GTP + 100 nM WT Rho	0.246 ± .007
Tb-GTP + 150 nM Y80C Rho	0.183 ± .003

In all the experiments, Tb-GTP complexes were made by incubating 150 μM Tb with 50 μM GTP. Majority of the Tb-GTP species were in bound form in the presence of indicated amount of hexameric Rho. Anisotropies were measured at 25 ^{o}C.

In general, quenching constant and anisotropy values did not change drastically because of the Y80C mutation, which suggests that the conformational changes induced by the mutation in the C-terminal domain are more subtle. To further corroborate these data, limited proteolytic digestions of the WT and Y80C Rho proteins was employed to probe the conformational changes with V8 protease, which cleaves preferably at glutamic acid residues. It was observed that a cluster of surface exposed glutamic acid residues (Figure 3.22(a)) near the dimeric interface of the C-terminal domain (Figure 3.22(b)) of both the WT and Y80C mutants were very sensitive to this protease. Interestingly, a new band corresponding to Glu226, close to this cluster (Figure 3.22(a) and (b)), was found to become sensitive to V8 digestion, specifically in the Y80C mutant. This observation further supports the proposal that the Y80C mutation in the primary RNA binding domain induces distinct but subtle conformational changes in the distal C-terminal domain, which might have affected the ATP binding domain and the surrounding regions.

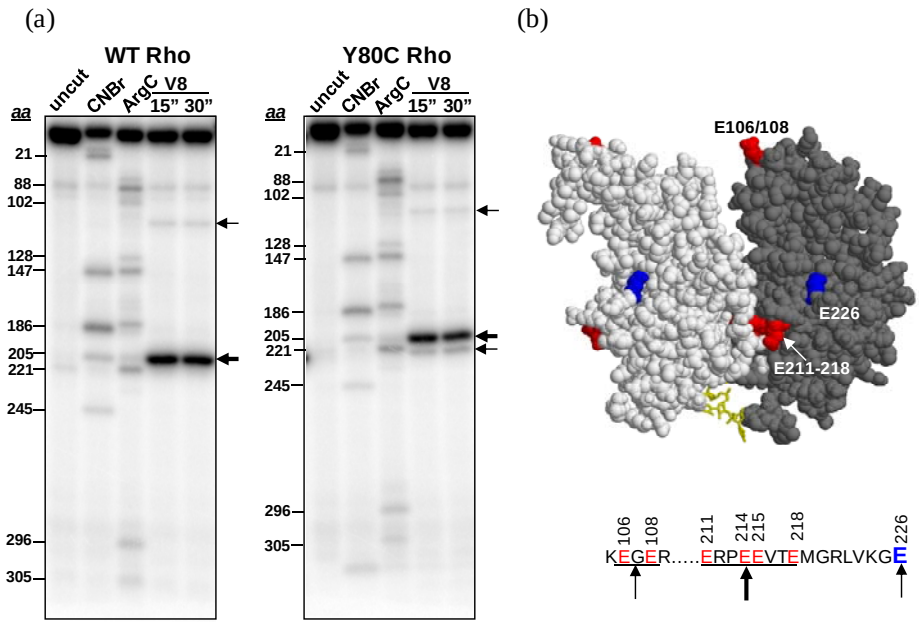

Figure 3.22

(a) Limited proteolysis of end-labeled WT and Y80C Rho proteins with V8 protease. Glutamic acid residues corresponding to the major cleavage products are indicated by arrows. These positions were identified from the calibration curve obtained from the molecular weight markers generated with CNBr and ArgC digestions of the same end-labeled Rho. The amino acid positions from N- to C-terminal are indicated to the left of the gel pictures. The thick arrow corresponds to the sensitivity towards the glutamic acids residues between 211 and 218. Individual amino acids are not resolved. Position of 106/108 and 226 are also indicated by thin arrows. (b) Locations of the V8 sensitive residues are indicated on the dimeric unit of the closed ring structure of Rho. The red spheres are the V8 sensitive patch comprising of glutamic acids at 211, 214, 215 and 218. Also E106/108 is also indicated as red spheres in the N-terminal domain. E226, which specifically became sensitive in the Rho Y80C is shown as a blue sphere.

3.3.12 RNA-release efficiency of the Rho mutants from stalled elongation complex

The majority of the Rho mutants are defective in secondary RNA binding, which might have affected the processivity during translocation along the nascent RNA and reduced the speed of translocation. It was hypothesized that if their termination defect is due to slow translocation only, these mutants may be able to release RNA from the stalled ECs if sufficient time is allowed. So the EC was stalled on an immobilized template at a particular position within the *trp t'* terminator region (Figure 3.23(a)) using the lac repressor as a roadblock (King et al., 2003). The stalled EC remains transcriptionally active and can restart transcription efficiently from this position upon removal of the lac repressor (King et al., 2003). Under this condition the mutant Rho proteins will eventually be able to "catch up" the stalled EC if sufficient time is allowed and release the RNA. Also in the stalled EC set-up, one can monitor only the Rho-dependent RNA release uncoupled from the

transcription elongation process and therefore the role of ATP and/or NusG on the different steps of the RNA release can be studied (see Figure 3.24).

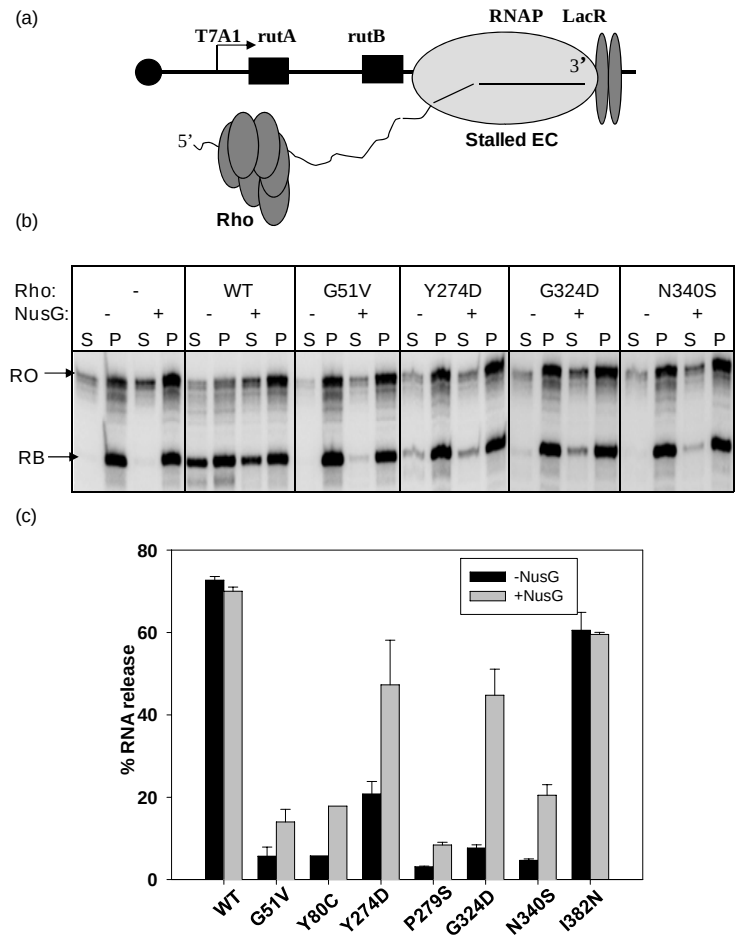

Figure 3.23: Rho-mediated RNA release from the stalled elongation complex.

(a) Cartoon showing the design of a stalled elongation complex using lac repressor as a roadblock. In this set-up, the EC was stalled at 161 position of the *trp t'* terminator. Rho was added to the reaction after the stalled complex is formed and RNA release was measured from the supernatant. (b) Autoradiogram showing the amount of released RNA in the supernatant by WT and different Rho mutants both in the absence and presence of NusG from the stalled EC. RB and RO denote the positions of roadblocked product and run-off product, respectively. The meaning of S and P is same as described for Figure 3.15. (c) The RNA release efficiencies shown by bar diagrams are calculated as: [2S]/[S+P].

To the stalled EC, WT or different mutant Rho proteins were added and the released RNA in the supernatant was monitored in the presence and absence of NusG. Under this experimental condition, WT Rho released ~70 to 80% of the RNA from the stalled EC. Considering the non-specific rebinding of the released RNA to the beads, these values suggest an efficient release of RNA from the stalled EC by Rho. In the absence of NusG, all the mutants except I382N were still defective in releasing RNA even from a stalled EC.

However, in the presence of NusG, a partial restoration in RNA release efficiency was observed for Y274D, G324D and N340S (Figure 3.22(b) and (c)), which is similar to that observed in continuous transcription assays (Figure 3.15(b), presence of NusG). This partial restoration of the RNA release efficiency from the stalled EC in the presence of NusG suggests that Y274D, G324D and N340S, unlike WT Rho, are very much dependent on NusG for interaction with the EC and possibly they are defective in the step(s) involving the release of RNA from the EC.

3.3.13 Effect of ATP and NusG on RNA-release efficiency of the Rho mutants from stalled elongation complex

In order to further identify the kinetic step(s) defective for these Rho mutants the time-course of RNA release from the stalled EC was followed in the presence of different concentrations of ATP. The concentration of ATP was varied to change the translocation rate. On template immobilized on magnetic beads, stalled EC was made, removed all the NTPs by extensive washing and WT or different mutant Rho proteins were added in the presence of 0.02 mM and 1 mM ATP. The time course of RNA release in the supernatant was followed for 30 min, both in the absence (Figure 3.24(a), (c) and (d)) and presence of NusG (Figure 3.24(b), (e) and (f)). The rate (slope of the curve) and the efficiency (maximum amount of released RNA) of RNA release remained the same for WT Rho at all the concentrations of ATP tested. A modest increment of rate but not the efficiency of RNA release was observed in the presence of NusG. RNA release efficiency by the P279S mutant did not improve significantly, even at 1 mM ATP and in the presence of NusG. Under the same conditions, a modest improvement in the RNA release efficiency was observed for G51V and Y80C mutants, but it never reached to the level of WT Rho. For Y274D, G324D and N340S, the efficiency of RNA release improved significantly when 1 mM ATP was present and NusG was absent. For these mutants, both the efficiency and rate of RNA release was observed to regain the WT Rho level in the presence of both 1 mM ATP and NusG. Higher concentrations of ATP might have increased the rate of ATP hydrolysis and as well as improved the processivity of Y274D, G324D and N340S Rho mutants, which in turn increased the overall rate of translocation. This has enhanced the chances of the Rho mutants to be in the vicinity of the stalled EC. These mutants may also have defects in the RNA release step, which most likely requires a direct interaction with the EC. The presence of NusG helped them to overcome this defect, which is reflected in the faster RNA release (Figure 3.24(f)).

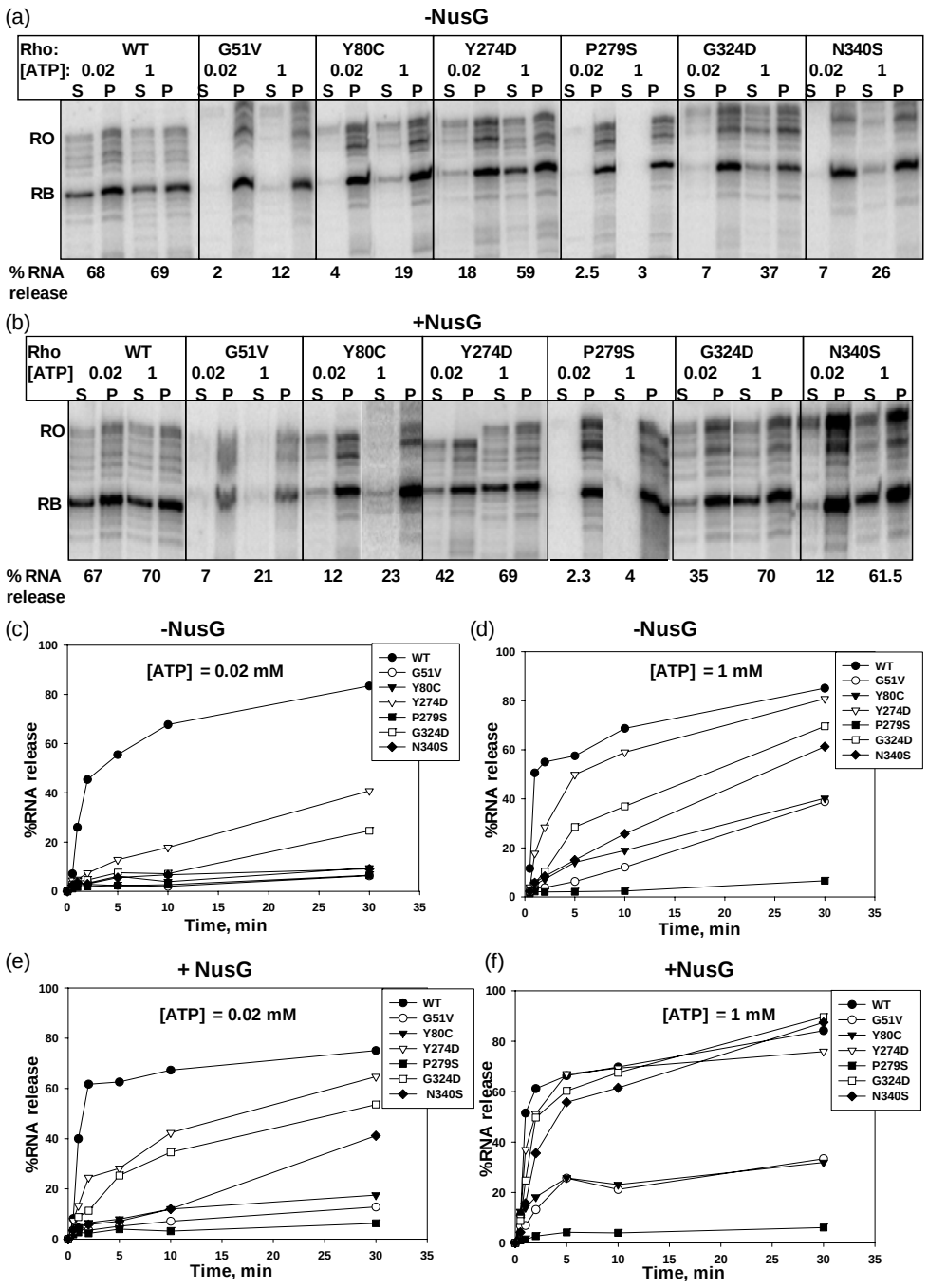

Figure 3.24

ATP and NusG dependence of Rho-mediated RNA release from a stalled elongation complex. Autoradiograms of the RNA release after 10 min of addition of different Rho mutants from the stalled EC (described in Figure 3.23) in the presence of different concentrations of ATP, both in the absence (a) and presence (b) of 200 nM NusG. (c)–(f) Curves showing the time courses of the RNA release upon addition of WT and different Rho mutants in the presence of indicated concentrations of ATP. The presence or absence of NusG in the reactions is also indicated. The RNA release efficiencies are calculated in the same way as described in Figure 3.23. I acknowledge Sharmistha Banerjee for providing major part of the data in this figure.

3.4 Discussion

In this work termination defective mutants of Rho were isolated through a random mutagenesis screen, characterized them and in the light of closed ring structure of Rho (Skordalakes and Berger, 2006), the involvement and importance of different functions of Rho in releasing RNA from the EC was studied. Different properties of the mutants are summarized in Table 7. All the termination defective mutants (except I382N) were found to be located in the previously identified functional domains, such as in the primary RNA binding domain and in the secondary RNA binding domain including Q-loop and R-loops. The termination defect of the mutants G51V, Y80C and P279S could not be overcome under the most relaxed conditions that have been tested, suggesting that the primary RNA binding domain and Q-loop are the most crucial elements for RNA release activity. These mutants are also defective for most of the other functions of Rho. The termination defects of the mutants (Y274D, G324D and N340S), which are mainly defective for secondary RNA binding and most likely for the translocase activity, could be restored under relaxed *in vitro* conditions. The functional defects of most of the mutants correlate with their spatial localization in the crystal structure. We also show that mutations in the primary RNA binding domain (Y80C) can affect functions and induce conformational changes in the distal C-terminal domain, which is not predictable from the structure of Rho. Any severe *in vitro* defect was not observed in I382N, which is inconsistent with its *in vivo* phenotype. Probably a modest *in vitro* defect can be amplified under more stringent *in vivo* conditions.

Importance of the polynucleotide interactions in the primary RNA binding domain of Rho in modulating other activities of Rho, apart from recognizing the *rut* site, had been envisioned earlier (Martinez et al., 1996; Pereira and Platt, 1995). Here we found that a specific mutation in position Y80, which directly interacts with the RNA at the primary site, intrinsically makes Rho defective for ATP binding (Table 5), induces conformational changes in the ATP-binding pocket (Figure 3.22(a) and Table 6) and in the surrounding C-terminal domain (Figure 3.22)b)). As the defect in ATP binding and other conformational changes occurred in the absence of RNA binding we propose that this mutation by itself has induced a major allosteric effect in the C-terminal domain, which is located far away from primary RNA binding domain.

Table 7: Summary of different properties of the termination-defective Rho mutants

Mutants	***1^{o} RNA Binding***	***2^{o} RNA[a] Binding***	***ATP Binding***	***Suppression of termination defect[c]***
G51V	++	+/-	++	No
Y80C	-	-	+[b]	No
Y274D	+	-	+	Yes
P279S	++	-	+	No
G324D	+	-	+	Yes
N340S	+	-	++	Yes
I382N	+	+	+++	Not defective *in vitro*
WT	+	++	+++	Not defective

All the activities of the mutants are expressed with respect to that of WT Rho.
[a] Binding activities are for rC_{10} and rC_{25} templates. +/- indicates ~100 fold reduced binding on rC_{25} template.
[b] For ATP binding of Y80C the K_m value is considered.
[c] For the mutants Y274D, G324D and N340S the RNA release efficiency from the stalled EC improves to the level of WT in the presence of 1 mM ATP and NusG.

On the other hand, mutation at G51, located in the same primary RNA binding domain, renders very stable binding with the nucleic acids (Table 3). This leads to severe defects in the RNA release and secondary RNA binding. This suggests that it is important that Rho leaves the *rut* site once it starts tracking the nascent RNA. Based on the properties of these two point mutations in the primary RNA binding domain we propose that this domain of Rho not only works as an "eye" to find the *rut* site but also exerts allosteric control over the downstream interactions upon binding to RNA. Therefore, mutations in this domain block the subsequent steps in the process of RNA release. Psu, an inhibitor of Rho, which inhibits Rho dependent termination by slowing down the rate of ATP hydrolysis, does not interact with the Y80C mutant (Pani et al., 2006). This lack of interaction between the Psu and Y80C mutant might also arise due to conformational changes in the ATP binding/hydrolysis domain.

What is the role of Q-loop? The Q-loop is a structural element, which is located at the entry point of secondary RNA binding domain and protrudes into the central hole of the Rho hexamer. A comparison of the open and closed ring structures of Rho reveals that this loop undergoes major conformational changes upon ring closure (Skordalakes and Berger, 2006) and was found to be protected in the Rho–poly(C) complex from the hydroxyl radical cleavage (Wei and Richardson, 2001a). P279S and earlier reported mutants in this loop (Wei and Richardson, 2001b) are defective in secondary RNA binding and in subsequent activities like ATP hydrolysis and translocation. Based on these results and the spatial location of this loop in the Rho hexamer (Figure 3.19(c)), we propose that this structural element works as a rudder that guides the RNA into the dimeric interface of the secondary RNA binding domain. This proposal is consistent with the "RNA handoff model", where the Q-loop is proposed to be involved in transferring RNA between the subunits during translocation (Skordalakes and Berger, 2006). It is known from the previous works that ATPase or NTPase activity of Rho is required for transcription termination (Howard and de Crombrugghe, 1976; Shigesada and Wu, 1980) and is believed that the free energy generated from the hydrolysis is required for the translocation of Rho along the RNA (Adelman et al., 2006; Brennan et al., 1987). Using a road blocked EC we have uncoupled the transcription elongation from the Rho-dependent RNA release from the EC, which enabled us for the first time to observe a direct correlation between ATP hydrolysis and RNA release by Rho from a stalled EC. The RNA release efficiency and the rate of RNA release improved at high concentration of ATP for the three mutants (Y274D, G324D and N340S) in the secondary RNA binding domain (Figure 3.24). These results suggest that a higher rate of ATP hydrolysis improved their processivity and overall rate of translocation and the free energy from the ATP hydrolysis is used to bring them in the vicinity of the EC. It is likely that the ATP hydrolysis helps Rho to remain bound to the nascent RNA during the "chase", because intrinsically the interactions in the secondary RNA binding domain are weak. On the other hand, RNA release kinetics experiments (Figure 3.24) suggest that NusG is involved only in the RNA release step(s) once Rho reaches the vicinity of the EC, which is consistent with role of NusG that was proposed earlier (Burns et al., 1999). WT Rho on its own is capable of releasing RNA, but the speed of RNA release is increased in the presence of NusG. Early termination that is usually

observed in the presence of NusG (Figure 3.15(a)) is the consequence of this enhanced rate of RNA release. So the requirement of NusG becomes mandatory under *in vivo* conditions where the RNA release has to be performed within a small time window. The RNA release step, in addition to their translocation defect, must be severely compromised in case of the mutants Y274D, G324D and N340S and therefore they are highly dependent on NusG. The final RNA release step may involve a direct interaction of Rho with the EC, so it is possible that the region of Rho defined by these amino acids is involved in the interaction with the EC. Based on the properties of different termination defective mutants of Rho and in the light of open and closed ring hexameric structures complexed with nucleic acids in primary and secondary RNA binding domains we sum-up the sequential steps that lead to the RNA release from the EC. (1) The primary RNA binding domain binds RNA and forms an open ring hexameric Rho. This interaction also involves conformational changes in the C-terminal domain. (2) RNA gets channeled into the secondary RNA binding domain via the Q-loop and the closed ring structure is formed. (3) This activates ATP hydrolysis and onsets the translocation of Rho along the mRNA, which brings Rho in the vicinity of the EC. (4) Rho then releases RNA possibly by pushing the EC or by pulling the RNA out of the EC by its translocase activity. It is also possible that Rho specifically interacts in the RNA exit channel and exerts allosteric effects on the stability of the EC. As NusG is only involved in increasing the rate of RNA release at this step, it is possible that NusG in the presence of Rho makes the EC more prone to termination.

CHAPTER IV

Interaction surface of NusG required for complex formation with the transcription termination factor Rho

4.1 Introduction

NusG is a transcription regulatory protein involved in the modulation of transcript elongation and termination processes. Though NusG is an essential protein in *E. coli,* it is not required for the growth of *Bacillus subtilis* and *Staphylococcus aureus* (Downing et al., 1990; Ingham et al., 1999; Xia et al., 1999). NusG is highly conserved among bacteria and archebacteria and has eukarytotic homologues in yeast and humans. *E. coli* NusG has two distinct globular domains connected by a flexible linker (Knowlton et al., 2003; Steiner et al., 2002). NusG accelerates the rate of transcription elongation both *in vitro* and *in vivo* (Burova et al., 1995) by suppressing transcriptional pauses that involve backtracking by RNAP. NusG in combination with NusA, NusB, NusE and other cellular factors can modify RNAP to create specialized antitermination complex that promote read-through of terminators within ribosomal *rrn* operons (Squires et al., 1993). NusG along with other Nus factors also enhances the stability of the λ N antitermination complex (Mason and Greenblatt, 1991; Nodwell and Greenblatt, 1991) and ensures efficient and processive elongation of the N modified RNAP through Rho dependent and independent terminators (Li et al., 1992).

The transcription terminator Rho interacts with the transcription elongation factor NusG to bring about the termination process efficiently. Knowledge of interaction surface involved in the Rho-NusG complex is essential for understanding the mechanism of termination process. To test whether the two-domains of NusG have a distinct function, the properties of the individual domains were separately investigated both *in vivo* and *in vitro*. In this study, to identify the domain of NusG involved in interaction with Rho, *in vivo* pulldown of Rho was attempted by individual NusG-NTD and NusG-CTD. Mutational and direct binding analyses were used to identify the areas on the solvent-accessible surface of NusG that interact with Rho protein. Experiments involving site-specific Cys-Cys di-sulphide bond formation between Rho and NusG further confirmed the results.

4.2 Materials and Methods

4.2.1 Cloning WT, NTD and CTD of NusG in pET21b, pET33b and pHYD3011

NusG was cloned into NdeI/XhoI sites of pET33b vector, to introduce both His- and HMK-tags at the N-terminal. For this, the *nusG* gene was PCR amplified using gene specific primers (RS114 and RS115) from plasmid pRS119 (Figure 4.1). The ligated DNA was transformed into ultracompetant *E. coli* DH5α cells. The recombinants having the insert were screened using colony PCR and the plasmids were sequenced. In order to specifically phosphorylate the end of NusG via a HMK (heart muscle kinase) tag, a naturally occurring cryptic HMK recognition site, RRKSE (at the position 57-61 amino acids), was removed by introducing a S60A mutation. To make pET33b and pET21b NusG S60A derivatives, Site Directed Mutagenesis (SDM) was done with QuickChange^{TM} XL site-directed kit (Stratagene) using oligos RS304 and RS305 on pRS600 and pRS119 respectively. NusG S60A was subcloned into NdeI/SalI sites of pHYD3011 (a derivative of pBAD vector) for *in vivo* studies. For this, the *nusG* gene was PCR amplified using gene specific primers (RS114 and RS115) from plasmid pRS612. The resultant plasmid was named as pRS695. Similar to earlier report (Richardson and Richardson, 2005), it was found that this mutation did not affect the activity of NusG both *in vivo* and *in vitro*. In all the assays, NusG referred as "WT" contains a S60A change.

To identify the domain of NusG involved in the interaction with Rho, N-terminal domain (NTD) (1-122 aa) and C-terminal domain (CTD) (117-181 aa) were cloned separately into NdeI/XhoI site of pET21b and pET33b vectors and NdeI/SalI sites of pHYD3011. NusG-NTD also carried the S60A mutation. For cloning NusG-NTD into pET33b and pHYD3011, insert was PCR amplified from pRS612 using primers RS114 and RS403. The insert was double digested with restriction enzymes NdeI/XhoI and cloned into double digested vectors (Figure 4.1).

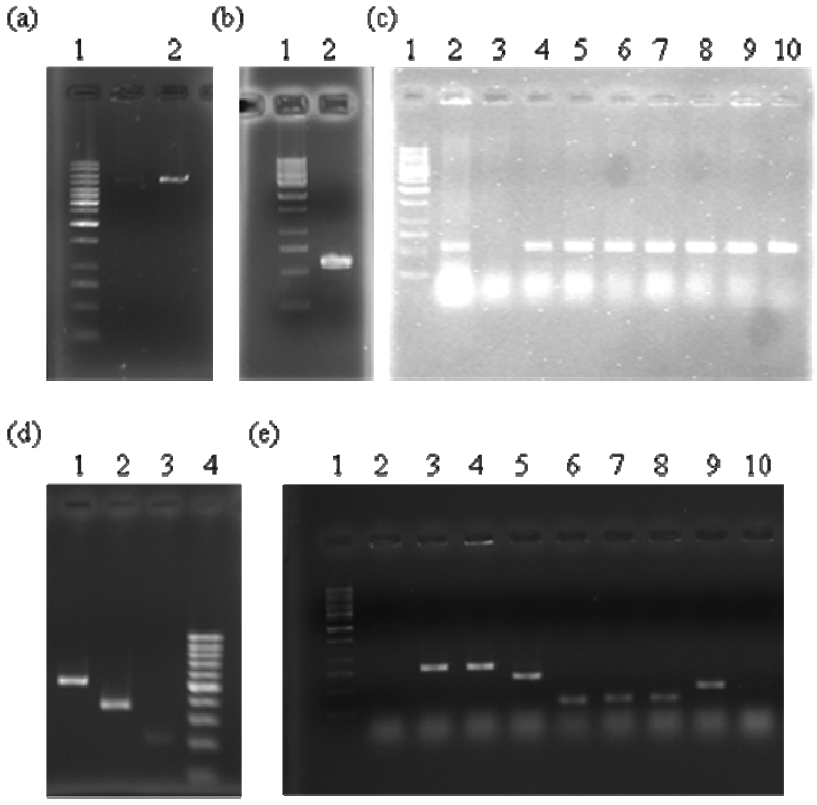

Figure 4.1: Cloning NusG derivatives in pET33b.

(a) Lanes: 1. 1 kb DNA marker; 2. NdeI/XhoI double digested pET33b plasmid (vector) (b) Lanes: 1. 1 kb DNA marker; 2. PCR amplified WT *nusG* gene (insert for cloning). (c) Colony PCR to screen for WT *nusG* in pET33b. Lanes:1. 1 kb DNA marker; 2 and 4-10 shows the *nusG* gene amplified using RS78 and RS79 primers from the recombinant plasmids. (d) Lanes: 1. PCR amplified NusG Δ 157-161 2. PCR amplified NTD of NusG (insert for cloning); 3. PCR amplified CTD of NusG (insert for cloning); 4. 100 bp DNA marker. (e) Colony PCR to screen for NusG derivatives in pET33b. Lanes: 1. 1 kb DNA marker; 3 and 4 shows the *nusG* Δ 157-161 gene amplified using RS78 and RS79 primers from the recombinant plasmids; 5. shows the NTD of NusG amplified using RS78 and RS79 primers from the recombinant plasmids; 9. shows the CTD of NusG amplified using RS78 and RS79 primers from the recombinant plasmids.

For subcloning NTD of NusG in pET21b, insert was PCR amplified from pRS612 using primers RS114 and RS309a. The downstream primer RS309a, did not have a stop codon and this allowed the addition of the 6-His tag from the vector to the C-terminus of NTD transcript (Figure 4.2). For cloning NusG-CTD into pET33b and pHYD3011, insert was PCR amplified from pRS612 using primers RS308 and RS115 (Figure 4.1). NusG-CTD PCR amplified using primers RS308 and RS116 from pRS612 was double digested with NdeI/XhoI and was cloned into the NdeI/XhoI sites of pET21b (Figure 4.2). Clonings were done following the same procedure as above.

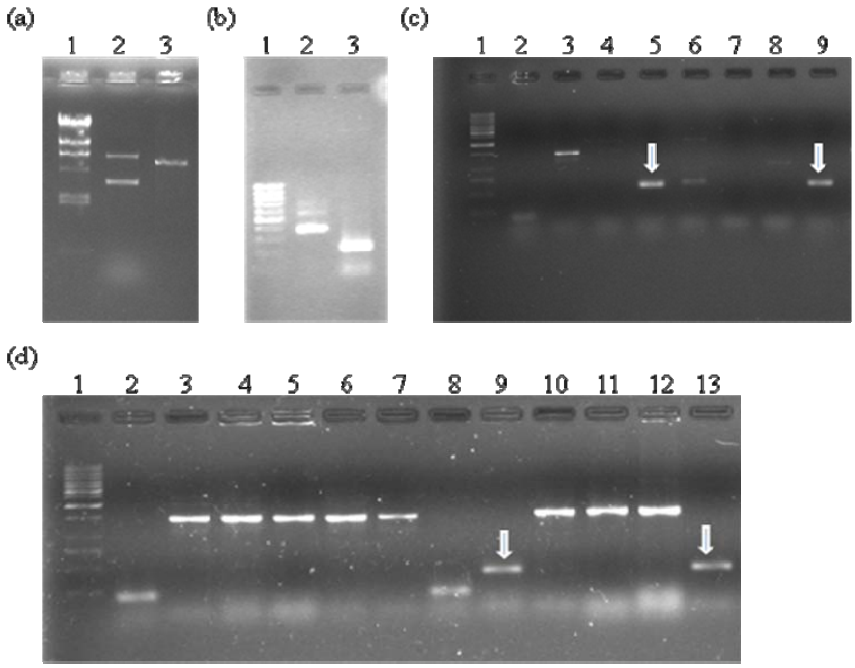

Figure 4.2: Cloning NTD and CTD of NusG in pET21b.

(a) Lanes: 1. λ Hind III DNA marker; 2. pET21b plasmid; 3.NdeI/XhoI double digested pET21b plasmid (vector) (b) Lanes: 1. 100 bp DNA marker; 2. PCR amplified NTD of NusG (insert for cloning); 3. PCR amplified CTD of NusG (insert for cloning). (c) Colony PCR to screen the recombinant plasmids for NTD of NusG with RS78/79 (T7 promoter and terminator specific) primers. (d) Colony PCR to screen the recombinant plasmids for CTD of NusG with RS78/79 primers. Positive clones are shown with arrows in the figure.

4.2.2 Cloning of deletion derivatives of NusG in pET21b and pHYD3011

Five deletion derivatives were constructed in the CTD of NusG of which, four (Δ145-149, Δ148-152, Δ157-161, Δ169-173) were 5 aa deletion derivatives while one was a 10 aa C-terminal deletion (Δ172-181). The insert for cloning NusG Δ145-149, Δ148-152 and Δ157-161 in pET21b were made by overlapping PCR. The C-terminal fragment downstream of the deletion in case of Δ145-149 was PCR amplified using primers RS330 and RS116 (Figure 4.3(a)). RS330 primer is a 30mer with 15 nucleotides upstream of the deletion and 15 nucleotides downstream of the deletion. The C-terminal fragment made from this PCR reaction (used as the reverse primer) and RS114 (forward primer from 5' end of NusG gene) were used for amplifying the NusG insert having the deletion (Figure 4.3(b) lane 3). The insert was double digested with restriction enzymes NdeI/XhoI and was cloned into the NdeI/XhoI sites of pET21b (Figure 4.3(d)). NusG Δ148-152 and Δ157-161 were cloned into pET21b, following the same procedure as above, with the exception that the

forward primers used for amplifying the NusG fragment downstream of the deletions were RS385 and RS331 respectively (Figure 4.3(c)). NusG Δ145-149, Δ148-152 and Δ157-161 were then PCR amplified from their corresponding pET21b plasmids using RS114 and RS115 primers and subcloned into pHYD3011 at NdeI/XhoI. NusG Δ157-161 was also subcloned into pET33b at NdeI/XhoI (Figure 4.1(e)). Insert for cloning NusG Δ169-173 and Δ172-181 in pHYD3011 were PCR amplified by using RS114 as forward primer and RS384 and RS383 as reverse primers respectively. NusG Δ169-173 was then PCR amplified from pHYD3011 NusG Δ169-173 plasmid using RS114 and RS116 primers (Figure 4.3(c) lane 4) and subcloned into pET21b at NdeI/XhoI sites (Figure 4.3(g)). NusG Δ172-181 insert PCR amplified by using RS114 and RS400 was double digested with NdeI/XhoI and was cloned into pET21b at NdeI/XhoI sites (Figure 4.3(h)). Clones were confirmed by sequencing.

4.2.3 Site Directed Mutagenesis (SDM) to make point mutations in NusG

It was reported that *in vivo*, G146D mutation in the CTD of NusG was defective for Rho-dependent termination (Harinarayanan and Gowrishankar, 2003). To make pET21b NusG G146D S60A, SDM was done using oligos RS304 and RS305 on pRS109 (pET21b NusG G146D). For *in vivo* studies NusG G146D S60A was then subcloned into NdeI/SalI sites of pHYD3011 from pRS618. Eleven other point mutants (NusG R135E, N145V, V148N, R157E, L158Q, K159D, V160N, I164A, R167E, T169A and V171N) were made on CTD of full length NusG by SDM to identify the residues involved in the Rho-NusG interaction. SDM were performed with QuickChange^{TM} XL site-directed kit (Stratagene) on pRS695 (pHYD3011 NusG S60A) using suitable primers (for oligos encoding the necessary aa substitutions, refer Appendix II). Seven of the above point mutants (NusG V148N, L158Q, V160N, I164A, R167E, T169A and V171N) were also made on pRS612 (pET21b NusG S60A). Six point mutants (NusG E19L, V22N, L26E, W80G, V83N and V89N) were made on NTD of full length NusG by SDM to study whether NTD of NusG is involved in Rho-NusG interaction. These point mutants were made on pRS612 (pET21b NusG S60A) using suitable primers (for oligos encoding the necessary aa substitutions, refer Appendix II). PCR products were subjected to DpnI digestion to digest the parental plasmid and transformed into DH5α ultra competent cells. Plasmids isolated from the transformants were sequenced to confirm the mutations.

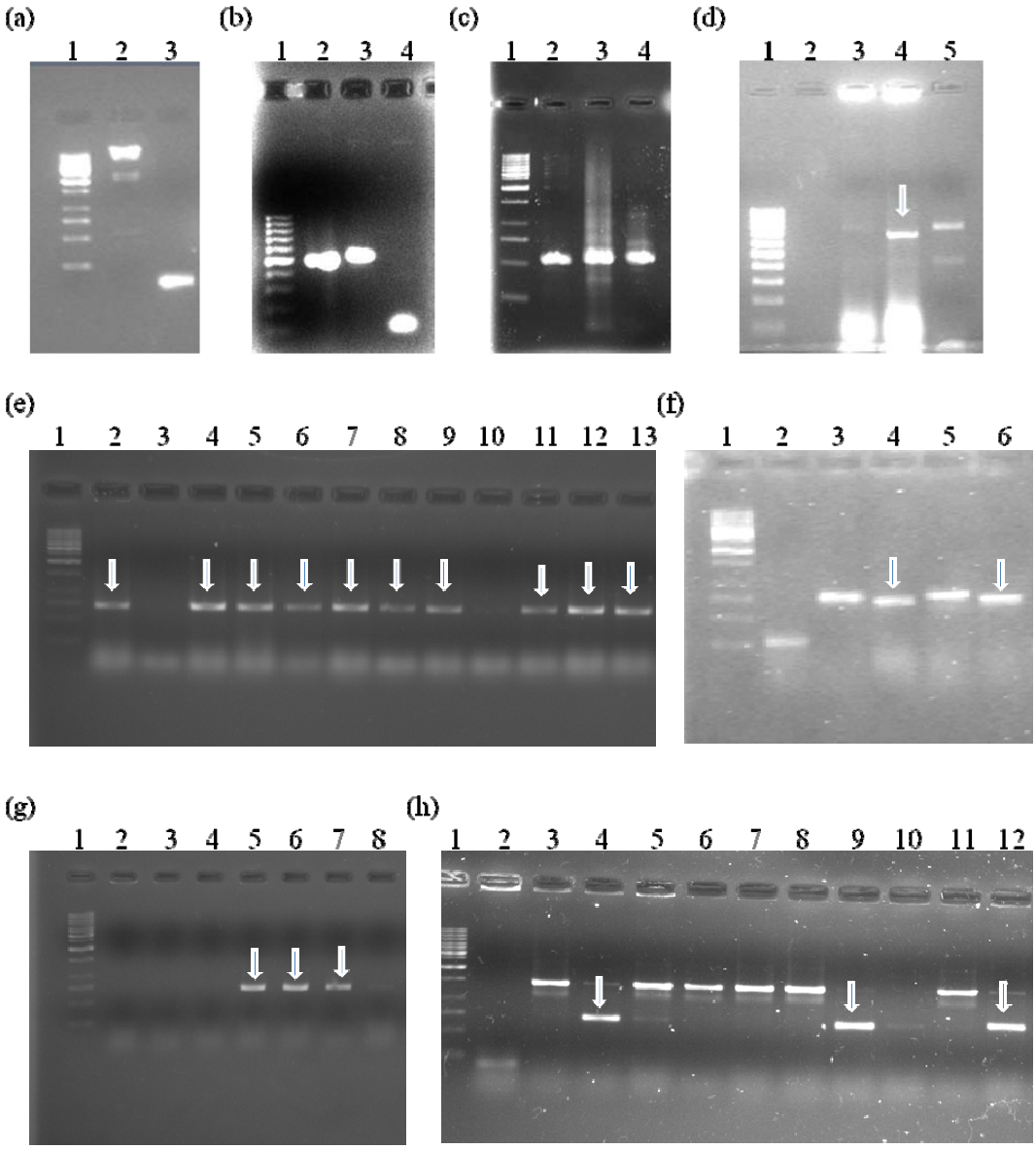

Figure 4.3: Cloning deletion mutants of NusG in pET21b.

(a) Lanes: 1. 1 kb DNA marker (MBI); 2. λ Hind III DNA marker; 3. PCR amplified C terminal fragment of Δ145-149 (b) Lanes: 1. 100 bp DNA marker; 2. PCR amplified NusG Δ172-181 gene (insert) used for cloning; 3. PCR amplified NusG Δ145-149; 4. PCR amplified C terminal fragment of NusG Δ148-152 (c) Lanes: 1. 1 kb DNA marker; 2. PCR amplified NusG Δ148-152; 3. PCR amplified NusG Δ157- 161; 4. PCR amplified NusG Δ169-173 (d) Colony PCR to screen the recombinant plasmids for NusG Δ145-149 with RS78/79 primers. (e) Colony PCR to screen the recombinant plasmids for NusG Δ148-152 (f) Colony PCR to screen the recombinant plasmids for NusG Δ157-161 (g) Colony PCR to screen the recombinant plasmids for NusG Δ169-173 (h) Colony PCR to screen the recombinant plasmids for NusG Δ172-181. Positive clones are shown with arrows in the figure.

4.2.4 SDM to make single cysteine derivatives of NusG

Chemical crosslinker Cu-phenanthroline that forms disulphide bond between two Cys residues can be used to study the interaction between Rho and NusG. As the WT NusG does not contain any Cys residue, eight single Cys derivatives of NusG at positions S25, S85, G119, T126, V147, S156, S161, A168 and a double Cys derivative NusG S25C S161C were made by using QuickChange^{TM} XL site-directed kit (Stratagene). SDM were done on pRS612 (pET21b NusG S60A) using suitable primers (for oligos encoding the necessary aa substitutions, refer Appendix II). PCR products were subjected to DpnI digestion to digest the parental plasmid and transformed into DH5α ultra competent cells. Plasmids isolated from the transformants were sequenced to confirm the mutations.

4.2.5 SDM to make single cysteine derivatives of Rho

For silencing the single Cys residue at 202 position of Rho, SDM was done to make C202S on pRS96 using primers RS409 and RS410. The resultant plasmid was named as pRS757. Rho R221C was PCR amplified from pHYD564 using DeepVent (NEB) proof reading enzyme and was cloned into NdeI/XhoI sites of pET21b. SDM was performed to make C202S on this plasmid so that the Rho protein from the resultant plasmid carries a single Cys at position 221. The two single Cys derivatives of Rho made on pRS757 by SDM were T217C and K224C. SDM were carried out using suitable primers (for oligos encoding the necessary aa substitutions, refer Appendix II) by following the methodology described in QuickChange^{TM} XL site-directed kit (Stratagene). Non His tag Rho T217C were also made by SDM on pRS100.

4.2.6 Strain constructions for *in vivo* assays

Bacterial strains, plasmids and phages used in this study are listed in Appendix I. Arabinose forms toxic intermediate compound in MC4100 strain due to the presence of a mutation in *araD* gene. To overcome this toxicity problem, either the strain was made *araD*$^{+}$ or *araBADC* genes were deleted so that NusG derivatives can be overexpressed from P_{BAD} promoter by using arabinose as inducer. RS689 was constructed by moving *Δara::tet*^{R} by P1 transduction from LMG194 into GJ3191. RS692 was made by replacing the shelter plasmid pHYD751 present in RS689 with pHYD763. This strain (RS692) containing a chromosomal disruption of *nusG* by a kanamycin resistance cassette was used

to determine if NusG variants could serve as the sole source of NusG in cells. The ability of individual domains of NusG to compete out WT NusG was tested by overexpressing NusG-NTD and NusG-CTD from P_{BAD} promoter in the presence of chromosomally encoded *nusG*. For this, *araD*$^{+}$ was transduced into MC4100 by using P1 lysate made on MG1655 and the resultant strain was named as RS353.

Recombinant λRS88 carrying P_{lac}-*lacZYA* construct was made as described in Chapter III. By lambda transduction using this recombinant λRS88, P_{lac}-*lacZYA* cassette was inserted as single copy at the phage λ attachment site of strain GJ3161 (RS257), resulting in strain RS445. Colony PCR of the lysogens were carried out using the RS58/RK1 primers to confirm the presence of the cassette in the chromosome of MC4100 (Figure 4.4(a)). *E. coli att*B and λ *att*P specific primers SBM15, 16 and 17 were used for PCR to confirm that they were single copy insertions at the λ phage insertion site in the bacterial chromosome (Powell et al., 1994) (Figure 4.4(b)). Refer Appendix III for protocol on λ lysate preparation and λ transduction. RS445 and GJ5153 strains transformed with pHYD763 were made *ΔnusG::kan*^{R} by P1 transduction using lysate made on GJ3191 resulting in strains RS714 and 801 respectively. *Δara::tet*^{R} was moved in to both of these strains by P1 transduction and named as RS715 and RS802 respectively.

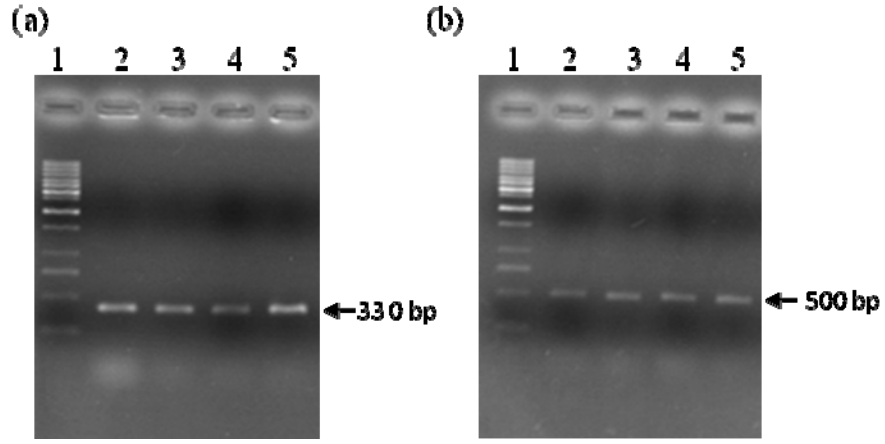

Figure 4.4: Colony PCR to screen the ΔT_{R1} lysogens

(a) ΔT_{R1} lysogens PCR amplified with RS58/RK1 primers. Lanes: 1. 1 kb DNA ladder (MBI); 2-5. Positive lysogens amplified to the expected size of 330 bp; (b) PCR to screen monolysogens. Lane 1. 1 kb DNA ladder (MBI). Lanes 2-5. Monolysogen recombinants amplified to the expected size of 500 bp using primers SBM 15, 16, and 17.

It was reported that NusG is essential in *E. coli* cells because it promotes Rho-dependent termination upstream of the toxic *rac* prophage *kil* gene (Cardinale et al., 2008). For testing the presence of *rac* prophage in the strains used for *in vivo* assays, colony PCR were carried out to amplify *rac* prophage sequence from different bacterial strains. As expected *rac* prophage sequence was amplified from strains MG1655 and MC4100 whereas there was no amplification from strains MDS42 and RSW472 (MGΔrac). Surprisingly it was found that from strains RS692, RS715 and RS802 *rac* prophage sequence was deleted (Figure 4.5).

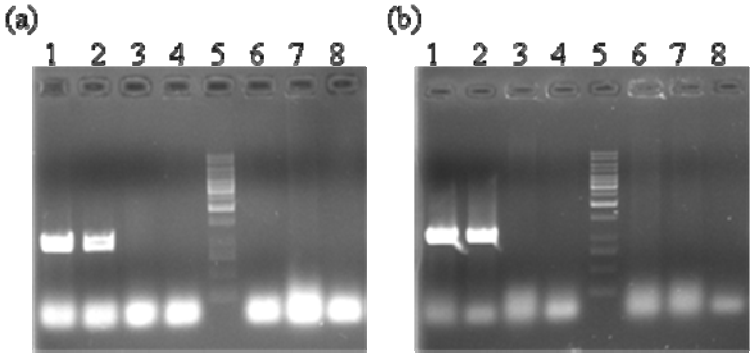

Figure 4.5: Colony PCR to amplify *rac* prophage sequence from different bacterial strains

(a) PCR amplification of *rac* sequence using primers RS405 and RS406. Lanes: 1. MG1655; 2. MC4100; 3. MDS42; 4. RSW472 (MGΔrac); 5. 1 kb DNA ladder (MBI); 6. RS692; 7. RS715; 8. RS802 (b) PCR amplification of *rac* sequence using primers RS407 and RS408. Lanes: 1. MG1655; 2. MC4100; 3. MDS42; 4. RSW472 (MGΔrac); 5. 1 kb DNA ladder (MBI); 6. RS692; 7. RS715; 8. RS802.

4.2.7 *In vivo* characterization of NusG mutants

4.2.7.1 Measurement of *in vivo* termination defects of the NusG mutants through beta- Galactosidase assay

To get a quantitative measure of the termination defects of the NusG mutants, the ratio of β-galactosidase made from a *lacZ* reporter fused to a Rho dependent terminator (P_{lac}-H-19B *nutR/*T_{R1}*-lacZYA*) to that without the terminator (P_{lac}-*lacZYA*) was measured (read-through efficiency =%RT). This Rho-dependent terminator is derived from the *nutR cro* region of a lambdoid phage H-19B. RS715 and RS802 strains with these reporter fusions in single copy were transformed with the plasmids carrying the WT and mutant derivatives of NusG under the arabinose inducible promoter P_{BAD}. The measurements of β-

galactosidase activities were done in a microtiter plate using a Spectramax plus plate reader following the procedure described in the Appendix III. Beta-Galactosidase values were average of four to five independent measurements. The ratio of beta–Galactosidase values in the presence and absence of T_{R1} terminator gives the efficiency of terminator read-through (%RT).

4.2.7.2 *In vivo* growth defect of NusG derivatives

Effect of overexpression of WT and individual domains of NusG (NTD and CTD) were studied by overexpressing them from the strong inducible P_{BAD} promoter (induced by arabinose) residing on the plasmid. Serially diluted overnight culture of RS353 strain transformed with these plasmid were spotted onto LB plates in the absence and in the presence of 0.2% arabinose and grown overnight at 37 °C.

To test the effect of the expression of NusG deletion derivatives on cell viability, plasmids encoding NusG Δ145-149, Δ148-152, Δ157-161, Δ169-173 and Δ172-181 under the control of the P_{BAD} promoter were transformed into RS692 strain. Transformants were repeatedly streaked and grown at 42 ˚C to remove the shelter plasmid pHYD763.

To study the *in vivo* growth defect of NusG point mutants, RS692 strain was transformed with pHYD3011 plasmid carrying WT or mutant derivatives of NusG under the control of arabinose inducible promoter P_{BAD}. Shelter plasmid was removed from these transformants by repeated streaking at 42 ˚C. A single colony was picked and inoculated in 1 ml LB and incubated at 37 ˚C overnight in shaking waterbath. 5 µl of serially diluted overnight culture of each strain were spotted onto LB plates in the absence and in the presence of 0.02% arabinose and grown overnight at 30 °C, 37 °C and 42 °C. Plated were scanned the next morning.

4.2.8 Purification of proteins

4.2.8.1 Purification of WT NusG, NusG-NTD and NusG-CTD

pET21b plasmid with WT, NTD and CTD of NusG cloned under the control of phage T7 promoter regulated through a lac operator and resident *lacI* gene were transformed into the BL21(DE3) strain that contains T7 RNA Polymerase gene under *lac OP* control. Proteins

were over expressed by inducing the culture at OD_{600} of 0.4 with 0.1 mM IPTG for 3 hr at 37 °C. His tagged NusG derivatives were purified using Ni-NTA column (Figure 4.6). The cells were collected by centrifuging the cell culture at 10000 rpm for 5 min. The cells were then resuspended in lysis buffer (pH 8.0) containing 100 mM NaH_2PO_4, 300 mM NaCl, 10 mM imidazole, 1 mg/ml Lysozyme and 50 µg/ml PMSF. After resuspending the cells thoroughly, Lysozyme was added and incubated on ice with constant stirring for 30 min. The cells were sonicated till solution turns yellowish and complete lysis takes place. The cells were centrifuged after lysis at 4 °C, 12000 rpm for 30 min. Supernatant was transferred to prechilled fresh tube. The Ni-NTA beads were packed in column that works under gravity. And the columns were equilibrated with 5 bed volumes of lysis buffer. The supernatant was applied to the column (typically 5 ml bed volume). The unbound fraction was allowed to flow through. The fraction was collected for analysis. The column was washed with 10 bed volumes of wash buffer (pH 8.0) containing 100 mM NaH_2PO_4, 300 mM NaCl, 20 mM imidazole. The protein was eluted with 15 ml elution buffer composed of 100 mM NaH_2PO_4, 300 mM NaCl, 500 mM imidazole. Various fractions were then checked on 10% SDS-PAGE. Pure protein was dialysed for 10 hr against storage buffer (10 mM Tris-HCl (pH 7.9), 0.1 mM EDTA, 0.1 mM DTT, 100 mM NaCl and 5% (v/v) glycerol) with three buffer changes and concentrated using Amicon YM10 (Millipore). Glycerol to the final concentration of 50% (v/v) was added to the concentrated pure protein and was aliquoted in to 100 µl fraction and stored at ⁻70 ºC.

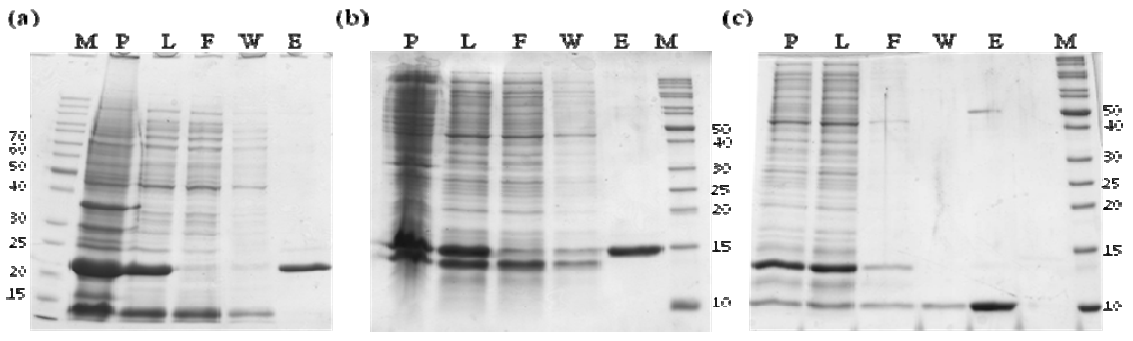

Figure 4.6: Purification of NusG S60A, NusG-NTD and NusG-CTD through Ni-NTA column

(a) Purification of WT NusG protein (b) Purification of NusG NTD protein (c) Purification of NusG CTD protein. M, Marker; P, Pellet, L, Lysate; F, Flowthrough, W, Wash, E, Elute.

4.2.8.2 Purification of deletion derivatives of NusG

The five aa NusG deletion derivatives having His tag at the C-terminal end were purified using Ni–NTA beads (Qiagen) (Figure 4.7). NusG Δ157-161was purified under native condition the same way as given above, whereas NusG Δ145-149, Δ148-152 and Δ169-173 were purified under denaturing conditions since they were largely in an insoluble form. These proteins were solubilized with 8 M urea and purified using Ni-NTA column. WT NusG was also purified under denaturing condition and its activity was tested to confirm that this purification procedure does not affect the activity of the proteins. NusG deletion derivatives cloned in the pET21b vector were transformed into *E. coli* BL21(DE3) strain. About 10-15 colonies were picked from the transformation plates and inoculated in 5 ml LB with ampicillin. This primary culture was grown at 37 ºC for about 3 hr and then 2% of the primary culture was subcultured in 200 ml LB with ampicillin. Culture was grown in a shaker incubator till an OD_{600} of 0.4-0.5 and was induced with IPTG to a final concentration of 0.1 mM. The growth was continued for another 3 hr and was stopped by chilling the culture on ice. The cells were harvested by centrifugation at 12000 rpm for 5 min at 4 °C. The pellet was then resuspended well by repeated pipeting, in 25 ml of lysis buffer (100 mM NaH_2PO_4, 10 mM Tris-HCl (pH 8.0), 300 mM NaCl, pH adjusted to 8.0) with 8 M urea. It was incubated for 1 hour at 4 °C, for the solubilization of the protein, with constant stirring. The lysate was centrifuged at 13,000 rpm for 30 min at 4 °C and the supernatant was carefully transferred to a fresh pre-cooled falcon tube. The lysate was loaded on to a Ni-NTA column pre-equilibrated with lysis buffer. The flow through was collected and the column was washed with 30 ml wash buffer (100 mM NaH_2PO_4, 10 mM Tris-HCl, 300 mM NaCl, pH adjusted to 6.3) with 8 M urea and the wash was collected. His tagged NusG deletion proteins were eluted with 15 ml of elution buffer (100 mM NaH_2PO_4, 10 mM Tris-HCl, 300 mM NaCl, pH adjusted to 4.5) with 6 M urea. The load, wash and elute samples were loaded onto a 15% SDS-PAGE for analyses. The elute were then dialyzed by giving buffer changes at 2 hr interval against storage buffer (10 mM Tris-HCl (pH 7.9), 0.1 mM EDTA, 0.1 mM DTT, 100 mM NaCl and 5% (v/v) glycerol) with 4 M, 3 M, 2 M and 1 M urea. Dialysis was further continued with two more buffer changes with storage buffer without urea. The protein was then centrifuged at 12000 rpm for 15 min at 4 °C to remove any protein aggregates and concentrated using Amicon YM10 (Millipore).

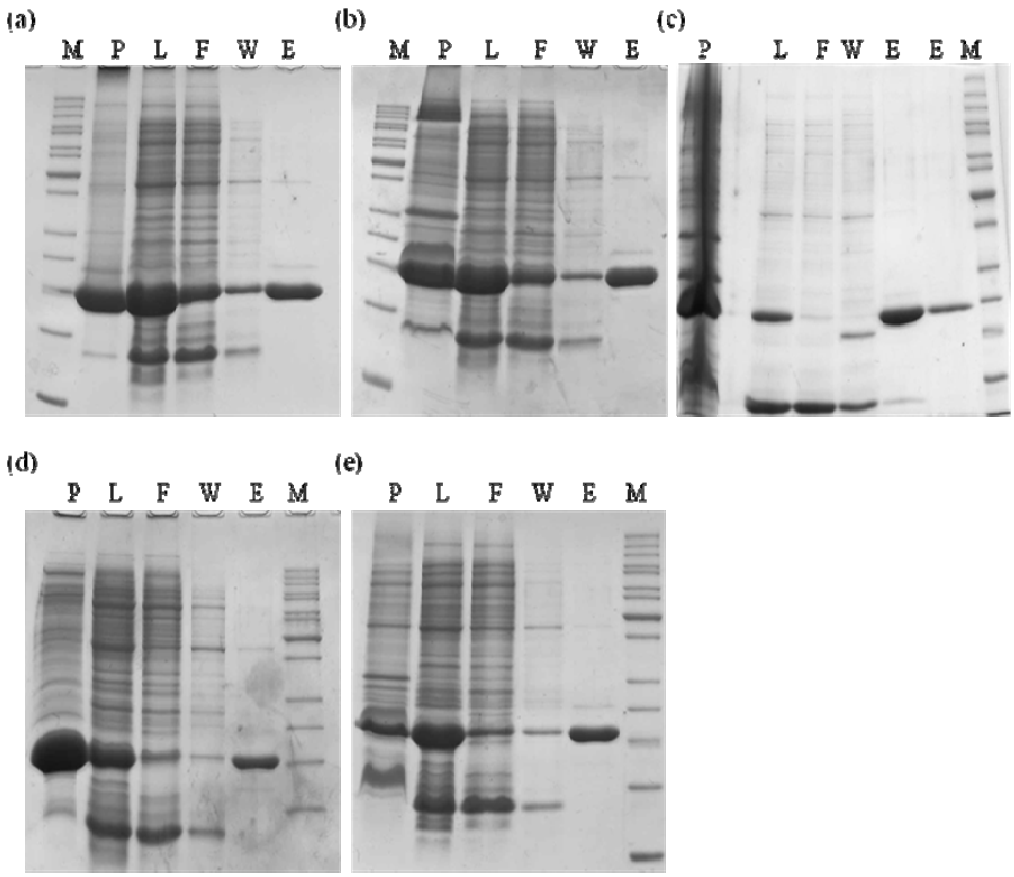

Figure 4.7: Purification of deletion mutants of NusG through Ni-NTA column

(a) Purification of NusG Δ145-149 protein under denaturing condition (b) Purification of NusG Δ148-152 protein under denaturing condition (c) Purification of NusG Δ157-161 protein under native condition (d) Purification of NusG Δ169-173 protein under denaturing condition (e) Purification of WT NusG protein under denaturing condition. M, Marker; P, Pellet, L, Lysate; F, Flow through, W, Wash, E, Elute.

4.2.8.3 Purification of point mutants of NusG

The pET21b vectors containing NusG L158Q, V160N, I164A, R167E, T169A were transformed into BL21(DE3) strain. They were purified from BL21(DE3) after induction at 37 ºC for 3 hr using Ni-NTA beads (Qiagen) under native condition (Figure 4.8). While NusG G146D, V148N and V171N protein over expression were induced at 18 ºC for 14 hr. Purifications were done using Ni-NTA beads under similar conditions as described earlier for WT NusG purification (Figure 4.8). NusG-NTD mutants E19L, V22N, L26E and V83N were purified under denaturing conditions while NusG W80G and V89N were purified under native conditions using Ni-NTA beads (Figure 4.9).

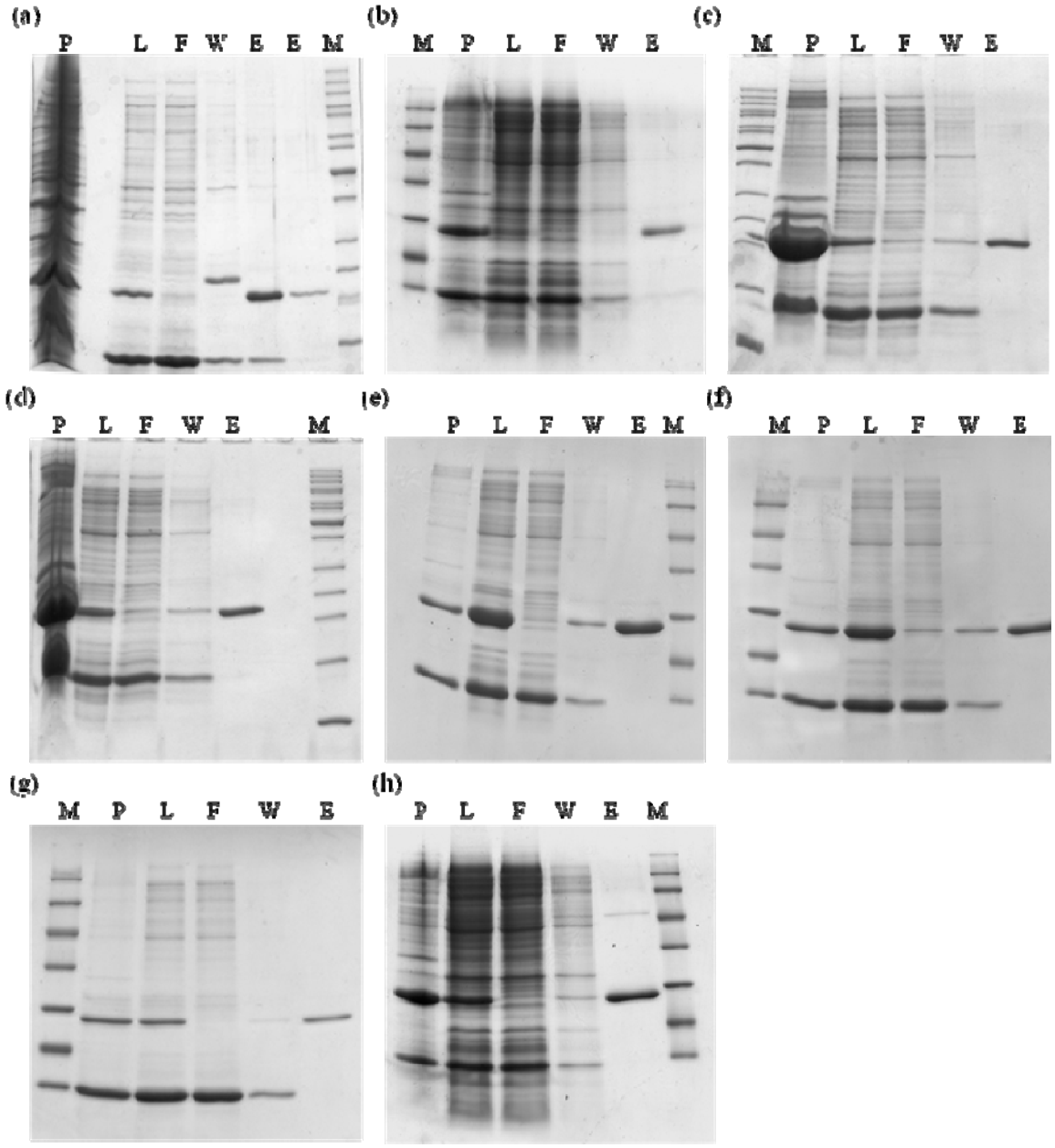

Figure 4.8: Purification of point mutants in NusG-CTD through Ni-NTA column

(a) Purification of NusG G146D (b) Purification of NusG V148N (c) Purification of NusG L158Q (d) Purification of NusG V160N (e) Purification of NusG I164A (f) Purification of NusG R167E (g) Purification of NusG T169A (h) Purification of NusG V171N. M, Marker; P, Pellet, L, Lysate; F, Flow through, W, Wash, E, Elute.

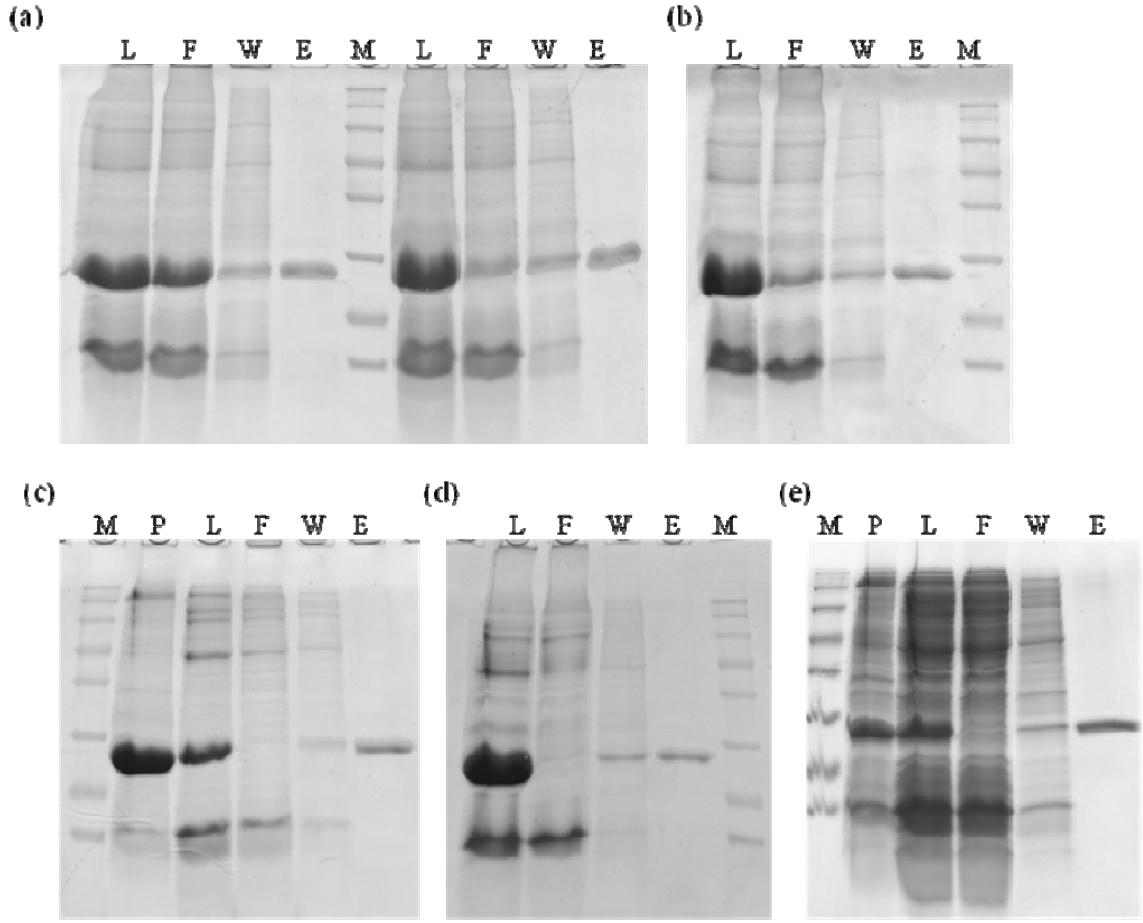

Figure 4.9: Purification of point mutations in NusG-NTD through Ni-NTA column

(a) Purification of NusG E19L and NusG L26E (b) Purification of NusG V22N (c) Purification of NusG W80G (d) Purification of NusG V83N (e) Purification of NusG V89N. M, Marker; P, Pellet, L, Lysate; F, Flow through, W, Wash, E, Elute.

4.2.8.4 Purification of single cysteine derivatives of NusG

Various Cys derivatives of NusG with His tag at C-terminal were purified from the BL21(DE3) strain transformed with pET21b plasmid containing the mutant *nusG* gene (Figure 4.10). Purifications were carried out under reducing condition to prevent the dimerisation of NusG. Protein was expressed in BL21(DE3) cells by inducing at OD_{600} of 0.4 with 0.1 mM IPTG at 37 °C. The cells were resuspended in lysis buffer (pH 8.0) containing 100 mM NaH_2PO_4, 300 mM NaCl, 10 mM imidazole, 20 mM 2-mercaptoethanol and 50 µg/ml PMSF. 1 mg/ml Lysozyme was added and incubated on ice with constant stirring for 30 min. The cells were sonicated till complete lysis.

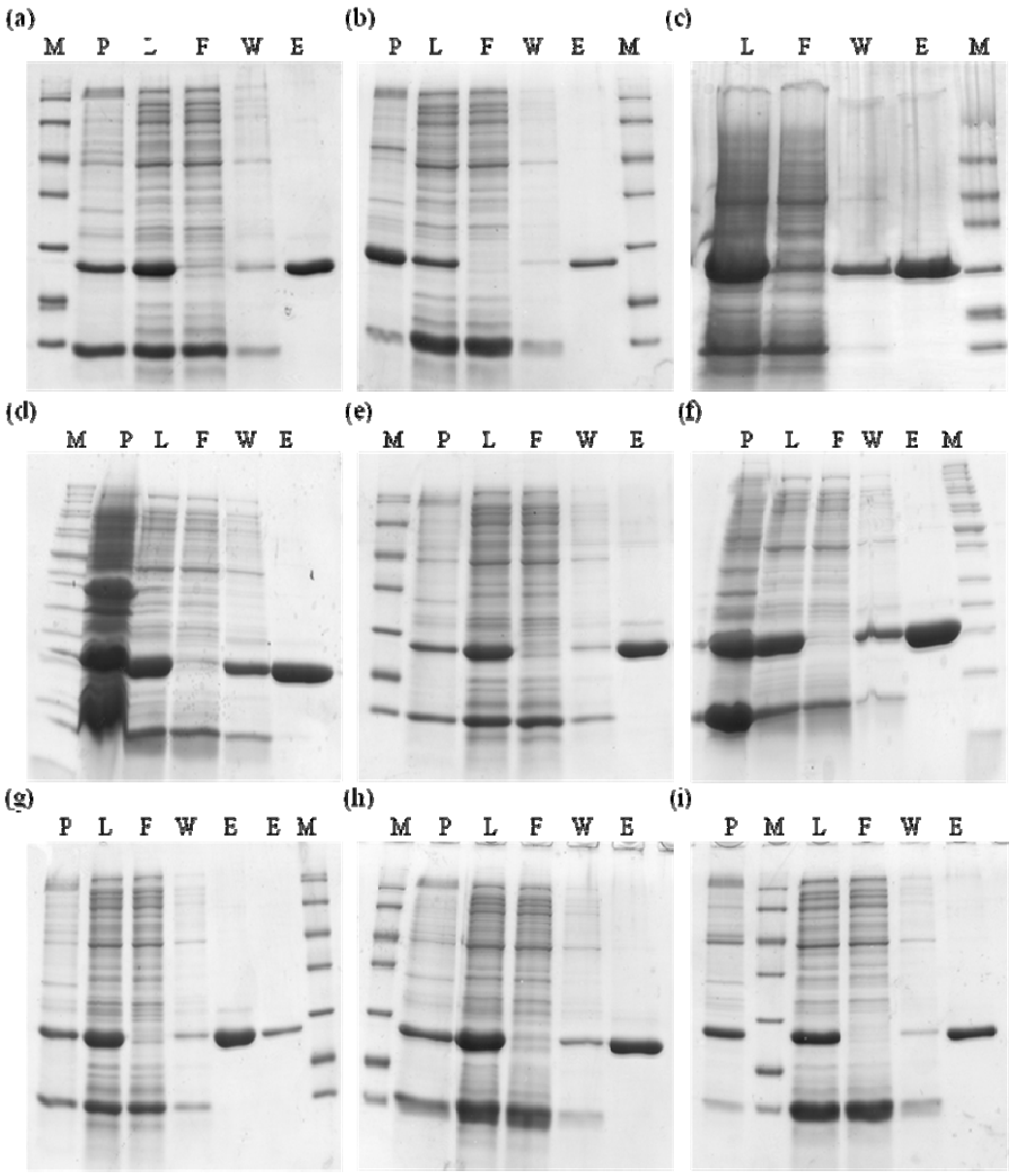

Figure 4.10: Purification of single Cys derivatives of NusG through Ni-NTA column

(a) Purification of NusG S25C (b) Purification of NusG S85C (c) Purification of NusG G119C (d) Purification of NusG T126C (e) Purification of NusG V147C (f) Purification of NusG S156C (g) Purification of NusG S161C (h) Purification of NusG A168C (i) Purification of NusG S25C S161C. M, Marker; P, Pellet, L, Lysate; F, Flowthrough, W, Wash, E, Elute.

The cells were centrifuged after lysis at 4 °C; 12000 rpm for 30 min. Supernatant was transferred to prechilled fresh tube. The Ni-NTA beads were packed in column. The columns were equilibrated with 5 bed volumes of lysis buffer. The supernatant was applied to the column (typically 5 ml bed volume). The unbound fraction was allowed to flow

through. The fraction was collected for analysis. The column was washed with 10 bed volumes of wash buffer (pH 8.0) containing 100 mM NaH_2PO_4, 300 mM NaCl, 20 mM imidazole, 20 mM 2-mercaptoethanol and 50 µg/ml PMSF. The protein was eluted with 15 ml elution buffer composed of 100 mM NaH_2PO_4, 300 mM NaCl, 250 mM imidazole, 50 mM 2-mercaptoethanol and 50 µg/ml PMSF. Pure protein was dialysed for 10 hr against storage buffer (10 mM Tris-HCl (pH 7.9), 0.1 mM EDTA, 100 mM NaCl, 50 mM DTT and 5% (v/v) glycerol) with three buffer changes. Protein was concentrated in Amicon YM10 and stored in storage buffer containing 50% (v/v) glycerol.

4.2.8.5 Purification of Non his tag WT Rho

Rho protein was expressed in BL21(DE3) over expression strain. Cells were induced at 0.5 OD_{600} with 1 mM IPTG for 3 hr at 32 °C. The cell pellet from 1 litre culture was about 5 g. The pellet was resuspended in grinding buffer (0.05 M Tris-HCl (pH 7.8), 2 mM EDTA, 0.1 mM DTT, 1 mM 2-mercaptoethanol, 0.233 M NaCl, 5% (v/v) glycerol and 50 µg/ml PMSF). Lysozyme was added to the final concentration of 1 mg/ml. The mix was incubated on ice for about 20 min. 0.05% sodium deoxycholate was then added to the mix and incubated on ice for an additional 30 min. The sample was sonicated for 6 min thrice or till complete lysis occurs. The lysate was collected after spinning the sonicated sample at 12000 rpm for 30 min. The lysate was incubated at 4 ºC and Polyethylamine (pH 7.9) was slowly added with constant stirring, to a final concentration of with 0.3%. The stirring was continued for another 30 min. The supernatant was again collected after spinning the sample at 12000 rpm for 30 min in cold. 50% ammonium sulphate was added to the supernatant and incubated in cold room for 45 min under constant stirring. The ammonium sulphate precipitate was collected and dissolved in TGED (10 mM Tris-HCl (pH 7.8), 0.1 mM EDTA, 0.1 mM DTT, 5% (v/v) glycerol) with 100 mM NaCl (Figure 4.11(a)). The protein was dialysed against the same buffer for about 12 hr with three buffer changes. The protein was loaded on Heparin column and the bound protein was eluted *via* a step gradient with increasing NaCl concentrations. The fractions were checked for the presence of protein by running in a 12% SDS-PAGE (Figure 4.11(b)). Since the fractions containing Rho thus obtained were not pure, those fractions were pooled and dialysed against 1 L of TGED with 0.1 M NaCl, with two buffer changes O/N. The protein was passed through Mono-S column (strong cation exchanger) using AKTA purifier (Amersham). Protein was eluted with a linear concentration gradient of NaCl in TGED buffer. Rho protein was not

bound to the column and came out in the flowthrough and wash fractions, while the contaminant proteins were present in the elute fractions (Figure 4.11(c)). The pure Rho protein fractions were pooled and concentrated in storage buffer (10 mM Tris-HCl (pH 8.0), 0.1 mM DTT, 0.1 mM EDTA, 100 mM KCl) with 5% (v/v) glycerol by using Amicon YM 100 (Millipore). After concentrating the sample to about 3 ml, the protein was dialysed against storage buffer with 50% (v/v) glycerol.

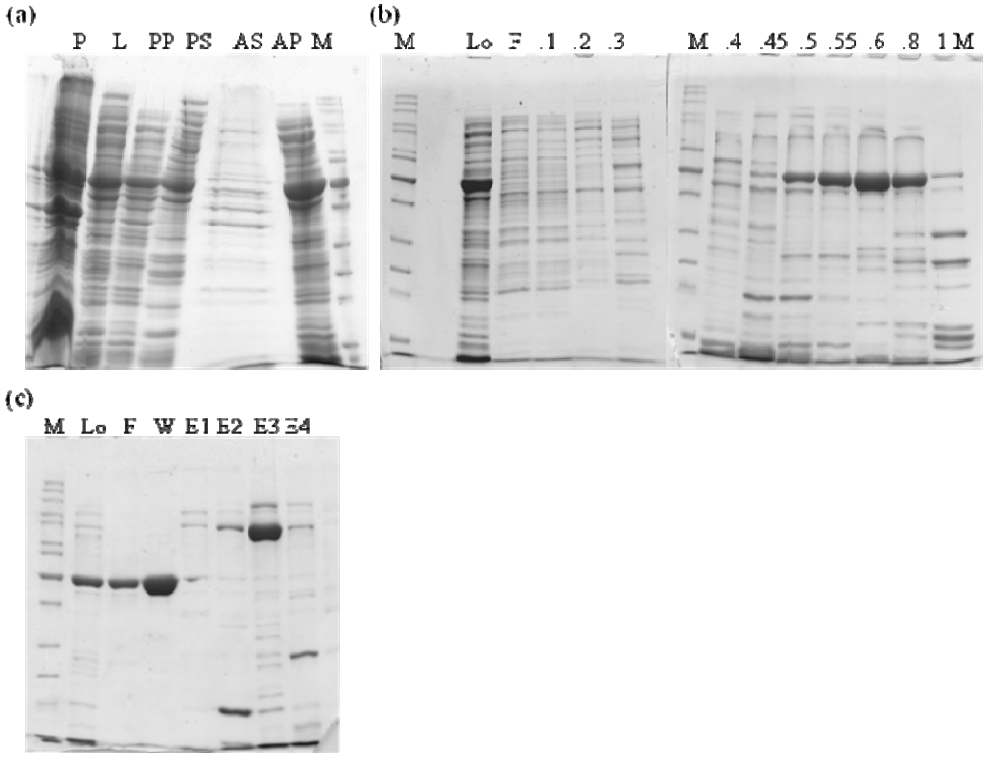

Figure 4.11: Purification of non His tag WT Rho

(a) P, Pellet; L, lysate; PP, Polymin P pellet; PS, Polymin P supernatant; AS, Ammonium sulphate supernatant, AP Ammonium sulphate pellet. (b) Purification through Heparin column by batch elution with NaCl gradient. M, Marker; Lo, Load; F, Flowthrough. Rho eluted at 0.5 - 0.8 M NaCl. (c) Purification through Mono S column. M, Marker; Lo, Load; F, Flowthrough; W, wash; E1, E2, E3, elution fractions. Rho protein was present in flow through and wash fractions.

4.2.8.6 Purification of single cysteine derivatives of Rho

E. coli strain BL21(DE3) harboring the recombinant plasmids with Rho single Cys derivatives were grown at 37 °C in LB medium containing ampicillin to OD_{600} 0.4 and then induced with IPTG (final concentration 1 mM). Cells were harvested 4 hr after induction and purified using Ni-NTA column followed by Heparin column as described earlier in Chapter III for WT Rho purification (Figure 4.12).

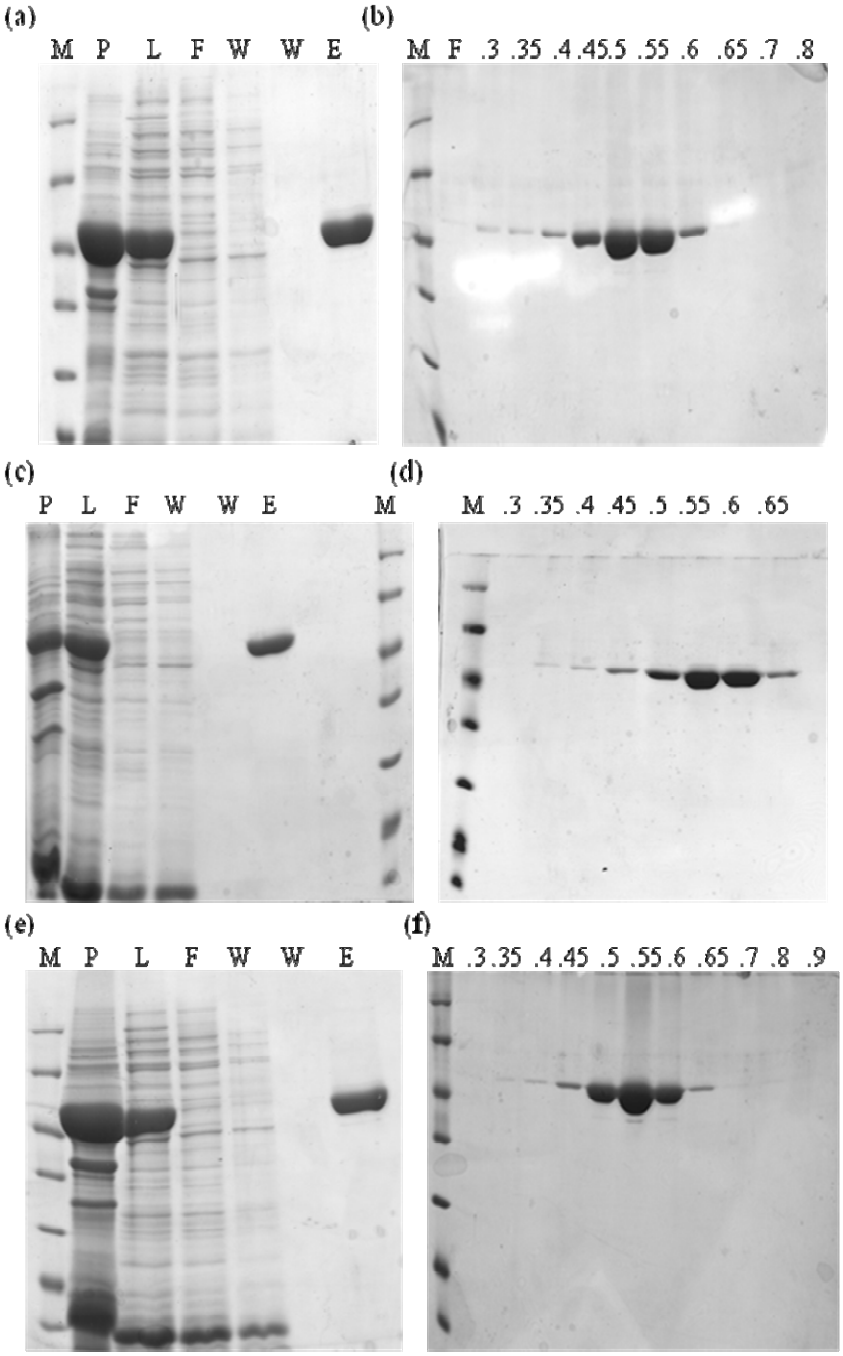

Figure 4.12: Purification of single Cys derivatives of Rho

(a) Purification of His Rho C202S T217C protein through Ni-NTA column (b) Purification through Heparin column by batch elution with NaCl gradient. Rho C202S T217C eluted at 0.4 M- 0.6 M NaCl. (c) Purification of His Rho C202S R221C protein through Ni-NTA column (d) Purification through Heparin column by batch elution with NaCl gradient. Rho C202S R221C eluted at 0.45 M- 0.65 M NaCl. (e) Purification of His Rho C202S K224C protein through Ni-NTA column (f) Purification through Heparin column by batch elution with NaCl gradient. Rho C202S K224C eluted at 0.45 M- 0.65 M NaCl.

4.2.9 *In vivo* pull down of Rho – NusG complex

Non-His tagged WT Rho and His-tagged NusG derivatives were co-overexpressed to demonstrate the *in vivo* interactions of Rho and WT and different derivatives of NusG. BL21(DE3) strain was transformed with plasmids of NusG (pET33b; Kan^R) and Rho (pET21b; Amp^R). The colonies obtained on the transformation plates were processed immediately. About 10-15 colonies were picked and inoculated in 1 ml LB. This was used as primary culture and 1% was subcultured in 100 ml LB with both the antibiotics ampicillin and kanamycin. The culture was grown at 37 ºC till the OD_{600} reached 0.4. The cultures were induced by adding IPTG to the final concentration of 100 µM. The proteins were expressed for 3 hr. The cells were collected and then resuspended in lysis buffer (pH 8.0) containing 100 mM NaH_2PO_4, 100 mM NaCl and 50 µg/ml PMSF. After resuspending the cells thoroughly, lysozyme was added to a final concentration of 1 mg/ml except for NusG-CTD and incubated on ice with constant stirring for 30 min. The cells were sonicated till complete lysis occured. NusG-CTD cells were sonicated without adding Lysozyme since both proteins co-migrated on gel. The lysed cells were centrifuged at 4 °C, 12000 rpm for 30 min. Supernatant was transferred to prechilled falcon. The Ni-NTA beads were packed into column. And the columns were equilibrated with 5 bed volumes of lysis buffer. The supernatant was poured onto the beads in the column (typically 2.5 ml bed volume). The flow through fraction was collected for analysis. The columns were washed with 6 bed volumes of wash buffer (pH 8.0) containing 100 mM NaH_2PO_4, 100 mM NaCl, 10 mM imidazole and 50 µg/ml PMSF. The wash fraction was also collected. The proteins were eluted with 5 ml of elution buffer composed of 100 mM NaH_2PO_4, 100 mM NaCl, 500 mM Imidazole and 50 µg/ml PMSF.

4.2.10 *In vitro* Rho – NusG binding assay

30 µg of His tagged NusG derivative and 6 µg of non His tagged WT Rho were mixed in 100 µl lysis buffer (pH 8.0) containing 100 mM NaH_2PO_4, 100 mM NaCl, 10 mM imidazole and 50 µg/ml PMSF and incubated at 37 ^oC for 10 min. Protein mixture was added to 100 µl of Ni-NTA beads equlibriated with lysis buffer and incubated at room temperature for 10 min. Supernatant was removed after spinning at 2000 rpm for 2 min. Beads were then washed with 100 µl of wash buffer (100 mM NaH_2PO_4, 100 mM NaCl,

50 mM imidazole) and proteins were eluted with 100 µl of elution buffer composed of 100 mM NaH_2PO_4, 100 mM NaCl, 500 mM imidazole. For *in vitro* competition of Rho-NusG complex, 6 µg of non His tagged Rho was added to the mixture of 10 µg of non His tagged NusG and 30 µg of His tagged NusG. Samples were loaded on 15% SDS-PAGE and stained by coomassie blue staining.

4.2.11 *In vitro* Rho dependent transcription termination assay

Linear DNA templates for *in vitro* transcription assays were made by PCR amplification using primers RS83 and RS177 from the plasmid pRS106 containing *trp t'* terminator following a strong T7A1 promoter. Reactions were performed in the transcription buffer (T buffer; 25 mM Tris-HCl, pH 8.0, 5 mM $MgCl_2$, and 50 mM KCl) at 37 °C. The reactions were initiated with 10 nM of DNA template, 40 nM RNA polymerase, 175 µM ApU, 5 µM each of GTP and ATP and 2.5 µM of CTP to make a 23-mer EC. [α-^{32}P] CTP (3000 Ci/mmole) was added to the reaction to label the EC_{23}. The complex was chased with 20 µM NTPs in presence of 10 µg/ml rifampicin for 5 min at 37 ^{o}C. 50 nM Rho and 200 nM of WT NusG or NusG derivatives were added to the chase solution. Effect of competition of WT NusG by NusG-NTD or NusG-CTD were checked by continuous transcription termination assay in the presence 50 nM WT Rho, 200 nM of WT NusG and increasing concentration of either NTD or CTD of NusG. Reactions were stopped by phenol extraction and mixed with equal volume of formamide loading dye. Products were analyzed on 10% sequencing gel, exposed to a phosphor imager screen (Amersham) and scanned by Typhoon 9200 Phosphorimager.

4.2.12 *In vitro* elongation rate assay

For the elongation rate assay, the template was prepared by PCR amplification from plasmid pRS106 using primers RS83 and RS177. EC_{23} made as described above was chased with 20 µM NTPs in presence of 10 µg/ml rifampicin and 200 nM of WT NusG or NusG derivatives. 8 µl aliquots were removed at indicated time and reactions were stopped by phenol extraction and mixed with equal volume of formamide loading dye. Products were analyzed on 10% sequencing gel, exposed to a phosphor imager screen (Amersham) and scanned using Typhoon 9200 Phosphorimager (Amersham). The transcript intensities were quantified using ImageQuant^{TL} software. The time for half of the RNAP molecules

elongating from position 23 to reach the full length transcript (RO) was measured by fitting the plot of the fraction of full length RNA against time to a sigmoidal curve. To determine the rate of elongation, the length of RNA from position 23 to RO was divided by the time for half of the RNAP molecules to transcribe it.

4.2.13 *In vitro ops* pause assay

For measuring *in vitro* pausing kinetics at *ops* pause, the template was PCR amplified using RS83/RS267 primers from pRS25 plasmid (Figure 4.13). Reactions were performed in the transcription buffer (T buffer; 25 mM Tris-HCl, pH 8.0, 5 mM $MgCl_2$, and 50 mM KCl) at 37 °C. At first EC_{23} was made by initiating the transcription with 175 μM of ApU, 5 μM each of GTP and ATP, 2.5 μM of CTP, [α-^{32}P]-CTP (3000 Ci/mmol, Amersham) and 500 nM of NusG derivatives. The EC_{23} was then chased in the presence of 100 μM each of UTP, CTP, and ATP and 10 μM GTP. 4 μl aliquots were removed at indicated time and mixed with equal volume of formamide loading dye. Products were analyzed on 8% sequencing gel. The amount of RNA in each pausing site was quantitated using ImageQuant software and plotted against time. The plots were fitted to the equation of exponential decay ($y=ae^{-\lambda t}$) to calculate the rate (λ) of escape from the paused site. The half-lives ($t_{1/2}$) of pausing were calculated from $t_{1/2}=\ln 2/\lambda$. All the curve fittings were performed using Sigmaplot.

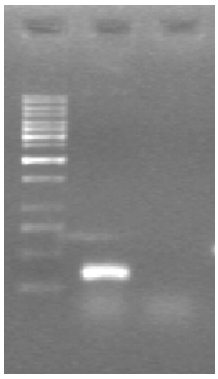

Figure 4.13: T7A1 *Ops* pause template PCR amplified from pRS25 using RS83/ RS267 primers

4.2.14 Copper phenanthroline crosslinking

The crosslinking reactions were carried out in the buffer containing, 25 mM Tris pH 7.0, 50 mM KCl, 100 mM NaCl. 10 mM stock of crosslinker was prepared by adding 1 μl of 1

M $CuSO_4$, 3 µl of 1M Phenanthroline to 96 µl of water. After incubating 250 nM of single Cys Rho and 2.5 µM of WT NusG or NusG single Cys derivatives in the buffer at 37 ºC for 10 min, the reaction was started by adding 1 µM of $Cu(P)_2$ and was continued at 37 ºC for 10 min. The crosslinking was stopped by adding equal volume of non-reducing SDS loading dye containing 100 mM iodoacetamide and was loaded on 10% SDS-PAGE. 100 mM of DTT was added after crosslinking and further incubated for 10 min before loading the gel wherever indicated.

The proteins were transferred to PVDF membrane for western blot analysis. The blots were blocked overnight in Phosphate buffered saline with Tween-20 (10 mM Na_2HPO_4, 1.76 mM KH_2PO_4, 137 mM NaCl, 2.7 mM KCl pH 7.4, 0.05% Tween-20 (PBST)) plus 5% non-fat dry milk. The blots were washed three times for 10 min each with PBST. The blots were then incubated for 2 hr in PBS with either 1:40,000 dilution of the primary NusG antisera or 1:60,000 dilution of the primary Rho antisera and washed three times for 10 min each with PBST. They were subsequently incubated with the antirabbit horseradish peroxidase-conjugated secondary antibody (Sigma), diluted 1:1,60,000 in PBST for 1 hr at room temperature and washed as before. The blots were developed with an ECL (enhanced chemiluminescence) kit (Amersham Pharmacia Biotech) and exposed to film.

4.3 Results

4.3.1 Two domains of NusG

4.3.1.1 *In vivo* pull down of Rho-NusG complex

In *E. coli,* NusG consists of two globular domains with a flexible segment connecting the two domains. By affinity chromatography columns it was previously shown that NusG can directly bind to Rho (Li et al., 1993). However the domain of NusG involved in the interaction is not identified. An understanding of the sites involved in the Rho–NusG complex formation will reveal the molecular basis of the interaction.

To determine the Rho-binding domain of NusG, His-tagged NusG-NTD (1-121) and NusG-CTD (117-181) domains (Figure 4.14(a)) were cloned separately. *In vivo* binding ability of each of the NusG derivative to Rho was measured by co-overexpression of His tagged NusG derivative (WT, NTD or CTD) and WT Rho (non-His tagged) from two

different pET vectors. After induction, the cell lysate was directly loaded onto Ni-NTA columns. The eluted fraction of WT NusG and NusG-CTD contained significant amount of Rho, whereas much smaller amounts of Rho were eluted with NusG-NTD (Figure 4.14(b)). The relative ability of the NusG-CTD to pull-down Rho suggested that this domain is important for the interaction with Rho and that the complex that had been pulled-down is a specific one.

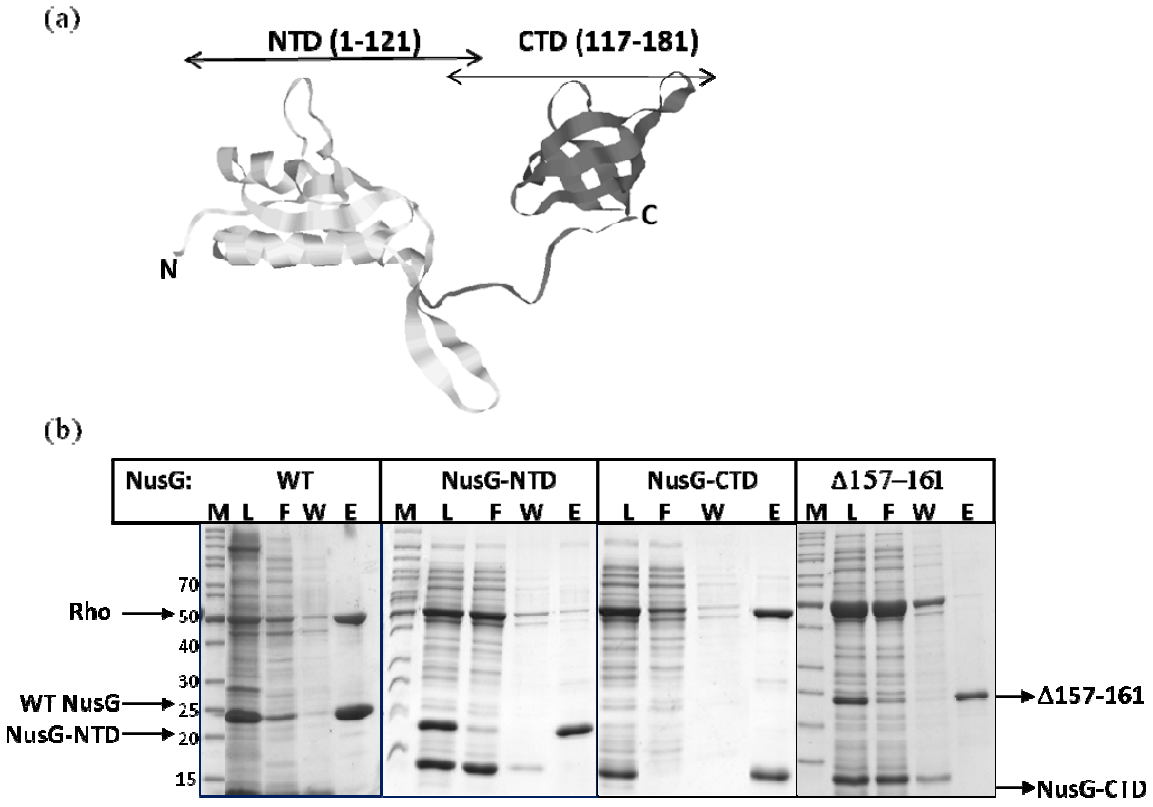

Figure 4.14

(a) Homology model of *E. coli* NusG showing the two domains, NusG-NTD (1-121) and NusG-CTD (117-181) connected by a flexible linker. (b) His tagged WT NusG and its different derivatives were co-overexpressed with Rho to assess the *in vivo* complex formation. Crude lysates were passed through Ni-NTA columns and different fractions L: whole lysate, F: flow-through fraction from the column, W: washed fraction, E: eluted fraction from the column and M: Molecular weight marker) were loaded onto SDS-PAGE and visualized by coomassie-blue staining. The presence of Rho in the fractions E indicates Rho–NusG complex formation *in vivo*. WT NusG and NusG-CTD could pull down Rho, but not by NusG-NTD or a NusG-CTD mutant of NusG.

4.3.1.2 *In vitro* Rho-NusG binding

In order to validate the *in vivo* observation that the binding to Rho takes place *via* NusG-CTD but not *via* NusG-NTD, *in vitro* Rho-NusG binding assay were carried out with purified His tagged NusG derivatives (WT, NTD or CTD) and WT Rho (non-His tagged). The His-tagged NusG derivative was incubated with a non His-tagged WT Rho and subsequently passed the mixture over Ni-NTA beads and measured quantitatively the fraction of Rho retained with Ni-NTA bound different NusG derivatives. Under this experimental condition ~60% to 80% of Rho was observed to be retained with either the full-length NusG or with the NusG-CTD. Interestingly the CTD fragment retained more Rho than the full-length NusG. Fraction of Rho retained with NusG-NTD was not significantly higher than the non-specific adsorption level (panel indicated as without NusG). Consistent with the *in vivo* data, the *in vitro* assay also showed that binding determinants of NusG for Rho reside in NusG-CTD (Figure 4.15 (a and b)).

4.3.1.3 Competition of Rho-NusG interaction by NusG-NTD and NusG-CTD

For testing whether the NusG-CTD can compete out WT NusG from NusG-Rho complex *in vitro*, a complex of non His tagged Rho and NusG was formed and passed the mixture through Ni-NTA columns bound to either WT NusG, to NusG-NTD or to NusG-CTD. Rho was observed to be eluted from the Ni-NTA columns bound to either WT-NusG or to NusG-CTD (Figure 4.15 (c)). Therefore, NusG-CTD can efficiently compete out WT NusG from a Rho-NusG complex which also indicated that NusG-CTD-Rho interaction *in vitro* is very specific.

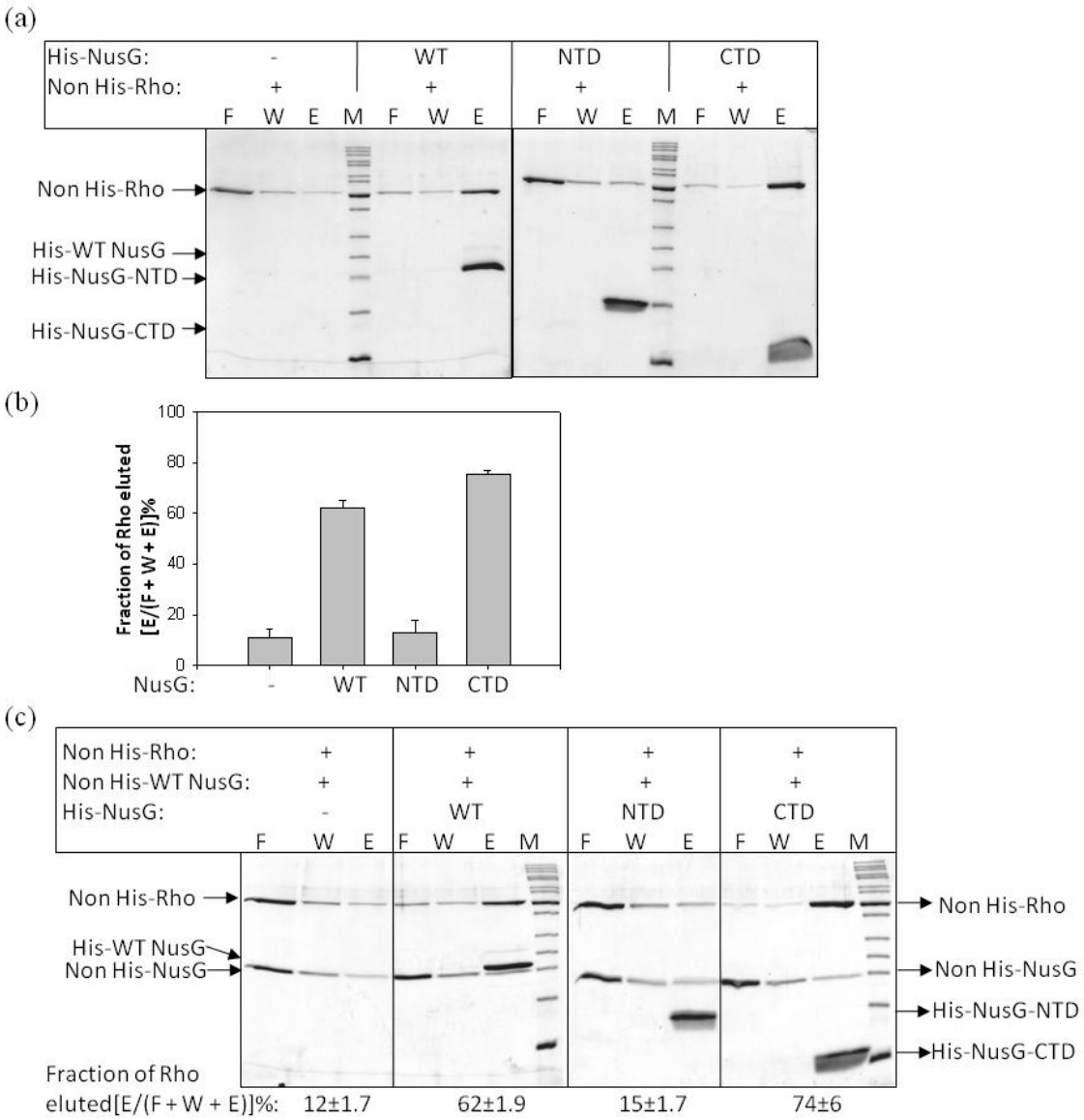

Figure 4.15: Specific interaction of NusG-CTD with Rho.

(a) Rho binding analysis of WT and individual domains of NusG. Rho was passed over different NusG derivatives attached to Ni-NTA beads. Rho was observed to be retained with either the WT NusG or with the NusG-CTD. While NusG-NTD was defective in binding to Rho. (b) Bar diagram showing the amount of Rho associated with different NusG derivatives. (c) Preformed Rho-NusG complex was mixed with His-tagged WT NusG or its different derivatives *in vitro* and loaded onto Ni-NTA columns and different fractions were loaded onto SDS-PAGE. Rho-NusG complex can be competed out efficiently by CTD alone, but not by NTD. This strongly suggests that binding determinants of NusG for Rho reside in CTD.

4.3.1.4 Effect of WT NusG, NTD and CTD on elongation enhancement

The ability of WT and individual domains of NusG (NTD and CTD) were tested for their effects on the overall rate of transcript elongation. A 23-mer elongation complex (EC_{23}) was made by withholding UTP during initiation on a linear DNA template with the *trp t'* terminator cloned downstream to the strong T7A1 promoter. EC_{23} was chased with 20 μM NTPs either in the presence or absence of WT or individual domains of NusG. The rate of transcription elongation was improved by about 25% upon addition of either WT NusG (3.73 nt/sec) or NusG-NTD (3.97 nt/sec) compared to that in the absence of NusG (2.99 nt/sec). NusG-CTD had no significant effect on the rate of transcription elongation (3.16 nt/sec) (Figure 4.16). This shows that NusG-NTD can work as effective as WT NusG in RNAP interaction and activity.

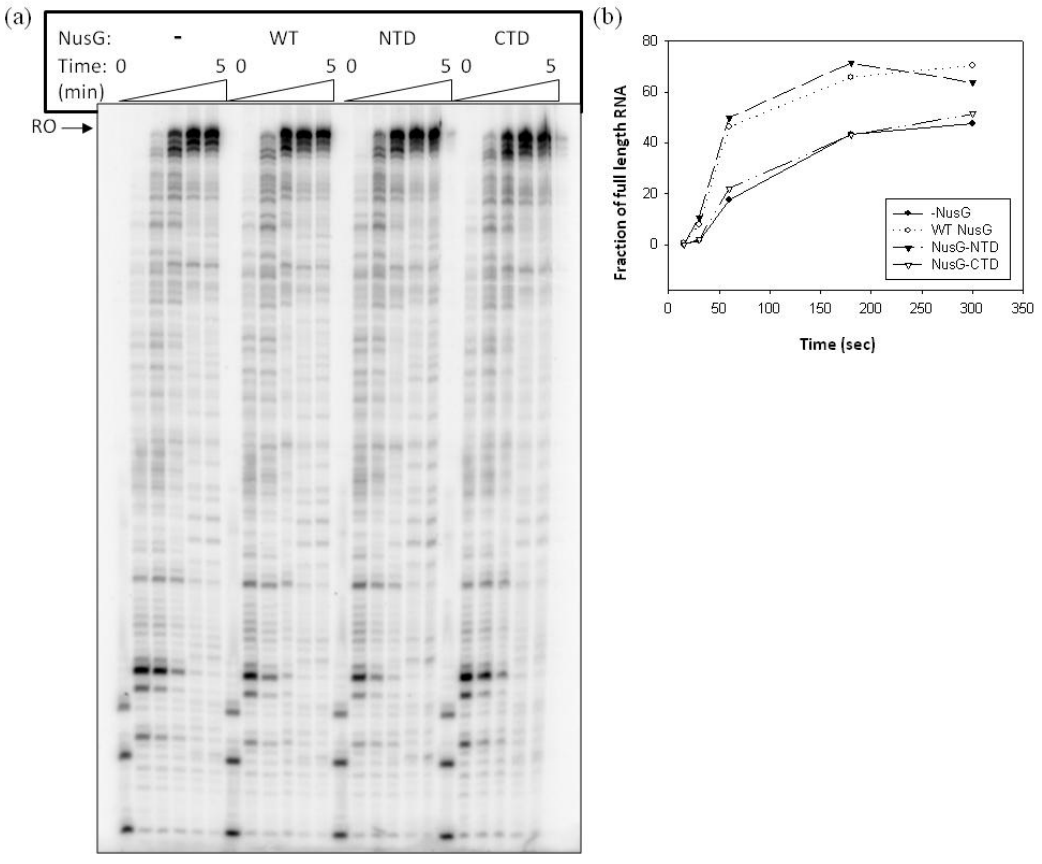

Figure 4.16

(a) Autoradiogram showing the time course of transcription elongation after the addition of the NTPs to the reaction mixtures without NusG, with WT NusG, NTD and CTD. Stimulation of transcription elongation by WT NusG and NTD is seen by the faster accumulation of the longer RNA products. (b) Plot showing the fraction of the full-length RNA as a function of time.

4.3.1.5 Functional competition of Rho-NusG complex by NusG-NTD and NusG-CTD

To test the hypothesis that expression of the NusG-NTD or CTD separately could inhibit WT function, WT and individual domains of NusG (NTD and CTD) were over expressed from the strong inducible P_{BAD} promoter (induced by arabinose) residing on the plasmid. This was done in the presence of a WT chromosomally encoded *nusG* that acts to promote termination. The cell viability of the strains expressing either WT or NusG derivatives proteins were monitored by spotting serial dilutions of saturated cultures on LB plates (Figure 4.17(a)). Over expression of either WT NusG or CTD did not reduce colony numbers significantly, and thus was not toxic to the bacteria. However, NusG-NTD over-expression resulted in clear inhibition of cell growth. This is consistent with the idea that the NTD maintains partial function, *i.e*. binds to RNAP, but is defective in another essential NusG activity. One possible explanation for the toxicity of the NTD is that it out-competes WT NusG in binding ECs but blocks Rho-dependent termination because it cannot interact with Rho.

At *trp t'* terminators WT NusG changes the pattern of termination by increasing the efficiency of Rho dependent termination at promoter proximal sites that are not preferred by Rho in the absence of NusG (Nehrke et al., 1993). The ability of the purified individual domains of NusG to modulate Rho dependent termination *in vitro* were assayed on a template containing *trp t'* terminator. The termination assays showed that neither NTD nor CTD affected Rho activity (Figure 4.17(b) panel 2 and 5). His tag and S60A point mutation did not interfere with the function of the NusG (Figure 4.17(b) panel 3 lane1). The result of competition of WT NusG by NTD and CTD in continuous transcription termination assay shows that NTD added in equimolar amounts to WT NusG (200 nM each) only slightly inhibited NusG activation of Rho (Figure 4.17(b) panel 3 lane1). NTD inhibition increased in a concentration-dependent manner, whereas CTD did not compete out WT NusG even at the highest concentration of CTD (2 µM) tested (Figure 4.17(b) panel 3 and 6). CTD by itself was found to be transcriptionally inert, whereas the NTD completely inhibits early termination by competing with WT NusG for interaction with EC. NTD did not reduce termination efficiency indicating that this domain does not directly inhibit Rho. This suggests that physical linkage of the CTD to the NTD is required for NusG to enhance Rho-EC interaction and termination.

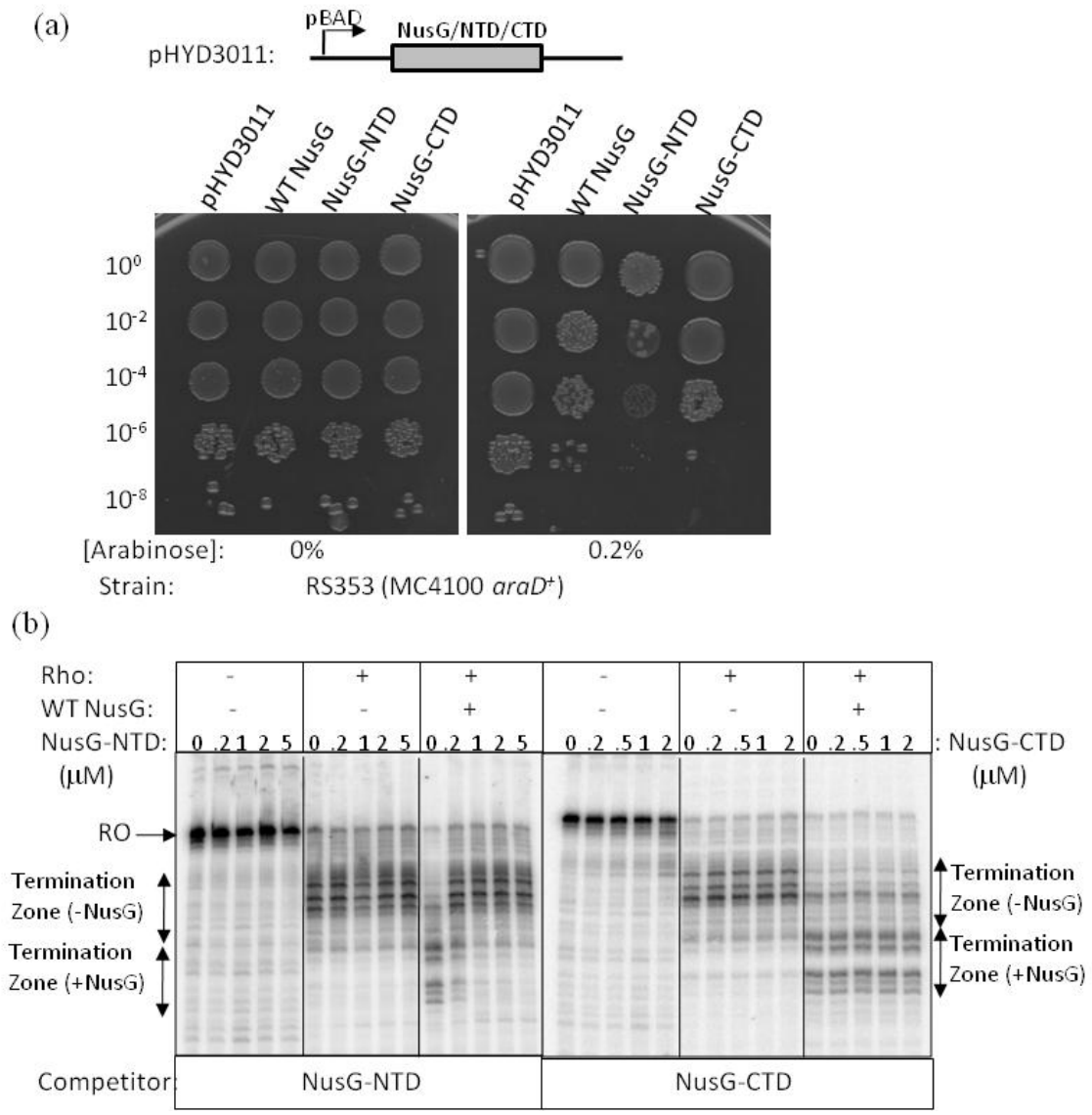

Figure 4.17: Functional competition of Rho-NusG complex by NusG-NTD and NusG-CTD

(a) WT NusG and its different derivatives were over-expressed from a strong P_{BAD} promoter in the presence of 0.2% arabinose. It was observed that over-expression of NusG-NTD is toxic to the cell but not NusG-CTD. (b) Autoradiograms of the *in vitro* transcription assays showing the Rho dependent termination in the *trp t'* terminator region in the absence and in the presence of WT and NusG-NTD or NusG-CTD as indicated. The transcript reaching the end of the template is indicated as RO. Addition of Rho stimulates termination, as seen by a decrease in the amount of the RO product and an increase in the amounts of shorter products. NusG additionally increases Rho termination at earlier template positions. The termination zone is indicated. Neither NTD nor CTD could directly modulate Rho termination. NusG-NTD but not NusG-CTD competes for RNAP binding with WT NusG as evidenced by the decreased NusG stimulation of termination with increasing amounts of competing NTD.

4.3.2 Micro-deletions in NusG-CTD

4.3.2.1 *In vivo* lethality of the mutants

NusG-CTD is highly conserved among bacteria and contains the KOW motif (Figure 4.18(a)). The NusG-CTD consists exclusively of β strands that fold into a compact globular five-stranded β barrel (β1: E132-V136, β2: F144-D152, β3: R157-I164, β4: R167-L173, β5: V178-K180). To further localize the binding region in the CTD, five micro-deletion mutants were made in the β sheets of NusG-CTD (Figure 4.18(b)). The effect of the expression of NusG deletion mutants on cell viability were tested in strains lacking WT NusG. For this plasmid encoding NusG Δ145-149, Δ148-152, Δ157-161, Δ169-173 and Δ172-181 under control of the P_{BAD} promoter which is induced by arabinose were used. All of them were found to be lethal in an *E. coli* MC4100 derivative strain RS692 (Figure 4.18(c)). It should be noted that in this strain *rac* prophage is deleted (Δ*rac*). Lethality of MC4100 strain due these micro-deletions is not consistent with the earlier observation that *nusG* deletion is not lethal in *E. coli* MG1655 Δ*rac* strain (Cardinale et al., 2008).

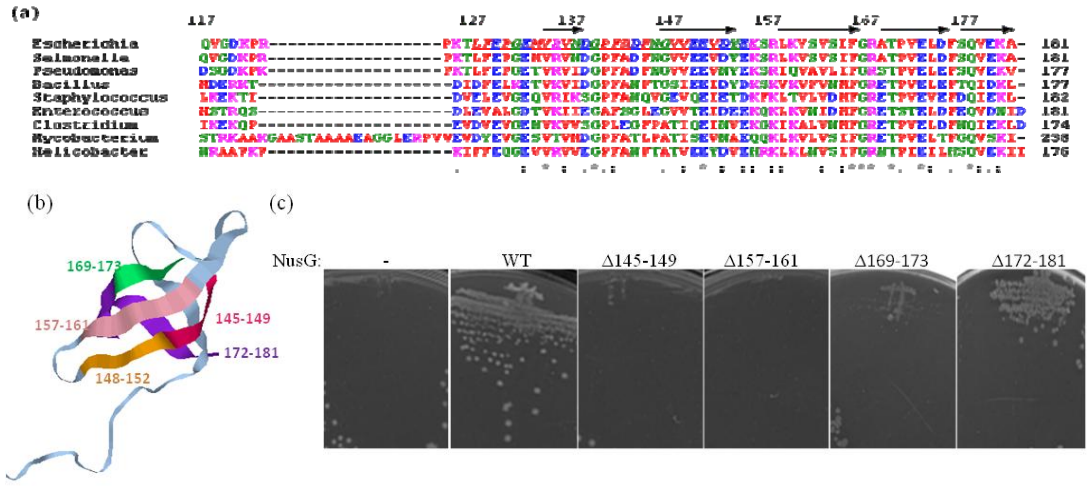

Figure 4.18

(a) Multiple amino acid sequence alignment of NusG-CTD using the program CLUSTAL W. Species and GenInfo numbers: *Escherichia coli* (16131812); *Salmonella enterica* (161505371); *Pseudomonas aeruginosa* (218889397); *Bacillus subtilis* (16077169); *Staphylococcus aureus* (82750244); *Enterococcus faecalis* (229549155); *Clostridium botulinum* (153933840); *Mycobacterium tuberculosis* (215402414); *Helicobacter pylori* (15645817). The conserved KOW motif is underlined. The relatedness of sequences are indicated as follows. '*' denotes an amino acid conserved by all protein sequences. ':' denotes conserved substitutions and '.' denotes semi-conserved substitutions. Colour coding for amino acids are red: small+ hydrophobic, blue: acidic, magenta: basic, green: hydroxyl + amine. (b) The micro deletions marked in different colours on homology model of *E. coli* NusG-CTD. (c) Complementation of *ΔnusG in vivo* with plasmids encoding NusG micro deletions. All the micro deletions were lethal.

4.3.2.2 Effect of NusG deletion mutants on *in vitro* transcription termination

Since NusG Δ145-149, Δ148-152 and Δ169-173 proteins were insoluble, for checking their *in vitro* activities; they were purified from inclusion bodies under denaturing condition and refolded, whereas NusG Δ157-161 was purified under native condition. Earlier it was reported that NusG W9L can be denatured and folded to yield active protein (Richardson and Richardson, 2005). Activity of WT NusG purified through re-folding procedure was similar to that purified under native condition (Figure 4.19(a) lane 4). *In vitro,* Rho terminates early in the presence of WT NusG which is indicative of Rho-NusG interaction (Nehrke et al., 1993). On a DNA template where a Rho-dependent terminator, *trp t'* was fused to a strong promoter T7A1, it was observed that none of these deletion mutants were able to induce early termination (Figure 4.19(a)).

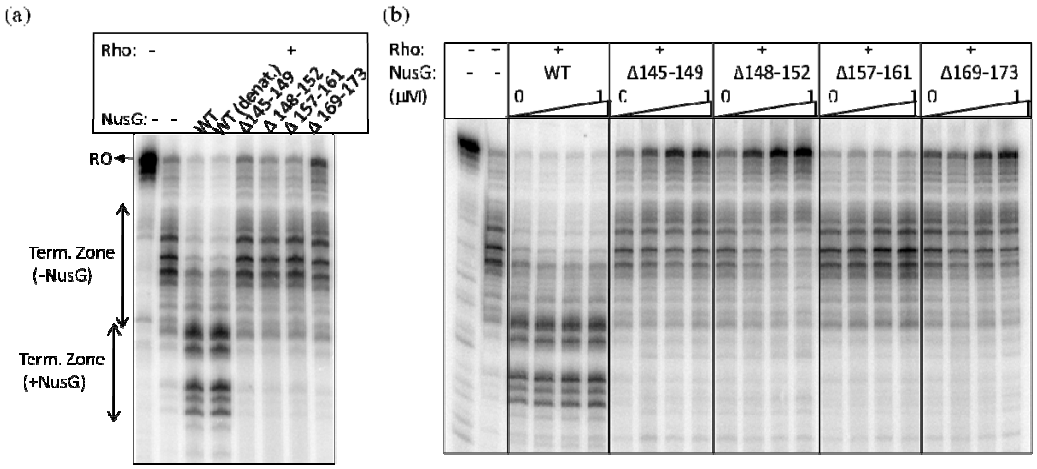

Figure 4.19

(a) Autoradiograms of the *in vitro* transcription assays showing the Rho dependent termination in the *trp t'* terminator region in the absence and in the presence of WT and NusG deletion mutants as indicated. WT (denat.) stands for the refolded WT protein. The termination zone is indicated. The transcript reaching the end of the template is indicated as RO. All the deletions are defective in Rho-dependent termination. (b) NusG deletion mutants tested at higher concentrations for enhancement of Rho termination. NusG Δ145-149, Δ148-152 and Δ169-173 inhibited Rho dependent transcription termination at higher concentrations.

4.3.2.3 Non-specific inhibition of termination by NusG deletion mutants

If NusG deletion mutants can interact with Rho but with reduced affinity, higher concentration of these proteins could enhance early termination at Rho dependent terminators. To test this hypothesis, *in vitro* transcription reactions were carried out with increasing concentration of NusG deletion mutants. NusG Δ157-161 neither inhibited Rho dependent transcription termination nor induced early termination even at higher

concentrations. Surprisingly it was found that NusG Δ145-149, Δ148-152 and Δ169-173 inhibited Rho dependent transcription termination rather than inducing early termination. Inhibition increased in a concentration-dependent manner (Figure 4.19(b)). As these deletions are insoluble, it is possible that their defect could arise from the altered conformations.

4.3.2.4 *In vitro* Rho binding analysis of different NusG deletion mutants

To demonstrate the level of direct Rho-NusG interaction, *in vitro* binding assay was carried out by various His tagged NusG deletion mutants. Non His tagged Rho was passed over different NusG deletion mutants attached to Ni-NTA beads. Compared to WT NusG much smaller amounts of Rho were eluted with NusG deletion mutants (Figure 4.20(a)). These results, represented graphically in Figure 4.20(b), demonstrate that these deletion mutants are defective for interacting with Rho.

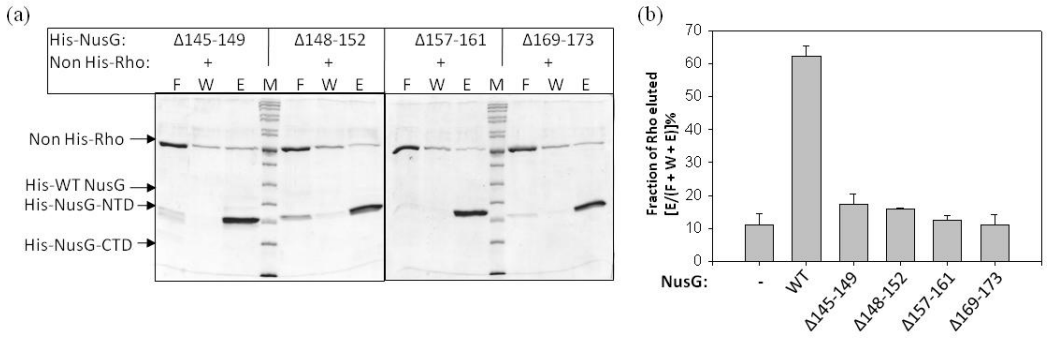

Figure 4.20

(a) Rho binding analysis of different NusG deletion mutants. All the deletions were defective in binding to Rho. (b) Bar diagrams showing the amount of WT Rho eluted with different NusG deletion mutants.

4.3.3 Point mutations in NusG-CTD

4.3.3.1 *In vivo* growth defects of the mutants

To test the role of the structure and sequences in the CTD of NusG, various unique point mutants were made by site directed muatgenesis on full-length NusG (Figure 4.21(a)). These point mutations were at first tested for their abilities to support bacterial growth. *In vivo* assays were performed in the strain RS692 where WT and different NusG mutants were supplied from a modified pBAD vector, pHYD3011. All these point mutants did not affect viability of this strain, unlike the deletion derivates described above. However, some of the mutants (G146D, V148N, L158Q, V160N and I164A) were observed to grow poorly at 30 ^{o}C (Figure 4.21(b)).

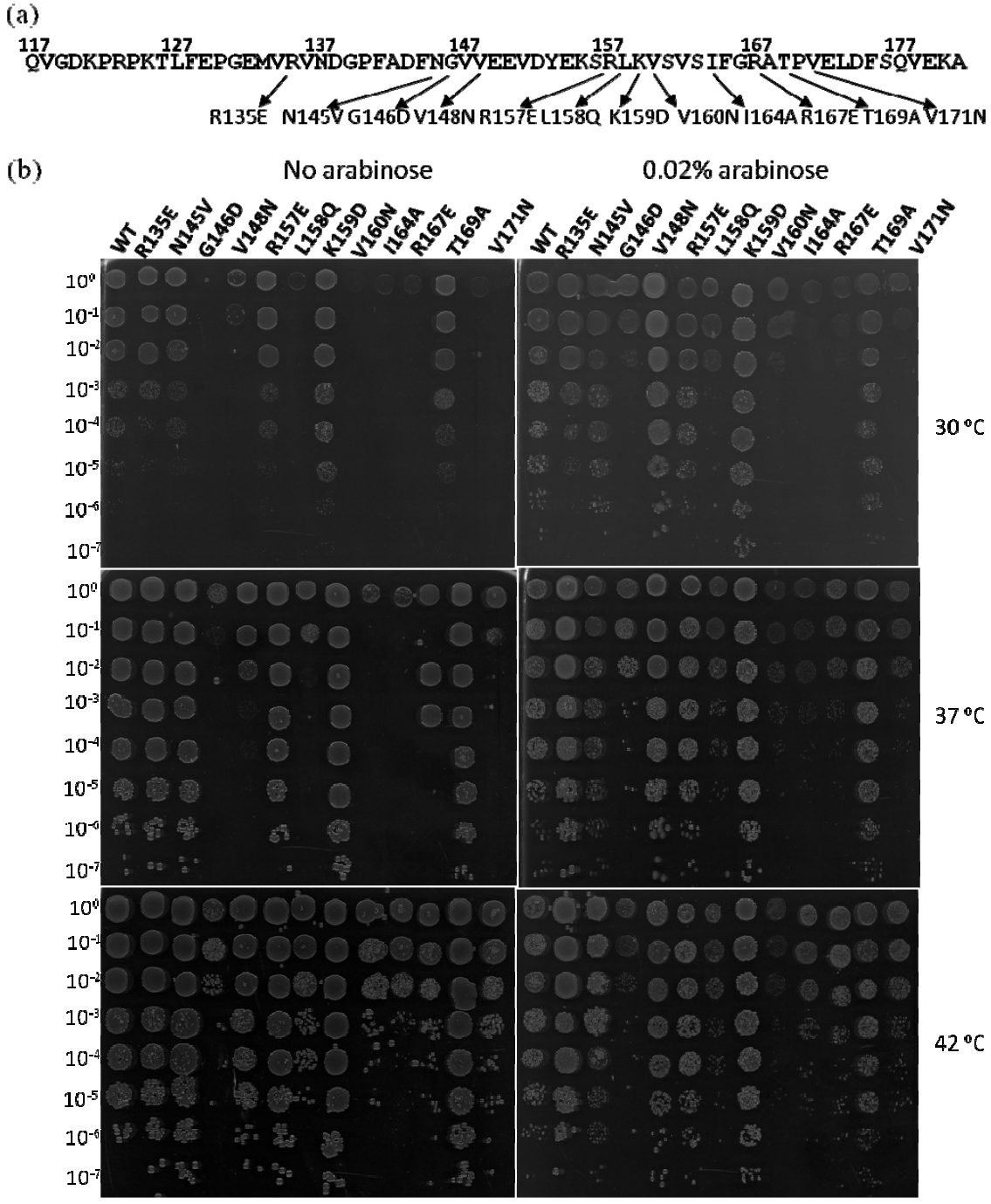

Figure 4.21: *In vivo* growth defect of the NusG mutants.

(a) Amino-acid sequence of NusG-CTD. Positions of the point mutations are indicated (below). (b) *In vivo* growth phenotype of NusG mutants in the strain RS692 in the absence and presence of 0.2% arabinose at different temperatures. Though NusG-CTD mutants were viable, NusG G146D, V148N, L158Q, V160N and I164A were observed to grow poorly at 30 ^{o}C.

4.3.3.2 *In vivo* termination defect of the mutants

To investigate the *in vivo* Rho-dependent termination defects of these mutants the activity of β-galactosidase enzyme made from the *lac* operon cloned downstream of a Rho-dependent terminator, T_{R1} (in the strain RS802; Appendix I) was measured. This terminator is cloned between the promoter and the structural genes (*lacZYA)* of the *lac* operon. Transcription was initiated from the P_{lac} promoter. The ratio of the enzyme activity (%RT) in the presence and absence (in the strain RS715; Appendix I) of the T_{R1} terminator gives the measure of read-through of the transcript from this terminator. Read-through (%RT) activities from this terminator in the presence of WT and different point mutants of NusG are described in table 8. Compared to WT NusG, the mutants G146D, V148N, L158Q, V160N and I164A showed 3 to 5-fold more read-through activity from this terminator.

Table 8: *In vivo* termination defects of NusG-CTD point mutants

NusG Alleles	β-galactosidase activity (arbitrary unit)[a] $+T_{R1}$	β-galactosidase activity (arbitrary unit)[b] $-T_{R1}$	%RT $(+T_{R1}/-T_{R1})$
WT	89.7±4.2	1514.2±36.0	5.9
R135E	49.6±13.6	1412.8±55.7	3.5
N145V	85.9±2.2	1625.6±13.2	5.3
G146D	292.5±18.3	1692.8±112.2	17.3
V148N	303.0±8.1	2076.8±10.2	14.6
R157E	84.7±2.6	1499.3±89.3	5.6
L158Q	307.1±17.4	2053.1±122.9	15.0
K159D	103.1±1.9	1601.1±36.8	6.4
V160N	263.5±16.5	1307.9±35.0	20.2
I164A	249.6±12.2	1504.3±27.6	16.6
R167E	144.6±16.2	1365.4±18.2	10.6
T169A	58.6±10.7	1339.8±45.7	4.4
V171N	98.1±6.7	1346.0±28.7	7.3

The above strains were transformed with the plasmids bearing different WT and NusG mutants. The ratio of β–galactosidase values in the presence and absence of T_{R1} terminator gives the efficiency of terminator read-through (%RT). This Rho-dependent terminator is derived from the *nutR-cro* region of a lambdoid phage H-19B and found to behave similar to the *nutR/*T_{R1} of λ phage. The averages of 4 to 5 independent measurements are shown.

4.3.3.3 Effect of NusG-CTD mutants on *in vitro* transcription termination

The His-tagged derivatives of the point mutants which were defective in *in vivo* Rho-dependent termination were purified and measured for their ability to induce early termination in the *in vitro* termination assays. Transcription assays were carried out on a linearized template where transcription was initiated from a strong T7A1 promoter and elongated through a Rho-dependent terminator cloned downstream of it, in the presence of 20 μM NTPs. Consistent with *in vivo* data, NusG G146D, V148N, L158Q, V160N and I164A were defective for early termination of Rho at *trp t'* terminators (Figure 4.22(a)). This indicates that these mutants are significantly defective for the Rho-dependent termination and the mutated amino acids may be involved in interaction with Rho.

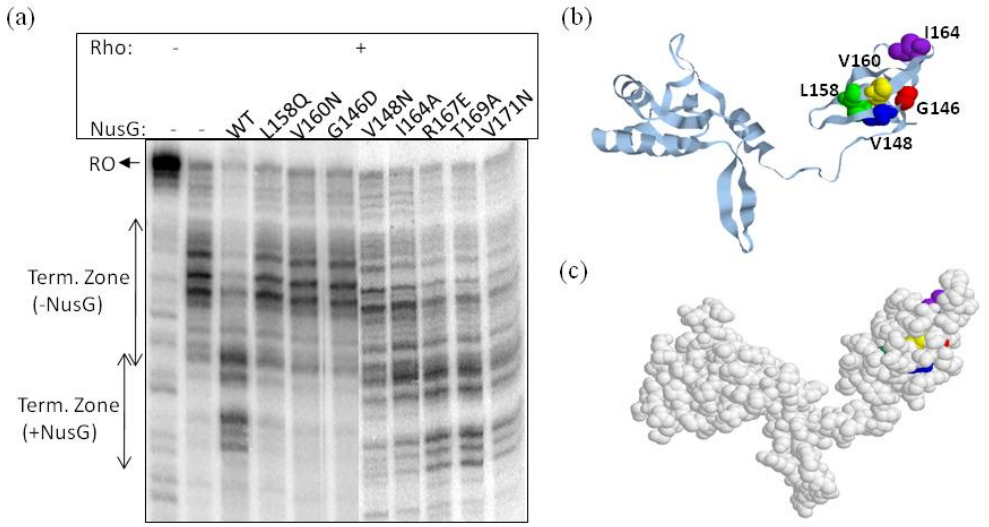

Figure 4.22

(a) *In vitro* termination defect of NusG-CTD mutants. Autoradiogram of the *in vitro* transcription assays showing the Rho dependent termination in the *trp t'* terminator region in the absence and in the presence of WT and NusG-CTD mutant proteins as indicated. The termination zone is indicated. The transcript reaching the end of the template is indicated as RO. Point mutants G146D, V148N, L158Q and V160N are defective but not the others. (b) Location of the defective point mutants are indicated on the ribbon representation of homology model of NusG. (c) Mapping of the amino acids in the NusG-CTD, changes of which caused defect in Rho-binding on the space-filled homology model of NusG. Color codes for the mutations are same as in (b).

While mapping the defective NusG-CTD mutants on the homology model of *E. coli* NusG, it was observed that they are located in the conserved β-sheet bundle (Figure 4.22(b)). Interestingly none of these mutants are highly surface exposed (Figure 2.22(c)). Therefore the interaction face of NusG must undergo conformational changes upon complex formation with Rho to make this region accessible.

4.3.3.4 Effect of mutants on *ops* pause

Failure in the enhancement of early Rho dependent termination by some NusG mutants can be either due to the defect in the interaction with RNAP or Rho. Interaction of NusG with the EC increases its elongation rate by suppressing transcriptional pauses that involves backtracking by RNAP (Artsimovitch and Landick, 2000). To test the effects of the NusG mutants on pausing, a model transcription system containing a known Class II pause site, the *ops* pause of the *E. coli pheP* gene (Artsimovitch and Landick, 2000), placed between the T7A1 promoter and an intrinsic terminator (from the *E. coli* his attenuator) was used. The pause half life at the *ops* sequence was measured in the presence of WT NusG and different point mutants (Figure 4.23(a)). WT NusG was observed to reduce the pause half life by ~2.5 fold similar to what reported earlier (Mooney et al., 2009). All the CTD mutants also induced similar level of reduction in pause half lives (Figure 4.23(b)). Therefore these mutants retained their anti-pausing activities. These results suggest that the lack of activity of these mutants in transcription termination were not because of an inability in its EC-binding function.

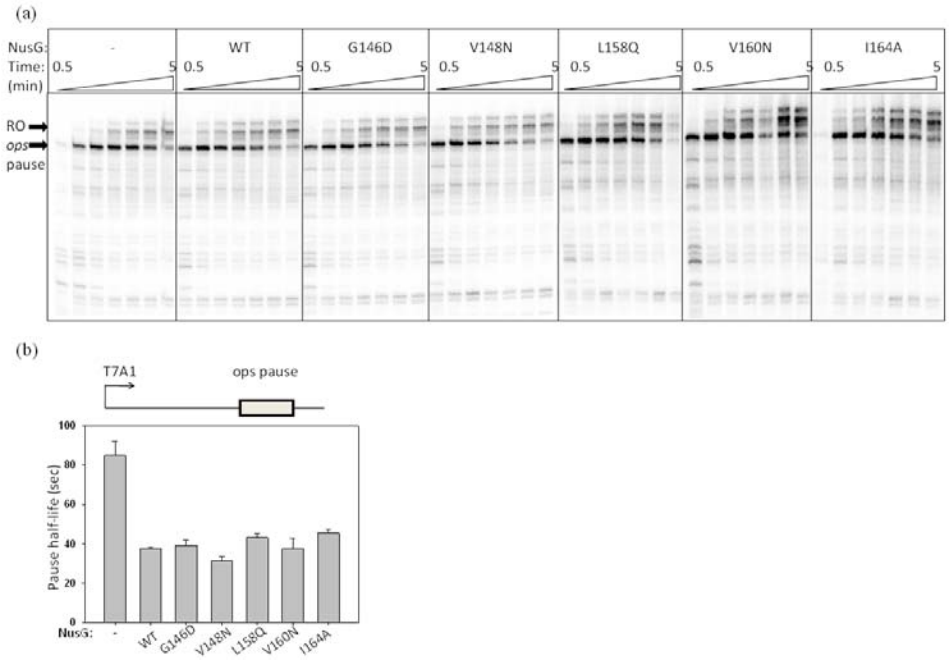

Figure 4.23: The effect of NusG-CTD mutants on *ops* pause suppression.

(a) Autoradiogram showing the time-course of transcription elongation through the *ops* pause sequence both in the absence and presence of either WT NusG or NusG-CTD mutants. The effect of NusG is seen by the faster decrease in RNAs paused at the *ops* pause (labeled *ops* pause) as ECs escape the pause and the faster accumulation of the longer RNA products (labeled RO for the run off products). (b) Schematic of *ops*-containing transcription template (top). Bar diagram showing the pause half-life determined from the transcription elongation kinetics through the *ops* pause site in the absence and presence of either WT NusG or NusG-CTD mutants. Pause half-life is the time taken by half of the complexes to escape the pause.

4.3.3.5 *In vitro* Rho – NusG binding

Binding analysis of the NusG-CTD mutants with Rho were performed in a similar way as described earlier. The eluted fractions revealed that WT NusG contained a significant amount of Rho, whereas a moderately reduced amount of Rho was eluted with NusG R167E, T169A and V171N indicating weak interaction with Rho. NusG V148N, G146D, L158Q, V160N and I164A failed to interact with Rho as evident from the significantly reduced amount of Rho eluted with these mutants (Figure 4.24). Therefore, the absence of interaction of these NusG mutants with Rho correlates with their lack of function in *in vivo* and *in vitro* transcription termination. The results from *in vivo* and *in vitro* studies indicate strongly that these mutants are specifically defective in Rho dependent termination and this defect is due to their inability to bind with Rho. These results also suggest that the amino acid positions corresponding to these mutations are either involved in direct interaction with Rho or these mutations affected the conformation of the interaction surface of NusG required to form a complex with Rho.

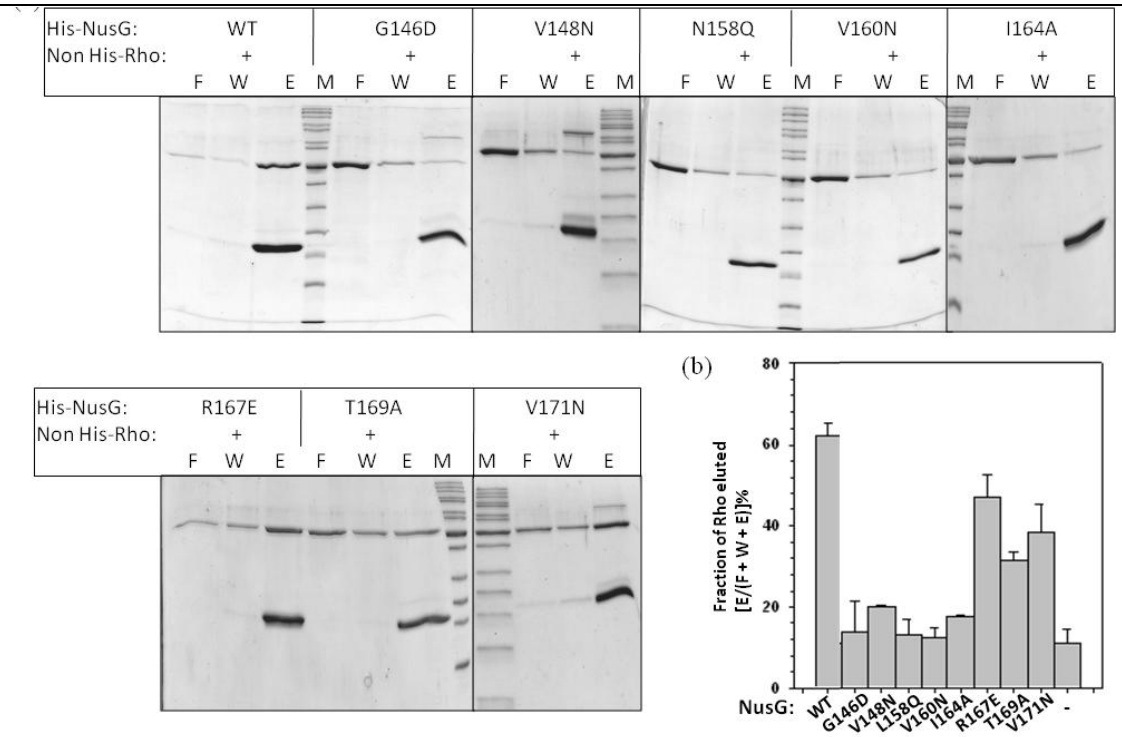

Figure 4.24: Point mutations in NusG-CTD are defective for Rho binding.

(a) Rho binding analysis of WT and different NusG-CTD point mutations. A mixture of WT Rho and different His tagged NusG proteins were passed through Ni-NTA agarose beads. NusG G146D, V148N, L158Q and V160N were defective in binding to Rho. (b) Bar diagrams showing the amount of WT Rho eluted with different NusG proteins. Error bars were calculated from 3 measurements.

4.3.4 Site-specific Cys-Cys di-sulphide bond formation between the regions of Rho and NusG

4.3.4.1 Activity assays of single derivatives

Mutational analysis described above strongly indicated that the major binding determinant of NusG for Rho is located in the CTD. In order to obtain more direct evidence to define the interaction surface involved in the Rho-NusG complex, the ability of different regions of NusG to form site-specific di-sulphide bonds with Rho were measured. For this purpose single Cys residues located in the different regions of NusG and in a specific region of the C-terminal domain of Rho were engineered.

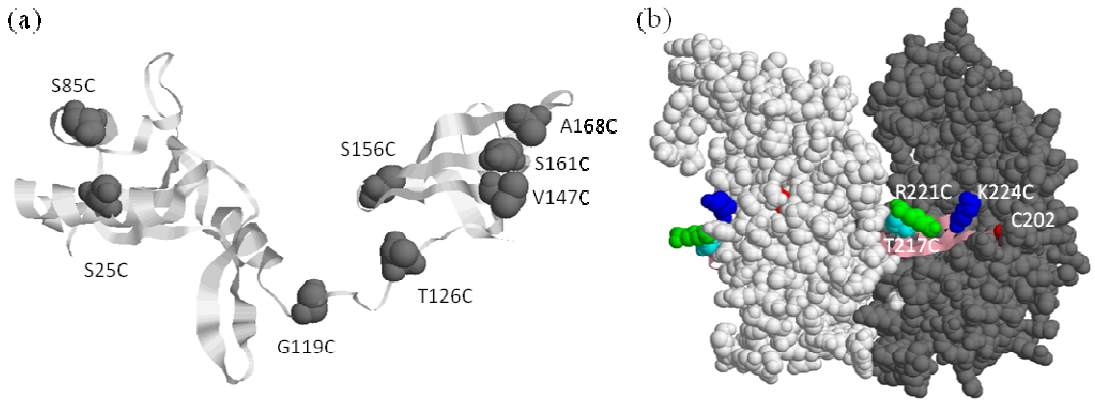

Figure 4.25

(a) Locations of engineered NusG single Cys are indicated on the the ribbon representation of homology model of NusG. (b) Locations of Rho single Cys residues are indicated on the dimeric unit of the closed ring structure of Rho. The amino acids which were changed to Cys are indicated in different colours. Cys residues were engineered on a conserved C-terminal region of Rho highlighted by a pink ribbon on the structure.

As NusG does not have any naturally occurring Cys, different non-conserved and surface exposed amino acids with Cys residues were replaced. Locations of these single Cys residues are indicated on the structure of the NusG (Figure 4.25(a)). It has been reported early that the R221C mutation in Rho can suppress the defect of G146D mutation in NusG (Harinarayanan and Gowrishankar, 2003) which indicates that this region of Rho may be involved in interaction with NusG. Also the only Cys residue of Rho, C202, is located near to this region. Therefore three single Cys derivatives of Rho, T217C, R221C and K224C were constructed in this region and the WT Rho served as a protein with single Cys at position 202. Locations of single Cys residues are shown on the dimeric structure of Rho

(Figure 4.25(b)). Cys derivatives of Rho and NusG with C-terminal His tag were purified using Ni-NTA column. All the single Cys derivatives of Rho and NusG except Rho T217C were active in Rho-dependent termination (Figure 4.26(a)) as confirmed by the *in vitro* transcription termination assay. This mutant was defective for termination. However, its NusG-binding ability was not affected (Figure 4.26(b)).

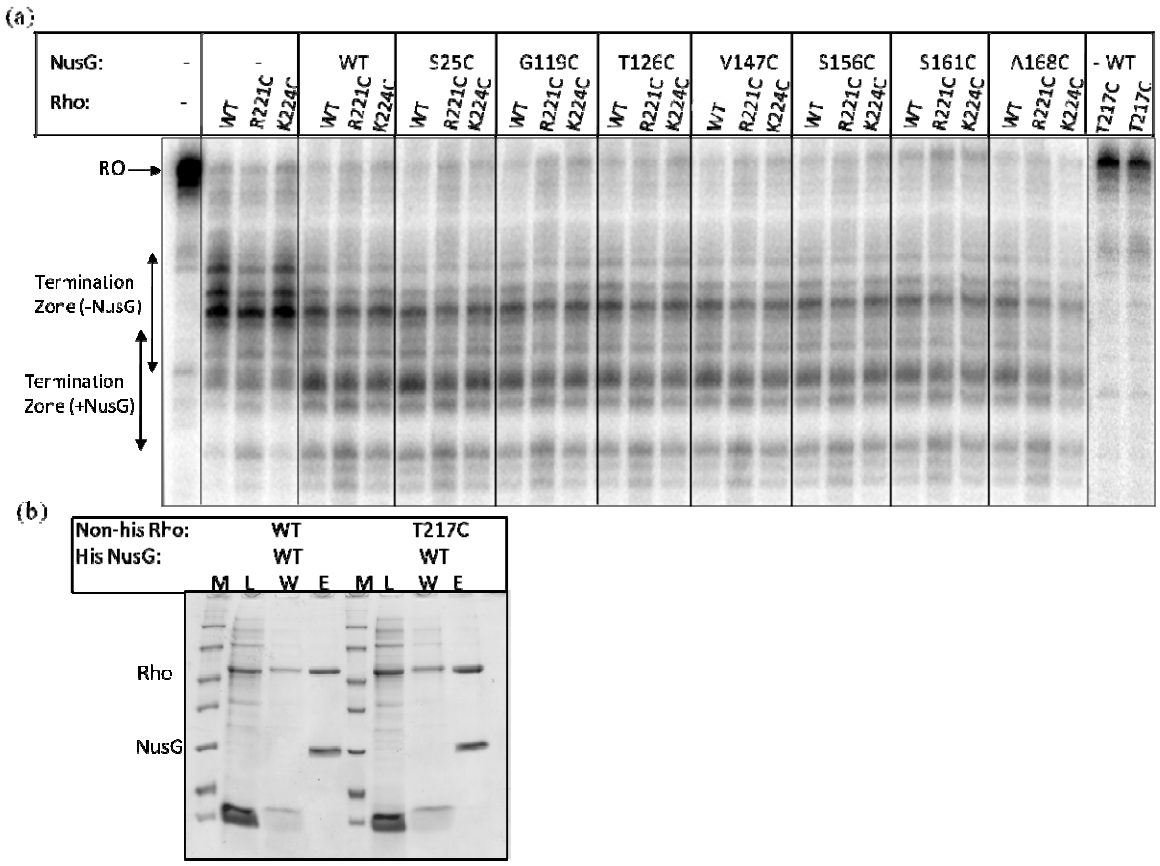

Figure 4.26

(a) Autoradiogram showing the single round *in vitro* Rho dependent transcription termination on *trp t′* terminator templates to determine the activity of Rho and NusG single Cys mutants. The termination zone is indicated. The transcript reaching the end of the template is indicated as RO. All the Cys derivatives of Rho and NusG except Rho T217C were active. (b) Binding analysis of WT Rho and Rho T217C with His tag WT NusG. Non His tag Rho was passed over NusG attached to Ni-NTA beads. Eluted fractions revealed that significant amount of both WT Rho and Rho T217C eluted with NusG.

4.3.4.2 Cu-phenanthroline induced di-sulphide bond formation between Rho and NusG Cys derivatives

Copper-phenanthroline (Cu-P) is an oxidizing agent that catalyzes Cys-Cys di-sulphide bond formation (Belogurov et al., 2007; Pani et al., 2009). Each of the single cys derivatives of NusG were mixed with all the four single Cys derivatives of Rho and Cys-Cys di-sulphide bond formation between Rho and NusG Cys derivatives were induced by adding Cu-P. The products were separated by non-reducing SDS-PAGE and analyzed different forms of NusG by western-blotting with NusG polyclonal antibodies (Figure 4.27(a)). Three types of species were observed: i) NusG monomer (<30 kD), ii) NusG dimer (between 40 to 50 kD) and iii) Rho-NusG di-sulphide bonded complex (between 90-100 kD). Species iii is denoted as a complex between a monomer of Rho and a monomer of NusG, even though it migrated at a higher position than the theoretical molecular weight of the complex (~70 kD) because of two reasons: 1) Presence of Rho in this species and 2) since single Cys derivatives of Rho and NusG were used, formation of one disulphide bonded species is only possible between a subunit of Rho and NusG. The higher migration could be attributed to an unusual conformation of the di-sulphide bonded species.

Significant amount of di-sulphide bonds were formed between the positions S25, S85, G119, V147, S161 and A168 of NusG with Rho R221C and K224C. Di-sulphide bridges were either not formed from the positions S156 of NusG and T217 of Rho or formed with very lower efficiency from the positions T126 of NusG and C202 of Rho (Figure 4.27(a)). Lack of interaction from some positions indicates that for the interaction to occur, residues have to be well surface exposed (T217 of Rho is buried and C202 of Rho is partially exposed; see figure 4.27(b) bottom panel) and should be present on the same interaction-face (S156 is in the opposite face of NusG and T126 is in the flexible linker) of NusG. No di-sulphide bonded species were detected when single Cys Rho was crosslinked with NusG without Cys residue (Figure 4.27(a)). Western blot analysis using polyclonal antibody of Rho confirmed the presence of Rho in the Rho-NusG di-sulphide bonded band (species iii) (Figure 4.27(b)). To eliminate the possibility that this complex formation was

an artefact of the existence of lower oligomeric states of Rho as the experiments were performed in the absence of any co-factors, the same experiments with S25C and A168C NusGs were performed in the presence of 1 mM ATP. Presence of 1 mM ATP stabilizes the hexameric form of Rho. Similar patterns of di-sulphide bridge formation were obtained (Figure 4.27(c)). Therefore, this methodology yielded physiologically relevant complex formation between Rho and NusG and defined the interaction face of NusG in the complex in the absence of the EC.

If Cys residues from NusG and Rho in the Rho-NusG complex are close enough, it is possible that they can form di-sulphide bridges by aerial-oxidation in the absence of the catalyst Cu-P. In the absence of Cu-P significant amount di-sulphide bond formation from the positions S25 and A168 of NusG with K224 position of Rho were observed (Figure 4.27(d)). Therefore, regions surrounding S25 and A168 of NusG and K224 of Rho indeed come within di-sulphide bonding distance (~4Å) in the Rho-NusG complex. Bands formed due to di-sulphide bond (species ii and iii) disappeared in the presence of reducing agent DTT, which suggests that these were indeed disulphide bonded (Figure 4.27(e)).

The above results suggests several interesting molecular nature of the Rho-NusG complex. 1) Formation of di-sulphide bridges from the positions V147, S156, S161 and A168 of NusG is consistent with the occurrence of mutants defective for Rho-binding in the same region and further reinforce the proposition that this part of NusG-CTD directly interacts with Rho. 2) Interactions from G119 position of NusG suggests that the flexible linker region may also come close to Rho. 3) Di-sulphide bond formation capability from the position S25 in the NusG-NTD both in the presence and absence of Cu-P, which incidentally is also on the same face of the interacting regions in NusG-CTD suggests that this region of NTD can also come within the interacting region of Rho in the absence of EC.

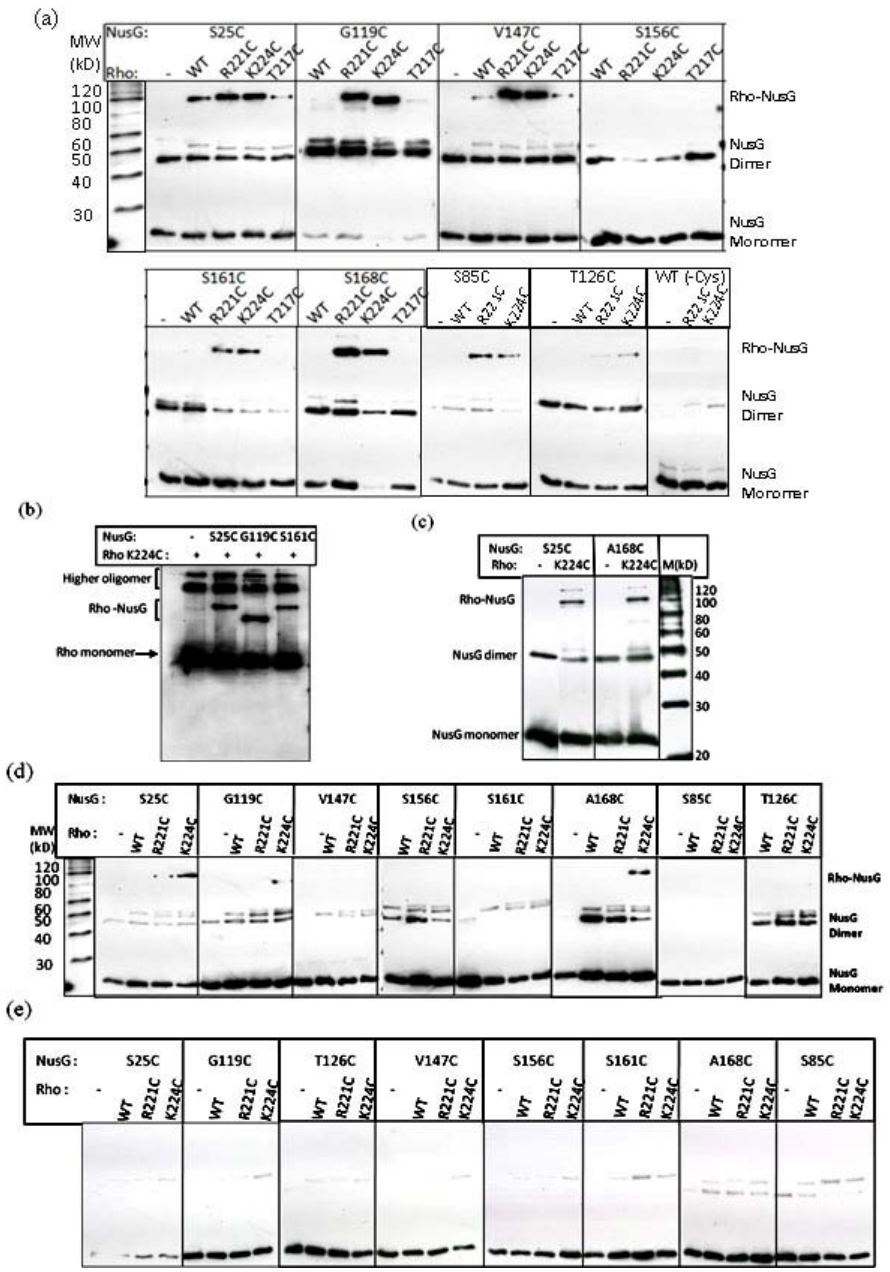

Figure 4.27: Site-specific Cys-Cys di-sulphide bond formation between different regions of NusG and Rho

(a) Western-blots probed with anti-NusG polyclonal antibody showing different NusG species in the presence of copper phenanthroline (Cu-P) between Rho and NusG single Cys mutants as indicated. Western-blot molecular weight marker (Magic Mark^{TM}) is indicated. Rho-NusG species indicates the di-sulphide bonded complexes between Rho and NusG. (b) Western-blot probed with anti-Rho polyclonal antibody showing the existence of Rho in the species labeled as Rho-NusG in the presence of Cu-P. (c) Western-blots probed with anti-NusG polyclonal antibody showing the formation of di-sulphide bonded species in the presence of Cu-P and 1 mM ATP. (d) Western-blots probed with NusG polyclonal antibody showing the formation of di-sulphide bonded species by aerial oxidation in the absence of Cu-P. (e) Western-blots probed with anti-NusG polyclonal antibody showing the absence of Cu-P induced di-sulphide bonded species in the presence of Cu-P and 100 mM DTT.

There can be two ways where two far-apart domains of NusG can form di-sulphide bridges with the same residues on Rho; either these two domains fold onto each other upon complex formation with Rho (species I in Figure 4.28(a)) or both the NusG-domains interact with the same residues which are located on the adjacent subunits of Rho (species II in figure 4.28(a)).

To resolve these issues S25C-S161C double Cys derivative of NusG was constructed. This species of NusG, capable of forming two di-sulphide bonds with Rho, upon complex formation will migrate as a Rho-monomer:NusG-monomer complex if species I is formed and will migrate as a Rho-dimer-NusG monomer if species II is formed in a non-reducing SDS-PAGE. This double derivative was incubated with either R221C or K224C Rho proteins and di-sulphide bridges were induced by Cu-P in a similar way as in Figure 4.27 (Figure 4.28(b)). NusG S25C-S161C formed Rho-dimer:NusG monomer complex with Rho (lanes 7 and 8). This species was not formed by NusG S25C-S161C either in the absence of Rho (lane 6) or in the presence of Rho C202S (lane 4 and 5). Single Cys derivative, S25C, also did not form this species. Therefore formation of Rho-dimer:NusG monomer complex was quite specific and we conclude that in the absence of EC, region around S25 of NusG-NTD can also interact with Rho but to the adjacent subunit to form the species II. The distances between S25 and S161 is ~50.5Å (Figure 4.28(c), upper panel), whereas the same between the two K224 residues from the adjacent subunits of Rho is ~47.5Å (Figure 4.28(c), lower panel). Therefore, structurally, formation of species II is also quite feasible.

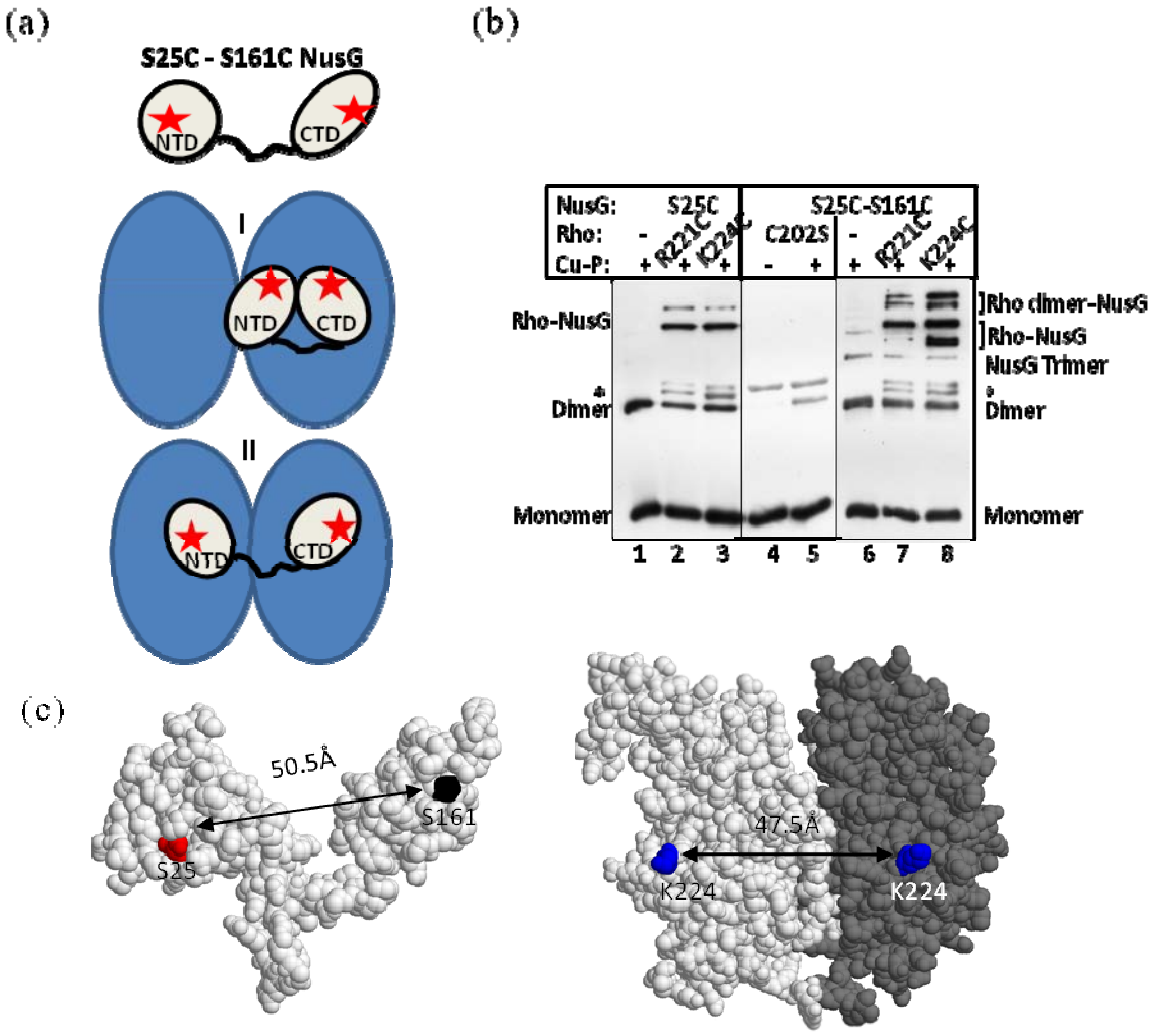

Figure 4.28: Site-specific di-sulphide bond formation between single Cys mutants of Rho and double Cys mutant of NusG:

(a) Cartoon of double Cys mutant of NusG showing the positions of two Cys residues (Top). Cartoon showing a probable di-sulphide bonded species in which two domains of NusG fold onto each other upon complex formation with Rho (indicated as species I) (Middle). Cartoon showing the second possibility in which both the NusG-domains interact with the same residues located on the adjacent subunits of Rho (indicated as species II) (Bottom). (b) Western-blot of non-reducing SDS-PAGE with anti-NusG polyclonal antibody showing the formation of di-sulphide bonded species in the presence of copper phenanthroline (Cu-P). NusG S25C-S161C formed Rho-dimer:NusG monomer complex (species II) with Rho R221C and Rho K224C. (c) Space filled structure of NusG showing the position of S25 and S161 and the distance between them (left). Space filled dimeric unit of the closed ring structure of Rho showing the position and the distance between the two K224 residues located in the two adjacent subunits of Rho (right). The structures and the distances were obtained using RASMOL software.

4.3.5 Point mutations in NusG-NTD

4.3.5.1 Effect of NusG-NTD mutants on *in vitro* transcription termination

As di-sulphide bonds with Rho can be formed from positions S25 and S85 of NusG-NTD, to investigate the functional importance of this region of NusG in Rho-NusG complex formation, different conserved amino acids of this region were mutated (Figure 4.29(a)). The ability of purified NusG variant proteins to stimulate Rho termination were assayed on a template containing *trp t'* terminator. The termination assays showed that NusG E19L, V22N, L26E and V83N failed to induce the early-termination (Figure 4.29(b)). These mutants were also not viable or had severe growth defect (indicated below the lanes in Figure 4.29(b)). This growth defects suggest that these mutants may have defect in interacting with the EC.

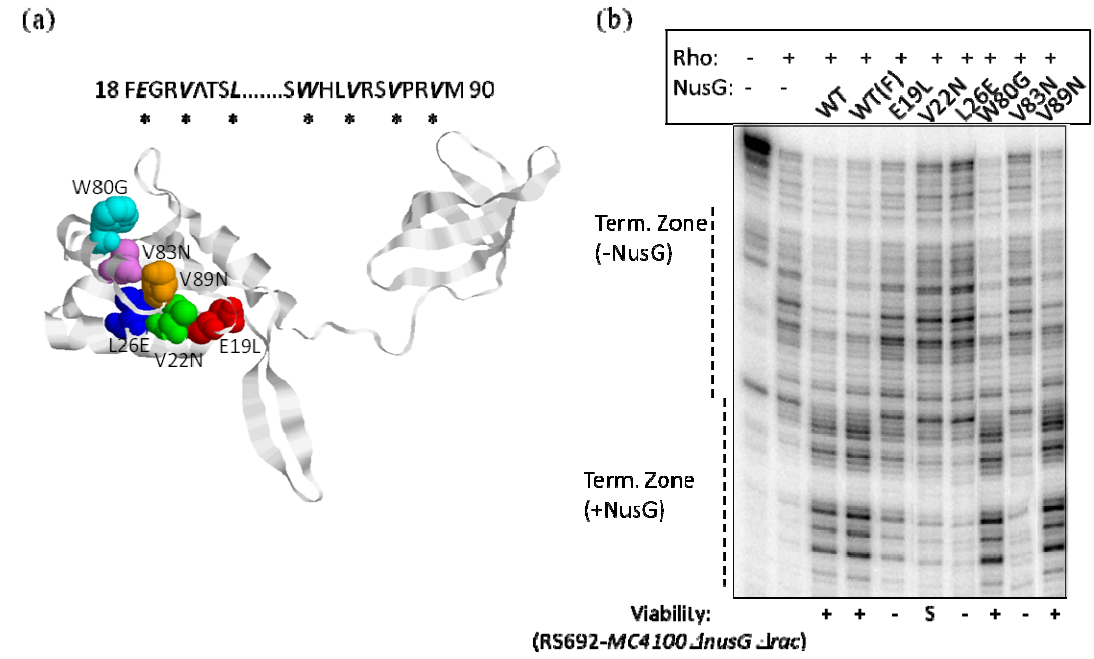

Figure 4.29: Mutations in NusG-NTD surrounding the di-sulphide forming sites:

(a) Locations of NusG-NTD mutants are shown on the NusG sequence (top) and on the ribbon representation of homology model of NusG (bottom). The asterisk (*****) indicates the residues mutated. (b) Autoradiogram of the *in vitro* transcription assays showing the Rho dependent termination in the *trp t'* terminator region in the absence and in the presence of WT and NusG-NTD mutant proteins as indicated. The termination zone is indicated. Point mutants NusG E19L, V22N, L26E and V83N failed to induce the early-termination but not the others. Result of *in vivo* complementation of *ΔnusG* with plasmids encoding WT and NusG-NTD mutants are indicated below each lane. '+' denotes viable, '-' denotes lethal and 'S' denotes smaller colony size compared to WT.

4.3.5.2 Effect of mutants on *ops* pause

NusG-NTD interacts with the EC and this interaction increases its elongation rate by suppressing transcriptional pauses. To directly measure the defects of the mutations in the NTD of NusG in interaction with the EC, their ability to induce anti-pausing at the *ops* pause site were assayed in a similar way as described earlier. It was observed that same mutants which were defective in inducing early-termination (Figure 4.29(b)) were also defective in anti-pausing activities (Figure 4.30). This suggests that even if this region of NusG-NTD interacts with Rho, it is also involved in the transcription elongation process.

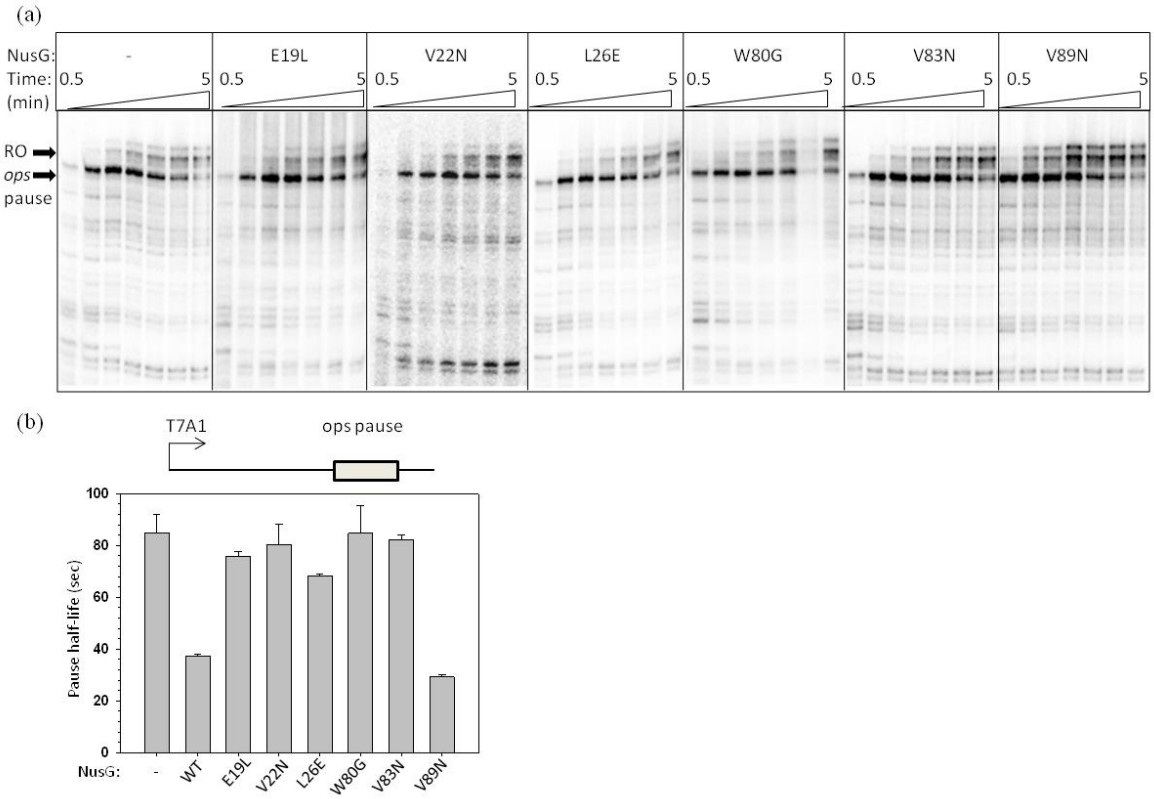

Figure 4.30: The effect of NusG-NTD mutants on *ops* pause suppression.

(a) Autoradiogram showing the time-course of transcription elongation through the *ops* pause sequence both in the absence and presence of NusG-NTD mutants. (b) Schematic of *ops*-containing transcription template (top). Bar diagrams showing the pausing half-lives at the *ops* pause in the absence and presence of NusG-NTD mutants. Pause half-life is the time taken by half of the complexes to escape the pause.

4.3.5.3 *In vitro* Rho – NusG binding

It is possible that the mutations in the NTD of NusG which failed to induce the early-termination produced functionally inactive NusG proteins. Binding analysis of the NusG-NTD mutants with Rho were performed in a similar way as described earlier. None of them showed very serious defects in retaining Rho (Figure 4.31), which was not surprising because in all these derivatives, NusG-CTD was intact and the later domain itself possessed the binding determinant for Rho (Figure 4.14). These results suggest that the lack of activity of these mutants were not because of production of functionally inactive NusG proteins and is due to an inability in its EC-binding function.

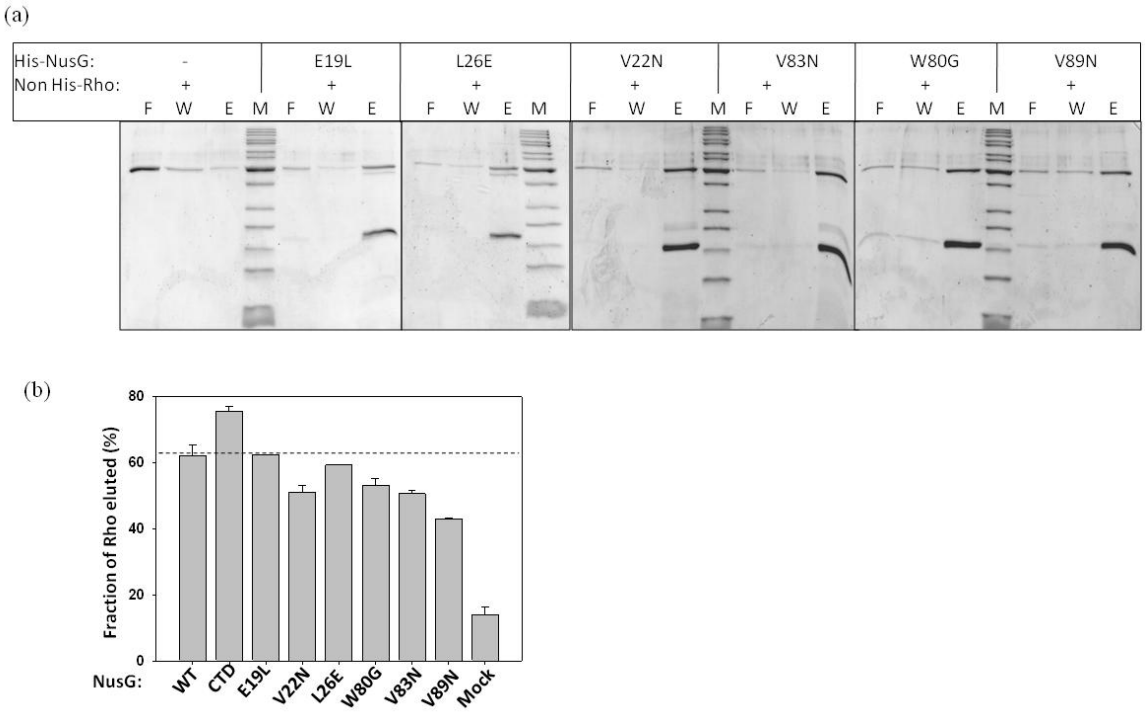

Figure 4.31: Rho binding analysis of WT and different NusG-NTD point mutations.

(a) Rho was passed over different NusG-NTD mutants attached to Ni-NTA beads. None of the NusG-NTD mutants were defective in binding to Rho. (b) Bar diagrams showing the amounts of Rho retained with different NusG-NTD mutants.

4.4 Discussion

Rho-dependent transcription termination is a well conserved process among the prokaryotes. Interaction of Rho with the transcription elongation factor NusG is required for efficient transcription termination (Cardinale et al., 2008). The binding surface of NusG involved in the Rho-NusG interaction is not yet known and the knowledge of which is essential for understanding the mechanism of termination process.

This study provides the following lines of evidence which strongly suggest that G146, V148, L158, V160 and I164 in the β-sheet bundles of NusG-CTD are involved in direct interactions with Rho.

1. NusG-CTD but not NusG-NTD could pulldown Rho from crude lysate.
2. NusG-CTD deletion mutants were lethal *in vivo* and failed to enhance early Rho dependent termination *in vitro.*
3. NusG-CTD point mutants (G146D, V148N, L158Q, V160N and I164A) exhibited significantly reduced *in vivo* termination efficiency and poor growth at 30 ^{o}C.
4. *In vitro* transcription studies showed that these mutants were unable to induce early termination.
5. NusG-CTD deletion mutants and point mutants (G146D, V148N, L158Q, V160N and I164A) failed to interact with Rho in *in vitro* Rho-NusG binding assay.
6. From this region of NusG, di-sulphide bridges can be induced with the surface exposed amino acids 202, 221 and 224 of Rho, which are located in the well conserved P-loop domain of Rho.

NusG-NTD enhanced the transcription elongation rate similar to WT NusG (Figure 4.16) and could compete out WT NusG both *in vivo* and *in vitro* (Figure 4.17). Thus the failure of NusG-NTD to interact with Rho can be the reason for the overexpression toxicity of NusG-NTD. Though NusG-CTD can bind to Rho and can compete out WT NusG from binding with Rho (Figure 4.15), neither its *in vivo* over expression was lethal nor could it compete out WT NusG during *in vitro* transcription (Figure 4.17). This inability of NusG–CTD to compete out WT NusG in the presence of EC could be due to the enhanced stability achieved by NusG through interaction with RNAP. These results shows that enhancement of Rho-dependent termination requires both the NusG domains.

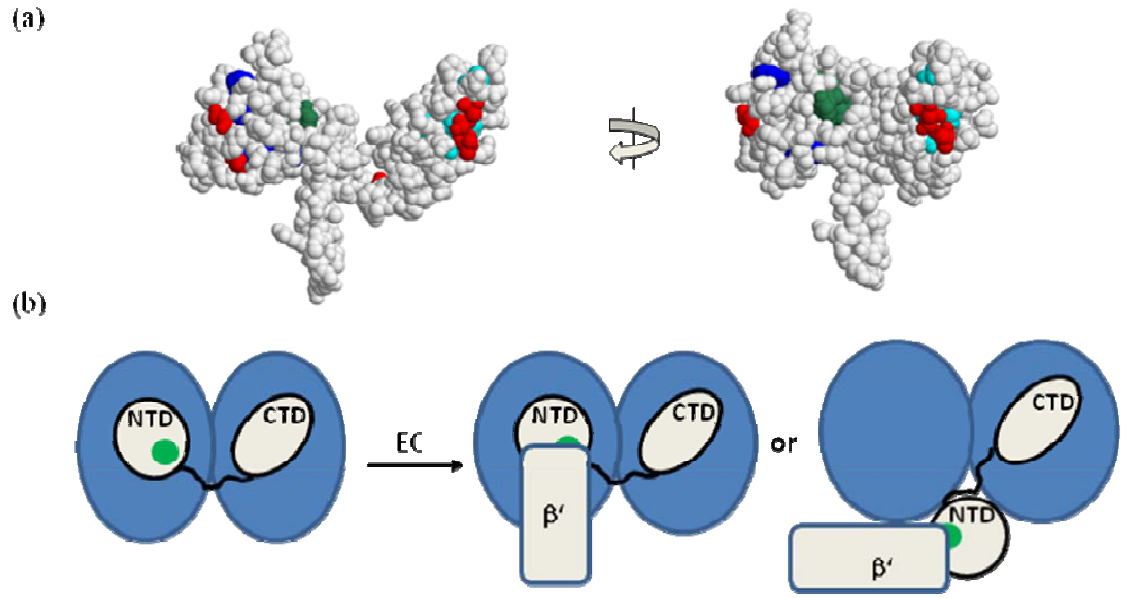

Figure 4.32

(a) Interaction faces of NusG for Rho. Location of defective NusG-NTD mutants (in blue), NusG-CTD mutants defective for Rho-binding (in cyan) and amino acid positions which forms di-sulphide bonds with Rho (in red) are shown on the homology model of NusG. The green spheres represent the hydrophobic patch that interacts with EC (Mooney et al., 2009). (b) Model of Rho-NusG interaction in the presence and absence of EC. The green circle denotes the hydrophobic patch on NusG-NTD located opposite to the Rho-binding face of NusG that interacts with the β' subunit of the RNAP of the EC.

Mapping of the defective NusG-NTD mutants (in blue) on the homology model of NusG (Figure 4.32(a)) revealed that they are located on the same face of NusG where the amino acids which are either forming di-sulphide bonds with Rho (in red) or defective for Rho-binding (in cyan) are located. Interestingly the hydrophobic patch (in green; (Belogurov et al., 2007)) that binds to the EC is located opposite to this whole face which interacts with Rho. This suggests that in the absence of EC, the whole face of NusG comprising of NusG-CTD and a part of NusG-NTD interacts with a dimer of Rho and in the presence of EC the β' subunit of RNAP interacts with the hydrophobic patch at the opposite face of NusG. This interaction of the NusG-NTD with the EC removes the less stable Rho-NusG-NTD contacts (Figure 4.32(b)).

Cys-Cys cross-linking with the S25C-S161C derivative of NusG revealed that in the absence of the EC, a monomer of NusG can be cross-linked to a dimer of Rho (Figure

4.28(b)). Earlier the stoichiometry of this complex was reported to be 1:1 between a monomer of NusG and a hexamer of Rho (Pasman and von Hippel, 2000). Therefore at a given time, only one of the NusG-binding sites on Rho is occupied and this suggests an existence of a negative co-operativity among these binding sites. Preference of a particular site will most likely be guided by the orientation of the Rho molecule during its translocation along the RNA.

Apart from being a component of the EC, NusG is also a key factor of N-and *rrn* gene antitermination machinery (Sen et al., 2008). Genomic analysis revealed that *E. coli* NusG has several interacting partners, including different ribosomal proteins (Butland et al., 2005). As the NusG-NTD is anchored to the EC, the NusG-CTD will be available to interact with ribosomal proteins and those from the antitermination machinery, and hence there will be a direct competition between Rho and these proteins for the CTD. This will in turn determine the efficiency and frequency of Rho-dependent termination. The possible interactions of NusG-CTD with ribosomal protein(s) could provide the mutual exclusiveness of a transcript to be either translated by ribosome or be terminated by Rho. Similarly, antitermination of Rho-dependent termination by the N-NusA-NusG complex could also occur by preventing the NusG-CTD-Rho interaction.

How does NusG modulate the Rho-dependent termination? Binding of NusG to Rho does not affect the latter's RNA binding, ATPase or helicase activities, but enhances its speed of RNA release. Therefore, the only way to enhance the speed and efficiency of RNA release is to recruit Rho close to the RNA-exit channel of the EC. It can be speculated that the docking of NusG at the C-terminal P-loop domain of Rho most likely orient the latter in such a way that its C-terminal RNA-entry point of the central hole faces the RNA-exit channel of the EC. This region of Rho may directly interact with EC (Epshtein et al., 2010) and could constitute the elusive "termination domain" of Rho. Protein-protein foot printing studies and site specific cleavage of Rho-NusG complex in the presence of EC will further help to identify the complete binding surface of Rho and NusG involved in the interaction.

References

Abbondanzieri, E. A., Greenleaf, W. J., Shaevitz, J. W., Landick, R., and Block, S. M. (2005). Direct observation of base-pair stepping by RNA polymerase. Nature 438, 460-465.

Adelman, J. L., Jeong, Y. J., Liao, J. C., Patel, G., Kim, D. E., Oster, G., and Patel, S. S. (2006). Mechanochemistry of transcription termination factor Rho. Mol Cell 22, 611-621.

Adhya, S., and Gottesman, M. (1978). Control of transcription termination. Annu Rev Biochem 47, 967-996.

Alifano, P., Rivellini, F., Limauro, D., Bruni, C. B., and Carlomagno, M. S. (1991). A consensus motif common to all Rho-dependent prokaryotic transcription terminators. Cell 64, 553-563.

Artsimovitch, I., and Landick, R. (2000). Pausing by bacterial RNA polymerase is mediated by mechanistically distinct classes of signals. Proc Natl Acad Sci U S A 97, 7090-7095.

Artsimovitch, I., and Landick, R. (2002). The transcriptional regulator RfaH stimulates RNA chain synthesis after recruitment to elongation complexes by the exposed nontemplate DNA strand. Cell 109, 193-203.

Banerjee, S., Chalissery, J., Bandey, I., and Sen, R. (2006). Rho-dependent transcription termination: more questions than answers. J Microbiol 44, 11-22.

Bar-Nahum, G., Epshtein, V., Ruckenstein, A. E., Rafikov, R., Mustaev, A., and Nudler, E. (2005). A ratchet mechanism of transcription elongation and its control. Cell 120, 183-193.

Bar-Nahum, G., and Nudler, E. (2001). Isolation and characterization of sigma(70)-retaining transcription elongation complexes from Escherichia coli. Cell 106, 443-451.

Bear, D. G., Andrews, C. L., Singer, J. D., Morgan, W. D., Grant, R. A., von Hippel, P. H., and Platt, T. (1985). Escherichia coli transcription termination factor rho has a two-domain structure in its activated form. Proc Natl Acad Sci U S A 82, 1911-1915.

Bear, D. G., Hicks, P. S., Escudero, K. W., Andrews, C. L., McSwiggen, J. A., and von Hippel, P. H. (1988). Interactions of Escherichia coli transcription termination factor rho with RNA. II. Electron microscopy and nuclease protection experiments. J Mol Biol 199, 623-635.

Belogurov, G. A., Vassylyeva, M. N., Sevostyanova, A., Appleman, J. R., Xiang, A. X., Lira, R., Webber, S. E., Klyuyev, S., Nudler, E., Artsimovitch, I., and Vassylyev, D. G. (2009). Transcription inactivation through local refolding of the RNA polymerase structure. Nature 457, 332-335.

Belogurov, G. A., Vassylyeva, M. N., Svetlov, V., Klyuyev, S., Grishin, N. V., Vassylyev, D. G., and Artsimovitch, I. (2007). Structural basis for converting a general transcription factor into an operon-specific virulence regulator. Mol Cell 26, 117-129.

Blatter, E. E., Ross, W., Tang, H., Gourse, R. L., and Ebright, R. H. (1994). Domain organization of RNA polymerase alpha subunit: C-terminal 85 amino acids constitute a domain capable of dimerization and DNA binding. Cell 78, 889-896.

Blumenthal, R. M., Reeh, S., and Pedersen, S. (1976). Regulation of transcription factor rho and the alpha subunit of RNA polymerase in Escherichia coli B/r. Proc Natl Acad Sci U S A 73, 2285-2288.

Bogden, C. E., Fass, D., Bergman, N., Nichols, M. D., and Berger, J. M. (1999). The structural basis for terminator recognition by the Rho transcription termination factor. Mol Cell 3, 487-493.

Borukhov, S., Polyakov, A., Nikiforov, V., and Goldfarb, A. (1992). GreA protein: a transcription elongation factor from Escherichia coli. Proc Natl Acad Sci U S A 89, 8899-8902.

Borukhov, S., Sagitov, V., and Goldfarb, A. (1993). Transcript cleavage factors from E. coli. Cell 72, 459-466.

Borukhov, S., and Severinov, K. (2002). Role of the RNA polymerase sigma subunit in transcription initiation. Res Microbiol 153, 557-562.

Bregeon, D., Colot, V., Radman, M., and Taddei, F. (2001). Translational misreading: a tRNA modification counteracts a +2 ribosomal frameshift. Genes Dev 15, 2295-2306.

Bregeon, D., Doddridge, Z. A., You, H. J., Weiss, B., and Doetsch, P. W. (2003). Transcriptional mutagenesis induced by uracil and 8-oxoguanine in Escherichia coli. Mol Cell 12, 959-970.

Brennan, C. A., Dombroski, A. J., and Platt, T. (1987). Transcription termination factor rho is an RNA-DNA helicase. Cell 48, 945-952.

Bridges, B. A. (1999). Dirty transcripts from clean DNA. Science 284, 62-63.

Brodolin, K., Zenkin, N., and Severinov, K. (2005). Remodeling of the sigma70 subunit non-template DNA strand contacts during the final step of transcription initiation. J Mol Biol 350, 930-937.

Bubunenko, M., Baker, T., and Court, D. L. (2007). Essentiality of ribosomal and transcription antitermination proteins analyzed by systematic gene replacement in Escherichia coli. J Bacteriol 189, 2844-2853.

Burgess, B. R., and Richardson, J. P. (2001a). RNA passes through the hole of the protein hexamer in the complex with the Escherichia coli Rho factor. J Biol Chem 276, 4182-4189.

Burgess, B. R., and Richardson, J. P. (2001b). Transcription factor Rho does not require a free end to act as an RNA-DNA helicase on an RNA. J Biol Chem 276, 17106-17110.

Burns, C. M., Nowatzke, W. L., and Richardson, J. P. (1999). Activation of Rho-dependent transcription termination by NusG. Dependence on terminator location and acceleration of RNA release. J Biol Chem 274, 5245-5251.

Burns, C. M., and Richardson, J. P. (1995). NusG is required to overcome a kinetic limitation to Rho function at an intragenic terminator. Proc Natl Acad Sci U S A 92, 4738-4742.

Burns, C. M., Richardson, L. V., and Richardson, J. P. (1998). Combinatorial effects of NusA and NusG on transcription elongation and Rho-dependent termination in Escherichia coli. J Mol Biol 278, 307-316.

Burova, E., and Gottesman, M. E. (1995). NusG overexpression inhibits Rho-dependent termination in Escherichia coli. Mol Microbiol 17, 633-641.

Burova, E., Hung, S. C., Chen, J., Court, D. L., Zhou, J. G., Mogilnitskiy, G., and Gottesman, M. E. (1999). Escherichia coli nusG mutations that block transcription termination by coliphage HK022 Nun protein. Mol Microbiol 31, 1783-1793.

Burova, E., Hung, S. C., Sagitov, V., Stitt, B. L., and Gottesman, M. E. (1995). Escherichia coli NusG protein stimulates transcription elongation rates in vivo and in vitro. J Bacteriol 177, 1388-1392.

Butland, G., Peregrin-Alvarez, J. M., Li, J., Yang, W., Yang, X., Canadien, V., Starostine, A., Richards, D., Beattie, B., Krogan, N., et al. (2005). Interaction network containing conserved and essential protein complexes in Escherichia coli. Nature 433, 531-537.

Callaci, S., Heyduk, E., and Heyduk, T. (1998). Conformational changes of Escherichia coli RNA polymerase sigma70 factor induced by binding to the core enzyme. J Biol Chem 273, 32995-33001.

Callaci, S., Heyduk, E., and Heyduk, T. (1999). Core RNA polymerase from E. coli induces a major change in the domain arrangement of the sigma 70 subunit. Mol Cell 3, 229-238.

Cardinale, C. J., Washburn, R. S., Tadigotla, V. R., Brown, L. M., Gottesman, M. E., and Nudler, E. (2008). Termination factor Rho and its cofactors NusA and NusG silence foreign DNA in E. coli. Science 320, 935-938.

Carpousis, A. J., and Gralla, J. D. (1980). Cycling of ribonucleic acid polymerase to produce oligonucleotides during initiation in vitro at the lac UV5 promoter. Biochemistry 19, 3245-3253.

Carpousis, A. J., and Gralla, J. D. (1985). Interaction of RNA polymerase with lacUV5 promoter DNA during mRNA initiation and elongation. Footprinting, methylation, and rifampicin-sensitivity changes accompanying transcription initiation. J Mol Biol 183, 165-177.

Carrano, L., Alifano, P., Corti, E., Bucci, C., and Donadio, S. (2003). A new inhibitor of the transcription-termination factor Rho. Biochem Biophys Res Commun 302, 219-225.

Chalissery, J., Banerjee, S., Bandey, I. and Sen, R. (2007). Transcription termination defective mutants of Rho: role of different functions of Rho in releasing RNA from the elongation complex. J Mol Biol. 371, 855-872.

Chan, B., and Busby, S. (1989). Recognition of nucleotide sequences at the Escherichia coli galactose operon P1 promoter by RNA polymerase. Gene 84, 227-236.

Chattopadhyay, S., Garcia-Mena, J., DeVito, J., Wolska, K., and Das, A. (1995). Bipartite function of a small RNA hairpin in transcription antitermination in bacteriophage lambda. Proc Natl Acad Sci U S A 92, 4061-4065.

Cheeran, A., Babu Suganthan, R., Swapna, G., Bandey, I., Achary, M. S., Nagarajaram, H. A., and Sen, R. (2005). Escherichia coli RNA polymerase mutations located near the upstream edge of an RNA:DNA hybrid and the beginning of the RNA-exit channel are defective for transcription antitermination by the N protein from lambdoid phage H-19B. J Mol Biol 352, 28-43.

Chen, X., and Stitt, B. L. (2004). The binding of C10 oligomers to Escherichia coli transcription termination factor Rho. J Biol Chem 279, 16301-16310.

Condon, C., Squires, C., and Squires, C. L. (1995). Control of rRNA transcription in Escherichia coli. Microbiol Rev 59, 623-645.

Das, A., Court, D., and Adhya, S. (1976). Isolation and characterization of conditional lethal mutants of Escherichia coli defective in transcription termination factor rho. Proc Natl Acad Sci U S A 73, 1959-1963.

Das, A., Merril, C., and Adhya, S. (1978). Interaction of RNA polymerase and rho in transcription termination: coupled ATPase. Proc Natl Acad Sci U S A 75, 4828-4832.

Davis, C. A., Bingman, C. A., Landick, R., Record, M. T., Jr., and Saecker, R. M. (2007). Real-time footprinting of DNA in the first kinetically significant intermediate in open complex formation by Escherichia coli RNA polymerase. Proc Natl Acad Sci U S A 104, 7833-7838.

de Smit, M. H., Verlaan, P. W., van Duin, J., and Pleij, C. W. (2008). Intracistronic transcriptional polarity enhances translational repression: a new role for Rho. Mol Microbiol 69, 1278-1289.

de Smit, M. H., Verlaan, P. W., van Duin, J., and Pleij, C. W. (2009). In vivo dynamics of intracistronic transcriptional polarity. J Mol Biol 385, 733-747.

Deaconescu, A. M., Chambers, A. L., Smith, A. J., Nickels, B. E., Hochschild, A., Savery, N. J., and Darst, S. A. (2006). Structural basis for bacterial transcription-coupled DNA repair. Cell 124, 507-520.

Dokland, T., Isaksen, M. L., Fuller, S. D., and Lindqvist, B. H. (1993). Capsid localization of the bacteriophage P4 Psu protein. Virology 194, 682-687.

Dolan, J. W., Marshall, N. F., and Richardson, J. P. (1990). Transcription termination factor rho has three distinct structural domains. J Biol Chem 265, 5747-5754.

Dombroski, A. J., and Platt, T. (1988). Structure of rho factor: an RNA-binding domain and a separate region with strong similarity to proven ATP-binding domains. Proc Natl Acad Sci U S A 85, 2538-2542.

Dombroski, A. J., Walter, W. A., and Gross, C. A. (1993a). Amino-terminal amino acids modulate sigma-factor DNA-binding activity. Genes Dev 7, 2446-2455.

Dombroski, A. J., Walter, W. A., and Gross, C. A. (1993b). The role of the sigma subunit in promoter recognition by RNA polymerase. Cell Mol Biol Res 39, 311-317.

Dombroski, A. J., Walter, W. A., Record, M. T., Jr., Siegele, D. A., and Gross, C. A. (1992). Polypeptides containing highly conserved regions of transcription initiation factor sigma 70 exhibit specificity of binding to promoter DNA. Cell 70, 501-512.

Downing, W. L., Sullivan, S. L., Gottesman, M. E., and Dennis, P. P. (1990). Sequence and transcriptional pattern of the essential Escherichia coli secE-nusG operon. J Bacteriol 172, 1621-1627.

Drivdahl, R. H., and Kutter, E. M. (1990). Inhibition of transcription of cytosine-containing DNA in vitro by the alc gene product of bacteriophage T4. J Bacteriol 172, 2716-2727.

Dutta, D., Chalissery, J., and Sen, R. (2008). Transcription termination factor rho prefers catalytically active elongation complexes for releasing RNA. J Biol Chem 283, 20243-20251.

Ebright, R. H. (2000). RNA polymerase: structural similarities between bacterial RNA polymerase and eukaryotic RNA polymerase II. J Mol Biol 304, 687-698.

Eisenmann, A., Schwarz, S., Prasch, S., Schweimer, K., and Rosch, P. (2005). The E. coli NusA carboxy-terminal domains are structurally similar and show specific RNAP- and lambdaN interaction. Protein Sci 14, 2018-2029.

Ellinger, T., Behnke, D., Bujard, H., and Gralla, J. D. (1994). Stalling of Escherichia coli RNA polymerase in the +6 to +12 region in vivo is associated with tight binding to consensus promoter elements. J Mol Biol 239, 455-465.

Enemark, E. J., and Joshua-Tor, L. (2006). Mechanism of DNA translocation in a replicative hexameric helicase. Nature 442, 270-275.

Epshtein, V., Cardinale, C. J., Ruckenstein, A. E., Borukhov, S., and Nudler, E. (2007). An allosteric path to transcription termination. Mol Cell 28, 991-1001.

Epshtein, V., Dutta, D., Wade, J., and Nudler, E. (2010). An allosteric mechanism of Rho-dependent transcription termination. Nature 463, 245-249.

Erie, D. A., Hajiseyedjavadi, O., Young, M. C., and von Hippel, P. H. (1993). Multiple RNA polymerase conformations and GreA: control of the fidelity of transcription. Science 262, 867-873.

Faber, C., Scharpf, M., Becker, T., Sticht, H., and Rosch, P. (2001). The structure of the coliphage HK022 Nun protein-lambda-phage boxB RNA complex. Implications for the mechanism of transcription termination. J Biol Chem 276, 32064-32070.

Feklistov, A., Barinova, N., Sevostyanova, A., Heyduk, E., Bass, I., Vvedenskaya, I., Kuznedelov, K., Merkiene, E., Stavrovskaya, E., Klimasauskas, S., et al. (2006). A basal promoter element recognized by free RNA polymerase sigma subunit determines promoter recognition by RNA polymerase holoenzyme. Mol Cell 23, 97-107.

Feng, G. H., Lee, D. N., Wang, D., Chan, C. L., and Landick, R. (1994). GreA-induced transcript cleavage in transcription complexes containing Escherichia coli RNA polymerase is controlled by multiple factors, including nascent transcript location and structure. J Biol Chem 269, 22282-22294.

Fisher, R. F., and Yanofsky, C. (1983). Mutations of the beta subunit of RNA polymerase alter both transcription pausing and transcription termination in the trp operon leader region in vitro. J Biol Chem 258, 8146-8150.

Fujita, N., Endo, S., and Ishihama, A. (2000). Structural requirements for the interdomain linker of alpha subunit of Escherichia coli RNA polymerase. Biochemistry 39, 6243-6249.

Geiselmann, J., Yager, T. D., Gill, S. C., Calmettes, P., and von Hippel, P. H. (1992a). Physical properties of the Escherichia coli transcription termination factor rho. 1. Association states and geometry of the rho hexamer. Biochemistry 31, 111-121.

Geiselmann, J., Yager, T. D., and von Hippel, P. H. (1992b). Functional interactions of ligand cofactors with Escherichia coli transcription termination factor rho. II. Binding of RNA. Protein Sci 1, 861-873.

Ghosh, P., Ishihama, A., and Chatterji, D. (2001). Escherichia coli RNA polymerase subunit omega and its N-terminal domain bind full-length beta' to facilitate incorporation into the alpha2beta subassembly. Eur J Biochem 268, 4621-4627.

Gogol, E. P., Seifried, S. E., and von Hippel, P. H. (1991). Structure and assembly of the Escherichia coli transcription termination factor rho and its interaction with RNA. I. Cryoelectron microscopic studies. J Mol Biol 221, 1127-1138.

Goldman, S. R., Ebright, R. H., and Nickels, B. E. (2009). Direct detection of abortive RNA transcripts in vivo. Science 324, 927-928.

Gowrishankar, J., and Harinarayanan, R. (2004). Why is transcription coupled to translation in bacteria? Mol Microbiol 54, 598-603.

Grachev, M. A., and Zaychikov, E. F. (1980). Initiation by Escherichia coli RNA-polymerase: transformation of abortive to productive complex. FEBS Lett 115, 23-26.

Gralla, J. D., Carpousis, A. J., and Stefano, J. E. (1980). Productive and abortive initiation of transcription in vitro at the lac UV5 promoter. Biochemistry 19, 5864-5869.

Greenblatt, J., and Li, J. (1981). Interaction of the sigma factor and the nusA gene protein of E. coli with RNA polymerase in the initiation-termination cycle of transcription. Cell 24, 421-428.

Greive, S. J., and von Hippel, P. H. (2005). Thinking quantitatively about transcriptional regulation. Nat Rev Mol Cell Biol 6, 221-232.

Grigorova, I. L., Phleger, N. J., Mutalik, V. K., and Gross, C. A. (2006). Insights into transcriptional regulation and sigma competition from an equilibrium model of RNA polymerase binding to DNA. Proc Natl Acad Sci U S A 103, 5332-5337.

Gruber, T. M., and Gross, C. A. (2003). Multiple sigma subunits and the partitioning of bacterial transcription space. Annu Rev Microbiol 57, 441-466.

Guajardo, R., and Sousa, R. (1997). A model for the mechanism of polymerase translocation. J Mol Biol 265, 8-19.

Guarente, L. P., and Beckwith, J. (1978). Mutant RNA polymerase of Escherichia coli terminates transcription in strains making defective rho factor. Proc Natl Acad Sci U S A 75, 294-297.

Gusarov, I., and Nudler, E. (1999). The mechanism of intrinsic transcription termination. Mol Cell 3, 495-504.

Gutierrez, P., Kozlov, G., Gabrielli, L., Elias, D., Osborne, M. J., Gallouzi, I. E., and Gehring, K. (2007). Solution structure of YaeO, a Rho-specific inhibitor of transcription termination. J Biol Chem 282, 23348-23353.

Harinarayanan, R., and Gowrishankar, J. (2003). Host factor titration by chromosomal R-loops as a mechanism for runaway plasmid replication in transcription termination-defective mutants of Escherichia coli. J Mol Biol 332, 31-46.

Harley, C. B., and Reynolds, R. P. (1987). Analysis of E. coli promoter sequences. Nucleic Acids Res 15, 2343-2361.

Hart, C. M., and Roberts, J. W. (1994). Deletion analysis of the lambda tR1 termination region. Effect of sequences near the transcript release sites, and the minimum length of rho-dependent transcripts. J Mol Biol 237, 255-265.

Haugen, S. P., Berkmen, M. B., Ross, W., Gaal, T., Ward, C., and Gourse, R. L. (2006). rRNA promoter regulation by nonoptimal binding of sigma region 1.2: an additional recognition element for RNA polymerase. Cell 125, 1069-1082.

Hawley, D. K., and McClure, W. R. (1983). Compilation and analysis of Escherichia coli promoter DNA sequences. Nucleic Acids Res 11, 2237-2255.

Hengge-Aronis, R. (1996). Back to log phase: sigma S as a global regulator in the osmotic control of gene expression in Escherichia coli. Mol Microbiol 21, 887-893.

Henthorn, K. S., and Friedman, D. I. (1996). Identification of functional regions of the Nun transcription termination protein of phage HK022 and the N antitermination protein of phage lambda using hybrid nun-N genes. J Mol Biol 257, 9-20.

Hitchens, T. K., Zhan, Y., Richardson, L. V., Richardson, J. P., and Rule, G. S. (2006). Sequence-specific interactions in the RNA-binding domain of Escherichia coli transcription termination factor Rho. J Biol Chem 281, 33697-33703.

Howard, B. H., and de Crombrugghe, B. (1976). ATPase activity required for termination of transcription by the Escherichia coli protein factor rho. J Biol Chem 251, 2520-2524.

Hsu, L. M., Vo, N. V., and Chamberlin, M. J. (1995). Escherichia coli transcript cleavage factors GreA and GreB stimulate promoter escape and gene expression in vivo and in vitro. Proc Natl Acad Sci U S A 92, 11588-11592.

Hughes, K. T., and Mathee, K. (1998). The anti-sigma factors. Annu Rev Microbiol 52, 231-286.

Hung, S. C., and Gottesman, M. E. (1995). Phage HK022 Nun protein arrests transcription on phage lambda DNA in vitro and competes with the phage lambda N antitermination protein. J Mol Biol 247, 428-442.

Igarashi, K., Fujita, N., and Ishihama, A. (1991a). Identification of a subunit assembly domain in the alpha subunit of Escherichia coli RNA polymerase. J Mol Biol 218, 1-6.

Igarashi, K., Hanamura, A., Makino, K., Aiba, H., Aiba, H., Mizuno, T., Nakata, A., and Ishihama, A. (1991b). Functional map of the alpha subunit of Escherichia coli RNA polymerase: two modes of transcription activation by positive factors. Proc Natl Acad Sci U S A 88, 8958-8962.

Igarashi, K., and Ishihama, A. (1991). Bipartite functional map of the E. coli RNA polymerase alpha subunit: involvement of the C-terminal region in transcription activation by cAMP-CRP. Cell 65, 1015-1022.

Imai, M., and Shigesada, K. (1978). Studies on the altered rho factor in a nitA mutants of Escherichia coli defective in transcription termination. I. Characterization and quantitative determination of rho in cell extracts. J Mol Biol 120, 451-466.

Ingham, C. J., Dennis, J., and Furneaux, P. A. (1999). Autogenous regulation of transcription termination factor Rho and the requirement for Nus factors in Bacillus subtilis. Mol Microbiol 31, 651-663.

Isaksen, M. L., Rishovd, S. T., Calendar, R., and Lindqvist, B. H. (1992). The polarity suppression factor of bacteriophage P4 is also a decoration protein of the P4 capsid. Virology 188, 831-839.

Iseki, M., Miyoshi, T., Konomi, T., and Imanaka, H. (1980). Biosynthesis of bicyclomycin. II. Biosynthetic conditions and incorporation of radioactive precursors into bicyclomycin by washed mycelium. J Antibiot (Tokyo) 33, 488-493.

Ishihama, A. (1981). Subunit of assembly of Escherichia coli RNA polymerase. Adv Biophys 14, 1-35.

Ishihama, A. (2000). Functional modulation of Escherichia coli RNA polymerase. Annu Rev Microbiol 54, 499-518.

Jager, S., Fuhrmann, O., Heck, C., Hebermehl, M., Schiltz, E., Rauhut, R., and Klug, G. (2001). An mRNA degrading complex in Rhodobacter capsulatus. Nucleic Acids Res 29, 4581-4588.

Jeon, Y. H., Negishi, T., Shirakawa, M., Yamazaki, T., Fujita, N., Ishihama, A., and Kyogoku, Y. (1995). Solution structure of the activator contact domain of the RNA polymerase alpha subunit. Science 270, 1495-1497.

Jeon, Y. H., Yamazaki, T., Otomo, T., Ishihama, A., and Kyogoku, Y. (1997). Flexible linker in the RNA polymerase alpha subunit facilitates the independent motion of the C-terminal activator contact domain. J Mol Biol 267, 953-962.

Jeong, Y. J., Kim, D. E., and Patel, S. S. (2004). Nucleotide binding induces conformational changes in Escherichia coli transcription termination factor Rho. J Biol Chem 279, 18370-18376.

Jin, D. J., Burgess, R. R., Richardson, J. P., and Gross, C. A. (1992). Termination efficiency at rho-dependent terminators depends on kinetic coupling between RNA polymerase and rho. Proc Natl Acad Sci U S A 89, 1453-1457.

Jin, D. J., and Gross, C. A. (1988). Mapping and sequencing of mutations in the Escherichia coli rpoB gene that lead to rifampicin resistance. J Mol Biol 202, 45-58.

Kainz, M., and Gourse, R. L. (1998). The C-terminal domain of the alpha subunit of Escherichia coli RNA polymerase is required for efficient rho-dependent transcription termination. J Mol Biol 284, 1379-1390.

Kainz, M., and Roberts, J. (1992). Structure of transcription elongation complexes in vivo. Science 255, 838-841.

Kalarickal, N. C., Ranjan, A., Kalyani, B. S., Wal, M., and Sen, R. (2010). A bacterial transcription terminator with inefficient molecular motor action but with a robust transcription termination function. J Mol Biol 395, 966-982.

Kamiya, T., Maeno, S., Hashimoto, M., and Mine, Y. (1972). Bicyclomycin, a new antibiotic. II. Structural elucidation and acyl derivatives. J Antibiot (Tokyo) 25, 576-581.

Kapanidis, A. N., Margeat, E., Ho, S. O., Kortkhonjia, E., Weiss, S., and Ebright, R. H. (2006). Initial transcription by RNA polymerase proceeds through a DNA-scrunching mechanism. Science 314, 1144-1147.

Kashlev, M., Nudler, E., Goldfarb, A., White, T., and Kutter, E. (1993). Bacteriophage T4 Alc protein: a transcription termination factor sensing local modification of DNA. Cell 75, 147-154.

Kassavetis, G. A., and Chamberlin, M. J. (1981). Pausing and termination of transcription within the early region of bacteriophage T7 DNA in vitro. J Biol Chem 256, 2777-2786.

Keilty, S., and Rosenberg, M. (1987). Constitutive function of a positively regulated promoter reveals new sequences essential for activity. J Biol Chem 262, 6389-6395.

Kim, D. E., and Patel, S. S. (1999). The mechanism of ATP hydrolysis at the noncatalytic sites of the transcription termination factor Rho. J Biol Chem 274, 32667-32671.

Kim, D. E., and Patel, S. S. (2001). The kinetic pathway of RNA binding to the Escherichia coli transcription termination factor Rho. J Biol Chem 276, 13902-13910.

Kim, H. C., and Gottesman, M. E. (2004). Transcription termination by phage HK022 Nun is facilitated by COOH-terminal lysine residues. J Biol Chem 279, 13412-13417.

Kim, H. C., Washburn, R. S., and Gottesman, M. E. (2006). Role of E.coli NusA in phage HK022 Nun-mediated transcription termination. J Mol Biol 359, 10-21.

Kim, H. C., Zhou, J. G., Wilson, H. R., Mogilnitskiy, G., Court, D. L., and Gottesman, M. E. (2003). Phage HK022 Nun protein represses translation of phage lambda N (transcription termination/translation repression). Proc Natl Acad Sci U S A 100, 5308-5312.

Kimura, M., and Ishihama, A. (1995a). Functional map of the alpha subunit of Escherichia coli RNA polymerase: amino acid substitution within the amino-terminal assembly domain. J Mol Biol 254, 342-349.

Kimura, M., and Ishihama, A. (1995b). Functional map of the alpha subunit of Escherichia coli RNA polymerase: insertion analysis of the amino-terminal assembly domain. J Mol Biol 248, 756-767.

King, R. A., Banik-Maiti, S., Jin, D. J., and Weisberg, R. A. (1996). Transcripts that increase the processivity and elongation rate of RNA polymerase. Cell 87, 893-903.

King, R. A., Madsen, P. L., and Weisberg, R. A. (2000). Constitutive expression of a transcription termination factor by a repressed prophage: promoters for transcribing the phage HK022 nun gene. J Bacteriol 182, 456-462.

King, R. A., Markov, D., Sen, R., Severinov, K., and Weisberg, R. A. (2004). A conserved zinc binding domain in the largest subunit of DNA-dependent RNA polymerase modulates intrinsic transcription termination and antitermination but does not stabilize the elongation complex. J Mol Biol 342, 1143-1154.

King, R. A., Sen, R., and Weisberg, R. A. (2003). Using a lac repressor roadblock to analyze the E. coli transcription elongation complex. Methods Enzymol 371, 207-218.

Knowlton, J. R., Bubunenko, M., Andrykovitch, M., Guo, W., Routzahn, K. M., Waugh, D. S., Court, D. L., and Ji, X. (2003). A spring-loaded state of NusG in its functional cycle is suggested by X-ray crystallography and supported by site-directed mutants. Biochemistry 42, 2275-2281.

Komissarova, N., Becker, J., Solter, S., Kireeva, M., and Kashlev, M. (2002). Shortening of RNA:DNA hybrid in the elongation complex of RNA polymerase is a prerequisite for transcription termination. Mol Cell 10, 1151-1162.

Koulich, D., Orlova, M., Malhotra, A., Sali, A., Darst, S. A., and Borukhov, S. (1997). Domain organization of Escherichia coli transcript cleavage factors GreA and GreB. J Biol Chem 272, 7201-7210.

Kulish, D., Lee, J., Lomakin, I., Nowicka, B., Das, A., Darst, S., Normet, K., and Borukhov, S. (2000). The functional role of basic patch, a structural element of Escherichia coli transcript cleavage factors GreA and GreB. J Biol Chem 275, 12789-12798.

Kumar, K. P., and Chatterji, D. (1990). Resonance energy transfer study on the proximity relationship between the GTP binding site and the rifampicin binding site of Escherichia coli RNA polymerase. Biochemistry 29, 317-322.

Kyrpides, N. C., Woese, C. R., and Ouzounis, C. A. (1996). KOW: a novel motif linking a bacterial transcription factor with ribosomal proteins. Trends Biochem Sci 21, 425-426.

Landick, R. (2001). RNA polymerase clamps down. Cell 105, 567-570.

Landick, R., Carey, J., and Yanofsky, C. (1985). Translation activates the paused transcription complex and restores transcription of the trp operon leader region. Proc Natl Acad Sci U S A 82, 4663-4667.

Landick, R., Wang, D., and Chan, C. L. (1996). Quantitative analysis of transcriptional pausing by Escherichia coli RNA polymerase: his leader pause site as paradigm. Methods Enzymol 274, 334-353.

Laptenko, O., Lee, J., Lomakin, I., and Borukhov, S. (2003). Transcript cleavage factors GreA and GreB act as transient catalytic components of RNA polymerase. Embo J 22, 6322-6334.

Lau, L. F., Roberts, J. W., and Wu, R. (1983). RNA polymerase pausing and transcript release at the lambda tR1 terminator in vitro. J Biol Chem 258, 9391-9397.

Li, J., Horwitz, R., McCracken, S., and Greenblatt, J. (1992). NusG, a new Escherichia coli elongation factor involved in transcriptional antitermination by the N protein of phage lambda. J Biol Chem 267, 6012-6019.

Li, J., Mason, S. W., and Greenblatt, J. (1993). Elongation factor NusG interacts with termination factor rho to regulate termination and antitermination of transcription. Genes Dev 7, 161-172.

Libby, R. T., Nelson, J. L., Calvo, J. M., and Gallant, J. A. (1989). Transcriptional proofreading in Escherichia coli. Embo J 8, 3153-3158.

Lim, H. M., Lee, H. J., Roy, S., and Adhya, S. (2001). A "master" in base unpairing during isomerization of a promoter upon RNA polymerase binding. Proc Natl Acad Sci U S A 98, 14849-14852.

Linderoth, N. A., and Calendar, R. L. (1991). The Psu protein of bacteriophage P4 is an antitermination factor for rho-dependent transcription termination. J Bacteriol 173, 6722-6731.

Linderoth, N. A., Tang, G., and Calendar, R. (1997). In vivo and in vitro evidence for an anti-Rho activity induced by the phage P4 polarity suppressor protein Psu. Virology 227, 131-141.

Liu, K., Zhang, Y., Severinov, K., Das, A., and Hanna, M. M. (1996). Role of Escherichia coli RNA polymerase alpha subunit in modulation of pausing, termination and anti-termination by the transcription elongation factor NusA. Embo J 15, 150-161.

Lonetto, M., Gribskov, M., and Gross, C. A. (1992). The sigma 70 family: sequence conservation and evolutionary relationships. J Bacteriol 174, 3843-3849.

Lowery, C., and Richardson, J. P. (1977). Characterization of the nucleoside triphosphate phosphohydrolase (ATPase) activity of RNA synthesi termination factor p. I. Enzymatic properties and effects of inhibitors. J Biol Chem 252, 1375-1380.

Magyar, A., Zhang, X., Kohn, H., and Widger, W. R. (1996). The antibiotic bicyclomycin affects the secondary RNA binding site of Escherichia coli transcription termination factor Rho. J Biol Chem 271, 25369-25374.

Marr, M. T., and Roberts, J. W. (1997). Promoter recognition as measured by binding of polymerase to nontemplate strand oligonucleotide. Science 276, 1258-1260.

Martin, F. H., and Tinoco, I., Jr. (1980). DNA-RNA hybrid duplexes containing oligo(dA:rU) sequences are exceptionally unstable and may facilitate termination of transcription. Nucleic Acids Res 8, 2295-2299.

Martinez, A., Burns, C. M., and Richardson, J. P. (1996a). Residues in the RNP1-like sequence motif of Rho protein are involved in RNA-binding affinity and discrimination. J Mol Biol 257, 909-918.

Martinez, A., Opperman, T., and Richardson, J. P. (1996b). Mutational analysis and secondary structure model of the RNP1-like sequence motif of transcription termination factor Rho. J Mol Biol 257, 895-908.

Mason, S. W., and Greenblatt, J. (1991). Assembly of transcription elongation complexes containing the N protein of phage lambda and the Escherichia coli elongation factors NusA, NusB, NusG, and S10. Genes Dev 5, 1504-1512.

Mason, S. W., Li, J., and Greenblatt, J. (1992). Host factor requirements for processive antitermination of transcription and suppression of pausing by the N protein of bacteriophage lambda. J Biol Chem 267, 19418-19426.

McClure, W. R., Cech, C. L., and Johnston, D. E. (1978). A steady state assay for the RNA polymerase initiation reaction. J Biol Chem 253, 8941-8948.

McSwiggen, J. A., Bear, D. G., and von Hippel, P. H. (1988). Interactions of Escherichia coli transcription termination factor rho with RNA. I. Binding stoichiometries and free energies. J Mol Biol 199, 609-622.

Miwa, Y., Horiguchi, T., and Shigesada, K. (1995). Structural and functional dissections of transcription termination factor rho by random mutagenesis. J Mol Biol 254, 815-837.

Miyamura, S., Ogasawara, N., Otsuka, H., Niwayama, S., and Tanaka, H. (1972). Antibiotic no. 5879, a new water-soluble antibiotic against gram-negative bacteria. J Antibiot (Tokyo) 25, 610-612.

Miyamura, S., Ogasawara, N., Otsuka, H., Niwayama, S., and Tanaka, H. (1973). Antibiotic 5879 produced by Streptomyces aizunensis, identical with bicyclomycin. J Antibiot (Tokyo) 26, 479-484.

Miyoshi, T., Iseki, M., Konomi, T., and Imanaka, H. (1980). Biosynthesis of bicyclomycin. I. Appearance of aerial mycelia negative strains (am-). J Antibiot (Tokyo) 33, 480-487.

Modrak, D., and Richardson, J. P. (1994). The RNA-binding domain of transcription termination factor rho: isolation, characterization, and determination of sequence limits. Biochemistry 33, 8292-8299.

Mooney, R. A., Darst, S. A., and Landick, R. (2005). Sigma and RNA polymerase: an on-again, off-again relationship? Mol Cell 20, 335-345.

Mooney, R. A., Davis, S. E., Peters, J. M., Rowland, J. L., Ansari, A. Z., and Landick, R. (2009a). Regulator trafficking on bacterial transcription units in vivo. Mol Cell 33, 97-108.

Mooney, R. A., Schweimer, K., Rosch, P., Gottesman, M., and Landick, R. (2009b). Two structurally independent domains of E. coli NusG create regulatory plasticity via distinct interactions with RNA polymerase and regulators. J Mol Biol 391, 341-358.

Morgan, W. D., Bear, D. G., Litchman, B. L., and von Hippel, P. H. (1985). RNA sequence and secondary structure requirements for rho-dependent transcription termination. Nucleic Acids Res 13, 3739-3754.

Morgan, W. D., Bear, D. G., and von Hippel, P. H. (1983). Rho-dependent termination of transcription. II. Kinetics of mRNA elongation during transcription from the bacteriophage lambda PR promoter. J Biol Chem 258, 9565-9574.

Morse, D. E., and Guertin, M. (1972). Amber suA mutations which relieve polarity. J Mol Biol 63, 605-608.

Mukhopadhyay, J., Das, K., Ismail, S., Koppstein, D., Jang, M., Hudson, B., Sarafianos, S., Tuske, S., Patel, J., Jansen, R., et al. (2008). The RNA polymerase "switch region" is a target for inhibitors. Cell 135, 295-307.

Mulligan, M. E., Brosius, J., and McClure, W. R. (1985). Characterization in vitro of the effect of spacer length on the activity of Escherichia coli RNA polymerase at the TAC promoter. J Biol Chem 260, 3529-3538.

Munson, L. M., and Reznikoff, W. S. (1981). Abortive initiation and long ribonucleic acid synthesis. Biochemistry 20, 2081-2085.

Murakami, K. S., Masuda, S., and Darst, S. A. (2002). Structural basis of transcription initiation: RNA polymerase holoenzyme at 4 A resolution. Science 296, 1280-1284.

Neely, M. N., and Friedman, D. I. (1998). Functional and genetic analysis of regulatory regions of coliphage H-19B: location of shiga-like toxin and lysis genes suggest a role for phage functions in toxin release. Mol Microbiol 28, 1255-1267.

Negishi, T., Fujita, N., and Ishihama, A. (1995). Structural map of the alpha subunit of Escherichia coli RNA polymerase: structural domains identified by proteolytic cleavage. J Mol Biol 248, 723-728.

Nehrke, K. W., and Platt, T. (1994). A quaternary transcription termination complex. Reciprocal stabilization by Rho factor and NusG protein. J Mol Biol 243, 830-839.

Nehrke, K. W., Zalatan, F., and Platt, T. (1993). NusG alters rho-dependent termination of transcription in vitro independent of kinetic coupling. Gene Expr 3, 119-133.

Nguyen, L. H., and Burgess, R. R. (1997). Comparative analysis of the interactions of Escherichia coli sigma S and sigma 70 RNA polymerase holoenzyme with the stationary-phase-specific bolAp1 promoter. Biochemistry 36, 1748-1754.

Nickels, B. E., and Hochschild, A. (2004). Regulation of RNA polymerase through the secondary channel. Cell 118, 281-284.

Nodwell, J. R., and Greenblatt, J. (1991). The nut site of bacteriophage lambda is made of RNA and is bound by transcription antitermination factors on the surface of RNA polymerase. Genes Dev 5, 2141-2151.

Nowatzke, W. L., Keller, E., Koch, G., and Richardson, J. P. (1997). Transcription termination factor Rho is essential for Micrococcus luteus. J Bacteriol 179, 5238-5240.

Nowatzke, W. L., and Richardson, J. P. (1996). Characterization of an unusual Rho factor from the high G + C gram-positive bacterium Micrococcus luteus. J Biol Chem 271, 742-747.

Nudler, E. (2009). RNA polymerase active center: the molecular engine of transcription. Annu Rev Biochem 78, 335-361.

Nudler, E., and Gottesman, M. E. (2002). Transcription termination and anti-termination in E. coli. Genes Cells 7, 755-768.

Oberto, J., Clerget, M., Ditto, M., Cam, K., and Weisberg, R. A. (1993). Antitermination of early transcription in phage HK022. Absence of a phage-encoded antitermination factor. J Mol Biol 229, 368-381.

Opalka, N., Chlenov, M., Chacon, P., Rice, W. J., Wriggers, W., and Darst, S. A. (2003). Structure and function of the transcription elongation factor GreB bound to bacterial RNA polymerase. Cell 114, 335-345.

Opperman, T., and Richardson, J. P. (1994). Phylogenetic analysis of sequences from diverse bacteria with homology to the Escherichia coli rho gene. J Bacteriol 176, 5033-5043.

Orlova, M., Newlands, J., Das, A., Goldfarb, A., and Borukhov, S. (1995). Intrinsic transcript cleavage activity of RNA polymerase. Proc Natl Acad Sci U S A 92, 4596-4600.

Pani, B. (2009). Studies on the inhibition of Rho dependent termination by a bacteriophage protein Psu. PhD thesis submitted to University of Manipal, India.

Pani, B., Banerjee, S., Chalissery, J., Abishek, M., Loganathan, R. M., Suganthan, R. B., and Sen, R. (2006). Mechanism of inhibition of Rho-dependent transcription termination by bacteriophage P4 protein Psu. J Biol Chem 281, 26491-26500.

Pani, B., Ranjan, A., and Sen, R. (2009). Interaction surface of bacteriophage P4 protein Psu required for complex formation with the transcription terminator Rho. J Mol Biol 389, 647-660.

Park, H. G., Zhang, X., Moon, H. S., Zwiefka, A., Cox, K., Gaskell, S. J., Widger, W. R., and Kohn, H. (1995). Bicyclomycin and dihydrobicyclomycin inhibition kinetics of Escherichia coli rho-dependent transcription termination factor ATPase activity. Arch Biochem Biophys 323, 447-454.

Park, J. S., Marr, M. T., and Roberts, J. W. (2002). E. coli Transcription repair coupling factor (Mfd protein) rescues arrested complexes by promoting forward translocation. Cell 109, 757-767.

Park, J. S., and Roberts, J. W. (2006). Role of DNA bubble rewinding in enzymatic transcription termination. Proc Natl Acad Sci U S A 103, 4870-4875.

Pasman, Z., and von Hippel, P. H. (2000). Regulation of rho-dependent transcription termination by NusG is specific to the Escherichia coli elongation complex. Biochemistry 39, 5573-5585.

Pereira, S., and Platt, T. (1995). Analysis of E. coli rho factor: mutations affecting secondary-site interactions. J Mol Biol 251, 30-40.

Peters, J. M., Mooney, R. A., Kuan, P. F., Rowland, J. L., Keles, S., and Landick, R. (2009). Rho directs widespread termination of intragenic and stable RNA transcription. Proc Natl Acad Sci U S A 106, 15406-15411.

Pichoff, S., Alibaud, L., Guedant, A., Castanie, M. P., and Bouche, J. P. (1998). An Escherichia coli gene (yaeO) suppresses temperature-sensitive mutations in essential genes by modulating Rho-dependent transcription termination. Mol Microbiol 29, 859-869.

Powell, B. S., Rivas, M. P., Court, D. L., Nakamura, Y., and Turnbough, C. L., Jr. (1994). Rapid confirmation of single copy lambda prophage integration by PCR. Nucleic Acids Res 22, 5765-5766.

Rees, W. A., Weitzel, S. E., Das, A., and von Hippel, P. H. (1997). Regulation of the elongation-termination decision at intrinsic terminators by antitermination protein N of phage lambda. J Mol Biol 273, 797-813.

Revyakin, A., Liu, C., Ebright, R. H., and Strick, T. R. (2006). Abortive initiation and productive initiation by RNA polymerase involve DNA scrunching. Science 314, 1139-1143.

Richardson, J. P. (1982). Activation of rho protein ATPase requires simultaneous interaction at two kinds of nucleic acid-binding sites. J Biol Chem 257, 5760-5766.

Richardson, J. P. (2002). Rho-dependent termination and ATPases in transcript termination. Biochim Biophys Acta 1577, 251-260.

Richardson, J. P. (2003). Loading Rho to terminate transcription. Cell 114, 157-159.

Richardson, J. P., and Carey III, J. L. (1982). rho Factors from polarity suppressor mutants with defects in their RNA interactions. J Biol Chem 257, 5767-5771.

Richardson, L. V., and Richardson, J. P. (2005). Identification of a structural element that is essential for two functions of transcription factor NusG. Biochim Biophys Acta 1729, 135-140.

Robert, J., Sloan, S. B., Weisberg, R. A., Gottesman, M. E., Robledo, R., and Harbrecht, D. (1987). The remarkable specificity of a new transcription termination factor suggests that the mechanisms of termination and antitermination are similar. Cell 51, 483-492.

Roberts, J. W. (1969). Termination factor for RNA synthesis. Nature 224, 1168-1174.

Robledo, R., Atkinson, B. L., and Gottesman, M. E. (1991). Escherichia coli mutations that block transcription termination by phage HK022 Nun protein. J Mol Biol 220, 613-619.

Ross, W., Gosink, K. K., Salomon, J., Igarashi, K., Zou, C., Ishihama, A., Severinov, K., and Gourse, R. L. (1993). A third recognition element in bacterial promoters: DNA binding by the alpha subunit of RNA polymerase. Science 262, 1407-1413.

Rozovskaia, T. A., Chenchik, A. A., and Bibilashvili, R. (1981). [Reaction of pyrophosphorolysis catalyzed by Escherichia coli RNA polymerase]. Mol Biol (Mosk) 15, 636-652.

Ryder, A. M., and Roberts, J. W. (2003). Role of the non-template strand of the elongation bubble in intrinsic transcription termination. J Mol Biol 334, 205-213.

Sambrook, J. and Russel, D.W (2001). *In* Molecular cloning, A laboratory manual. Third edition; Cold Spring Harbor Laboratory Press. Cold Spring Harbor, New York.

Santangelo, T. J., Mooney, R. A., Landick, R., and Roberts, J. W. (2003). RNA polymerase mutations that impair conversion to a termination-resistant complex by Q antiterminator proteins. Genes Dev 17, 1281-1292.

Santangelo, T. J., and Roberts, J. W. (2004). Forward translocation is the natural pathway of RNA release at an intrinsic terminator. Mol Cell 14, 117-126.

Sasse-Dwight, S., and Gralla, J. D. (1989). KMnO4 as a probe for lac promoter DNA melting and mechanism in vivo. J Biol Chem 264, 8074-8081.

Sasse-Dwight, S., and Gralla, J. D. (1991). Footprinting protein-DNA complexes in vivo. Methods Enzymol 208, 146-168.

Sauer, B., Ow, D., Ling, L., and Calendar, R. (1981). Mutants of satellite bacteriophage P4 that are defective in the suppression of transcriptional polarity. J Mol Biol 145, 29-46.

Savery, N. J. (2007). The molecular mechanism of transcription-coupled DNA repair. Trends Microbiol 15, 326-333.

Schmidt, M. C., and Chamberlin, M. J. (1984). Binding of rho factor to Escherichia coli RNA polymerase mediated by nusA protein. J Biol Chem 259, 15000-15002.

Selby, C. P., and Sancar, A. (1993). Molecular mechanism of transcription-repair coupling. Science 260, 53-58.

Sen, R., and Dasgupta, D. (2003). Simple fluorescence assays probing conformational changes of Escherichia coli RNA polymerase during transcription initiation. Methods Enzymol 370, 598-605.

Sen, R., Chalissery, J. and Muteeb, G. (2008). Nus factors of *Escherichia coli*. In *EcoSal-Eschericia coli and Salmonella;* Cellular and Molecular Biology (A. Böck, R. Curtiss III, J. B. Kaper, P. D. Karp, F. C. Neidhardt, T. Nyström, J. M. Slauch, and C. L. Squires eds.). ASM press, Washington DC; http://www.ecosal.org.

Severinov, K., Kashlev, M., Severinova, E., Bass, I., McWilliams, K., Kutter, E., Nikiforov, V., Snyder, L., and Goldfarb, A. (1994). A non-essential domain of Escherichia coli RNA polymerase required for the action of the termination factor Alc. J Biol Chem 269, 14254-14259.

Sevostyanova, A., Svetlov, V., Vassylyev, D. G., and Artsimovitch, I. (2008). The elongation factor RfaH and the initiation factor sigma bind to the same site on the transcription elongation complex. Proc Natl Acad Sci U S A 105, 865-870.

Shigesada, K., and Wu, C. W. (1980). Studies of RNA release reaction catalyzed by E. coli transcription termination factor rho using isolated ternary transcription complexes. Nucleic Acids Res 8, 3355-3369.

Shin, D. H., Nguyen, H. H., Jancarik, J., Yokota, H., Kim, R., and Kim, S. H. (2003). Crystal structure of NusA from Thermotoga maritima and functional implication of the N-terminal domain. Biochemistry 42, 13429-13437.

Simons, R. W., Houman, F., and Kleckner, N. (1987). Improved single and multicopy lac-based cloning vectors for protein and operon fusions. Gene 53, 85-96.

Skordalakes, E., and Berger, J. M. (2003). Structure of the Rho transcription terminator: mechanism of mRNA recognition and helicase loading. Cell 114, 135-146.

Skordalakes, E., and Berger, J. M. (2006). Structural insights into RNA-dependent ring closure and ATPase activation by the Rho termination factor. Cell 127, 553-564.

Skordalakes, E., Brogan, A. P., Park, B. S., Kohn, H., and Berger, J. M. (2005). Structural mechanism of inhibition of the Rho transcription termination factor by the antibiotic bicyclomycin. Structure 13, 99-109.

Sloan, S. B., and Weisberg, R. A. (1993). Use of a gene encoding a suppressor tRNA as a reporter of transcription: analyzing the action of the Nun protein of bacteriophage HK022. Proc Natl Acad Sci U S A 90, 9842-9846.

Snyder, L., Gold, L., and Kutter, E. (1976). A gene of bacteriophage T4 whose product prevents true late transcription on cytosine-containing T4 DNA. Proc Natl Acad Sci U S A 73, 3098-3102.

Sosunov, V., Zorov, S., Sosunova, E., Nikolaev, A., Zakeyeva, I., Bass, I., Goldfarb, A., Nikiforov, V., Severinov, K., and Mustaev, A. (2005). The involvement of the aspartate triad of the active center in all catalytic activities of multisubunit RNA polymerase. Nucleic Acids Res 33, 4202-4211.

Sosunova, E., Sosunov, V., Kozlov, M., Nikiforov, V., Goldfarb, A., and Mustaev, A. (2003). Donation of catalytic residues to RNA polymerase active center by transcription factor Gre. Proc Natl Acad Sci U S A 100, 15469-15474.

Sparkowski, J., and Das, A. (1992). Simultaneous gain and loss of functions caused by a single amino acid substitution in the beta subunit of Escherichia coli RNA polymerase: suppression of nusA and rho mutations and conditional lethality. Genetics 130, 411-428.

Squires, C. L., Greenblatt, J., Li, J., Condon, C., and Squires, C. L. (1993). Ribosomal RNA antitermination in vitro: requirement for Nus factors and one or more unidentified cellular components. Proc Natl Acad Sci U S A 90, 970-974.

Stebbins, C. E., Borukhov, S., Orlova, M., Polyakov, A., Goldfarb, A., and Darst, S. A. (1995). Crystal structure of the GreA transcript cleavage factor from Escherichia coli. Nature 373, 636-640.

Stefano, J. E., and Gralla, J. D. (1982). Spacer mutations in the lac ps promoter. Proc Natl Acad Sci U S A 79, 1069-1072.

Steiner, T., Kaiser, J. T., Marinkovic, S., Huber, R., and Wahl, M. C. (2002). Crystal structures of transcription factor NusG in light of its nucleic acid- and protein-binding activities. Embo J 21, 4641-4653.

Steinmetz, E. J., Brennan, C. A., and Platt, T. (1990). A short intervening structure can block rho factor helicase action at a distance. J Biol Chem 265, 18408-18413.

Steinmetz, E. J., and Platt, T. (1994). Evidence supporting a tethered tracking model for helicase activity of Escherichia coli Rho factor. Proc Natl Acad Sci U S A 91, 1401-1405.

Stitt, B. L., and Xu, Y. (1998). Sequential hydrolysis of ATP molecules bound in interacting catalytic sites of Escherichia coli transcription termination protein Rho. J Biol Chem 273, 26477-26486.

Straney, D. C., and Crothers, D. M. (1985). Intermediates in transcription initiation from the E. coli lac UV5 promoter. Cell 43, 449-459.

Sullivan, S. L., and Gottesman, M. E. (1992). Requirement for E. coli NusG protein in factor-dependent transcription termination. Cell 68, 989-994.

Sullivan, S. L., Ward, D. F., and Gottesman, M. E. (1992). Effect of Escherichia coli nusG function on lambda N-mediated transcription antitermination. J Bacteriol 174, 1339-1344.

Sunshine, M., and Six, E. (1976). Relief of P2 bacteriophage amber mutant polarity by the satellite bacteriophage P4. J Mol Biol 106, 673-682.

Surratt, C. K., Milan, S. C., and Chamberlin, M. J. (1991). Spontaneous cleavage of RNA in ternary complexes of Escherichia coli RNA polymerase and its significance for the mechanism of transcription. Proc Natl Acad Sci U S A 88, 7983-7987.

Svetlov, V., Belogurov, G. A., Shabrova, E., Vassylyev, D. G., and Artsimovitch, I. (2007). Allosteric control of the RNA polymerase by the elongation factor RfaH. Nucleic Acids Res 35, 5694-5705.

Taddei, F., Hayakawa, H., Bouton, M., Cirinesi, A., Matic, I., Sekiguchi, M., and Radman, M. (1997). Counteraction by MutT protein of transcriptional errors caused by oxidative damage. Science 278, 128-130.

Temiakov, D., Zenkin, N., Vassylyeva, M. N., Perederina, A., Tahirov, T. H., Kashkina, E., Savkina, M., Zorov, S., Nikiforov, V., Igarashi, N., et al. (2005). Structural basis of transcription inhibition by antibiotic streptolydigin. Mol Cell 19, 655-666.

Thomsen, N. D., and Berger, J. M. (2009). Running in reverse: the structural basis for translocation polarity in hexameric helicases. Cell 139, 523-534.

Toulokhonov, I., Artsimovitch, I., and Landick, R. (2001). Allosteric control of RNA polymerase by a site that contacts nascent RNA hairpins. Science 292, 730-733.

Toulokhonov, I., and Landick, R. (2003). The flap domain is required for pause RNA hairpin inhibition of catalysis by RNA polymerase and can modulate intrinsic termination. Mol Cell 12, 1125-1136.

Travers, A. A., and Burgess R. R. (1969). Cyclic re-use of the RNA polymerase sigma factor. Nature 222, 537-540.

Tsurushita, N., Hirano, M., Shigesada, K., and Imai, M. (1984). Isolation and characterization of rho mutants of Escherichia coli with increased transcription termination activities. Mol Gen Genet 196, 458-464.

Tuske, S., Sarafianos, S. G., Wang, X., Hudson, B., Sineva, E., Mukhopadhyay, J., Birktoft, J. J., Leroy, O., Ismail, S., Clark, A. D., Jr., et al. (2005). Inhibition of bacterial RNA polymerase by streptolydigin: stabilization of a straight-bridge-helix active-center conformation. Cell 122, 541-552.

Uptain, S. M., Kane, C. M., and Chamberlin, M. J. (1997). Basic mechanisms of transcript elongation and its regulation. Annu Rev Biochem 66, 117-172.

Vassylyev, D. G., Sekine, S., Laptenko, O., Lee, J., Vassylyeva, M. N., Borukhov, S., and Yokoyama, S. (2002). Crystal structure of a bacterial RNA polymerase holoenzyme at 2.6 A resolution. Nature 417, 712-719.

Vassylyev, D. G., Vassylyeva, M. N., Perederina, A., Tahirov, T. H., and Artsimovitch, I. (2007). Structural basis for transcription elongation by bacterial RNA polymerase. Nature 448, 157-162.

Vassylyeva, M. N., Svetlov, V., Dearborn, A. D., Klyuyev, S., Artsimovitch, I., and Vassylyev, D. G. (2007). The carboxy-terminal coiled-coil of the RNA polymerase beta'-subunit is the main binding site for Gre factors. EMBO Rep 8, 1038-1043.

von Hippel, P. H. (1998). An integrated model of the transcription complex in elongation, termination, and editing. Science 281, 660-665.

Wada, T., Takagi, T., Yamaguchi, Y., Ferdous, A., Imai, T., Hirose, S., Sugimoto, S., Yano, K., Hartzog, G. A., Winston, F., et al. (1998). DSIF, a novel transcription elongation factor that regulates RNA polymerase II processivity, is composed of human Spt4 and Spt5 homologs. Genes Dev 12, 343-356.

Wang, D., Bushnell, D. A., Westover, K. D., Kaplan, C. D., and Kornberg, R. D. (2006). Structural basis of transcription: role of the trigger loop in substrate specificity and catalysis. Cell 127, 941-954.

Warne, S. E., and deHaseth, P. L. (1993). Promoter recognition by Escherichia coli RNA polymerase. Effects of single base pair deletions and insertions in the spacer DNA separating the -10 and -35 regions are dependent on spacer DNA sequence. Biochemistry 32, 6134-6140.

Washburn, R. S., Wang, Y., and Gottesman, M. E. (2003). Role of E.coli transcription-repair coupling factor Mfd in Nun-mediated transcription termination. J Mol Biol 329, 655-662.

Watnick, R. S., and Gottesman, M. E. (1998). Escherichia coli NusA is required for efficient RNA binding by phage HK022 nun protein. Proc Natl Acad Sci U S A 95, 1546-1551.

Watnick, R. S., and Gottesman, M. E. (1999). Binding of transcription termination protein nun to nascent RNA and template DNA. Science 286, 2337-2339.

Watnick, R. S., Herring, S. C., Palmer, A. G., 3rd, and Gottesman, M. E. (2000). The carboxyl terminus of phage HK022 Nun includes a novel zinc-binding motif and a tryptophan required for transcription termination. Genes Dev 14, 731-739.

Wei, R. R., and Richardson, J. P. (2001a). Identification of an RNA-binding Site in the ATP binding domain of Escherichia coli Rho by H2O2/Fe-EDTA cleavage protection studies. J Biol Chem 276, 28380-28387.

Wei, R. R., and Richardson, J. P. (2001b). Mutational changes of conserved residues in the Q-loop region of transcription factor Rho greatly reduce secondary site RNA-binding. J Mol Biol 314, 1007-1015.

Weisberg, R. A., and Gottesman, M. E. (1999). Processive antitermination. J Bacteriol 181, 359-367.

Wilson, K. S., and von Hippel, P. H. (1994). Stability of Escherichia coli transcription complexes near an intrinsic terminator. J Mol Biol 244, 36-51.

Xia, M., Lunsford, R. D., McDevitt, D., and Iordanescu, S. (1999). Rapid method for the identification of essential genes in Staphylococcus aureus. Plasmid 42, 144-149.

Xu, Y., Kohn, H., and Widger, W. R. (2002). Mutations in the rho transcription termination factor that affect RNA tracking. J Biol Chem 277, 30023-30030.

Yang, J. T., Wu, C. S., and Martinez, H. M. (1986). Calculation of protein conformation from circular dichroism. Methods Enzymol 130, 208-269.

Yang, X. J., and Roberts, J. W. (1989). Gene Q antiterminator proteins of Escherichia coli phages 82 and lambda suppress pausing by RNA polymerase at a rho-dependent terminator and at other sites. Proc Natl Acad Sci U S A 86, 5301-5305.

Yarnell, W. S., and Roberts, J. W. (1992). The phage lambda gene Q transcription antiterminator binds DNA in the late gene promoter as it modifies RNA polymerase. Cell 69, 1181-1189.

Yarnell, W. S., and Roberts, J. W. (1999). Mechanism of intrinsic transcription termination and antitermination. Science 284, 611-615.

Young, B. A., Anthony, L. C., Gruber, T. M., Arthur, T. M., Heyduk, E., Lu, C. Z., Sharp, M. M., Heyduk, T., Burgess, R. R., and Gross, C. A. (2001). A coiled-coil from the RNA polymerase beta' subunit allosterically induces selective nontemplate strand binding by sigma(70). Cell 105, 935-944.

Yu, X., Horiguchi, T., Shigesada, K., and Egelman, E. H. (2000). Three-dimensional reconstruction of transcription termination factor rho: orientation of the N-terminal domain and visualization of an RNA-binding site. J Mol Biol 299, 1279-1287.

Zaychikov, E., Martin, E., Denissova, L., Kozlov, M., Markovtsov, V., Kashlev, M., Heumann, H., Nikiforov, V., Goldfarb, A., and Mustaev, A. (1996). Mapping of catalytic residues in the RNA polymerase active center. Science 273, 107-109.

Zenkin, N., Kulbachinskiy, A., Yuzenkova, Y., Mustaev, A., Bass, I., Severinov, K., and Brodolin, K. (2007). Region 1.2 of the RNA polymerase sigma subunit controls recognition of the -10 promoter element. Embo J 26, 955-964.

Zhang, G., Campbell, E. A., Minakhin, L., Richter, C., Severinov, K., and Darst, S. A. (1999). Crystal structure of Thermus aquaticus core RNA polymerase at 3.3 A resolution. Cell 98, 811-824.

Zhang, G., and Darst, S. A. (1998). Structure of the Escherichia coli RNA polymerase alpha subunit amino-terminal domain. Science 281, 262-266.

Zheng, C., and Friedman, D. I. (1994). Reduced Rho-dependent transcription termination permits NusA-independent growth of Escherichia coli. Proc Natl Acad Sci U S A 91, 7543-7547.

Zwiefka, A., Kohn, H., and Widger, W. R. (1993). Transcription termination factor rho: the site of bicyclomycin inhibition in Escherichia coli. Biochemistry 32, 3564-3570.

Appendix

Appendix I: Bacterial Strains, Phages and plasmids used

AI.1 Bacterial Strains

Strain	Description	Source or reference
BL21(DE3)	F-omp ThsdSB(rB-mB-) gal dcm(DE3)	Novagen
GJ3161 (RS257)	MC4100 *galEp3*	(Harinarayanan and Gowrishankar, 2003)
DH5α	Δ *(argF-lac)U169 supE44 hsdR17 recA1 endA1 gyrA96 thi-1 relA1 (ø80lacZΔM15)*	
GJ3073 (RS417)	MC4100 *galEp3*, λRS45 lysogen carrying P_{lac} – H-19B *nutR- T_{R1} -lacZYA*, ilv: Tn*10* Tet^R	Dr. J. Gowrishankar
GJ3183 (RS324)	MC4100 *galEp3 trpE9851(Oc) zci-506::*Tn*10 nusG*-G146D *rho*-R221C	(Harinarayanan and Gowrishankar, 2003)
GJ3191 (RS331)	MC4100 *galEp3 ΔnusG::*Kan^R with pHYD751, Amp^R	(Harinarayanan and Gowrishankar, 2003)
GJ3192 (RS330)	MC4100 *galEp3 Δrho::*Kan R with pHYD1201, Amp^R	(Harinarayanan and Gowrishankar, 2003)
GJ5153	MC4100 *galEp3 nusG* G146D, λRS45 lysogen carrying P_{lac} – H-19B *nutR- T_{R1} -lacZYA*	Dr. J. Gowrishankar
LMG194	*F-ΔlacX74 galE thi rpsL ΔphoA(PvuII)* Δ*ara714 leu*::Tn*10*	Invitrogen
MC4100	Δ *(argF-lac)U169 rpsL150 relA1 araD139 flbB5301 deoC1 ptsF25*	
MDS42 (RS726)	MG1655 deleted for ~14% of genome	(Cardinale et al., 2008)
MG1655	WT	
RpoB2	MG1655, *rpoB2* Tet^R Rif^R	(Jin and Gross, 1988)
RpoB8	MG1655, *rpoB8* Tet^R Rif^R	(Jin and Gross, 1988)
RSW472 (RS764)	MG1655 Δ*rac*::Cam^R	(Cardinale et al., 2008)
RS336	GJ3192, *trpE9851*(Oc) Tet^R	This study
RS353	MC4100 $araD^+$	This study
RS364	RS336, λRS45 lysogen carrying P_{lac} – H-19B *nutR- T_{R1} -lacZYA*	This study
RS391	RS336, λRS88 lysogen carrying P_{lac} *–lacZYA*	This study
RS445	GJ3161, λRS88 lysogen carrying P_{lac} *–lacZYA*	This study
RS446	GJ3192, *rpoB8* Tet^R Rif^R	This study
RS449	RS 446, λRS45 lysogen carrying P_{lac} – H-19B *nutR- T_{R1} -lacZYA*	This study
RS450	RS 446, λRS88 lysogen carrying P_{lac} *–lacZYA*	This study
RS451	GJ3192, *rpoB2* Tet^R Rif^R	This study
RS689	GJ3191, Δ*ara*::Tet^R	This study

RS692	RS689 with pHYD763, Cam^R	This study
RS714	RS445, Δ*nusG*::Kan^R with pHYD763, Cam^R	This study
RS715	RS714, Δ*ara*:Tet^R	This study
RS801	GJ5153, ΔnusG::Kan^R with pHYD763, Cam^R	This study
RS802	RS801, Δara::Tet^R	This study
XL1-Red	*endA1 gyrA96 thi-1 hsdR17 supE44 relA1 lac mutD5 mutS mutT* Tn*10* (Tet^R)	Stratagene

AI.2 Phages

Phage	Description	Source
λRS45		Dr. J. Gowrishankar
λRS88		Dr. Robert Weisberg
P1*kc* (P1 phage)		Dr. J. Gowrishankar

AI.3 Plasmids

Plasmid	Description	Source or reference
pHYD564	3.3 kb chromosomal NsiI fragment carrying rho-R221C cloned into PstI site of pCL1920 (pSC101; Sp^R, Sm^R)	(Harinarayanan and Gowrishankar, 2003)
pHYD567	3.3kb NsiI fragment carrying rho^+ cloned from l phage 556 of Kohara library into PstI site of pCL1920 (pSC101; Sp^R, Sm^R)	(Harinarayanan and Gowrishankar, 2003)
pHYD751	2.1 kb chromosomal fragment carrying $nusG^+$ cloned into Eco RI-Sal I sites of pAM34 (pMB1; Amp^R)	(Harinarayanan and Gowrishankar, 2003)
pHYD763	3.8 kb BamHI-Sac I fragment carrying nusG subcloned from pHYD547 into BamHI-Sac I sites of pMAK705 (pSC101; Cam^R)	(Harinarayanan and Gowrishankar, 2003)
pHYD1201	3.3kb HindIII-SalI fragment carrying rho+ subcloned from pHYD567 into HindIII-SalI sites of pAM34 (pMB1; IPTG dependent replicon, Amp^R)	(Harinarayanan and Gowrishankar, 2003)
pHYD3011	pBAD18 vector with the MCS and RBS of pET vector, Amp^R	Dr. J. Gowrishankar
pK8628	pTL61T with P_{lac} – H-19B *nutR(TR1) -lacZAY* fusion, Amp^R	(Cheeran et al., 2005)
pRS25	pTL61T with pT7A1-H-19B *nutR (ΔcII)* $T_R{}'T_1T_2$-*lacZYA*,Amp^R	(Cheeran et al., 2005)
pRS96	WT rho cloned at NdeI/XhoI site of pET21b, His-tag at C-terminal, Amp^R	(Pani, B. 2009. PhD thesis, Chalissery et al., 2007)
pRS100	WT Rho cloned at NdeI/XhoI site of pET21b, non-His-tagged, Amp^R	(Pani et al., 2006)

pRS106	pT7A1 cloned at EcoRI/HindIII sites upstream of *trp t'* cloned at HindIII/BamHI sites of pK8641,	(Pani et al., 2006)
pRS109	NusG G146D cloned at NdeI/XhoI site of pET21b, His-tag at C-terminal, Amp^R	This study
pRS119	NusG WT cloned at NdeI/XhoI site of pET21b, His-tag at C-terminal, Amp^R	(Cheeran et al., 2005)
pRS236	lacI cloned at NdeI/XhoI site of pET21b, Amp^R	(Pani, B. 2009. PhD thesis, Chalissery et al., 2007)
pRS262	NusG WT cloned at NdeI/XhoI site of pET21b, non-His-tagged, Amp^R	(Pani et al., 2006)
pRS338	WT rho cloned at NdeI/XhoI site of pET21b, HMK tag and His-tag at C-terminal, Amp^R	This study
pRS341	pHYD567-rho P279S, Sp^R, Sm^R	This study
pRS342	pHYD567-rho G51V, Sp^R, Sm^R	This study
pRS344	pHYD567-rho G324D, Sp^R, Sm^R	This study
pRS346	pHYD567-rho N340S, Sp^R, Sm^R	This study
pRS347	pHYD567-rho P279L, Sp^R, Sm^R	This study
pRS350	pHYD567-rho Y80C, Sp^R, Sm^R	This study
pRS377	rho P279S cloned at NdeI/XhoI site of pET21b, His-tag at C-terminal, Amp^R	This study
pRS378	rho G51V cloned at NdeI/XhoI site of pET21b, His-tag at C-terminal, Amp^R	This study
pRS379	rho G324D cloned at NdeI/XhoI site of pET21b, His-tag at C-terminal, Amp^R	This study
pRS380	rho N340S cloned at NdeI/XhoI site of pET21b, His-tag at C-terminal, Amp^R	This study
pRS381	rho Y80C cloned at NdeI/XhoI site of pET21b, His-tag at C-terminal, Amp^R	This study
pRS387	pHYD567-rho G53V, Sp^R, Sm^R	This study
pRS397	pHYD567-rho Y274D, Sp^R, Sm^R	This study
pRS399	pHYD567-rho I382N, Sp^R, Sm^R	This study
pRS431	pTL61T with P_{lac} – *lacZAY* by deletion of H-19B *nutR-TR1* between HindIII and BamHI from PK8628, Amp^R	This study
pRS432	rho I382N cloned at NdeI/XhoI site of pET21b, His-tag at C-terminal, Amp^R	This study
pRS433	rho Y274D cloned at NdeI/XhoI site of pET21b, His-tag at C-terminal, Amp^R	This study
pRS600	WT NusG cloned at NdeI/ XhoI site of pET33b, HMK tag and His-tag at N-terminal, Kan^R	This study
pRS602	rho Y80C cloned at NdeI/XhoI site of pET21b, HMK tag and His-tag at C-terminal, Amp^R	This study
pRS607	pET33b NusG S60A by SDM of pRS600, HMK tag and His-tag at N-terminal, Kan^R	This study

pRS612	pET21b NusG S60A by SDM of pRS262, His-tag at C-terminal, Amp^R	This study
pRS613	Rho R221C cloned at NdeI/XhoI site of pET21b, His-tag at C-terminal, Amp^R	This study
pRS616	pET21b NusG G119C S60A by SDM of pRS612, His-tag at C-terminal, Amp^R	This study
pRS618	pET21b NusG G146D S60A, by SDM of pRS109, His-tag at C-terminal, Amp^R	This study
pRS620	NusG Δ145-149 S60A, cloned at NdeI/XhoI site of pET21b, His-tag at C-terminal, Amp^R	This study
pRS621	NusG Δ157-161 S60A, cloned at NdeI/XhoI site of pET21b, His-tag at C-terminal, Amp^R	This study
pRS622	NusG-NTD S60A, cloned at NdeI/XhoI site of pET21b, His-tag at C-terminal, Amp^R	This study
pRS623	NusG-CTD, cloned at NdeI/XhoI site of pET21b, His-tag at C-terminal, Amp^R	This study
pRS638	NusG Δ157-161 S60A cloned at NdeI/ XhoI site of pET33b, HMK tag and His-tag at N-terminal, Kan^R	This study
pRS646	pET21b NusG T126C S60A by SDM of pRS612, His-tag at C-terminal, Amp^R	This study
pRS647	pET21b NusG S156C S60A by SDM of pRS612, His-tag at C-terminal, Amp^R	This study
pRS693	NusG-NTD cloned at NdeI/ XhoI site of pET33b, HMK tag and His-tag at N-terminal, Kan^R	This study
pRS694	NusG-CTD cloned at NdeI/ XhoI site of pET33b, HMK tag and His-tag at N-terminal, Kan^R	This study
pRS695	NusG S60A cloned at NdeI/SalI site of pHYD3011, Amp^R	This study
pRS696	NusG Δ145-149 S60A cloned at NdeI/SalI site of pHYD3011, Amp^R	This study
pRS697	NusG Δ157-161 S60A cloned at NdeI/SalI site of pHYD3011, Amp^R	This study
pRS698	NusG-NTD S60A cloned at NdeI/SalI site of pHYD3011, Amp^R	This study
pRS699	NusG-CTD cloned at NdeI/SalI site of pHYD3011, Amp^R	This study
pRS700	NusG G146D S60A cloned at NdeI/SalI site of pHYD3011, Amp^R	This study
pRS727	pHYD3011 NusG R157E S60A by SDM of pRS695, Amp^R	This study
pRS728	pHYD3011 NusG L158Q S60A by SDM of pRS695, Amp^R	This study
pRS729	pHYD3011 NusG V160N S60A by SDM of pRS695, Amp^R	This study
pRS730	pHYD3011 NusG K159D S60A by SDM of pRS695, Amp^R	This study

pRS731	NusG Δ172-181 S60A cloned at NdeI/SalI site of pHYD3011, Amp^R	This study
pRS732	NusG Δ169-173 S60A cloned at NdeI/SalI site of pHYD3011, Amp^R	This study
pRS733	NusG Δ148-152 S60A , cloned at NdeI/XhoI site of pET21b, His-tag at C-terminal, Amp^R	This study
pRS740	NusG Δ169-173 S60A, cloned at NdeI/XhoI site of pET21b, His-tag at C-terminal, Amp^R	This study
pRS743	NusG Δ172-181 S60A , cloned at NdeI/XhoI site of pET21b, His-tag at C-terminal, Amp^R	This study
pRS744	pET21b NusG L158Q S60A by SDM of pRS612, His-tag at C-terminal, Amp^R	This study
pRS745	pET21b NusG V160N S60A by SDM of pRS612, His-tag at C-terminal, Amp^R	This study
pRS748	NusG Δ148-152 S60A cloned at NdeI/SalI site of pHYD3011, Amp^R	This study
pRS757	pET21b Rho C202S by SDM of pRS96, His-tag at C-terminal, Amp^R	This study
pRS758	pET21b Rho R221C C202S by SDM of pRS613, His-tag at C-terminal, Amp^R	This study
pRS760	pHYD3011 NusG N145V S60A by SDM of pRS695, Amp^R	This study
pRS762	pET21b Rho T217C C202S by SDM of pRS757, His-tag at C-terminal, Amp^R	This study
pRS763	pET21b Rho K224C C202S by SDM of pRS757, His-tag at C-terminal, Amp^R	This study
pRS770	pHYD3011 NusG R135E S60A by SDM of pRS695, Amp^R	This study
pRS771	pHYD3011 NusG V148N S60A by SDM of pRS695, Amp^R	This study
pRS772	pHYD3011 NusG I164A S60A by SDM of pRS695, Amp^R	This study
pRS773	pHYD3011 NusG R167E S60A by SDM of pRS695, Amp^R	This study
pRS774	pHYD3011 NusG T169A S60A by SDM of pRS695, Amp^R	This study
pRS775	pHYD3011 NusG V171N S60A by SDM of pRS695, Amp^R	This study
pRS776	pET21b NusG V147C S60A by SDM of pRS612, His-tag at C-terminal, Amp^R	This study
pRS777	pET21b NusG S161C S60A by SDM of pRS612, His-tag at C-terminal, Amp^R	This study
pRS778	pET21b NusG A168C S60A by SDM of pRS612, His-tag at C-terminal, Amp^R	This study
pRS779	pET21b NusG V148N S60A by SDM of pRS612, His-tag at C-terminal, Amp^R	This study

pRS794	pET21b NusG I164A S60A by SDM of pRS612, His-tag at C-terminal, Amp^R	This study
pRS795	pET21b NusG R167E S60A by SDM of pRS612, His-tag at C-terminal, Amp^R	This study
pRS796	pET21b NusG T169A S60A by SDM of pRS612, His-tag at C-terminal, Amp^R	This study
pRS797	pET21b NusG V171N S60A by SDM of pRS612, His-tag at C-terminal, Amp^R	This study
pRS805	pET21b NusG S25C S60A by SDM of pRS612, His-tag at C-terminal, Amp^R	This study
pRS806	pET21b NusG S85C S60A by SDM of pRS612, His-tag at C-terminal, Amp^R	This study
pRS870	pET21b NusG S25C S161C S60A by SDM of pRS777, His-tag at C-terminal, Amp^R	This study
pRS874	pET21b Rho T217C C202S by SDM of pRS100, Amp^R	This study
pRS884	pET21b NusG V22N S60A by SDM of pRS612, His-tag at C-terminal, Amp^R	This study
pRS885	pET21b NusG L26E S60A by SDM of pRS612, His-tag at C-terminal, Amp^R	This study
pRS886	pET21b NusG E19L S60A by SDM of pRS612, His-tag at C-terminal, Amp^R	This study
pRS887	HYD3011 NusG V22N S60A by SDM of pRS695, Amp^R	This study
pRS903	pET21b NusG W80G S60A by SDM of pRS612, His-tag at C-terminal, Amp^R	This study
pRS904	pET21b NusG V83N S60A by SDM of pRS612, His-tag at C-terminal, Amp^R	This study
pRS905	pET21b NusG V89N S60A by SDM of pRS612, His-tag at C-terminal, Amp^R	This study
pRS906	pHYD3011 NusG W80G S60A by SDM of pRS695, Amp^R	This study
pRS907	pHYD3011 NusG V83N S60A by SDM of pRS695, Amp^R	This study
pRS908	pHYD3011 NusG V89N S60A by SDM of pRS695, Amp^R	This study
pRS909	pHYD3011 NusG E19L S60A by SDM of pRS695, Amp^R	This study
pRS910	pHYD3011 NusG L26E S60A by SDM of pRS695, Amp^R	This study

Appendix II: Oligos used in this study

Oligo	Sequence	Description
RK1	CGCCAGGGTTTTCCCAGTCACGAC	RP in the *lacZ* gene
RS58	ATAAACTGCCAGGAATTGGGGATC G	FP of pTL61T (and all its derivatives like pRS106, pRS25) vector sequence
RS78	GCTAGTTATTGCTCAGCGGT	T7 terminator sequence
RS79	TAATACGACTCACTATAGGG	T7 promoter sequence
RS83	ATAAACTGCCAGGAATTGGGGATC G	5' biotinylated RS58
RS84new	GCG CGC CTC GAG TGA GCG TTT CAT CAT TTC	rho RP with XhoI site and without stop codon
RS114	GCGCGCGCCATATGTCTGAAGCTCC TAAAAAGCGC	nusG FP with NdeI site
RS115	GCGCGCGCCTCGAGTTAGGCTTTTT CAACCTGGC	nusG RP with stop codon and XhoI site
RS116	GCG CGC CTC GAG GGC TTT TTC AAC CTG GCT G	nusG RP XhoI site and without stop codon
RS117	TGATGGTTCT GCTGATCGAC GAACGTCCGG	rho internal FP, 610-640 nt
RS118	CCGCAACCTGAAGTGGCGAGATCG GG	rho internal RP, 703-733 nt
RS140	GTCCGGATTGGAGCTTGGGATCC	rho internal RP, 703-733 nt
RS153	GCG CGC CTC GAG AAC AGA TGC ACG ACG TGA GCG TTT CAT CAT TTC GAA G	rho RP with HMK tag, XhoI site and without stop codon
RS156	CCTGCAGCAGGTTTGTGATAAGCCG CGTC	FP to make NusG G119C by SDM
RS157	GACGCGGCTTATCACAAACCTGCTG CAGG	RP to make NusG G119C by SDM
RS166	TCCTCGACGCTAACCTGGC	FP- 150 bp upstream of rho leader sequence
RS167	ACATCGCCAGCGCGGCAT	RP-70 bp downstream of rho stop codon
RS177	GAA TTG TGA GCG CTC ACA ATT C GGATATATATTAACAATTACCTG	RP with lac operator sequence at 161U of *trp t'* terminator used to generate roadblock downstream of rut sites of T7A1-*trp t'* template
RS205	AGCTTGCGCTTGCGCTTGCGCG	Sequence complementary to RS206 with HindIII adapter for making ΔT_{R1} template
RS206	GATCCGCGCAAGCGCAAGCGCA	Sequence complementary to RS205 with BamHI adapter for making ΔT_{R1} template

RS267	GGTATGCGTGGAAAAAACGCACGC TACCGCCTGGCCTTAGTTGGTCAGA TATATTGGG	RP for amplifying ops pause sequence from pRS25
RS304	GTCAGCGTCGCAAAGCAGAACGTA AATTC	FP to make NusG S60A by SDM
RS305	GAATTTACGTTCTGCTTTGCGACGC TGAC	RP to make NusG S60A by SDM
RS308	GCG CGC CAT ATG CAGGTTGGTGATAAGCC	Internal FP with NdeI site for cloning NusG-CTD in pET 21b
RS309a	GCG CGC CTC GAG CGGCTTATCACCAACCTG	Internal RP with XhoI site and without stop codon for cloning NusG-NTD in pET 21b
RS330	GATGGTCCGTTCGCTGACTTCGAAG TGGATTACGAGAAATC	Internal NusG FP for amplifying C terminal of NusG which is to be used as RP for cloning NusG Δ145-149
RS331	GAAGTGGATTACGAGAAATCTGTTT CTATCTTCGGTCGTGC	Internal NusG FP for amplifying C terminal of NusG which is to be used as RP for cloning NusG Δ157-161
RS353	GAT AAG CCG CGT CCG AAA TGC CTG TTT GAA CCG GGT G	FP to make NusG T126C by SDM
RS354	CAC CCG GTT CAA ACA GGC ATT TCG GAC GCG GCT TAT C	RP to make NusG T126C by SDM
RS355	GAA GTG GAT TAC GAG AAA TGC CGT CTG AAA GTG TCT GTT TC	FP to make NusG S156C by SDM
RS356	ACA GAC ACT TTC AGA CGG CAT TTC TCG TAA TCC ACT TC	RP to make NusG S156C by SDM
RS383	GAT ATA CTC GAG TTA TAC CGG GGT CGC ACG ACC	Internal RP with stop codon and XhoI site for cloning NusG Δ172-181
RS384	GAT ATA CTC GAG TTAGGC TTT TTC AAC CTG GCT GAA GTC CGC ACG ACC GAA GAT AG	RP with stop codon and XhoI site for cloning NusG Δ169-173
RS385	CGCTGACT TCAACGGTGT T TACG AGAAATCTCG TCTG	Internal NusG FP for amplifying C terminal of NusG which is to be used as RP for cloning NusG Δ148-152
RS391	GTG GAT TAC GAG AAA TCT GAA CTG AAA GTG TCT G	FP to make NusG R157E by SDM
RS392	CAG ACA CTT TCA GTT CAG ATT TCT CGT AAT CCA C	RP to make NusG R157E by SDM
RS393	GAT TAC GAG AAA TCT CGT CAG AAA GTG TCT GTT TC	FP to make NusG L158Q by SDM
RS394	GAA ACA GAC ACT TTC TGA CGA GAT TTC TCG TAA TC	RP to make NusG L158Q by SDM
RS395	GAG AAA TCT CGT CTG GAC GTG TCT GTT TCT ATC	FP to make NusG K159D by SDM
RS396	GAT AGA AAC AGA CAC GTC CAG ACG AGA TTT CTC	RP to make NusG K159D by SDM

RS397	GAG AAA TCT CGT CTG AAA AAC TCT GTT TCT ATC TTC G	FP to make NusG V160N by SDM
RS398	CGA AGA TAG AAA CAG AGT TTT TCA GAC GAG ATT TCT C	RP to make NusG V160N by SDM
RS403	GCG CGC CTC GAG TTA CGGCTTATCACCAACCTG	Internal RP with stop codon and XhoI site for cloning NusG-NTD
RS405	ACAAGATGTGAGATTCGCAAAATG C	FP-rac1
RS406	GGACTAACATGACTTTTAACTGTGC	RP-rac1
RS407	CCATAAAGAGTCGGTCTTGTCTG	FP-rac2
RS408	GCAGGCTATTTCTTTCAGATTTCAC	RP-rac2
RS409	CAA CCA CCC GGA TTG TCT GCT GAT GGT TCT GC	FP to make Rho C202S by SDM
RS410	GCA GAA CCA TCA GCA GAC AAT CCG GGT GGT TG	RP to make Rho C202S by SDM
RS411	CGT CCG GAA GAA GTA TGT GAG ATG CAG CGT C	FP to make Rho T217C by SDM
RS412	GAC GCT GCA TCT CAC ATA CTT CTT CCG GAC G	RP to make Rho T217C by SDM
RS413	G ATG CAG CGT CTG GTA TGT GGT GAA GTT GTT GC	FP to make Rho K224C by SDM
RS414	GCA ACA ACT TCA CCA CAT ACC AGA CGC TGC ATC	RP to make Rho K224C by SDM
RS417	CCG TTC GCT GAC TTC GTG GGT GTT GTT GAA GAA G	FP to make NusG N145V by SDM
RS418	CTT CTT CAA CAA CAC CCA CGA AGT CAG CGA ACG G	RP to make NusG N145V by SDM
RS424	CCG GGT GAA ATG GTC GAA GTT AAT GAT GGT CCG	FP to make NusG R135E by SDM
RS425	CGG ACC ATC ATT AAC TTC GAC CAT TTC ACC CGG	RP to make NusG R135E by SDM
RS426	GTG TCT GTT TCT GCT TTC GGT CGT GCG ACC	FP to make NusG I164A by SDM
RS427	GGT CGC ACG ACC GAA AGC AGA AAC AGA CAC	RP to make NusG I164A by SDM
RS428	GTT TCT ATC TTC GGT GAA GCG ACC CCG GTA GAG	FP to make NusG R167E by SDM
RS429	CTC TAC CGG GGT CGC TTC ACC GAA GAT AGA AAC	RP to make NusG R167E by SDM
RS430	CTT CGG TCG TGC GGC GCC GGT AGA GC	FP to make NusG T169A by SDM
RS431	GCT CTA CCG GCG CCG CAC GAC CGA AG	RP to make NusG T169A by SDM
RS432	CGT GCG ACC CCG AAC GAG CTG GAC TTC	FP to make NusG V171N by SDM

RS433	GAA GTC CAG CTC GTT CGG GGT CGC ACG	RP to make NusG V171N by SDM
RS434	GCT GAC TTC AAC GGT TGC GTT GAA GAA GTG GAT TAC	FP to make NusG V147C by SDM
RS435	GTA ATC CAC TTC TTC AAC GCA ACC GTT GAA GTC AGC	RP to make NusG V147C by SDM
RS436	CTC GTC TGA AAG TGT GCG TTT CTA TCT TCG GTC G	FP to make NusG S161C by SDM
RS437	CGA CCG AAG ATA GAA ACG CAC ACT TTC AGA CGA G	RP to make NusG S161C by SDM
RS438	CTA TCT TCG GTC GTT GCA CCC CGG TAG AGC	FP to make NusG A168C by SDM
RS439	GCT CTA CCG GGG TGC AAC GAC CGA AGA TAG	RP to make NusG A168C by SDM
RS440	GCT GAC TTC AAC GGT GTT AAC GAA GAA GTG GAT TAG	FP to make NusG V148N by SDM
RS441	CTA ATC CAC TTC TTC GTT AAC ACC GTT GAA GTC AGC	RP to make NusG V148N by SDM
RS457	CGC GTA GCA ACG TGC CTG CGT GAG CAT ATC	FP to make NusG S25C by SDM
RS458	GAT ATG CTC ACG CAG GCA CGT TGC TAC GCG	RP to make NusG S25C by SDM
RS459	CAC CTG GTG CGC TGC GTA CCG CGT GTG ATG	FP to make NusG S85C by SDM
RS460	CAT CAC ACG CGG TAC GCA GCG CAC CAG GTG	RP to make NusG S85C by SDM
RS468	GCG TTT TCC GGT TTT CTG GGC CGC GTA GCA ACG	FP to make NusG E19L by SDM
RS469	CGT TGC TAC GCG GCC CAG AAA ACC GGA AAA CGC	RP to make NusG E19L by SDM
RS470	GTT TTG AAG GCC GCA ACG CAA CGT CGC TGC GTG	FP to make NusG V22N by SDM
RS471	CAC GCA GCG ACG TTG CGT TGC GGC CTT CAA AAC	RP to make NusG V22N by SDM
RS472	CCG CGT AGC AAC GTC GGA ACG TGA GCA TAT CAA ATT AC	FP to make NusG L26E by SDM
RS473	GTA ATT TGA TAT GCT CAC GTT CCG ACG TTG CTA CGC GG	RP to make NusG L26E by SDM
SBM15	GAGGTACCAGCGCGGTTTGATC	FP upstream of *E. coli* attB
SBM16	TTTAATATATTGATATTTATATCATT TTACGTTTCTCGTTC	FP upstream of λ attP
SBM17	ACTCGTCGCGAACCGCTTTC	RP within the λ int gene

Appendix III: Genetics and Molecular biology techniques employed

AIII.1 Phage P1 lysate preparation

A single colony of the donor strain was inoculated into 3 ml LB supplemented with 1.0 mM $CaCl_2$ and required antibiotic and was grown overnight at 37 ºC. 0.3 ml of this culture was taken into a sterile eppendorf tube and was mixed with 10^7 plaqueforming units (pfu) of a stock P1 lysate prepared on MG1655. Adsorption was allowed to occur at 30 ºC for 30 min. 10 ml LB medium supplemented with 5 mM $CaCl_2$ and Tetracycline was added to this and kept on a shaker incubator set at 37 ºC for 3-4 hr and monitored for cell lysis. Once visible cell lysis occurs, this lysate was treated with chloroform (0.3 ml chloroform/10 ml lysate), shaken well, transferred into a sterile glass test tube, centrifuged at 4000 rpm. After centrifugation, the clear supernatant was removed into a sterile test tube, twice treated with chloroform as earlier and the clear lysate was stored at 4 ºC. To quantitative the P1 phage lysate preparations, titration was done using a P1-sensitive indicator strain such as MG1655. 100 µl each of serial dilutions of the recombinant P1 phage made (typically 10^{-5}, 10^{-6}) were mixed with 0.1 ml of the fresh culture. After 15 min adsorption at 37 ºC without shaking, each mixture was added in a soft agar overlay to LB agar plates, and incubated overnight at 37 ºC. The phage titer was calculated from the number of plaques obtained on the plates.

AIII.2 P1 transduction

2 ml of overnight culture of the recipient strain, (grown in LB supplemented with 5 mM $CaCl_2$) was spun at 4000 rpm, the supernatant was removed and was re-suspended in 0.5 ml fresh LB supplemented with 2.5 mM $CaCl_2$. This was mixed with 10^7 plaque-forming units (pfu) of a recombinant P1 lysate prepared on strains as required. Adsorption was allowed to occur at 37 ºC for 30 min. This was then spun at 4000 rpm to remove the un-adsorbed P1 phage. The bacterial pellet was resuspended in 4 ml of fresh LB supplemented with 150 µl of 1 M Sodium Citrate (to prevent further adsorption P1 phage). This was incubated for 30 min at 30 ºC with slow shaking to allow for phenotypic expression of the antibiotic resistance gene. This was then spun at 4000 rpm, the supernatant was taken out and the bacterial pellet was resuspended in 0.3 ml of Citrate buffer. The mixture was then centrifuged at 4000 rpm, and the pellet was resuspended in

0.3 ml of citrate buffer. 100 µl aliquots were plated on appropriate antibiotic containing plates supplemented with 2.5 mM sodium citrate. A control tube without the addition of the P1 lysate was processed in the similar way as described above. The plates were incubated O/N at 37 ºC, the transductants that came up in the plate were streaked onto fresh plates with the same medium and grown O/N at 37 °C.

AIII.3 Preparation of lambda lysate

A λ-sensitive host (MC4100) was grown overnight in 3 ml of LB containing 0.4% maltose and 10 mM $MgSO_4$. To 1 ml of this culture, 0.1 ml of λ phage lysate (or to a titer value ~10^9 pfu/ml) was added in the presence of 5 mM $MgSO_4$ and after 20 min of infection; the mixture was diluted with 10-20 ml of LB containing 5 mM $MgSO_4$. This was grown with shaking until lysis occurred after ~ 4-6 hr. Once visible cell lysis occurs, this lysate was treated with chloroform (0.3 ml chloroform/10 ml lysate), shaken well, transferred into a sterile glass test tube, centrifuged at 4000 rpm. After centrifuging down the debris, the clear supernatant was removed into a sterile test tube, treated again with chloroform (0.3 ml), spun at 4000 rpm and the clear lysate was stored at 4 ºC with Chloroform. The lysate thus obtained usually contained 10^9 pfu/ml phage particles. To quantitate the lysate preparation, a titration was done using a sensitive indicator strain such as MG1655. 100 µl each of serial dilutions of the λ RS45 phage made (typically 10^{-5}, 10^{-6}) were mixed with 0.1 ml of the fresh culture. After 15 min adsorption at 37 ºC without shaking, each mixture was added in a soft agar overlay to LB agar plates supplemented with 10 mM $MgSO_4$, and incubated overnight at 37 ºC. The phage titer was calculated from the number of plaques obtained on the plates.

AIII.4 Preparation of recombinant lambda lysate

E. coli strain MC4100 was transformed with the plasmid carrying the required *lac* cassette to be inserted in to the host chromosome. Lambda phage vector (λ RS45 or λ RS88) was propagated on this strain as described above. 0.3 ml overnight culture of MC4100 and 10^7 plaque-forming units (pfu) or phage to an MOI of 0.01 of the recombinant phage suspended in soft agar maintained at around 37 ºC was mixed quickly and overlaid on to the LB agar plate supplemented with X-Gal IPTG (to a concentration

of 40 μg/ml for X-Gal and 1 mM for IPTG), 0.4% maltose and 10 mM $MgSO_4$. The recombinant phage harboring the sequence of interest was picked up based on color of the plaque and propagated as follows.

AIII.5 Purification of lambda phage from single plaques

A single plaque of λ contains approximately 10^5-10^6 pfu/ml of phage. The method of propagation of λ from a single plaque was as follows. The contents of a single isolated plaque were drawn into a sterile 1-ml pipette tip and dispensed into 0.5 ml of LB. After addition of a drop of chloroform, the contents were vortexed for short bursts and centrifuged. The lysate was purified to homogeneity for phages expressing the desired plaque color by passing it once again through fresh MC4100 cells by growing the adsorbed phage-bacterial cells as above in LB X-Gal plates and picking up plaques from it and repeating the lysate preparation from the picked up plaque, as above. The clear supernatant obtained was mixed with 0.3 ml of MC4100 cells grown O/N in LB supplemented with 10 mM $MgSO_4$ and incubated for 20 min at room temperature for adsorption. The infection mixture was then added into 10 ml of LB supplemented with 5 mM $MgSO_4$ and incubated at 37 ºC with shaking until lysis. The lysate was mixed with chloroform and was purified by centrifugation as given above and clear lysate was stored at 4 ºC.

AIII.6 Lambda transduction

A bacterial lawn of MC4100 was prepared by mixing 0.3 ml of O/N culture of MC4100 (grown in LB containing 10 mM $MgSO_4$) with 3 ml soft agar (kept at a temperature of around 37 °C- 40 °C) and overlaying it by pouring it into an LB agar plate supplemented with 10 mM $MgSO_4$ and allowing it to solidify for 10 min, inside the laminar air flow chamber. Dilutions of (10^{-5} and 10^{-6} in LB) of the recombinant λ lysate was spotted onto this lawn and allowed to adsorb on to the lawn for 30 min. The plate was then incubated for 18-20 hr in a 37 °C incubator. Lysogens which were visible on the clearings in the bacterial lawn brought about by phage mediated lysis were picked up using a toothpick and streaked onto a LB agar plate onto and incubated O/N at 37 °C. The lysogens were re-streaked into fresh plates and a colony PCR using the primers specific for the upstream

and downstream regions of the sequence to be inserted was carried out, to confirm the presence of the cassette in the chromosome of MC4100. The lysogens obtained after transduction were checked to confirm that they were single copy insertions (prophage copy number) at the λ phage insertion site in the bacterial chromosome by PCR screening using *E. coli att*B and λ *att*P specific primers by following the methodology described by Powell et al., 1994.

AIII.7 Betagalactosidase assay

A single colony was picked and inoculated in 1 ml LB with appropriate antibiotic and incubated at 37 ˚C overnight in shaking water bath. 1% of the primary inoculum was subcultured in 1 ml of LB broth with required antibiotic. The cells were grown till O.D of 0.2 is reached. The cells were then induced with various concentration of arabinose for 30 min. 200 µl of the culture was taken in a microplate (Plate #1) and O.D was taken at 600 nm wavelength in a spectramax system. The culture was taken in eppendorf and 40 µl chloroform was added to each. The cells were lysed by vortexing and spun down. 20 µl of the lysate was taken in another microtiter plate (Plate #2). 140 µl of Z buffer was added to each well and 40 µl of 4 mg/ml ONPG was added. Immediately the reading was taken in plate #2 in kinetic mode of Spectramax system. LB was used as the blank in plate #1, in plate #2 160 µl Z buffer + 40 µl ONPG were used as blank.

AIII.8 Isolation of plasmid DNA

The rapid alkaline lysis method of plasmid isolation, as described by Sambrook (Sambrook et al., 2001) was followed with minor modifications. Bacterial pellet from 3 ml of stationary-phase culture was resuspended in 200 µl of ice-cold solution I (50 mM glucose, 25 mM Tris-Cl pH 8.0, 10 mM EDTA pH 8.0 containing 1 mg/ml lysozyme) by vortexing. After 5 min incubation at room temperature, 400 µl of freshly prepared solution II (0.2 N NaOH, 1% SDS) was added and the contents were mixed, by gently inverting the tube several times. This was followed by the addition of 300 µl of ice-cold solution III (5 M potassium acetate, pH 4.8) and gentle mixing. The tube was incubated on ice for 10 min and centrifuged at 12,000 rpm for 15 min at 4 °C. The clear supernatant was removed into a fresh tube and, if required, was extracted with an equal volume of

phenol: chloroform mixture. The supernatant was precipitated with either two volumes of cold 95% ethanol or 0.6 volumes of isopropanol at room temperature for 30 min. The nucleic acids were pelleted by centrifugation, washed with 70% ethanol, vacuum dried, and dissolved in appropriate volume of TE buffer. If required, the sample was treated for 30 min with DNase free RNase at a final concentration of 20 µg/ml. The plasmid DNA was checked on a 0.8% agarose gel and stored at –20 °C. The plasmid DNA thus isolated was suitable for procedures such as restriction digestion, ligation, and preparation of radiolabeled probes. Alternatively, in cases where high purity of the plasmid preparation is required (for example, for procedures such as automated DNA sequencing), plasmid DNA was also prepared by using the commercial kit for plasmid DNA isolation (mini prep and midi prep) from Qiagen, following the manufacturer's protocols.

AIII.9 Agarose gel electrophoresis

The DNA samples were mixed with the appropriate volumes of the 6X loading dye (0.25% bromophenol blue, 0.25% xylene cyanol and 30% glycerol in water) and subjected to electrophoresis through agarose gel (0.8% for plasmid DNA and 1%-1.6% for PCR products, as per the size variations of the DNA fragments) in either 1x TBE or 1x TAE buffer. The gel was stained in 1 µg/ml of Ethidium Bromide solution prepared in Ix TAE for 10 min at room temperature and the bands were visualized by fluorescence under UV-light.

AIII.10 PCR Reactions

Polymerase Chain Reactions (PCR) was carried out for amplifying DNA on PCR machines (Mastercycler, Eppendorf). The concentrations of the components were as follows: DNA 20-50 ng, Primers (forward and reverse)- 0.5 µM; dNTPs - 0.25 mM; $MgCl_2$- 2.5 mM; Taq DNA Polymerase (Roche), as per manufacturer’s instructions. Proof reading DNA Polymerases (Pfu-Stratagene, DeepVent-NEB and Dnazyme-Finnzymes) were used for amplifying DNA used in cloning and for templates in transcription reactions, concentration of which ranged from 1-2.5 U/50 µl, as per the length of DNA to be amplified. The initial denaturation was done at 95 °C for 2 min; denaturation, annealing (at 55 °C) and extension (72 °C) were for 30 sec, 30 sec and 2

min respectively, reaction was for 30 cycles. The final extension was done at 72 °C for 10 min. For larger DNA products (above 1 kb), we have used the following cycle: The initial denaturation was at 95 °C for 2 min; denaturation, annealing (at 55 °C) and extension (72 °C) were for 30 sec, 1 min and 2 min respectively and reaction was for 30 cycles. The final extension was at 72 °C for 15 min.

AIII.11 Restriction enzyme digestion and analysis

0.5-1 μg of DNA was used for each restriction enzyme digestion. 2-4 units of the restriction enzymes with the appropriate 10X buffers supplied by the manufacturers and BSA (as when required) were used in the reactions. The digestion was allowed to proceed for 3-6 hr at the temperature recommended by the manufacturer. The DNA fragments were visualized by Ethidium Bromide staining following electrophoresis on agarose gels. Commercially available DNA size markers were run along with the digestion samples to compare with and to estimate the sizes of the restriction fragments. The restriction digested DNA samples that were to be used for cloning purposes were phenol extracted and ethanol precipitated or purified and concentrated by passing through Centricon centrifugal filters before the next step.

AIII.12 Purification of DNA fragments by elution from the gel

DNA fragments to be used for specific purposes such as ligation or radioactive labeling were eluted from the agarose gel, after the electrophoresis. The gel piece containing the desired band of DNA was sliced out using afresh scalpel blade and the DNA was purified from the gel using the purification kits available for this purpose, following the manufacturer's protocols. Qiagen gel extraction and purification kits were used throughout this study. The efficiency of elution was determined by checking a small aliquot of DNA sample on the gel.

AIII.13 Ligation of DNA

Typically, 50-150 ng of DNA was used in each ligation reaction. The ratio of vector to insert was maintained between 1:3 and 1:5. The reactions were usually done in a 10 μl

volume containing ligation buffer (provided by the manufacturer) and 0.05 Weiss units of T4 DNA ligase, and the reactions were incubated at 16 °C for 12-16 hr.

AIII.14 End labeling of DNA markers

DNA markers were radiolabelled with T4 Polynucleotide Kinase (NEB). Reactions were carried out essentially as per manufacturer's protocols, with the buffer provided along with the enzyme and [γ-^{32}P] ATP (Amersham/BRIT). The labeled DNA was purified by passing through G-25 spin columns (Amersham).

AIII.15 Transformation protocols

AIII.15.1 Calcium chloride method: For routine plasmid transformations, where high efficiency is not required, the following method, which is a modification of that described by Sambrook et al. was used. An overnight culture of the recipient strain was subcultured in fresh LB with the appropriate antibiotics as required and grown till mid-exponential phase. The culture was chilled on ice for 15 min, and the steps hereafter were done on ice or at 4 °C. The culture was centrifuged, and the pellet was resuspended in one-third volume of cold 0.1 M $CaCl_2$. After 15 min incubation on ice, the cells were again recovered by centrifugation. If the competent cells prepared were to be stored for later use, storage purposes, $CaCl_2$ with 20% glycerol was added and stored in $^{-}$70 °C as 100 µl aliquots. Alternatively, if directly using for transformation, the pellet was resuspended in one-tenth volume of cold 0.1 M $CaCl_2$. The suspension was incubated on ice for 5 min and aliquoted 100 µl each, in sterile eppendorf tubes; incubated for 30 min and then DNA was added (~10-100 ng of DNA in less than 10 µl volume). The mixture was again incubated on ice for 30 min, and then was subjected to a heat shock for 90 sec at 42 °C. The tubes were plunged into ice immediately after the 90 sec heat shock, incubated in ice for 2 min and then 0.9 ml of LB broth was added to the tube, incubated at 37 °C for 45 min for phenotypic expression of the antibiotic marker before being plated on selective medium at various dilutions or as a whole, after centrifuging the cells at 4000 rpm and plating the whole pellet resuspended in 100 µl LB. A negative control tube (with no plasmid DNA addition) was also routinely included in each of the experiments.

AIII.15.2 Preparation of high efficiency competent cells (ultra competent cells)

Competent cells for high efficiency transformation were prepared according to Inoue's method (Sambrook and Russel, 2001). An overnight culture of the recipient strain was subcultured into fresh LB broth at 1:100 dilution and allowed to grow with good shaking at 37 °C till an A_{600} of ~0.5. The cells were chilled on ice for 15 min and centrifuged at 4000 rpm at 4 °C. The pellet was resuspended in one-third volume of ice-cold Transformation Buffer (10 mM PIPES (free acid), 15 mM $CaCl_2.2H_2O$, 250 mM KCl, and 55 mM $MnCl_2.2H_2O$; pH adjusted to 6.8 with 1 N KOH and filter sterilized) and incubated on ice for 20 min. The cells were recovered after centrifugation at 4000 rpm at 4 °C and the pellet was resuspended in one-twelth volume of ice-cold transformation buffer with DMSO (to a final concentration of 7%) as the cryo-protectant. The cell suspension was again incubated on ice for 15 min, and 100 µl aliquots were then distributed into pre-chilled microfuge tubes. The aliquots were flash-frozen in liquid nitrogen and stored at ⁻70 °C till further use. For transformation, the tube was thawed on ice, DNA was added to it and the subsequent protocol followed was as described early, for transformation.

AIII.16 Electroporation

AIII.16.1 Preparation of electro competent cells

E. coli cell cultures were grown in LB with good aeration to an A_{600} of ~ 0.6 to 0.8. The culture was chilled on ice for 20 min and all subsequent steps were carried out on ice or at 4 °C. The cells were harvested by centrifugation, washed three times with ice-cold sterile distilled water, then once with ice-cold 10% glycerol, and finally resuspended in the latter in $1/500^{th}$ the volume of the original culture. The thick cell suspension was dispensed into aliquots of 50 µl, flash frozen using liquid nitrogen and stored at ⁻70 °C. Aliquoted tubes were taken when required, was thawed on ice and used for electroporation as described below.

AIII.16.2 Electroporation: A 20 µl aliquot of electro competent cells was transferred into an electroporation cuvette, the DNA to be electroporated was added to it, and the mix was kept on ice for 5 min. The amount of DNA that can be added is limited by the

salt concentration in the DNA used (typically, from a ligation mix, 1-2 µl of DNA was used). Electroporation was carried out in an electroporator (Biorad) following the manufacturer's instructions. Generally, a pulse, at a resistance of 200 Ω and at 1800 V was used for electroporation of the *E. coli* electro competent cells. Immediately after electroporation, SOB medium was added to the cells in the cuvette. The cells were transferred to a sterile glass tube, was incubated for 30 min to 1 hr with shaking for aeration and then plated into the appropriate selection plates.

AIII.17 Glycerol Stock Preparation:

Single colonies of the required bacteria were inoculated into 3 ml LB with the appropriate antibiotics and grown overnight in a shaker incubator at the required temperature. The overnight culture was centrifuged at 4000 rpm and the supernatant was discarded without disturbing the bacterial pellet. The pellet was then resuspended in 750 µl of sterile 10 mM $MgSO_4$. This was then transferred into sterile cryovials with proper labeling. 250 µl of sterile 80% glycerol was added into this (final concentration of glycerol becomes 20%), mixed well and was stored in $^{-}$70 °C deep freezer.

Appendix IV: Media and reagents

All the media and buffers (except those which were heat labile) were sterilized by autoclaving for 15 min at 121 °C. Media and buffers used in this study are described below.

LB medium:

Tryptone	10 g
Yeast extract	5 g
NaCl	10 g
Water to	1000 ml, pH adjusted to 7.0 - 7.2 with 1 N NaOH.

LB agar:

LB medium	1000 ml
Bacto-agar	15 g

LB soft agar:

LB medium	100 ml
Bacto-agar	0.6 g

MacConkey agar:

MacConkey Agar (Difco)	51.5 g
Water to	1000 ml

Citrate buffer: (0.1 M; pH 5.5)

Citric acid (0.1 M)	4.7 volumes
Sodium citrate (0.1 M)	15.4 volumes

Z Buffer IM, for IL

$Na_2HPO_4.7H_2O$ (O.06 M)	16.10 g/L
$NaH_2PO_4.7H_2O$ (0.04 M)	5.50 g/L
KCl (0.01 M)	0.75 g/L
$MgSO_4 .7H_2O$ (0.001 M)	0.25 g/L

pH was adjusted to 7.0 and stored at 4 °C. Prior to use, added βME (270 µl for 100 ml).

ONPG

80 mg O- Nitro Phenyl-β-D-Galactosidase to 20 ml milliQ water (4 mg/ml)

1.0 M Na_2CO_3

Na_2CO_3 - 10.6 g/L; stored at room temperature.

TE buffer: 10 mM Tris-Cl (pH 8.0) and 1 mM EDTA.

TBE and TAE buffers:

TBE: 90 mM Tris-borate, 2 mM EDTA (pH 8.0) and TAE: 40 mM Tris-acetate, 2 mM EDTA (pH 8.0) were used as standard electrophoresis buffers. TBE and TAE were prepared as 10X and 50X concentrated stock solutions, respectively, and used at 1X concentration. (Alternatively, 10X solution of TBE was made by dissolving 10X TBE concentrate powder from Ambion and dissolving in 1 L RO water).

Sequencing Gel mix (For 500 ml)

10X TBE – 1X- 50 ml

40% Acrylamide (19:1 Acrylamide: BisAcrylamide) mix to the required percentage.

7 M Urea - 210 g

Double distilled water-to make up till the final amount (1 L)

Sequencing gel mix was also purchased from Ambion.

For casting sequencing gels, to the pre-made mix of 25 ml, 200 µl of 10% APS and 20 µl of TEMED were added.

Antibiotics

Antibiotics were used at the following final concentrations (µg/ml):

Ampicillin (for plasmids)	100
Chloramphenicol (for plasmids)	50
Kanamycin	50
Rifampicin	100
Spectinomycin	50
Tetracycline	15

Biochemicals and enzymes

Most chemicals were obtained from commercial sources. The sources for some of the fine chemicals used in this study are given below. Most of the chemicals such as antibiotics, sugars, IPTG, ONPG, DTT, DMF, X-Gal, oligo$(dC)_{34}$, rC_{10}, rC_{25}, Protein kinase A, acrylamide and $TbCl_3$ were obtained from Sigma Chemical Co. NTPs and poly(C) were from Amersham. The media components for the growth of bacteria were mostly from Difco laboratories. The materials used in the recombinant DNA experiments such as restriction endonucleases, T4 DNA ligase, polynucleotide kinase, DNA polymerase and DNA size markers were obtained from companies including New England Biolabs, MBI, Sigma, Finnzyme, Gibco-BRL, Promega and Amersham (USB). Ni-NTA beads and kits used for plasmid isolation, purification of DNA fragments from agarose gel were purchased from Qiagen. The oligonucleotide primers used in this study were mainly synthesized from Sigma Aldrich and MWG Biotech. The radioactive NTPs were from BRIT, Mumbai as well as from Amersham, UK. WT *E. coli* RNA polymerase holoenzyme was purchased from Epicenter Biotechnologies. Taq DNA polymerase was from Roche. *Staphyloccocal aureus* V8 protease and Submaxillary protease (Arg-C) were from Pierce. CNBr was obtained from Fluka.

Publications

1. **Chalissery, J.,** Muteeb, G., Jisha, V., Mohan, S. and Sen, R. Interaction surface required for the complex formation between a transcription terminator and an antiterminator. Manuscript submitted.

2. Dutta, D., **Chalissery, J.** and Sen, R. (2008). Transcription termination factor Rho prefers catalytically active elongation complex for releasing RNA. Journal of Biological Chemistry. 283 (29), 20243-20251.

3. Sen, R., **Chalissery, J.** and Muteeb, G. (2008). Nus factors of *Escherichia coli*. Invited chapter of the book *Escherichia coli* and *Salmonella*: Cellular and Molecular Biology, ASM press. http://www.ecosal.org.

4. **Chalissery, J.**, Banerjee, S., Bandey, I. and Sen, R. (2007). Transcription termination defective mutants of Rho: role of different functions of Rho in releasing RNA from the elongation complex. Journal of Molecular Biology. 371, 855-872.

5. Pani, B., Banerjee, S., **Chalissery, J**., Abhishek, M., Ramya, M. L., Suganthan, R. and Sen, R. (2006). Mechanism of inhibition of Rho-dependent transcription termination by bacteriophage P4 protein Psu. Journal of Biological Chemistry. 281(36), 26491-26500.

6. Banerjee, S., **Chalissery, J.**, Bandey, I and Sen, R. (2006). Rho-dependent transcription termination. More questions than answers. Journal of Microbiology, 44(1), 11-22.

doi:10.1016/j.jmb.2007.06.013 J. Mol. Biol. (2007) 371, 855–872

JMB

Available online at www.sciencedirect.com

ScienceDirect

ELSEVIER

Transcription Termination Defective Mutants of Rho: Role of Different Functions of Rho in Releasing RNA from the Elongation Complex

Jisha Chalissery, Sharmistha Banerjee†, Irfan Bandey† and Ranjan Sen*

Laboratory of Transcription Biology, Centre for DNA Fingerprinting and Diagnostics ECIL Road, Nacharam Hyderabad-500076, India

*Corresponding author

The transcription termination factor Rho of *Escherichia coli* is a RNA binding protein which can translocate along the RNA and unwind the RNA:DNA hybrid using the RNA-dependent ATPase activity. In order to investigate the involvement of each of these functions in releasing RNA from the elongation complex, we have isolated different termination defective mutants of Rho by random mutagenesis, characterized them for their different functions and established the structure–function correlations from the available structural data of Rho. These mutations are located within the two domains; the N-terminal RNA binding domain (G51V, G53V, and Y80C) and in the C-terminal ATP binding domain (Y274D, P279S, P279L, G324D, N340S, I382N) including the two important structural elements, the Q-loop (P279S, P279L) and R-loop (G324D). Termination defects of the mutants in primary RNA binding domain and Q-loop could not be restored under any conditions that we tested and these were also defective for most of the other functions of Rho. The termination defects of the mutants (Y274D, G324D and N340S), which were mainly defective for secondary RNA binding and likely defective for translocase activity, could be restored under relaxed *in vitro* conditions. We also show that a mutation in a primary RNA binding domain (Y80C) can cause a defect in ATP binding and induce distinct conformational changes in the distal C-terminal domain, and these allosteric effects are not predictable from the crystal structure. We conclude that the interactions in the primary RNA binding domain and in the Q-loop are mandatory for RNA release to occur and propose that the interactions in the primary RNA binding modulate most of the other functions of Rho allosterically. The rate of ATP hydrolysis regulates the processivity of translocation along the RNA and is directly correlated with the efficiency of RNA release. NusG improves the speed of RNA release and is not involved in any other step.

Keywords: RNA polymerase; Rho; NusG; transcription termination; mutagenesis

Introduction

Once the process of transcription is initiated, RNA polymerase (RNAP) makes a stable elongation complex with the DNA and the nascent RNA.[1–3] Elongation complex (EC) only dissociates in response to *cis* or *trans* termination signals. Distinguished by their mechanism and structural features, there are two types of terminators in the *Escherichia coli* genome. (a) Intrinsic terminators characterized by a GC-rich inverted repeat followed by a oligo(dT) stretch that induce RNA polymerase to disengage RNA; and (b) the factor-dependent terminators, which depend on an essential protein factor, called Rho, for termination.[4,5]

Rho is a homo-hexameric RNA/DNA helicase or translocase that dissociates RNA polymerase from

† S.B. and I.B. contributed equally to the work.

Abbreviations used: RNAP, RNA polymerase; EC, elongation complex; %RT, read-through efficiency.

E-mail address of the corresponding author: rsen@cdfd.org.in

DNA template and releases RNA. RNA-dependent ATPase activity of Rho provides free energy for these activities.[6–8] The primary RNA binding site (residues 22–116) can bind to a single-stranded DNA molecule as well as a single-stranded RNA molecule and is responsible for recognizing the Rho utilization (*rut*) site.[9] Amino acid residues 179–183 form the P-loop, a highly conserved region among the RecA family of ATPases and is involved in ATP binding and ATPase activity.[10] The Q-loop and R-loop have been defined as the secondary RNA binding sites. The Q-loop is formed by an eight-residue segment within 278–290 amino acid residues,[10–13] while the R-loop spans between 322–326 amino acid residues.[11,14,15]

Rho-dependent termination involves a series of sequential events. At first Rho binds to the C-rich regions of the nascent RNA, called the *rut* site[16–18] through its primary RNA binding domain. This binding leads to the positioning of the RNA into the secondary RNA binding domain, which in turn activates the ATPase activity. It utilizes the free energy derived from the ATP hydrolysis for its translocase/RNA–DNA helicase functions,[6,7] which eventually leads to the release of the RNA from the elongation complex. It is commonly believed that the translocase/helicase activities of Rho is instrumental in pulling out RNA from the elongating RNA polymerase.[7] However, it is not well understood how each of these events is related to the RNA release process.

Here, we investigated the involvement of different functions of Rho in releasing the RNA from the elongation complex. We randomly mutagenized the *rho* gene, isolated the termination defective mutants, characterized each of them for their defects in other functions and established a structure–function relationship of the effects of these mutations based on the recent closed ring structure of Rho.[19] This is in contrast to earlier mutagenesis approaches which were only restricted to identify the different functional domains of Rho.[13,14,20] We also established an *in vitro* experimental set-up to measure the Rho-mediated RNA release from a stalled EC, uncoupled from the transcription elongation process. This set-up enabled us to find the conditions under which some of these mutants regained the efficiency of RNA release and to understand the specific roles of ATP and NusG in the process of Rho-dependent termination. We concluded that the mutations in the N-terminal primary RNA binding domain can exert allosteric effects in the distal C-terminal domain, and this domain may act as a "master switch" that governs all the other functions of Rho. The primary RNA binding domain and the Q-loop are the most crucial structural elements for the RNA release function. Altered interactions in the secondary RNA binding domain only reduce the rate of ATPase activity which most likely slows down the translocation rate of Rho along the RNA. The rate of ATP hydrolysis is directly correlated with the efficiency of RNA release and involvement of NusG is restricted only to the final step of RNA release from the EC.

Results

Isolation of termination defective mutants of Rho

We have randomly mutagenized the whole *rho* gene and screened for mutants defective for termination at two Rho-dependent terminators (see Materials and Methods). After screening about 100,000 colonies, we isolated nine unique mutations in Rho which were severely defective for termination. These mutations are G51V, G53V, Y80C, Y274D, P279S, P279L, G324D, N340S and I382N. G51V and I382N mutations were independently isolated at least six times. G51V and G53V were also isolated earlier from a localized mutagenesis screen of the primary RNA binding domain.[20] Although the positions of the mutations indicate that the mutagenesis was random, the classical polarity suppressor mutations[21] were not isolated by this method, the reason of which is not clear to us. Termination defects exhibited by these mutations on three Rho-dependent terminators (defect for $nutR/TR_1$ terminator is described below) suggest that the defect is not specific for a particular terminator. We also observed that mutants other than G51V, Y80C and Y274D caused a growth defect at 42 °C.

In vivo termination defects of the Rho mutants

To get a quantitative measure of the termination defects of the Rho mutants, the ratio of β-galactosidase made from a *lacZ* reporter fused to a Rho-dependent terminator (P_{lac}-H-19B $nutR/TR_1$-*lacZYA*) to that without the terminator (P_{lac}-*lacZYA*) was measured (read-through efficiency=%RT). This Rho-dependent terminator is derived from the *nutR-cro* region of a lambdoid phage H-19B[22] and found to behave similar to the $nutR/T_{R1}$ of λ phage. These reporter fusions were present as a single copy prophage (see Materials and Methods and Table 6 for the strains). Different strains with these reporter fusions were transformed with the plasmids carrying the Rho mutants. The measurements were done in the presence of either wild-type (WT) or B8 (rpoB, Q513P) RNA polymerase in the chromosome and either in the presence of a WT or chromosomal deletion of Rho.

Compared to WT Rho, all the mutants showed a significant defect in termination as evident from the 10 to 20-fold increase in terminator read-through efficiency (Table 1, column 4). Even in the presence of a WT copy of Rho, the read-through efficiency of the mutants was significantly high (Table 1, column 7). This could be attributed to the multi-copy (copy number of pCL1920 is ~5)[23] dominance of the mutant Rho over WT Rho. The partial suppression of the defects could also arise from the mixing of WT and mutant protomers of Rho.

The kinetic coupling model of Rho-dependent termination predicts that a slow moving RNA polymerase can suppress the effect of defective Rho.[24] So

Table 1. *In vivo* termination defects of the Rho mutants

Rho alleles	WT RNAP β-Galactosidase (arbitrary units)						B8 RNAP β-Galactosidase (arbitrary units)		
	Δ*rho: kan*[a]			*WT rho*[b]			Δ*rho: kan*[c]		
	$+T_{R1}$	$-T_{R1}$	%RT	$+T_{R1}$	$-T_{R1}$	%RT	$+T_{R1}$	$-T_{R1}$	%RT
WT	42±2	973±28	4.3	37±2	839±68	4.4	78.5±10	564±83	13.9
G51V	334±20	690±24	49.0	360±17	860.5±62	41.8	445±32	782±128	56.9
G53V	548.5±54	678±22	80.9	433±11	1055±45	41.0	458±48	636±96	72.1
Y80C	435±12	687±11	63.3	422±23	1072±46	39.3	645±60	850±180	75.8
Y274D	605.5±45	729±34	83.1	324±14	1183±44	27.4	435±45.5	623±115	69.8
P279S	362±8	677±25	53.4	308±6	870±10	35.4	345±42	633±122	54.5
P279L	686±39	1116±39	61.5	317±22	852±42	37.2	772±36	1304±84	59.2
G324D	636.5±24	1074±52	59.3	298±13	839±33	35.5	847±116	1127±18.5	75.1
N340S	732±45.5	1102±35	66.4	284±15.5	973±33	29.2	1272±93	1553±275	81.9
I382N	750±54	1158±24	64.8	290±11	1057±24	27.5	1050±33	1247±182	84.1

These above strains were transformed with the plasmids bearing different WT and *rho* mutants. The ratio of β–galactosidase values in the presence and absence of T_{R1} terminator gives the efficiency of terminator read-through (%RT). This Rho-dependent terminator is derived from the *nutR-cro* region of a lambdoid phage H-19B and found to behave similar to the *nutR*/T_{R1} of λ phage. The averages of five to six independent measurements are shown.

[a] Strains RS364 and RS391 with WT RNA polymerase and deletion of *rho* in the chromosome.

[b] Strains GJ3073 and RS445 with WT RNA polymerase and WT *rho* in the chromosome.

[c] Strains RS449 and RS450 with B8 RNA polymerase and deletion of *rho* in the chromosome.

we wanted to know whether the defects of these mutants could be suppressed by B8 (rpoB, Q513P), a slow elongating RNA polymerase.[25] Similar measurements of termination read-through in the presence of B8 RNAP showed that defects of none of the Rho mutants were suppressed by the "slow" RNAP (Table 1, column 10), which is in contrast to earlier observations of different Rho mutants being suppressed by this RNAP.[24,26] According to the kinetic coupling model, slow RNAP will suppress only the Rho mutants which are defective in translocation along the RNA. Thus, either these mutants translocate too slow to catch up B8 RNAP or these mutants are defective in other steps of Rho-dependent termination. It is also noted that none of these mutants were compatible with a fast moving RNAP, B2 (rpoB, H526Y). It was difficult to obtain transformants in the strain having B2 RNAP in the chromosome with all the plasmids bearing Rho mutants. The defects of these Rho mutants might have amplified in the presence of a fast moving RNAP that caused this lethality. We also observed increased read-through activity with the slow RNAP (B8), which was unexpected (Table 1, column 10) and the reason for this is not clear.

In vitro termination defects of the Rho mutants

In vitro transcription termination activity of the Rho mutants was studied at the *trp t'*terminator[21,27,28] using purified WT and all the mutant Rho proteins, except G53V and P279L. We could not purify G53V and P279L mutants because they formed inclusion bodies under overexpression conditions. A linear DNA template with the *trp t'* terminator cloned downstream to the strong T7A1 promoter was used for transcription assays (see Materials and Methods). In order to observe the released RNA at the Rho-dependent termination points, the templates were immobilized on streptavidin-coated magnetic beads. In the assays, the supernatant fractions contain the released RNA. The WT Rho protein showed about 85% efficiency in termination. Consistent with their *in vivo* phenotype, all the Rho mutants except I382N showed significantly reduced termination efficiency (Figure 1(a) and (b)). The presence of NusG during the chase improved the termination efficiency of Y274D, G324D and N340S by about twofold (Figure 1(a) and (b)). NusG, however, did not bring about early termination in these mutants as observed for the WT Rho (Figure 1(a)).

In order to validate the *in vivo* observation that the termination defects of the Rho mutants could not be suppressed by B8 RNAP, *in vitro* transcriptions were also carried out with the B8 enzyme. Consistent with the *in vivo* data (Table 1), the *in vitro* assays (Figure 1(c)) also showed that B8 RNAP does not improve the termination efficiency of the mutants significantly, except for Y274D. For Y274D and G324D mutants, termination efficiency was improved ~1.5-to twofold in the presence of NusG. These mutants (and N340S; see Figure 1(a) and (b)) might have defects in the RNA release step(s) from the EC, and NusG is likely to be involved in this step during the Rho-dependent termination process.

Location of the mutations on the crystal structure of Rho and prediction of functional defects

We mapped the positions of the mutations on the recently reported hexameric closed ring structure of Rho, which has both the primary and secondary RNA binding sites occupied with nucleic acids[19] (Figure 2(a) and (b)). In general, the mutations are located within or close to the previously identified

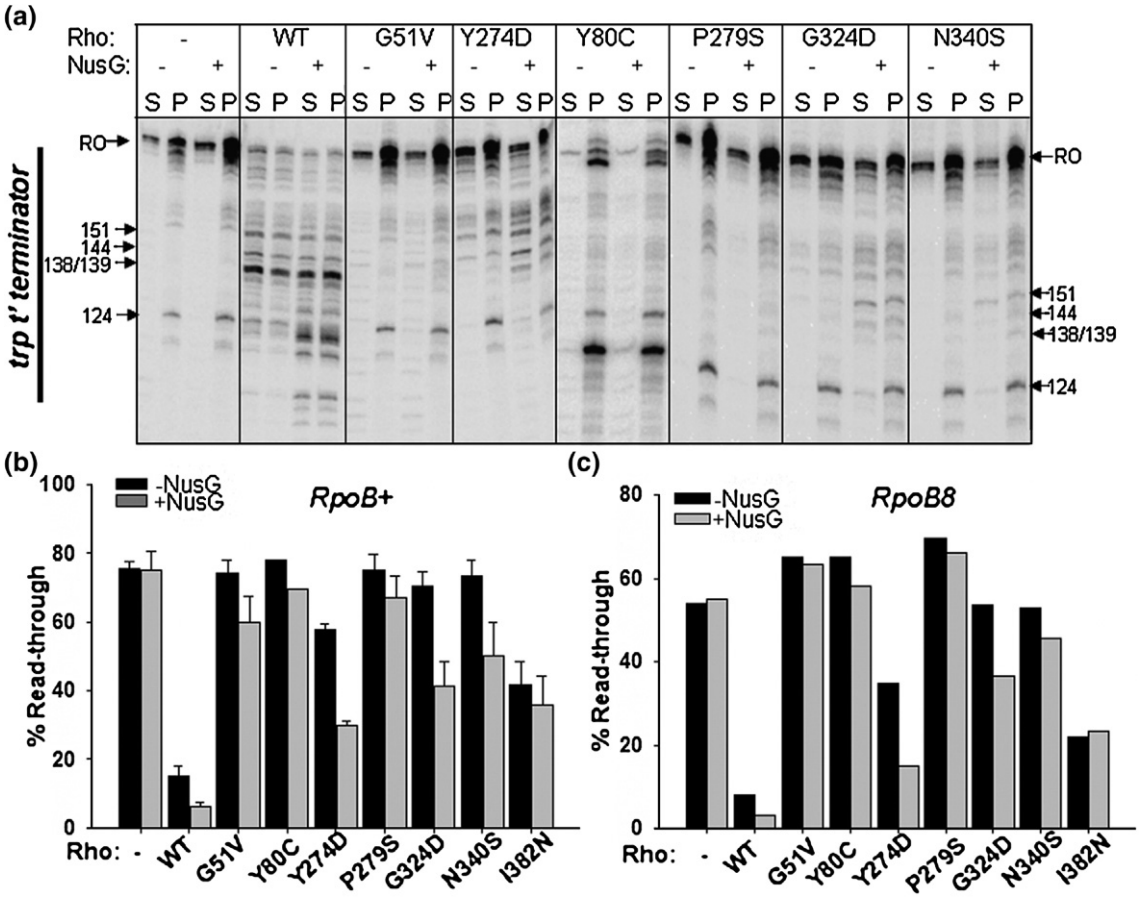

Figure 1. *In vitro* termination defects of the mutant Rho proteins. (a) Autoradiogram of the *in vitro* transcription termination by different Rho mutants both in the absence and presence of 200 nM NusG. Transcription was initiated from T7A1 promoter. The DNA template was immobilized on magnetic beads. Rho-dependent RNA release starts from 100 nt downstream of the transcription start site in the *trp t'* terminator region (as indicated). Major termination positions are marked. Half of the supernatant is denoted as S (released RNA) and the rest of the reaction mixture containing both supernatant and pellet is denoted as P (total RNA). RO denotes the run-off product. The read-through efficiency (RT) for each case was calculated from the P lanes as: RT=[RO product]/[RO product + all the products ≥ 100 nt]. (b) Measured RT for each of the mutants is shown as bar diagrams using WT RNA polymerase. Higher read through efficiencies of the Rho mutants reflect their termination defect. (c) Read through efficiencies measured in the presence of B8 RNA polymerase.

important functional domains of Rho. Among them, G51V, G53V and Y80C are in the primary RNA binding domain (Figure 2(c)). Y274D, P279S and P279L are in or close to the Q-loop (Figure 2(d)). G324D and N340S are close to the secondary RNA binding domain and G324D is in the R-loop (Figure 2(d)). The mutation I382N could not be located on the structure as the C-terminal end of the closed ring structure of Rho is not resolved. Interestingly, mutations in these important structural elements of Rho did not have a lethal phenotype.

It is revealed from the structure that amino acid Y80 makes direct contact with the nucleic acid in the primary RNA binding domain[29] (Figure 2(c)). So there is a high probability that Y80C change will affect the primary RNA binding drastically. Amino acids G51 and G53 also come within 12–14 Å of the nucleic acid in the crystal structure and changes in these amino acids can also affect the primary RNA binding (see the distance calculations in Figure 2(e)). The crystal structure revealed the binding of only two nucleotides, whereas about ten nucleotides can be occupied in the primary RNA binding site of a monomer.[30] Therefore it is likely that other amino acids of this domain (including G51 and G53) will take part in the primary RNA binding.[31] Defect in the primary RNA binding due to the change in these three amino acids will subsequently affect the secondary RNA binding and the RNA release processes.

The amino acids G324 and N340 are situated close to the RNA in the secondary RNA binding site (Figure 2(d) and (e)). It is likely that G324, located in the R-loop, will take part directly in the interaction with RNA. Therefore, it can be predicted that changes in these two amino acids will cause a defect in the secondary RNA binding and in the ATP hydrolysis activities. This may in turn affect the processive translocation of Rho along the RNA, which will lead to a termination defect.

P279S and P279L changes in the Q-loop can alter the loop conformation by extending the length of the preceding helix. The closed ring structure of Rho revealed that the Q-loop is about 30 Å (Figure 2(e))

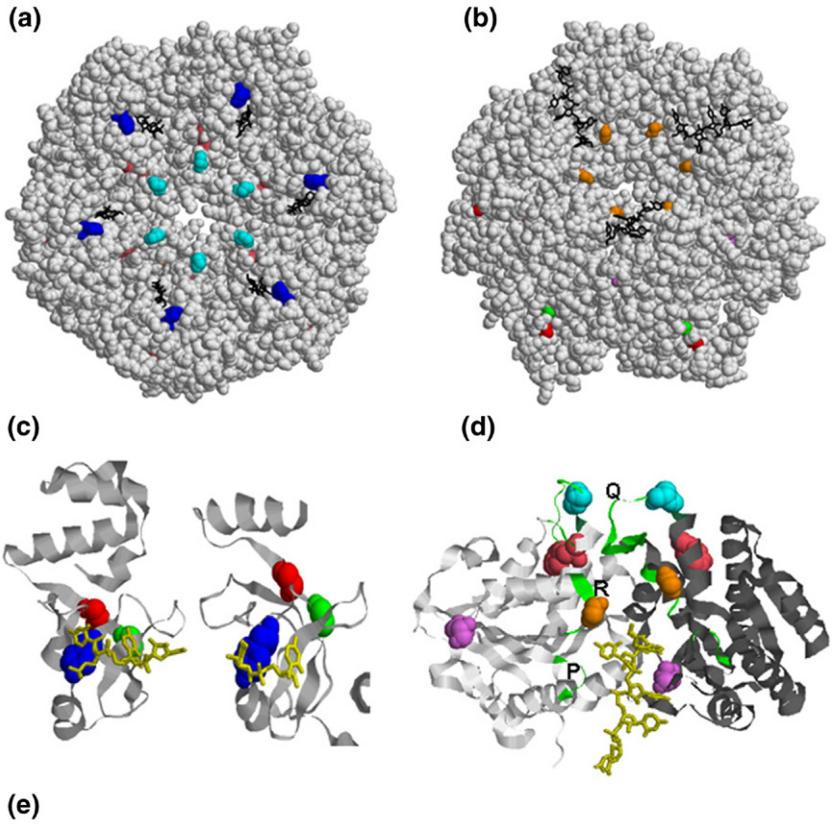

(e)

Mutant Rho	Distance to the 1° RNA binding site (Å)	Distance to the 2° RNA binding site (Å)	Distance to ATP binding site (Å)
G51V	14.3	48.6	38.5
G53V	12.3	41.5	32.0
Y80C	5.3	46.3	39.2
Y274D	17.6	22.2	22.7
P279S	16.2	29.4	32.2
G324D	34.1	4.9*	17.1
N340S	36.0	14.2	19.6

Figure 2. Location of the mutations on the crystal structure of Rho. In (a) and (b) the space-filled model of hexameric closed ring structure of Rho was generated from the available co-ordinates of the dimeric unit of Rho (2HT1[19]) and the Figures were prepared using RASMOL. Positions of the mutations are indicated. The color codes are as follows. G51V, red; G53V, green; Y80C, blue; Y274D, pink; P279S/P279L, cyan; G324D, orange; N340S, violet. The position of I382N is not resolved in this structure. In (a) the view is from primary RNA binding domain and that in (b) is from secondary RNA binding domain. (c) The primary RNA binding domain of Rho generated from the co-ordinates of the structure of N-terminal domain (2A8V[29]; left) and closed ring (2HT1; right) structures. The RNA oligonucleotide is shown in yellow and locations of G51V, G53V and Y80C are also shown as spheres with the same color code as in (a) and (b). (d) The secondary RNA binding domain is shown in the dimeric unit of the closed ring structure with the RNA (in yellow) bound at the interface of the two monomers (chains are shown in grey and black). P, Q and R loops are shown in green and the locations of Y274D, P279S/P279L, G324D and N340S are also indicated as spheres. Color codes for the mutations are same as in (a) and (b). (e) Distances of the positions of different mutations from important functional domains. The distances were calculated using the RASMOL program. For calculating the distances from primary (1°) and secondary (2°) RNA binding domains, the nearest RNA residues were considered and that from the P-loop, Cα atom of residue 184 was considered.

away from the nearest RNA residue in the secondary RNA binding site. In the closed ring structure of Rho, the Q-loop forms a hairpin-like structure from the disordered conformations observed in the open ring structure.[19] This alteration may be important for attaining the active conformation of Rho and the change in the loop conformation due to the mutations will affect its function. On the other hand Y274, which is located just outside this loop, may come on the pathway of the RNA passing through the dimeric interface of two Rho protomers (Figure 2(d)). So Y274D may have similar defects as G324D and N340S changes.

In order to test these predictions of the additional defects of these mutants in different properties of Rho, we assayed their efficiencies for primary and secondary RNA binding as well as for their ATP binding and hydrolysis activities.

Primary RNA-binding properties of the Rho mutants

There are two distinct types of polynucleotide interaction sites in Rho.[10,32] The primary RNA-binding site, located in the N-terminal region, recognizes both single-stranded DNA and RNA, whereas the secondary binding site located at the central hole of the oligomer, binds specifically to the RNA. To investigate whether interactions in these two sites were affected by these mutations, we monitored the interactions specifically at the primary binding site by estimating the dissociation constant (K_d) of each of the mutants for a 34-mer DNA oligonucleotide, $(dC)_{34}$. Occupancy of a DNA oligomer only in the primary RNA binding site of the Rho crystal[15] and protection of primary RNA binding domain by DNA oligomer in the protein

footprinting studies,[10] strongly suggest that DNA can specifically bind to this site and not to the secondary RNA binding site.

The dissociation constants (K_d) for oligo$(dC)_{34}$ of different Rho mutants were measured by both gel retardation and filter binding assays (Table 2, column 2). The K_d value for WT Rho was ~10 nM. None of the mutants were defective for binding to oligo$(dC)_{34}$ except Y80C, which did not show significant binding in both the gel retardation and filter binding assays. In order to check whether this defect is specific for a DNA oligo, we checked the efficiency of binding of a radiolabeled RNA oligo, rC_{10} to Y80C by UV cross-linking. This mutant showed significantly reduced cross-linking efficiency even at 20 μM of rC_{10} and did not show any gel-shift compared to WT Rho (data not shown). The binding defect of this mutation is consistent with the fact that this amino acid directly stacks against the base of the oligonucleotide[29] (Figure 2(c)). Previously reported mutants in this region also exhibited similar defects in primary RNA binding.[33]

G51V and P279S have about a threefold higher affinity for oligo$(dC)_{34}$ compared to WT. Therefore the stability of the oligonucleotide-bound complexes of these two mutants in the presence of both single-stranded DNA and RNA as competitors was tested. Rho complexed with end-labeled oligo$(dC)_{34}$ was challenged with increasing concentrations of either unlabeled oligo$(dC)_{34}$ (Figure 3, upper panel) or H-19B *cro* RNA having a *rut* site (Figure 3, lower panel). It was observed that the G51V–oligo$(dC)_{34}$ complex was significantly resistant to both the competitors compared to either WT or P279S complexes. This unusually stable interaction at the primary RNA binding site, which was not predicted from the crystal structure, could affect the proper release of RNA from the primary RNA binding site of G51V during the translocation process. It should be noted that the position of G51 is about 14 Å away from the nearest RNA residue (Figure 2(e)). Earlier it was reported that a termination defective Rho mutant G99V, in this same domain, also had a tighter (~2.5-fold higher compared to WT Rho) primary RNA binding.[21] Even though the amino acid P279 comes within 16 Å of the RNA in the primary RNA binding site (Figure 2(e)), it is difficult to envision from the available structural data why a mutation in Q-loop will increase the affinity for DNA in the primary RNA binding site. The distortion of the loop conformation due to this mutation might have an allosteric effect in the nearby primary RNA binding domain. In this context it is also to be mentioned that a high affinity primary RNA binding does not lead to a formation of a "super Rho".

Secondary RNA binding

Interaction of RNA in the secondary site is mandatory to activate ATP hydrolysis.[10,32] It has been reported that due to the weak interactions at the secondary RNA binding site, it is difficult to observe the RNA binding at this site by using direct binding assays.[34,35] So we measured the concentrations of poly(C), oligos rC_{10} (10-mer) and rC_{25} (25-mer) required to elicit half-maximal ATPase activities in the presence of excess ATP for estimating the binding efficiency to this site. For the oligos, rC_{10} and rC_{25}, measurements were done in the presence of oligo $(dC)_{34}$ at the primary site, because short RNA oligos ($rC_{5–8}$) can elicit ATPase activity by binding to the secondary site only in the presence of oligo(dC).[14,36]

None of the mutants showed a significant defect in utilizing poly(C) as substrate (Table 2, column 3).

Table 2. *In vitro* primary and secondary RNA binding properties of the Rho mutants

Rho mutants	K_d[a] $(dC)_{34}$ (nM)	[poly(C)] at half-maximal ATPase activity[b] (μM)	ATPase activity on poly(C) RNA[c] (nmol of ATP/min per μg Rho)	[rC_{25}] at half-maximal ATPase activity[d] (μM)	[rC_{10}] at half-maximal ATPase activity[e] (μM)
WT	10±0.9	0.59±0.02	29.1±3.5	0.13±0.01	13.2±2.6
G51V	3±0.3	0.46±0.04	15.5±0.2	15.45±1.75	>200
Y80C	>3000	0.14±0.06	20.4±0.2	>500	>200
Y274D	12±1.4	0.43±0.02	14.1±1.0	>500	>200
P279S	3±0.1	0.78±0.03	33.1±2.3	>500	>200
G324D	10±2	0.72±0.05	19.6±4.0	>500	>200
N340S	11±2	0.51±0.09	23.6±1.4	>500	>200
I382N	12±3	0.30±0.02	20.4±0.05	0.39±0.01	32.3±1.0

[a] K_d values were average of those obtained from gel shift and filter binding assays using end-labeled $(dC)_{34}$. Fractions of bound complexes were plotted against the concentration of Rho and the plot was fitted to a hyperbolic binding isotherm to determine the dissociation constant. Concentration of oligo$(dC)_{34}$ is expressed in terms of DNA ends. For Y80C there was no binding up to 3 μM.

[b] Amount of radiolabeled inorganic phosphate release from [γ-^{32}P]ATP was plotted against the increasing concentration of poly(C). Concentration of poly(C) corresponding to the half-maximal ATPase activity was determined by fitting the plot to a sigmoidal curve. The concentration range of poly(C) was 0 to 5 μM, in terms of the nucleotides. The concentration of ATP was 500 μM. Poly(C) will bind both to the primary and secondary RNA binding sites. However, the measurements are based on the activities solely in the secondary RNA binding site, so the values obtained by this method will reflect binding defects, if any, in the secondary site.

[c] The initial rate of ATP hydrolysis in the presence of poly(C) as cofactor was determined by fitting the plot of the amount of unhydrolyzed ATP against time to the equation $y = y_o \exp(-\lambda t)$, where λ is the rate constant. The time-points in the linear region (up to 5 min) were considered for the calculations. Concentrations of ATP and poly(C) were 1 mM and 20 μM, respectively.

[d] Except for WT, G51V and I382N, a significant amount of ATPase activity was not observed up to 500 μM rC_{25}. Concentration of rC_{25} is expressed in terms of RNA ends. The concentration of ATP was 1 mM.

[e] Except for WT and I382N, a significant amount of ATPase activity was not observed up to 200 μM rC_{10}. Concentration of rC_{10} is expressed in terms of RNA ends. The concentration of ATP was 1 mM.

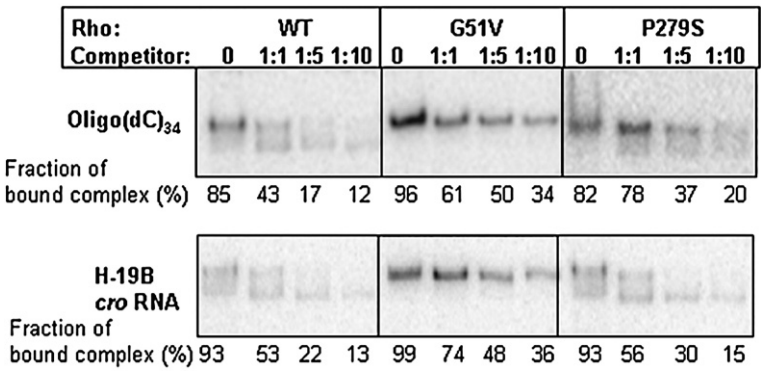

Figure 3. Stability of Rho–oligo $(dC)_{34}$ complexes. Autoradiograms of native PAGE showing the amount of labeled oligo$(dC)_{34}$ complexed with WT and different mutant Rho proteins survived in the presence of increasing concentrations of competitors: upper panel, unlabeled oligo $(dC)_{34}$; lower panel, H-19B *cro* RNA. The fraction of bound complex was calculated as: [bound oligo]/[free oligo+bound oligo]. The 5 nM labeled oligo$(dC)_{34}$ was used to form complex with 50 nM of WT and mutant Rho proteins.

Only P279S and G324D showed slightly less affinity compared to others. This was further supported by the fact that the rates of ATP hydrolysis with poly(C) were also not significantly different for the mutants (Table 2, column 4). It was observed that a strong substrate like poly(C) can mask the defects in secondary site binding,[12,37] so we used two shorter RNA oligos, rC_{10} and rC_{25}, to assess the binding defects in the secondary site. All the mutants, except I382N, failed to show significant amounts of ATP hydrolysis even at a very high concentration of the oligo, rC_{10} (Table 2, column 6). Even with the longer oligo rC_{25}, the affinity for G51V was only increased, but still it showed ~100-fold weaker affinity compared to WT (Table 2, column 5). In general, we concluded that except I382N, all the mutants were defective in secondary RNA binding or they had an extremely slow rate of ATP hydrolysis. This defect should have contributed significantly in their inability to terminate.

Most likely, the defect in binding of oligo $(dC)_{34}$ to the primary site of the Y80C mutant did not stimulate the ATPase activity with the shorter oligos at the secondary site. In case of G51V, the unusual mode of binding of $(dC)_{34}$ in the primary site, might have failed to elicit the allosteric effect in the secondary site. Earlier, the reported tight binding mutant, G99V, also had a similar defect in binding to oligo rC_{10}.[21] Defects of G324D and N340S for secondary RNA binding were predictable from their locations close to this site. Although according to the crystal structure[19] (Figure 2(e)), amino acids Y274 and P279 are more than 20 Å away from the closest RNA residue in the secondary site, these data and the previously obtained protein footprinting results with Q-loop mutants[12] strongly suggest that this region of Rho also takes part in interactions with the RNA in the secondary site.

ATP binding

We measured the apparent dissociation constant ($K_{d,app}$) of ATP for WT and mutant Rho proteins in the absence of the RNA cofactor by using the UV-cross-linking technique. The apparent affinity of ATP for mutants Y274D, P279S and G324D was observed to be reduced by five-to eightfold, whereas it was comparable to WT for mutants N340S, G51V and I382N (Table 3). Mutations in R and Q-loops might have allosteric effects on the proximal P-loop, the ATP binding site. Cross-talk between the R-loop and P-loop has also been proposed from the closed ring crystal structure of Rho.[19] There was no significant cross-linking of ATP for the Y80C mutant.

Cross-linking efficiency of the radiolabeled ATP varied among different mutants to the extent that it was negligible for Y80C. Absence of cross-linking means that either the binding affinity for ATP is very poor or some unusual conformational changes due to the mutation has impaired the chemistry of cross-linking. As Y80C can hydrolyze ATP in the presence of poly(C) (Table 2) the mutant must have the ability to bind ATP. Therefore, we measured the K_m value of ATP for this mutant using poly(C) as cofactor and compared with the WT Rho (Table 3, data in parentheses). Y80C, indeed showed about fourfold increase in K_m value, which indicated that the binding of ATP has been affected due to this mutation. It is of interest to note that a mutation in the primary RNA binding domain can affect the

Table 3. ATP binding of the Rho mutants

Rho mutants	$K_{d,\ app}$ (μM)
WT	0.54±0.06 (11.7±2.2)
G51V	1.35±0.26
Y80C	No cross-linking (43.2±0.8)
Y274D	3.15±0.26
P279S	4.28±0.54
G324D	2.45±0.15
N340S	1.09±0.12
I382N	0.60±0.1

Apparent dissociation constant ($K_{d,app}$) of ATP was determined by UV-cross-linking. The intensities of the cross-linked species were plotted against increasing concentrations of [γ-^{32}P]ATP and K_d values were obtained from the hyperbolic fitting of the plots. For Y80C, no cross-linking was observed up to 30 μM [γ-^{32}P]ATP. K_m values of ATP for WT and Y80C are shown in parenthesis. The concentration of WT and mutant Rho was 50 nM in hexamer.

conformations in the ATP binding domain which is located ~40 Å away (Figure 2(e)).

Y80C change in the N-terminal causes conformational changes in the distal C-terminal domain

Besides impairing the primary RNA binding, the Y80C mutation also caused significant defect in ATP binding. This led us to hypothesize that this change may cause conformational changes in the distal (~40 Å) C-terminal domain allosterically. To test this hypothesis, we probed the conformations of WT and mutant Rho by limited proteolytic cleavages, fluorescence anisotropy and fluorescence quenching.

We monitored the surface accessibility of the single tryptophan residue (W381), located ~15 Å away from the ATP-binding site, by the fluorescence quenching technique using acrylamide as a neutral quencher.[38] This tryptophan residue emits a fluorescence signal at 350 nm upon excitation at 295 nm. Quenching of this signal was plotted against the

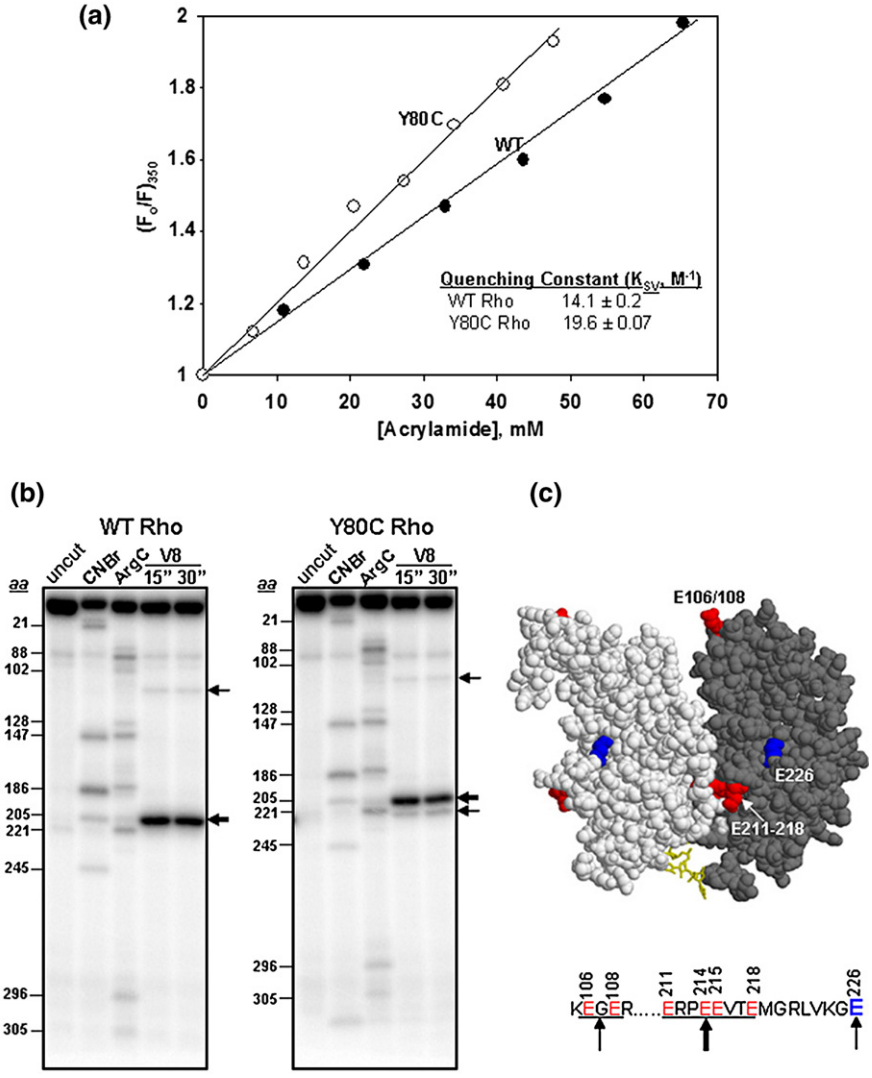

Figure 4. Conformational changes in the C-terminal domain of the Y80C mutant. (a) Stern–Volmer plots for acrylamide quenching of tryptophan fluorescence of WT and Y80C Rho proteins. The quenching constant (K_{SV}) was calculated from these plots using the equation: $(F_0/F)_{350} = 1 + K_{SV}[Q]$, where Q is the concentration of the quencher, acrylamide. (b) Limited proteolysis of end-labeled WT and Y80C Rho proteins with V8 protease. Glutamic acid residues corresponding to the major cleavage products are indicated by arrows. Thickness of the arrow corresponds to the intensity of the bands. These positions were identified from the calibration curve obtained from the molecular weight markers generated with CNBr and ArgC digestions of the same end-labeled Rho. The amino acid positions from N to C-terminal are indicated to the left of the gel pictures. The thick arrow corresponds to the sensitivity towards the glutamic acids residues between 211 and 218. Individual amino acids are not resolved. Position of 106/108 and 226 are also indicated by thin arrows. (c) Locations of the V8 sensitive residues are indicated on the dimeric unit of the closed ring structure of Rho. The red spheres are the V8 sensitive patch comprising of glutamic acid residues at 211, 214, 215 and 218. Also E106/108 is also indicated as red spheres in the N-terminal domain. E226, which specifically became sensitive in the Y80C Rho is shown as a blue sphere.

increasing concentration of acrylamide to obtain the quenching constant (K_{sv}) (Figure 4(a)). The value of K_{sv} increases as the tryptophan becomes more surface accessible. We observed that this tryptophan in the Y80C mutant is more surface accessible compared to the WT.

We used a fluorescent analogue of GTP, Tb-GTP, which is a complex of terbium chloride and GTP,[39,40] to see the local conformational flexibilities at the ATP binding pocket. Here we assumed Tb-GTP will bind to the same ATP binding site as GTP is also a good substrate of Rho.[41,42] We measured the anisotropy (r) of the Tb-GTP moiety upon binding to the ATP binding pocket. The anisotropy (r) of a fluorophore gives the measure of the rotational freedom of the species and reports the conformational flexibility of the surroundings.[39] A higher value of r means less rotational freedom of the fluorescent probe. A lower value of r for Tb-GTP bound to Y80C compared to that obtained for WT Rho (Table 4) suggested more conformational disorders in the ATP-binding pocket.

In general, quenching constant and anisotropy values did not change drastically because of the Y80C mutation, which suggests that the conformational changes induced by the mutation in the C-terminal domain are more subtle. To further corroborate these data, we employed limited proteolytic digestions of the WT and Y80C Rho proteins to probe the conformational changes with V8 protease, which cleaves preferably at glutamic acid residues. We observed that a cluster of surface exposed glutamic acid residues (Figure 4(b)) near the dimeric interface of the C-terminal domain (Figure 4(c)) of both the WT and Y80C mutants were very sensitive to this protease. Interestingly, a new band corresponding to Glu226, close to this cluster (Figure 4(c) and (d)), was found to become sensitive to V8 digestion, specifically in the Y80C mutant. This observation further supports the proposal that the Y80C mutation in the primary RNA binding domain induces distinct but subtle conformational changes in the distal C-terminal domain, which might have affected the ATP binding domain and the surrounding regions.

RNA-release efficiency of the Rho mutants from stalled elongation complex

The majority of the Rho mutants are defective in secondary RNA binding, which might have affected the processivity during translocation along the nascent RNA and reduced the speed of translocation. We hypothesized that if their termination defect is due to slow translocation only, these mutants may be able to release RNA from the stalled ECs if sufficient time is allowed. So we stalled the EC on an immobilized template at a particular position within the *trp t′* terminator region (Figure 5(a)) using the lac repressor as a roadblock.[43] The stalled elongation complex remains transcriptionally active and can restart transcription efficiently from this position upon removal of the lac repressor[43] (data not shown). Under this condition the mutant Rho proteins will eventually be able to "catch up" the stalled EC if sufficient time is allowed and release the RNA. Also in the stalled EC set-up, one can monitor only the Rho-dependent RNA release uncoupled from the transcription elongation process and therefore the role of ATP and/or NusG on the different steps of the RNA release can be studied (see Figure 6).

To the stalled EC, WT or different mutant Rho proteins were added and the released RNA in the supernatant was monitored in the presence and absence of NusG. Under this experimental condition, WT Rho released ~70 to 80% of the RNA from the stalled EC. Considering the non-specific rebinding of the released RNA to the beads, these values suggest an efficient release of RNA from the stalled EC by Rho. In the absence of NusG, all the mutants except I382N were still defective in releasing RNA even from a stalled EC. However, in the presence of NusG, a partial restoration in RNA release efficiency was observed for Y274D, G324D and N340S (Figure 5(b) and (c)), which is similar to that observed in continuous transcription assays (Figure 1(b), presence of NusG). This partial restoration of the RNA release efficiency from the stalled EC in the presence of NusG suggests that Y274D, G324D and N340S, unlike WT Rho, are very much dependent on NusG for interaction with the EC and possibly they are defective in the step(s) involving the release of RNA from the EC.

Table 4. Fluorescence anisotropy (r) values of Tb-GTP

Species	Anisotropy (r)
Free Tb-GTP [150 μM: 50 μM]	0.096±.005
Tb-GTP+ 100 nM WT Rho	0.246±.007
Tb-GTP+ 150 nM Y80C Rho	0.183±.003

In all the experiments, Tb-GTP complexes were made by incubating 150 μM Tb with 50 μM GTP. The majority of the Tb-GTP species were in bound form in the presence of the indicated amount of hexameric Rho. Anisotropies were measured at 25 °C.

High concentration of ATP and the presence of NusG restore the RNA release activity of the mutants Y274D, G324D and N340S

In order to further identify the kinetic step(s) defective for these Rho mutants we followed the time-course of RNA release from the stalled EC in the presence of different concentrations of ATP. We varied the concentrations of ATP to change the translocation rate. We preformed stalled EC, immobilized on magnetic beads, removed all the NTPs by extensive washing and WT or different mutant Rho proteins were added in the presence of 0.02 mM, 0.1 mM (data not shown) and 1 mM ATP. The time-course of RNA release in the supernatant was followed for 30 min, both in the absence (Figure 6(a), (c) and (d)) and presence of NusG (Figure 6(b), (e) and (f)). The rate (slope of the curve) and the efficiency (maximum amount of released RNA) of

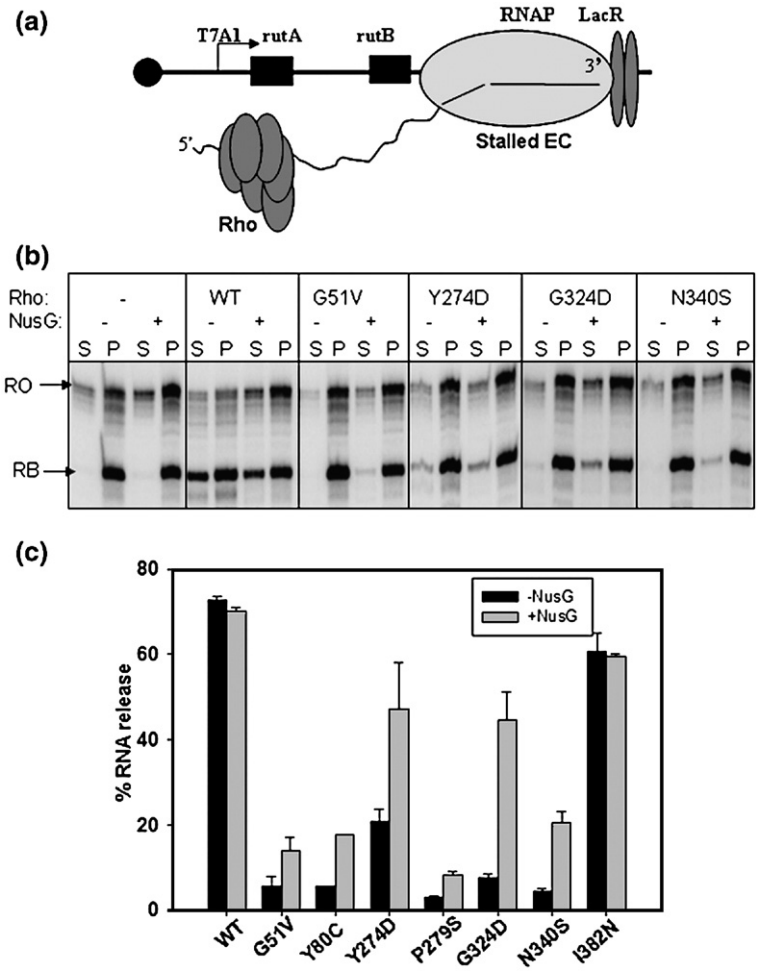

Figure 5. Rho-mediated RNA release from the stalled elongation complex. (a) Cartoon showing the design of a stalled elongation complex using lac repressor as a roadblock. In this set-up, the EC was stalled at 161 position of the *trp t'* terminator. Rho was added to the reaction after the stalled complex is formed and RNA release was measured from the supernatant. (b) Autoradiogram showing the amount of released RNA in the supernatant by WT and different Rho mutants both in the absence and presence of 200 nM NusG from the stalled EC. RB and RO denote the positions of roadblocked product and run-off product, respectively. The meaning of S and P is same as described for Figure 1. (c) The RNA release efficiencies shown by bar diagrams are calculated as: [2S]/[S+P].

RNA release remained the same for WT Rho at all the concentrations of ATP tested. A modest increment of rate but not the efficiency of RNA release was observed in the presence of NusG. RNA release efficiency by the P279S mutant did not improve significantly, even at 1 mM ATP and in the presence of NusG. Under the same conditions, a modest improvement in the RNA release efficiency was observed for G51V and Y80C mutants, but it never reached to the level of WT Rho. For Y274D, G324D and N340S, the efficiency of RNA release improved significantly when 1 mM ATP was present and NusG was absent. For these mutants, both the efficiency and rate of RNA release was observed to regain the WT Rho level in the presence of both 1 mM ATP and NusG.

Higher concentrations of ATP might have increased the rate of ATP hydrolysis and as well as improved the processivity of Y274D, G324D and N340S Rho mutants, which in turn increased the overall rate of translocation. This has enhanced the chances of the Rho mutants to be in the vicinity of the stalled EC. These mutants may also have defects in the RNA release step, which most likely requires a direct interaction with the EC. The presence of NusG helped them to overcome this defect, which is reflected in the faster RNA release (Figure 6(f)).

Discussion

Here we report the isolation and characterization of the termination defective mutants of Rho from a random mutagenesis screen and attempt to find the involvement and importance of different functions of Rho in releasing RNA from the EC in light of the recent crystal structure of Rho.[19] Different properties of the mutants are summarized in Table 5. All the termination defective mutants (except I382N) were found to be located in the previously identified functional domains, such as in the primary RNA binding domain and in the secondary RNA binding domain including Q-loop and R-loops. The termination defect of the mutants G51V, Y80C and P279S could not be overcome under the most relaxed conditions that have been tested, suggesting that the primary RNA binding domain and Q-loop are the most crucial elements for RNA release activity. These mutants are also defective for most of the other functions of Rho. The termination defects of the mutants (Y274D, G324D and N340S), which are mainly defective for secondary RNA binding and most likely for the translocase activity, could be restored under relaxed *in vitro* conditions. The functional defects of most of the mutants correlate with their

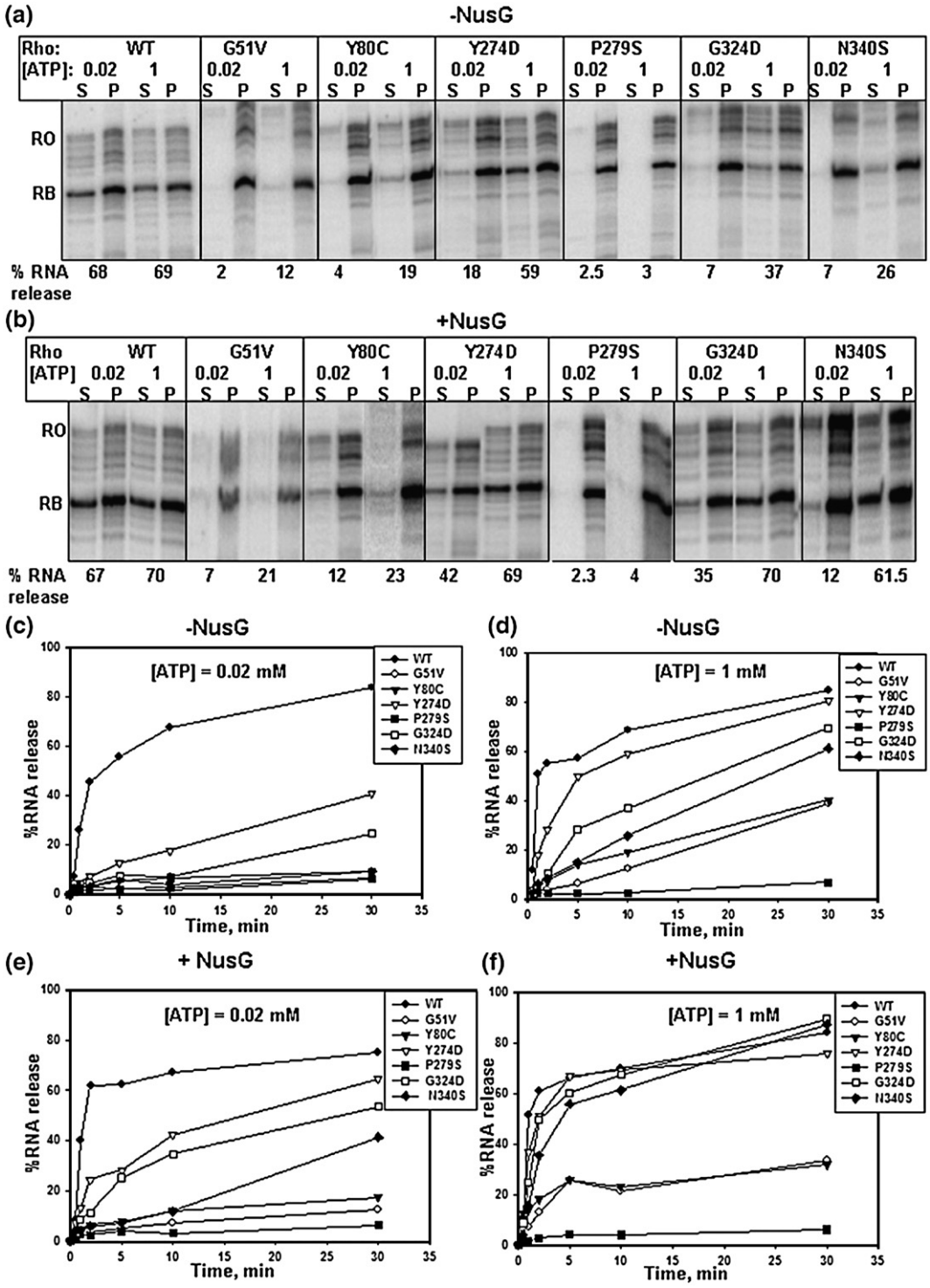

Figure 6. ATP and NusG dependence of Rho-mediated RNA release from a stalled elongation complex. Autoradiograms of the RNA release after 10 min of addition of different Rho mutants from the stalled EC (described in Figure 5) in the presence of different concentrations of ATP, both in the absence (a) and presence (b) of 200 nM NusG. (c)–(f) Curves showing the time courses of the RNA release upon addition of WT and different Rho mutants in the presence of indicated concentrations of ATP. The presence or absence of NusG in the reactions is also indicated. The RNA release efficiencies are calculated in the same way as described in Figure 5.

spatial localization in the crystal structure. We also show that mutations in the primary RNA binding domain (Y80C) can affect functions and induce conformational changes in the distal C-terminal domain, which is not predictable from the structure of Rho. We did not observe any severe *in vitro* defect in I382N, which is not consistent with its *in vivo* phenotype. Probably a modest *in vitro* defect can be amplified under more stringent *in vivo* conditions.

Table 5. Summary of different properties of the termination-defective Rho mutants

Mutants	1° RNA binding	2° RNA[a] binding	ATP binding	Suppression of termination defect[b]
G51V	++	+/−	++	No
Y80C	−	−	+[c]	No
Y274D	+	−	+	Yes
P279S	++	−	+	No
G324D	+	−	+	Yes
N340S	+	−	++	Yes
I382N	+	+	+++	Not defective *in vitro*
WT	+	++	+++	Not defective

All the activities of the mutants are expressed with respect to that of WT Rho.

[a] Binding activities are for rC_{10} and rC_{25} templates. +/− indicates ~100 fold reduced binding on rC_{25} template.

[b] For the mutants Y274D, G324D and N340S the RNA release efficiency from the stalled EC improves to the level of WT in the presence of 1 mM ATP and NusG.

[c] For ATP binding of Y80C the K_m value is considered.

Importance of the polynucleotide interactions in the primary RNA binding domain of Rho in modulating other activities of Rho, apart from recognizing the *rut* site, had been envisioned earlier.[21,33] Here we found that a specific mutation in position Y80, which directly interacts with the RNA at the primary site, intrinsically makes Rho defective for ATP binding (Table 3), induces conformational changes in the ATP-binding pocket (Figure 4(a) and Table 4) and in the surrounding C-terminal domain (Figure 4(b)). As the defect in ATP binding and other conformational changes occurred in the absence of RNA binding we propose that this mutation by itself has induced a major allosteric effect in the C-terminal domain, which is located far away from primary RNA binding domain. On the other hand, mutation at G51, located in the same primary RNA binding domain, renders very stable binding with the nucleic acids (Table 2 and Figure 3). This leads to severe defects in the RNA release and secondary RNA binding. This suggests that it is important that Rho leaves the *rut* site once it starts tracking the nascent RNA. Based on the properties of these two point mutations in the primary RNA binding domain we propose that this domain of Rho not only works as an "eye" to find the *rut* site but also exerts allosteric control over the downstream interactions upon binding to RNA. Therefore, mutations in this domain block the subsequent steps in the process of RNA release. We have recently found that Psu, an inhibitor of Rho, which inhibits Rho-dependent termination by slowing down the rate of ATP hydrolysis, does not interact with the Y80C mutant.[44] This lack of interaction between the Psu and Y80C mutant might also arise due to conformational changes in the ATP binding/hydrolysis domain.

What is the role of Q-loop? The Q-loop is a structural element, which is located at the entry point of secondary RNA binding domain and protrudes into the central hole of the Rho hexamer. A comparison of the open and closed ring structures of Rho reveals that this loop undergoes major conformational changes upon ring closure[19] and was found to be protected in the Rho–poly(C) complex from the hydroxyl radical cleavage.[10] P279S and earlier reported mutants in this loop[12] are defective in secondary RNA binding and in subsequent activities like ATP hydrolysis and translocation. Based on these results and the spatial location of this loop in the Rho hexamer (Figure 4(c)), we propose that this structural element works as a rudder that guides the RNA into the dimeric interface of the secondary RNA binding domain. This proposal is consistent with the "RNA handoff model", where the Q-loop is proposed to be involved in transferring RNA between the subunits during translocation.[19]

It is known from the previous works that ATPase or NTPase activity of Rho is required for transcription termination[45,46] and is believed that the free energy generated from the hydrolysis is required for the translocation of Rho along the RNA.[47,48] Using a roadblocked EC we have uncoupled the transcription elongation from the Rho-dependent RNA release from the EC, which enabled us for the first time to observe a direct correlation between ATP hydrolysis and RNA release by Rho from a stalled EC. The RNA release efficiency and the rate of RNA release improved at high concentration of ATP for the three mutants (Y274D, G324D and N340S) in the secondary RNA binding domain (Figure 6). These results suggest that a higher rate of ATP hydrolysis improved their processivity and overall rate of translocation and the free energy from the ATP hydrolysis is used to bring them in the vicinity of the EC. It is likely that the ATP hydrolysis helps Rho to remain bound to the nascent RNA during the "chase", because intrinsically the interactions in the secondary RNA binding domain are weak.

On the other hand, RNA release kinetics experiments (Figure 6) suggest that NusG is involved only in the RNA release step(s) once Rho reaches the vicinity of the EC, which is consistent with role of NusG that was proposed earlier.[49] WT Rho on its own is capable of releasing RNA, but the speed of RNA release is increased in the presence of NusG. Early termination that is usually observed in the presence of NusG (Figure 1(a)) is the consequence of this enhanced rate of RNA release. So the requirement of NusG becomes mandatory under *in vivo* conditions where the RNA release has to be performed within a small time window. The RNA release step, in addition to their translocation defect, must be severely compromised in case of the mutants Y274D, G324D and N340S and therefore they are highly dependent on NusG. The final RNA release step may involve a direct interaction of Rho with the EC, so it is possible that the region of Rho defined by these amino acids is involved in the interaction with the EC.

Based on the properties of different termination defective mutants of Rho and in the light of open and closed ring hexameric structures complexed with nucleic acids in primary and secondary RNA

binding domains we sum-up the sequential steps that lead to the RNA release from the EC. (1) The primary RNA binding domain binds RNA and forms an open ring hexameric Rho. This interaction also involves conformational changes in the C-terminal domain. (2) RNA gets channeled into the secondary RNA binding domain *via* the Q-loop and the closed ring structure is formed. (3) This activates ATP hydrolysis and onsets the translocation of Rho along the mRNA, which brings Rho in the vicinity of the EC. (4) Rho then releases RNA possibly by pushing the EC or by pulling the RNA out of the EC by its translocase activity. It is also possible that Rho specifically interacts in the RNA exit channel and exerts allosteric effects on the stability of the EC. As NusG is only involved in increasing the rate of RNA release at this step, it is possible that NusG in the presence of Rho makes the EC more prone to termination.

How important is Rho-dependent termination *in vivo*? All the termination defective mutants of Rho that we have isolated are viable. Among them, Y80C is defective for most of the functions of Rho. Surprisingly, these apparent severe defects did not cause lethality to the cells. This raises the question, that how important is the process of Rho-dependent termination when the cells are growing exponentially and why Rho is essential to *E. coli*. We speculate that due to the multi-functional nature of Rho, it may very well have other essential function(s), which is more important than transcription termination.

Materials and Methods

Biochemicals and enzymes

NTPs, poly(C), [γ-^{32}P]ATP (6000 Ci/mmol, 3000 Ci/mmol and 30 Ci/mmol) and [α-^{32}P]CTP (3000 Ci/mmol) were purchased from Amersham. Antibiotics, IPTG, lysozyme, DTT and BSA were from USB. Primers for PCR, oligo(dC)$_{34}$, rC$_{10}$, rC$_{25}$, galactose, Protein kinase A, acrylamide and $TbCl_3$ were obtained from Sigma. Restriction endonucleases, polynucleotide kinase and T4 DNA ligase were from New England Biolabs. WT *E. coli* RNA polymerase holoenzyme was purchased from Epicenter Biotechnologies. *Taq* DNA polymerase was from Roche. *Staphyloccocal aureus* V8 protease and Submaxillary protease (Arg-C) were from Pierce. CNBr was obtained from Fluka.

Strain construction

Bacterial strains, plasmids and phages used in this study are listed in Table 6. *trpE9851*(Oc)[50] was moved by P1 transduction from GJ3183 into GJ3192 and designated as RS336. The P$_{lac}$-H-19B *nutR/T$_{R1}$-lacZYA* cassette obtained from pK8628[22] was inserted as single copy at the phage λ attachment site of strain RS336, resulting in strain RS364. Similarly, single copy fusion without H-19B T$_{R1}$ rho-dependent terminator (P$_{lac}$-*lacZAY* from pRS431) was constructed and designated as RS391. *rpoB8*[25] and *rpoB2*[25] genes were also moved into GJ3192 and named as RS446 and RS451, respectively. P$_{lac}$-H-19B *nutR/T$_{R1}$-lacZYA* and P$_{lac}$-*lacZAY* were inserted into RS446 in single copy resulting in the strains RS449 and RS450, respectively. Strain RS445 was constructed by single copy insertion of P$_{lac}$-*lacZAY* in GJ3161.

Random mutagenesis and screening of Rho mutants

The plasmid pHYD567 with the WT *rho* gene was transformed into XL1-Red mutator strain (Stratagene). The mutagenized plasmid library was isolated and electroporated into the background strain RS336 with a chromosomal deletion in the *rho* gene. In this strain, Rho is supplied from a shelter plasmid carrying WT *rho* gene, which has an IPTG dependent conditional replicon (pHYD1201).

The transformants were plated on MacConkey agar plates supplemented with 1% (w/v) galactose and appropriate antibiotics. The strain was propagated in the absence of IPTG to remove the shelter plasmid so that the sole supply of Rho will be from the mutagenized plasmid library. The *galEP3* mutation in the strain confers Rho-dependent transcriptional polarity on the downstream genes, so that the cell is unable to utilize galactose to satisfy its auxotrophy in the presence of a functional Rho.[51] Rho mutants can release polarity in such a strain and can make the strain able to utilize galactose. *gal*$^+$ transformants were picked, purified three times by streaking in the same medium.

Mutant strains were streaked on a minimal anthranilate plate to confirm the mutations. The *trpE9851*(Oc) mutation confers Rho-dependent transcriptional polarity on the downstream *trpCDBA* genes, so that the cell is unable to utilize anthranilate in the presence of functional Rho. The strain with WT Rho is incapable of growing on a minimal anthranilate plate while Rho mutant strains can overcome the polarity of the *trpE9851*(Oc) mutation. The putative Rho mutant plasmids were isolated and re-transformed into the background strain for ensuring the mutant phenotypes. The full-length *rho* gene was sequenced from each of these plasmids to identify the mutation and to ensure that no other mutations were present in the gene.

Measurement of *in vivo* termination

The strains RS364 and RS391 were transformed with the mutants and WT Rho plasmids to estimate the *in vivo* termination efficiency at the H-19B T_{R1} rho-dependent terminator. Similarly RS449 and RS450 were transformed with the mutants and WT Rho plasmids to get the activities with B8 RNAP. The strains GJ3073 and RS445 were used to get the β-galactosidase activities in the presence of WT Rho. The measurements of β-galactosidase activities were done in a microtiter plate using a Spectramax plus plate reader following the published procedure.[52]

Cloning and purification of wild-type and mutants of Rho, NusG and B8 RNA polymerase

The WT and mutant *rho* genes were PCR amplified using proof-reading DNA polymerase from pHYD567 and its derivatives (Table 6) and were cloned into the XhoI/NdeI site of pET21b to introduce a His-tag at the C-terminal end. All the mutant (except I382N) plasmids were then transformed into the BL21(DE3) over expressing strain. I382N was over expressed in salt-inducible strain BL21SI (Invitrogen). After induction, His-tagged

Table 6. Bacterial strains, plasmids and phages used in this study

Strain/plasmid/phage	Description	Source or reference
A. *Strains*		
GJ3192	MC4100 *galEp3* Δ*rho*::Kan^R with pHYD1201, Amp^R	56
GJ3183	MC4100 *galEp3 trpE9851(Oc) zci-506::Tn10 nus*G-G146D *rho*-R221C	56
RS336	GJ3192, *trpE9851(Oc)* Tet^R	This study
RS364	RS336, λRS45 lysogen carrying P_{lac} – H-19B *nutR-*T_{R1}*-lacZYA*	This study
RS391	RS336, λRS88 lysogen carrying P_{lac} –*lacZYA*	This study
GJ3073	MC4100 *galEp3,* λRS45 lysogen carrying P_{lac} – H-19B *nutR-*T_{R1}*-lacZYA*	Dr J. Gowrishankar
GJ3161	MC4100 *galEp3*	56
RS445	GJ3161, λRS88 lysogen carrying P_{lac} –*lacZYA*	This study
RpoB8	MG1655, *rpoB8* Tet^R Rif^R	25
RS446	GJ3192, *rpoB8* Tet^R Rif^R	This study
RS449	RS 446, λRS45 lysogen carrying P_{lac} – H-19B *nutR-*T_{R1}*-lacZYA*	This study
RS450	RS 446, λRS88 lysogen carrying P_{lac} –*lacZYA*	This study
RpoB2	MG1655, *rpoB2* Tet^R Rif^R	25
RS451	GJ3192, *rpoB2* Tet^R Rif^R	This study
B. *Plasmids*		
pHYD567	3.3 kb NsiI fragment carrying *rho*$^+$ cloned from λ phage 556 of Kohara library into PstI site of pCL1920 (pSC101; Sp^R, Sm^R)	56
pHYD1201	3.3 kb HindIII-SalI fragment carrying *rho*$^+$ sub-cloned from pHYD567 into HindIII-SalI sites of pAM34 (pMB1; IPTG dependent replicon, Amp^R)	56
pRS342	pHYD567-*rho* G51V, Sp^R, Sm^R	This study
pRS387	pHYD567-*rho* G53V, Sp^R, Sm^R	This study
pRS350	pHYD567-*rho* Y80C, Sp^R, Sm^R	This study
pRS397	pHYD567-*rho* Y274D, Sp^R, Sm^R	This study
pRS341	pHYD567-*rho* P279S, Sp^R, Sm^R	This study
pRS347	pHYD567-*rho* P279L, Sp^R, Sm^R	This study
pRS344	pHYD567-*rho* G324D, Sp^R, Sm^R	This study
pRS346	pHYD567-*rho* N340S, Sp^R, Sm^R	This study
pRS399	pHYD567-*rho* I382N, Sp^R, Sm^R	This study
pK8628	pTL61T with P_{lac} – H-19B *nutR(*T_{R1}*)-lacZAY* fusion, Amp^R	22
pRS431	pTL61T with P_{lac} – *lacZAY* by deletion of H-19B *nutR-*T_{R1}between HindIII and BamHI from PK8628, Amp^R	This study
pRS106	pT7A1 cloned at EcoRI/HindIII sites upstream of *trpt* cloned at HindIII/BamHI sites of pK8641, Amp^R	44
pRS96	WT *rho* cloned at NdeI/XhoI site of pET21b, His-tag at C-terminal, Amp^R	This study
pRS378	*rho* G51V cloned at NdeI/XhoI site of pET21b, His-tag at C-terminal, Amp^R	This study
pRS381	*rho* Y80C cloned at NdeI/XhoI site of pET21b, His-tag at C-terminal, Amp^R	This study
pRS433	*rho* Y274D cloned at NdeI/XhoI site of pET21b, His-tag at C-terminal, Amp^R	This study
pRS377	*rho* P279S cloned at NdeI/XhoI site of pET21b, His-tag at C-terminal, Amp^R	This study
pRS379	*rho* G324D cloned at NdeI/XhoI site of pET21b, His-tag at C-terminal, Amp^R	This study
pRS380	*rho* N340S cloned at NdeI/XhoI site of pET21b, His-tag at C-terminal, Amp^R	This study
pRS432	*rho* I382N cloned at NdeI/XhoI site of pET21b, His-tag at C-terminal, Amp^R	This study
pRS119	WT *nusG* cloned at NdeI/XhoI site of pET21b, His-tag at C-terminal, Amp^R	53
pRS236	*lacI* cloned at NdeI/XhoI site of pET21b, Amp^R	This study
pRS338	WT *rho* cloned at NdeI/XhoI site of pET21b, HMK tag and His-tag at C-terminal, Amp^R	This study
pRS602	*rho* Y80C cloned at NdeI/XhoI site of pET21b, HMK tag and His-tag at C-terminal, Amp^R	This study
C. *Phages*		
λRS45		Dr J. Gowrishankar
λRS88		Dr Robert Weisberg

WT and mutant Rho proteins were purified using Ni-NTA beads (Qiagen) as per the manufacturer's protocol. The proteins were eluted in the presence of 500 mM immidazole and further purified by passing through a heparin-Sepharose column (Amersham). The expression levels for all the mutants, except Y80C, were high and the majority of the proteins were present in the soluble fraction. As the expression level of Y80C was low, to avoid the contamination from the WT Rho expressed from chromosome, the purification was done in the presence of 1 M NaCl. For all the mutants the contamination from WT Rho protomers was also checked by passing the mutant Rho proteins through Ni-NTA columns in the presence of 1 M NaCl. Due to the dissociation of the subunits at high salt, non-His tagged WT protomers, if present, would be eluted in the wash-fractions only. We estimated that the contamination from the WT protomer was less than 5% for all the mutants. In all experiments concentrations of Rho is expressed in terms of hexamer. Cloning and purification of NusG has been described.[53] B8 RNAP was purified according to the published protocol.[54]

Solubility of mutant Rho proteins was reasonably good and we did not observe any aggregation over the period of performing the experiments. Chemical cross-linking showed that like WT Rho,[55] all the mutant Rho proteins remained as hexamer above the concentration of 1 μM (data not shown). CD spectra of the different mutants were similar to that of the WT Rho, indicating that the overall structural integrity of the mutants was maintained during the course of the experiments (data not shown).

The composition of the different secondary structural elements for WT and mutant Rho proteins are as follows. α–Helix, 24–27%; β–sheet, 24–32%; turn, 13–17%; random coil, 28–32%. So the differential activities and loss of specific functions of the mutants in various assays were not due to instability of the mutants or presence of inactive fractions in the preparations.

Gel retardation and filter retention assays

RNA binding to the primary RNA-binding site of the WT and mutant Rho proteins was measured by gel-retardation and filter retention assays using an end-labeled 34-mer oligo(dC). 10 nM of labeled oligo was used for the binding assays in the transcription buffer (25 mM Tris–HCl (pH 8.0), 5 mM $MgCl_2$, 50 mM KCl, 1 mM DTT and 0.1 mg/ml of BSA) with the increasing concentrations of the WT or the mutant Rho (0.1 nM to 300 nM). The reactions were performed at 37 °C for 5 min before loading onto a 5% (w/v) native acrylamide gel. Fraction of bound species was quantified by Image Quant software of the phosphor-imager Typhoon 9200. Gel-shift assays with labeled rC_{10} were also done in the same way. For the filter retention assays, 5 μl of reaction mixtures (as above) were spotted onto a nitrocellulose membrane in duplicate and kept in a dot-blot apparatus (Bio-Rad). Each spot was washed with 500 μl of transcription buffer under vacuum. The fraction of bound $oligo(dC)_{34}$ was estimated from the ratio of the intensity of the washed (retained) and unwashed (total) spots using Image-Quant software. The dissociation constant values were calculated by hyperbolic fitting of the binding isotherms. For the competition assays, 10 nM $oligo(dC)_{34}$ was allowed to bind to 50 nM of WT or mutant Rho proteins for 5 min at 37 °C followed by adding 10 nM (1:1), 50 nM (1:5) and 100 nM (1:10) of either cold $oligo(dC)_{34}$ or H-19B *cro* RNA and incubating the reaction for further 5 min at 37 °C. The amount of bound fraction that survived the competitor was estimated from the band intensities.

ATPase assays

ATPase activity of the WT and mutant Rho proteins was measured from the release of inorganic phosphate (Pi) from ATP after separating on the polyethyleneimine TLC sheets (Macherey-Nagel) using 0.75 M KH_2PO_4 (pH 3.5) as the mobile phase. In all the ATPase assays the composition of the reaction mixtures was 25 mM Tris–HCl (pH 8.0), 50 mM KCl and 5 mM $MgCl_2$, 1 mM DTT and 0.1 mg/ml of BSA. The reactions were stopped with 1.5 M formic acid at the indicated time points. To determine the concentration of poly(C) required for half-maximal ATPase activity (Table 2, column 3), 25 nM Rho was incubated with different concentrations of poly(C) at 37 °C. Reaction was initiated with 500 μM ATP together with [γ-^{32}P]ATP (6000 Ci/mmol) and was stopped after 15 min by formic acid. Release of Pi was analyzed by exposing the TLC sheets to a Phosphorimager screen for 5 min and subsequently by scanning using Typhoon 9200 (Amersham) and quantified by Image QuantTL software. The concentration of poly(C) corresponding to half-maximal ATPase activity was determined by fitting the plot of amount of Pi release against concentration of poly(C) to a sigmoidal curve. To determine the concentration of rC_{10} and rC_{25} corresponding to half-maximal ATPase activity (Table 3, columns 4 and 5), the titrations were done in the presence of 1 μM $oligo(dC)_{34}$. The concentration of ATP was 1 mM. Other conditions were similar to those described above.

To calculate the K_m values of ATP for WT and Y80C mutant of Rho, in the same reaction mixture as described above, 5 nM of Rho was incubated with 10 μM of poly(C) at 30 °C for 10 min and ATP hydrolysis was initiated by the addition of different concentration of ATP (10 μM – 100 μM). Aliquots were removed and mixed with 1.5 M formic acid at various time points. The product formation was linear in the time range (up to 5 min) that we used for calculating the initial rate of reaction. The initial rates of the reaction were determined by plotting the amount of ATP hydrolyzed *versus* time using linear regression method. Then the K_m values were determined from the double-reciprocal Lineweaver–Burk plots.

The rate of ATP hydrolysis in the presence of poly(C) was measured in the same reaction mixture as described above. The concentrations of Rho, ATP and poly(C) were 10 nM, 1 mM and 20 μM, respectively. Reactions were performed at 30 °C and aliquots were removed at different time points (at 30 s intervals up to 5 min) and mixed with 1.5 M formic acid.

Photo-affinity labeling of ATP and rC_{10} to Rho

To determine the apparent dissociation constant ($K_{d,app}$) of ATP, UV cross-linking of labeled ATP was performed with 50 nM Rho and varying concentrations of [γ-^{32}P]ATP (30 Ci/mmol) in a 10 μl reaction mixture containing 25 mM Tris–HCl (pH 8.0), 50 mM KCl, 5 mM $MgCl_2$and 1 mM DTT. The samples were irradiated for 5 min at room temperature in CL-1000 Ultraviolet cross-linker from UVP. This method of determining the apparent dissociation constant was used earlier.[14,34] In a similar way the cross-linking of labeled rC_{10} to WT and Y80C mutant of Rho were performed. The samples were separated by SDS–PAGE, followed by scanning the gels in the phosphor-imager Typhoon 9200 and quantified by Image-Quant software.

Fluorescence quenching and anisotropy measurements

All the fluorescence experiments were performed in the buffer containing 10 mM Tris–HCl (pH 7.0) and 100 mM KCl at 25 °C in a Perkin Elmer LS 55 Luminescence spectrometer. Changes in the tryptophan (W381) fluorescence at 350 nm of WT and Y80C Rho were monitored upon exciting at 295 nm. Fluorescence quenching was measured in the presence of different concentrations of a neutral quencher, acrylamide. Normalized emission was plotted against increasing concentrations of acrylamide and the quenching constant (K_{SV}) was obtained using Stern-Volmer equation: $(F_0/F)_{350} = 1 + K_{SV}[Q]$, where, F_0 is the initial fluorescence intensity and Q is the concentration of acrylamide.

TbGTP (3:1; 150 μM of terbium chloride and 50 μM of GTP) complex upon excitation at 295 nm gives rise to an emission signal characterized by two emission peaks at 488 nm and 545 nm.[39,40] We measured the fluorescence anisotropies of this complex at 545 nm both in the absence and presence of either WT or Y80C Rho proteins.

Limited proteolysis of Rho by V8 protease

The conformational changes induced by the Y80C mutation were probed from the limited proteolysis pattern generated by V8 protease. For the purpose of end-labeling the protein, we used heart muscle protein kinase (HMK)

tagged WT and Y80C Rho. The tag was introduced at the C terminus by PCR amplification using appropriate primers and was cloned in pET21b vector. The resultant Rho proteins have both His and HMK-tags at the C-terminal end. They were purified in a similar way as described above and the termination assays showed that these two tags did not interfere with the function of the WT Rho. HMK-tagged Rho proteins were radiolabeled with [γ-^{32}P]ATP (3000 Ci/mmol) using protein kinase A. The labeling reaction was done in buffer containing 20 mM Tris–HCl (pH 8.0), 150 mM NaCl, 10 mM $MgCl_2$ and 10 μM ATP. 30 μg of Rho were incubated with 60 units of the kinase for 2 h at 21 °C. After labeling, 0.8 μM of labeled Rho were incubated with 0.05 μg of V8 protease in transcription buffer supplemented with 1 mM ATP for the indicated time at 37 °C. The reactions were stopped by adding 6X SDS-loading dye and were stored on ice. Samples were heated to 95 °C for 3 min, prior to loading onto a SDS–12.5%(w/v) PAGE. Gels were exposed overnight to a phosphorimager screen and were scanned using Phosphor-imager Typhoon 9200 and analyzed by Image-Quant software. Molecular weight markers of end-labeled Rho were generated by cyanogen bromide (CNBr) and Sub-maxillary protease (Arg-C) mediated cleavages. Methionine-specific cleavage reactions using CNBr contained (pH adjusted to pH2 with 1 M HCl) 0.8 μM of labeled Rho, 1 M CNBr and 0.4%(w/v) SDS in a 10 μl reaction. Reaction mixtures for arginine specific cleavage contained 0.8 μM of labeled Rho, 2 μg of Sub-maxillary protease and 0.1%(w/v) SDS in a 10 μl reaction. Reactions were terminated after 10 min at 37 °C by addition of 6X SDS-loading dye followed by boiling.

Templates for *in vitro* transcription

Plasmid pRS106 containing *trp t′* terminator following a strong T7A1 promoter was constructed by replacing the H-19B *nutR*-triple terminator cassette from plasmid pRS25.[53] Linear DNA templates for *in vitro* transcription were made by PCR amplification using the plasmid pRS106. In order to immobilize the template on streptavidin-coated magnetic beads, a biotinylated upstream primer was used. The lac operator sequence was incorporated in a downstream primer to make the templates with lac-operator at the downstream edge.[43]

In vitro Rho-dependent transcription termination assay

In vitro Rho-dependent termination reactions were performed in T buffer (25 mM Tris–HCl (pH 8.0), 5 mM $MgCl_2$, 50 mM KCl, 1 mM DTT and 0.1 mg/ml of BSA) at 37 °C. The template DNA was immobilized on the streptavidin-coated magnetic beads (Promega), wherever required, before starting the reaction. The reactions were initiated with 10 nM DNA, 40 nM WT RNA polymerase, 175 μM ApU, 5 μM each of GTP and ATP and 2.5 μM CTP to make a 23-mer elongation complex (EC_{23}). [α-^{32}P]CTP (3000 Ci/mmol) was added to the reaction to label the EC_{23}. The complex was chased with 20 μM NTPs in the presence of 10 μg/ml of rifampicin for 5 min at 37 °C. 50 nM WT Rho or Rho mutants and 200 nM NusG were added to the chase solution as indicated. The reaction was stopped by adding 20 μl of phenol after 5 min of incubation at 37 °C and the released RNA was phenol extracted. RNA was fractionated in a 10% sequencing gel. For the reactions with B8 RNAP, the enzyme concentration was 100 nM and the EC was chased with 100 μM NTPs.

RNA release from stalled elongation complex by WT and Rho mutants

trp t′ template with the lac operator sequence at position 161 was used to study RNA release from stalled elongation complex (RB) by WT and Rho mutants. In order to make the stalled roadblocked complex on streptavidin beads, lac repressor was added before addition of the chasing solution. EC_{23} was made first and then was chased with 20 μM NTPs and 10 μg/ml of rifampicin for 2 min to make the RB. This was followed by addition of 50 nM of either WT or mutant Rho proteins in the presence or absence of 200 nM NusG. The reaction was incubated at 37 °C for 5 min and the supernatant was separated from streptavidin beads on a magnetic stand to measure the released RNA from the EC (Figure 5).

For the kinetics of RNA release from the RB, under different concentrations of ATP both in the presence or absence of NusG, RB was at first formed at position 161 of the *trp t′* template as described above, except that EC_{23} was chased with 50 μM NTPs. The RB was then washed extensively to remove the unincorporated NTPs and was re-suspended in T buffer supplemented with different concentrations of ATP (Figure 6). Following which 50 nM WT Rho or Rho mutants with or without 200 nM NusG were added to it. Half of the supernatant (S) was removed at various time points and added to the equal volume of RNA loading dye (Ambion). The rest of the reaction (half of the supernatant + pellet; P) was phenol extracted and mixed with the dye.

Acknowledgements

We are grateful to Professor T. Ramasarma and other laboratory members for critically reading the manuscript and Dr Ding Jin for providing strains with B2 and B8 RNA polymerases. We thank Dr J. Gowrishankar for providing us with different *E. coli* strains and his laboratory members for helping us in performing different genetic experiments. We thank Mohammad Akif for helping in structural analysis of different Rho mutants. We are thankful to R. Suganthan for cloning and purifying lac repressor protein and Nanci R. Kolli for the technical help in purifying B8 RNA polymerase. We also thank the CDFD sequencing facility for all the sequencing reactions. This work is supported by a Wellcome Trust Senior Research fellowship (to R.S.). J.C. is a University Grants Commission, Senior Research Fellow.

References

1. Wilson, K. S. & von Hippel, P. H. (1994). Stability of *Escherichia coli* transcription complexes near an intrinsic terminator. *J. Mol. Biol.* **244**, 36–51.
2. Mooney, R. A., Artsimovitch, I. & Landick, R. (1998). Information processing by RNA polymerase: recognition of regulatory signals during RNA chain elongation. *J. Bacteriol.* **180**, 3265–3275.
3. Yarnell, W. S. & Roberts, J. W. (1999). Mechanism of intrinsic transcription termination and antitermination. *Science*, **284**, 611–615.

4. Richardson, J. P. (1993). Transcription termination. *Crit. Rev. Biochem. Mol. Biol.* **28**, 1–30.
5. Uptain, S. M., Kane, C. M. & Chamberlin, M. J. (1997). Basic mechanisms of transcript elongation and its regulation. *Annu. Rev. Biochem.* **66**, 117–172.
6. Richardson, J. P. (2003). Loading Rho to terminate transcription. *Cell*, **114**, 157–159.
7. Richardson, J. P. (2002). Rho-dependent termination and ATPases in transcript termination. *Biochim. Biophys. Acta*, **1577**, 251–260.
8. Banerjee, S., Chalissery, J., Bandey, I. & Sen, R. (2006). Rho-dependent transcription termination: more questions than answers. *J. Microbiol.* **44**, 11–22.
9. Modrak, D. & Richardson, J. P. (1994). The RNA-binding domain of transcription termination factor rho: isolation, characterization, and determination of sequence limits. *Biochemistry*, **33**, 8292–8299.
10. Wei, R. R. & Richardson, J. P. (2001). Identification of an RNA-binding Site in the ATP binding domain of *Escherichia coli* Rho by H2O2/Fe-EDTA cleavage protection studies. *J. Biol. Chem.* **276**, 28380–28387.
11. Burgess, B. R. & Richardson, J. P. (2001). RNA passes through the hole of the protein hexamer in the complex with the Escherichia coli Rho factor. *J. Biol. Chem.* **276**, 4182–4189.
12. Wei, R. R. & Richardson, J. P. (2001). Mutational changes of conserved residues in the Q-loop region of transcription factor Rho greatly reduce secondary site RNA-binding. *J. Mol. Biol.* **314**, 1007–1015.
13. Xu, Y., Kohn, H. & Widger, W. R. (2002). Mutations in the rho transcription termination factor that affect RNA tracking. *J. Biol. Chem.* **277**, 30023–30030.
14. Miwa, Y., Horiguchi, T. & Shigesada, K. (1995). Structural and functional dissections of transcription termination factor rho by random mutagenesis. *J. Mol. Biol.* **254**, 815–837.
15. Skordalakes, E. & Berger, J. M. (2003). Structure of the Rho transcription terminator: mechanism of mRNA recognition and helicase loading. *Cell*, **114**, 135–146.
16. Alifano, P., Rivellini, F., Limauro, D., Bruni, C. B. & Carlomagno, M. S. (1991). A consensus motif common to all Rho-dependent prokaryotic transcription terminators. *Cell*, **64**, 553–563.
17. Morgan, W. D., Bear, D. G., Litchman, B. L. & von Hippel, P. H. (1985). RNA sequence and secondary structure requirements for rho-dependent transcription termination. *Nucl. Acids Res.* **13**, 3739–3754.
18. Bear, D. G., Hicks, P. S., Escudero, K. W., Andrews, C. L., McSwiggen, J. A. & von Hippel, P. H. (1988). Interactions of *Escherichia coli* transcription termination factor rho with RNA. II. Electron microscopy and nuclease protection experiments. *J. Mol. Biol.* **199**, 623–635.
19. Skordalakes, E. & Berger, J. M. (2006). Structural insights into RNA-dependent ring closure and ATPase activation by the Rho termination factor. *Cell*, **127**, 553–564.
20. Martinez, A., Opperman, T. & Richardson, J. P. (1996). Mutational analysis and secondary structure model of the RNP1-like sequence motif of transcription termination factor Rho. *J. Mol. Biol.* **257**, 895–908.
21. Pereira, S. & Platt, T. (1995). Analysis of *E. coli* rho factor: mutations affecting secondary-site interactions. *J. Mol. Biol.* **251**, 30–40.
22. Neely, M. N. & Friedman, D. I. (1998). Functional and genetic analysis of regulatory regions of coliphage H-19B: location of shiga-like toxin and lysis genes suggest a role for phage functions in toxin release. *Mol. Microbiol.* **28**, 1255–1267.
23. Lerner, C. G. & Inouye, M. (1990). Low copy number plasmids for regulated low-level expression of cloned genes in *Escherichia coli* with blue/white insert screening capability. *Nucl. Acids Res.* **18**, 4631.
24. Jin, D. J., Burgess, R. R., Richardson, J. P. & Gross, C. A. (1992). Termination efficiency at rho-dependent terminators depends on kinetic coupling between RNA polymerase and rho. *Proc. Natl Acad. Sci. USA*, **89**, 1453–1457.
25. Jin, D. J. & Gross, C. A. (1988). Mapping and sequencing of mutations in the Escherichia coli rpoB gene that lead to rifampicin resistance. *J. Mol. Biol.* **202**, 45–58.
26. Guarente, L. P. & Beckwith, J. (1978). Mutant RNA polymerase of *Escherichia coli* terminates transcription in strains making defective rho factor. *Proc. Natl Acad. Sci. USA*, **75**, 294–297.
27. Magyar, A., Zhang, X., Abdi, F., Kohn, H. & Widger, W. R. (1999). Identifying the bicyclomycin binding domain through biochemical analysis of antibiotic-resistant rho proteins. *J. Biol. Chem.* **274**, 7316–7324.
28. Pereira, S. & Platt, T. (1995). A mutation in the ATP binding domain of rho alters its RNA binding properties and uncouples ATP hydrolysis from helicase activity. *J. Biol. Chem.* **270**, 30401–30407.
29. Bogden, C. E., Fass, D., Bergman, N., Nichols, M. D. & Berger, J. M. (1999). The structural basis for terminator recognition by the Rho transcription termination factor. *Mol. Cell*, **3**, 487–493.
30. Geiselmann, J., Yager, T. D. & von Hippel, P. H. (1992). Functional interactions of ligand cofactors with *Escherichia coli* transcription termination factor rho. II. Binding of RNA. *Protein Sci.* **1**, 861–873.
31. Hitchens, T. K., Zhan, Y., Richardson, L. V., Richardson, J. P. & Rule, G. S. (2006). Sequence-specific interactions in the RNA-binding domain of *Escherichia coli* transcription termination factor Rho. *J. Biol. Chem.* **281**, 33697–33703.
32. Richardson, J. P. (1982). Activation of rho protein ATPase requires simultaneous interaction at two kinds of nucleic acid-binding sites. *J. Biol. Chem.* **257**, 5760–5766.
33. Martinez, A., Burns, C. M. & Richardson, J. P. (1996). Residues in the RNP1-like sequence motif of Rho protein are involved in RNA-binding affinity and discrimination. *J. Mol. Biol.* **257**, 909–918.
34. Dolan, J. W., Marshall, N. F. & Richardson, J. P. (1990). Transcription termination factor rho has three distinct structural domains. *J. Biol. Chem.* **265**, 5747–5754.
35. McSwiggen, J. A., Bear, D. G. & von Hippel, P. H. (1988). Interactions of *Escherichia coli* transcription termination factor rho with RNA. I. Binding stoichiometries and free energies. *J. Mol. Biol.* **199**, 609–622.
36. Richardson, J. P. & Carey, J. L. (1982). 3rd rho Factors from polarity suppressor mutants with defects in their RNA interactions. *J. Biol. Chem.* **257**, 5767–5771.
37. Chen, X. & Stitt, B. L. (2004). The binding of C10 oligomers to Escherichia coli transcription termination factor Rho. *J. Biol. Chem.* **279**, 16301–16310.
38. Lakowicz, J. R. (1999). *Principles of Flurescence Spectroscopy*, 2nd edit. Kluwer Academic/Plenum, New York.
39. Kumar, K. P. & Chatterji, D. (1990). Resonance energy transfer study on the proximity relationship between the GTP binding site and the rifampicin binding site of *Escherichia coli* RNA polymerase. *Biochemistry*, **29**, 317–322.
40. Sen, R. & Dasgupta, D. (2003). Simple fluorescence assays probing conformational changes of *Escherichia*

coli RNA polymerase during transcription initiation. *Methods Enzymol.* **370**, 598–605.
41. Lowery, C. & Richardson, J. P. (1977). Characterization of the nucleoside triphosphate phosphohydrolase (ATPase) activity of RNA synthesis termination factor p. I. Enzymatic properties and effects of inhibitors. *J. Biol. Chem.* **252**, 1375–1380.
42. Nowatzke, W. L. & Richardson, J. P. (1996). Characterization of an unusual Rho factor from the high G+ C Gram-positive bacterium *Micrococcus luteus*. *J. Biol. Chem.* **271**, 742–747.
43. King, R. A., Sen, R. & Weisberg, R. A. (2003). Using a lac repressor roadblock to analyze the *E. coli* transcription elongation complex. *Methods Enzymol.* **371**, 207–218.
44. Pani, B., Banerjee, S., Chalissery, J., Abhishek, M., Malarini, L. R., Suganthan, R. & Sen, R. (2006). Mechanism of inhibition of RHO-dependent transcription termination by bacteriophage P4 protein PSU. *J. Biol. Chem.* **281**, 26491–26500.
45. Shigesada, K. & Wu, C. W. (1980). Studies of RNA release reaction catalyzed by *E. coli* transcription termination factor rho using isolated ternary transcription complexes. *Nucl. Acids Res.* **8**, 3355–3369.
46. Howard, B. H. & de Crombrugghe, B. (1976). ATPase activity required for termination of transcription by the *Escherichia coli* protein factor rho. *J. Biol. Chem.* **251**, 2520–2524.
47. Brennan, C. A., Dombroski, A. J. & Platt, T. (1987). Transcription termination factor rho is an RNA-DNA helicase. *Cell*, **48**, 945–952.
48. Adelman, J. L., Jeong, Y. J., Liao, J. C., Patel, G., Kim, D. E., Oster, G. & Patel, S. S. (2006). Mechanochemistry of transcription termination factor Rho. *Mol. Cell*, **22**, 611–621.
49. Burns, C. M., Nowatzke, W. L. & Richardson, J. P. (1999). Activation of Rho-dependent transcription termination by NusG. Dependence on terminator location and acceleration of RNA release. *J. Biol. Chem.* **274**, 5245–5251.
50. Morse, D. E. & Guertin, M. (1972). Amber suA mutations which relieve polarity. *J. Mol. Biol.* **63**, 605–608.
51. Das, A., Merril, C. & Adhya, S. (1978). Interaction of RNA polymerase and rho in transcription termination: coupled ATPase. *Proc. Natl Acad. Sci. USA*, **75**, 4828–4832.
52. Menzel, R. (1989). A microtiter plate-based system for the semiautomated growth and assay of bacterial cells for beta-galactosidase activity. *Anal. Biochem.* **181**, 40–50.
53. Cheeran, A., Babu Suganthan, R., Swapna, G., Bandey, I., Achary, M. S., Nagarajaram, H. A. & Sen, R. (2005). *Escherichia coli* RNA polymerase mutations located near the upstream edge of an RNA:DNA hybrid and the beginning of the RNA-exit channel are defective for transcription antitermination by the N protein from lambdoid phage H-19B. *J. Mol. Biol.* **352**, 28–43.
54. Kashlev, M., Nudler, E., Severinov, K., Borukhov, S., Komissarova, N. & Goldfarb, A. (1996). Histidine-tagged RNA polymerase of *Escherichia coli* and transcription in solid phase. *Methods Enzymol.* **274**, 326–334.
55. Geiselmann, J., Seifried, S. E., Yager, T. D., Liang, C. & von Hippel, P. H. (1992). Physical properties of the *Escherichia coli* transcription termination factor rho. 2. Quaternary structure of the rho hexamer. *Biochemistry*, **31**, 121–132.
56. Harinarayanan, R. & Gowrishankar, J. (2003). Host factor titration by chromosomal R-loops as a mechanism for runaway plasmid replication in transcription termination-defective mutants of *Escherichia coli*. *J. Mol. Biol.* **332**, 31–46.

Edited by M. Gottesman

(Received 4 April 2007; received in revised form 1 June 2007; accepted 1 June 2007)
Available online 9 June 2007